Cruise Report

The Gulf of Mexico Gas Hydrate Joint Industry Project

Covering the cruise of the Drilling Vessel *Uncle John*
Mobile, Alabama to Galveston, Texas
Atwater Valley Blocks 13/14 and Keathley Canyon Block 151
17 April to 22 May 2005

DISCLAIMER

Cruise Participants*

Shipboard Scientific Party

George E. Claypool
Chief Scientist
University of California, San Diego
9500 Gilman Dr, GRD 0244
La Jolla, CA 92093-0244
USA
geclaypool@aol.com

Timothy S. Collett
Downhole Logging Scientist
U.S. Geological Survey
Denver Federal Center
MS-939, Box 25046
Denver, CO 80225
USA
tcollett@usgs.gov

Brandon Dugan
Physical Properties Specialist
Rice University
Department of Earth Sciences – MS126
P.O. Box 1892
Houston, TX 77251-1892
USA
dugan@rice.edu

Barry Freifeld
X-ray Imaging Specialist
Lawrence Berkeley National Laboratory
MS 90-1116
One Cyclotron Rd
Berkeley, CA 94720
USA
bmfreifeld@lbl.gov

Melanie Holland
IR Imaging Specialist
GeoTek Ltd
3 Faraday Close
Drayton Fields
Daventry
Northamptonshire, NN11 5RD
UK
melanie@geotek.co.uk

Miriam Kastner
Geochemist
University of California, San Diego
9500 Gilman Dr, GRD 0212
La Jolla, CA 92093-0212
USA
mkastner@ucsd.edu

Thomas D. Lorenson
Geochemist
U.S. Geological Survey
345 Middlefield Rd, MS999
Menlo Park, CA 94025
USA
tlorenson@usgs.gov

Peter Schultheiss
Core Logging Scientist
GeoTek Ltd
3 Faraday Close
Drayton Fields
Daventry
Northamptonshire, NN11 5RD
UK
peter@geotek.co.uk

John Roberts
Core Logging Scientist
GeoTek Ltd
3 Faraday Close
Drayton Fields
Daventry
Northamptonshire, NN11 5RD
UK
john@geotek.co.uk

Tae Sup Yun
Physical Properties Specialist
Georgia Institute of Technology
790 Atlantic Dr.
Mason 299
Atlanta, GA 30332-0355
USA
taesup.yun@gmail.com

*contact information as of May 21, 2005

Guillermo A. Narsilio
Physical Properties Specialist
Georgia Institute of Technology
790 Atlantic Dr.
(Mason 299)
Atlanta, GA 30332-0355
USA
guillermo.narsilio@ce.gatech.edu

Brian Buczkowski
Curator/Data Management Specialist
U.S. Geological Survey
Woods Hole Science Center
384 Woods Hole Rd
Woods Hole, MA 02543
USA
bbuczkowski@usgs.gov

Jennifer Dougherty
Gas Geochemistry Specialist
U.S. Geological Survey
345 Middlefield Rd, MS999
Menlo Park, CA 94025
USA
jdougherty@usgs.gov

Rebecca Fenwick
Curator/Data Manager
University of California, San Diego
9500 Gilman Dr, GRD 0244
La Jolla, CA 92093-0244
USA
rfenwick@ucsd.edu

Gretchen Robertson
Pore Water Specialist
University of California, San Diego
9500 Gilman Dr, GRD 0212
La Jolla, CA 92093-0212
USA
grobertson@ucsd.edu

Christie Lindemann
Curator/Data Manager
University of California, San Diego
9500 Gilman Dr, GRD 0244
La Jolla, CA 92093-0244
USA
clindemann@ucsd.edu

Robert Monroe
Science Writer
University of California, San Diego
9500 Gilman Dr, 0206
La Jolla, CA 92093-0206
USA
rmonroe@ucsd.edu

JIP Shipboard Personnel and Project Representatives

Aaron Conte
Operations Manager
ChevronTexaco Energy Technology Co.
1500 Louisiana St.
Houston, TX 77002
USA
aconte@chevrontexaco.com

Emrys Jones
Project Manager
ChevronTexaco Energy Technology Co.
2811 Hayes Road
Houston, TX 77082-6696
USA
ejones@chevrontexaco.com

Ben Bloys
Operations Manager
ChevronTexaco Energy Technology Co.
3901 Briarpark
Houston, TX 77042
Ben.bloys@chevrontexaco.com

Ray Boswell
U. S. Department of Energy
National Energy Technology Lab
Collins Ferry Road
Morgantown, WV
RAY .BOSWELL@netl.doe.gov

Fugro McClelland Shipboard Personnel

Gary Humphry	Project Manager	ghumphry@fugro.com
Fabian Hippe	Project Engineer	fabian.hippe@gmx.de
Yew Choong (Patrick) Lee	Shift Engineer	
Ricardo Alvarez	Soil Tech	
Brian Ferri	Drilling Supervisor	
David Fendley	Senior Driller	
David Garcia	Electro Mechanical Tech	drgave@earthlink.net
David Mooney	Senior Driller	
Miguel Quiros	Electro Mechanical Tech	
Jeff Scott	Engineer	jscott@fugro.com
Louis Semien	Soil Tech	

Fugro Engineers B.V.

Sander Rutgers	Sr. Operator	srutgers@tiscali.nl
Roeland Baas	Operator	r.baas@fugro.nl

ITE Institute of Petroleum Engineering

Martin Rothfuss	Engineer/Scientist	martin.rothfuss@tu-clausthal.de
Marcel Diedrich	Mech. Tech	

Fugro Chance Inc.

Michael Brent	Surveyor
Steven Spruell	Surveyor

Cal Dive Shipboard Personnel

Chuck Schaeffler	Superintendent
Jeff Davis	Superintendent
Bill Bishop	Supervisor
CJ Kirwer	Supervisor
Angkau Melai	Rigger Forman
Mingu Yabu	Rigger Forman
Miles Tucker	EHS Advisor/Medic
Danny Batten	EHS Advisor/Medic
William Allen	Crane Operator
John Cavilier	Crane Operator
Johnathan Ilong	Rigger
Usin Budong	Rigger
Peter Celica	Rigger
Ambol Banta	Rigger
Juin Sintau	Rigger
Kasa Jabing	Rigger

C-Mar Shipboard Personnel

Derek Newham	Master
Viru Narona	Master
Scott McKenzie	Chief Officer
George Milanovic	Chief Officer
Ed Woodley	Chief Engineer
Calvin Austin	2nd Engineer
Colin Maynard	2nd Engineer
Jason Sheils	Bosun
Alan Lawson	Bosun
Frank Miles	Bosun
Andy Little	Chief Engineer
Ulchai Thamoothang	Welder
Kosol Chanpoon	Welder
Scott McKenzie	Chief Officer
Stephen Park	DPO/2nd Officer
Frank Sobrink	Senior DPO
Louis Walsh	2nd Mate/DPO
Derrick Martin	Head Cook
Sunny Garcia	Night Cook

Canyon Offshore Shipboard Personnel

Robert Collins	ROV Supervisor
Steve Hebert	ROV Supervisor
Rod Heckle	ROV Pilot/Technician
Kirby Keddy	ROV Pilot/Technician
James Lafferty	ROV Pilot/Technician
George Wilson	ROV Supervisor
Marcus Martens	ROV Supervisor

Schlumberger Shipboard Personnel

Alexandra Carey	Wireline Field Engineer	acarey@slb.com
Kelvin Hoong	LWD/MWD Tech	hhoong@slb.com
Lake Loh	LWD/MWD Tech	lloh@slb.com
Joy Araujo	LWD/MWD Tech	
Neil Commeaux	Wireline Tech	
Scott Davis	Wireline Tech	
Jared Naquin	Wireline Tech	
Shelia Noeth	Wellbore Stability	
Tom Smith	Seismic Engineer	

Secorp Shipboard Personnel

Richard (Quake) McKnight	HES Representative/H_2S Technician

GeoCet Shipboard Personnel

Steve Olsen	Marine Mammal Observer
Zach Roddenberry	Marine Mammal Observer
Gina Zingarelli	Marine Mammal Observer

Cruise Report Gulf of Mexico JIP

Contents

Sections (as individual files on CD):

Gulf of Mexico Gas Hydrates Joint Industry Project
Operational Summary of 2005 Drilling and Coring Program

Aaron Conte and Ben Bloys
Chevron Corporation
Houston, TX

Focus and Objectives

A primary focus of the drilling and coring operations was to conduct the program in a manner consistent with the highest standards of health-environment-safety (HSE), and to achieve incident-free operations. As a result the program achieved:

- More than 48,300 man-hours worked with the vessel at 102 person capacity for nearly the entire project;
- No injuries or spills were recorded;
- Minerals Management Service inspections found no noncompliance incidents;
- One near-miss incident was reported.

The drilling and coring program was part of a larger US Department of Energy-supported joint industry project (JIP) to better characterize *in situ* gas hydrate in sediments of the Gulf of Mexico. Some of the principle objectives were to:

- Collect log data in shallow sections;
- Determine seismic velocities;
- Recover cores for sediment, pore water and gas analyses;
- Determine formation temperatures and pressures.

The objectives were limited by the budget available (~$7.6 MM) for the offshore operations portion of the project. A 35 offshore day project schedule was developed (including 10% contingency) and the objectives prioritized accordingly. A total of seven boreholes covering 5540 ft (1.82 km) were completed in the Atwater Valley (AT) and Keathley Canyon (KC) protraction areas during the available time:

- AT13#1 – Logging while drilling (LWD) hole to 809 ft (265 m) below mud line (BML);
- AT14#1 – LWD hole to 941 ft (309 m) BML;
- AT13#2 – Cored hole to 656 ft (215 m) BML;
- AT M1 – Cored hole to 80 ft (26.2 m) BML;
- AT M2 – Cored hole to 103 ft (33.8 m) BML;
- KC151 #2 – LWD hole to 1506 ft (494 m) BML;
- KC151 #3 – Cored hole to 1445 ft (474 m) BML.

The Atwater Valley and Keathley Canyon drilling and coring locations in the deepwater Gulf of Mexico are shown in Figure 1.

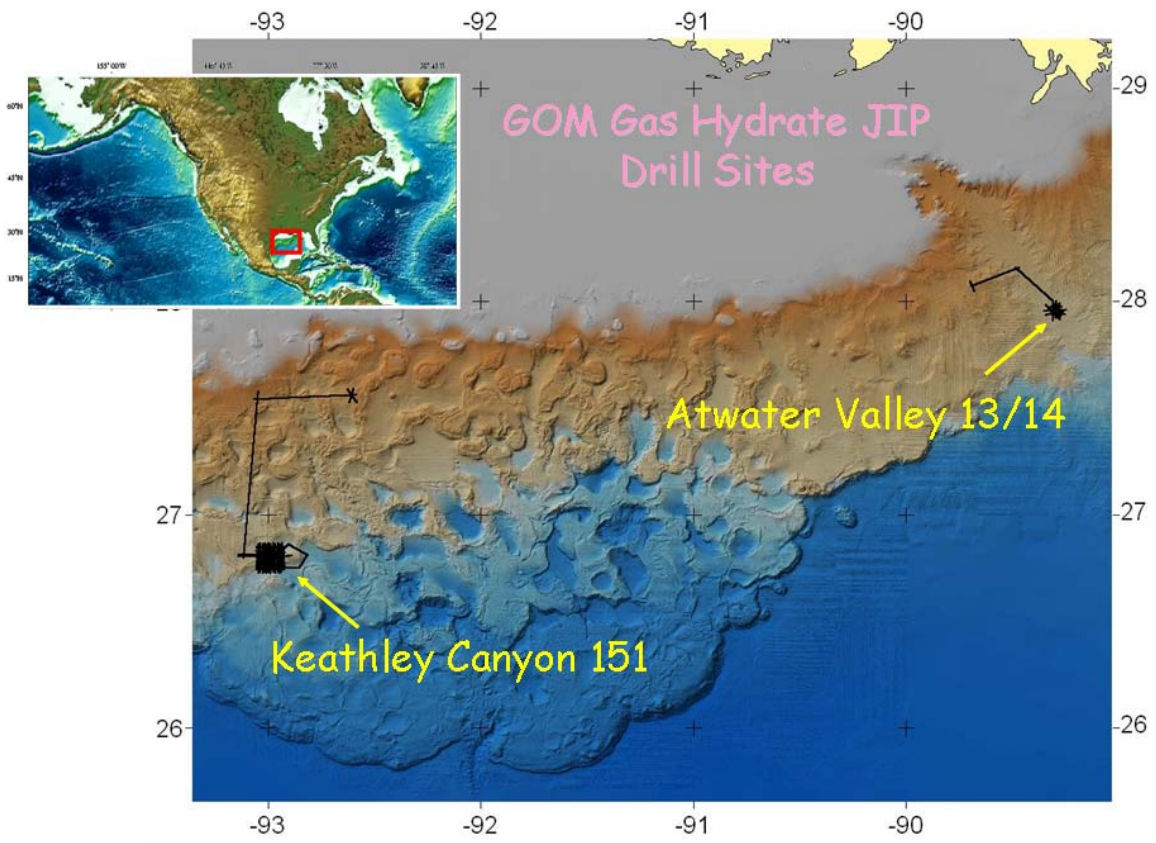

Figure 1.—Bathymetric relief map of Northern Gulf of Mexico continental slope showing general location of Atwater Valley and Keathley Canyon JIP drilling sites.

Logistics

Chevron Gulf of Mexico Shelf Logistics provided support for numerous transfers of equipment and personnel during the drilling and coring program. Atwater Valley operations were serviced from Venice, with the *Gilbert McCall* (150 ft crew boat) used for equipment load outs and four helicopter flights used for personnel transfers. Keathley Canyon operations were supported from Intracoastal City by the *Genesis* and *Gilbert McCall* crewboats, and by four helicopter flights for personnel transfers. The Fourchon deepwater port was available for use if needed, and a contractor used one helicopter flight from Leeville for a family emergency. Shore-based logistical support from all locations included the requirement for customs clearance for all personnel and equipment.

Drilling Vessel

The Cal Dive semi-submersible *Uncle John* was used for the drilling and coring program, after the previously contracted geotechnical drill ship *Fugro Explorer* was unavailable due to program delays and schedule conflicts. The *Uncle John* is a dynamically positioned vessel equipped with a 150 metric ton derrick, a National hydraulic top drive, a Hydraudyne Compensator, and a pipe handling system for 30-ft drill pipe up to 5-1/2 inch diameter. The vessel has 1100 square meters of deck space, a 350 metric ton project

load limit, and two 100 metric ton Aker cranes. The *Uncle John* had no mud system, mud pumps or cement unit.

Mobilization

Mobilizaton took place April 14-16, 2005 at the dock in Middle Bay port, Mobile, Alabama, during which trucks delivered and loaded all required equipment for the initial stage of the cruise. Cal-Dive personnel installed piping for the mud system and commissioned the system including tanks and pumps. Chevron personnel performed the required inspections and notation of required action items prior to formal acceptance of the vessel. Special equipment for hazardous gas detection was installed and required training of response teams was performed during the mobilization.

Mud System and Program

The mud system consisted of a 100 barrel mixing tank with a shear hopper (Aqua Shear), a 250-barrel storage tank for 12.0 pound per gallon kill mud, and a diesel powered PZ-8 mud pump. A line was constructed to provide direct seawater feed to the mud pump, and six-inch suction lines equipped with pneumatic valves connected the tanks to the mud pump. The mud system took up a large proportion of the deck space.

The mud program employed viscous sweeps mixed with seawater and 32 pound per barrel (ppb) of attapulgite. Twenty barrel sweeps were planned as needed based on hole conditions. Mud mixing was done manually using the Aqua Shear hopper, which enabled rapid mixing and the appropriate yield of attapulgite. Mud mixing required the use of 2000-pound bags and palletized sacks of both attapulgite and barite. The mud program was supplemented with XCD (xanthan gum biopolymer used to raise the viscosity of water-based drilling fluids) as needed.

Remotely Operated Vehicle (ROV)

The ROV was used for various purposes and was critical to several phases of cruise operations. At each site the ROV was used to deploy compats for positioning, and to collect bottom water samples and shallow push cores of surface sediments. The ROV enabled visual verification of the sea bottom for the initiation of coring, was used to clamp the drill string to the sea bed frame for operation of the pressure coring equipment, and allowed re-entry into the sea bed frame. Holes were continuously monitored by the ROV video camera for any flows during and after drilling operations.

Transits

The *Uncle John* is a self-propelled vessel with about twenty-five-foot draft. The 160-mile transit from Mobile to the Atwater Valley locations averaged a speed of six knots, the 220-mile transit from Atwater Valley to Keathley Canyon averaged eight knots, and the 170-mile transit from Keathley Canyon to Galveston averaged 6 knots. The *Uncle John*

moved between the Atwater Valley Block 13 and Block 14 sites in dynamic positioning mode, with the drill string hanging below the vessel, at a speed of 0.2 to 0.5 knots.

Ship Positioning

The *Uncle John* is dynamically positioned, with a differential global positioning satellite and acoustic positioning tied into the Fugro Chance survey system. Compats (acoustic "pingers") were deployed on the sea floor, on the ROV, and on the sea bed frame for supplemental positioning purposes. The exact position of the boreholes was determined by placing the ROV-mounted compat next to the bit for the LWD, and by the compat mounted on the sea bed frame for the cored holes. The accuracy of acoustic positioning was +/- 20 feet, or 0.5 percent of water depth (4300 feet).

Weather-Loop Current

Weather was generally excellent, with only one minor squall during the 35-day JIP cruise. The main problem was currents in the Atwater Valley location, which ran consistently 2-3 knots at the surface with subsurface effects felt down to about 1000 feet. The ship had no working current meter, and the strong loop current created problems for the *Uncle John* in holding position, causing thruster loads frequently above critical redundancy levels. Subsurface currents caused the drill pipe to drift at an angle beneath the vessel and created difficulties in tripping the pipe. A total of nine hours of downtime were attributed to problems created by currents.

Sea Floor Sampling

The ROV was used to sample water and sediments at or near the sea floor. Core tubes and Niskin bottles were lowered in a basket by winch. The manipulator arm of the ROV could trigger the Niskin bottles and insert the core tubes while being viewed on the ROV video camera. Short (2-3 ft) cores were collected at each site and analyzed for pore water, dissolved gas, and physical properties. This Niskin bottle technique was also used to sample a sea floor plume associated with a shallow flow at Keathley Canyon 151 #2.

Atwater Valley 13/14 LWD Holes

The initial LWD hole (AT 13 #1) was spudded at 23:00 CT on19 April 2005 in water depth of 4234 ft (1290.5 m). AT 13#1 (Figure 2) was intended as a reference hole for the general region. The hole was started with low (100 gallon per minute, gpm) circulation and rotation (50 revolutions per minute, rpm) rates in order to minimize hole enlargement/washout and obtain better battery-operated Geovision Tool (GVR) log response in the shallowest sediments. Rates were increased to 300 gpm and 75 rpm when the NMR tool reached the mud line in order to turn on the tool string. The rate of penetration (ROP) was maintained at less than 100 ft per hour. Each joint of pipe was backreamed 2 or 3 times, and a 20 bbl gel sweep was added every other joint. Flow rates were increased to 350 gpm with backreaming of each joint. The hole was tight, stalling rotary on connections. The equivalent circulating density (ECD) reached 14.9 ppg

estimated mud weight due to hole collapse. AT 13#1 was abandoned at 06:35 on 21 April 2005 at a total depth of 5086 ft or 809 ft (247 meters) below the seafloor with mud filling the hole.

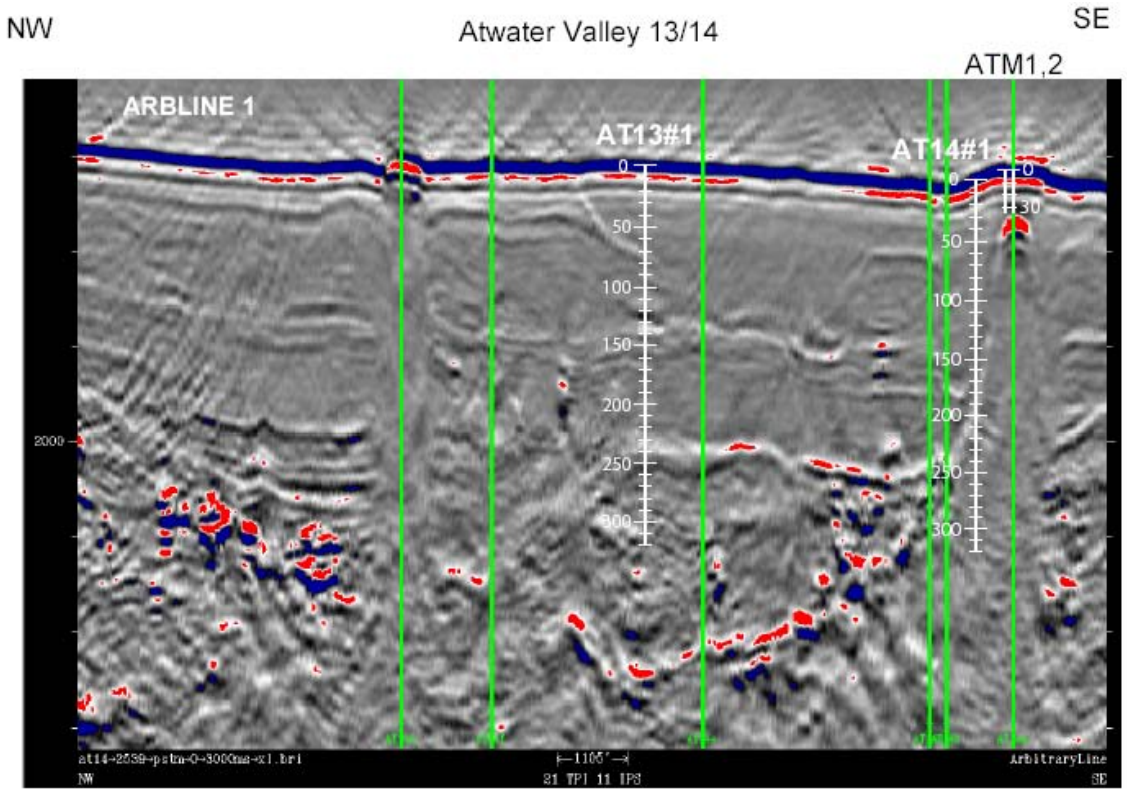

Figure 2.—Seismic line showing four drilling sites in Atwater 13/14 blocks. White lines indicate position of two logging while drilling sites (AT13#1, AT14#2), and coring sites (AT13#2 at same location as AT13#1, and mound sites ATM1, ATM2). Green lines are locations of previously proposed drilling locations.

After a short (~1.6 km) dynamic positioning (DP) move from AT 13#1 and without tripping the bottom-hole assembly (BHA) and LWD tools, AT 14#1 was spudded at 01:17 on 22 April in water depth of 4266 ft (1300.3 m). AT 14 #1 was intended to penetrate the side of an intrusive feature, expressed at the surface as Mound F. The hole was spudded with rates of 100 gpm and 50 rpm, but no GVR data were recovered because batteries were exhausted. Rates were increased to 330 gpm and 75 rpm when the NMR tool reached the mudline. An instantaneous penetration rate of 75 ft per hour was maintained, and each pipe joint was backreamed 3 or 4 times. The hole was cleaned and stabilized using XCD and 11 ppg gel sweeps. Flow rate was increased to 350 gpm and the hole was maintained in much better condition than at AT 13#1. The ECD reached 14.9 ppg EMW due to hole collapse, and the hole was terminated at a total depth of 809 ft (246.6 m) below the mudline. Hole AT 14#1 was abandoned with drilling mud in the hole (ECD = 14.8 ppg EMW).

Coring Operations

The following equipment was used for recovery of core:

- Common BHA for all core tools
- Fugro Hydraulic Piston Corer (FHPC)
- Fugro Corer (FC)
- Fugro Pressure Corer (FPC)
- Hyace Rotary Corer (HRC)
- Temperature sensor in cutting shoe
- Seabed frame
- Wireline BOP

The FHPC has either 15 ft (4.6 m) or 23 ft (7 m) core barrel that is deployed on the sandline. The barrel lands out in the BHA and build-up of pressure on the drill string shears pins and fires the core shoe and barrel into the formation until it either fully strokes or it meet stiff sediment. Typical firing pressures are 1200-2000 psi depending on the type of shear pins (steel/aluminum) and anticipated sediment strength. The FHPC averaged about 95% core recovery with core gas voids intact. A cutting shoe with temperature sensor could be used for in situ temperature measurements. The maximum depth below mudline for using the FHPC on this cruise was 1022 ft (311.5 m), with maximum depth determined by the required pull-out force.

The FC has either 10 ft (3 m) or 15 ft (4.6 m) barrel also deployed on the sandline. The barrel lands out on the formation just outside the bit. The core is taken by pressure on the drill string pushing the barrel into the formation and using a mud hammer effect to push the core shoe through stiffer sediment. Typical hammering pressures are 400-900 psi. The FC averaged 59% recovery but gas retention was much lower (no gas voids). The cutting shoe on the FC could also be replaced with one containing a temperature sensor. This coring tool was used for deeper sediments in Keathley Canyon and was not run in Atwater Valley.

The FPC has a 3 ft (1 m) long pressure-retaining core barrel. The core retracts into an autoclave closed by a flapper valve. The FPC uses a percussion coring mechanism similar to the FC. The FPC was deployed nine times with three successful recoveries of core under pressure. The average core recovery was 38%. The tool is depth-limited due to pull out force. The use of the common BHA created problems for the FPC in soft sediment due to the absence of a landing ring.

The HRC has a 3.2 ft (1 m) long core barrel and also is designed to retain pressure. A small mud motor rotates the cutting shoe and takes the core. Two of nine runs successfully recovered core under pressure, with 20% of footage recovered. The tool is mainly designed for stiffer sediments.

Fugro adapted the Sea Bed Reaction Frame specifically for this project. The frame has ten metric ton reaction mass, with beams for landing in the moon pool, and was run on the lifting sub that was part of the BHA, with locking plates on the frame that allowed it

to be carried on the drill string. Use of the frame allowed for compensation while taking cores by clamping jaws around the drill pipe and activating the drill string compensator. The clamp mechanism was activated by the ROV with a hot stab and an open/close valve. The sea bed frame provided re-entry capability by means of the funnel guide at the top, and a compat was mounted for positioning.

Core Processing Container and Core Handling Process

A forty-foot container/van was outfitted with a core-handling rack and track-mounted IR camera. The container was kept at ~50ºF by means of two roof-mounted refrigeration units. Processing of FHPC and FC cores was done inside the container, as well as transfer and some measurements on pressurized (FPC and HRC) cores.

The core barrel was wireline-retrieved, broken out from the piston/firing assembly at the tool joint on the rig floor, and raised up and laid out on the pipe handler. The core barrel was then transferred via the port-aft crane to the ice trough. After packing in ice, the cutting shoe was broken off and the core liner was pulled out of the inner barrel and into the core processing container/van using a motorized tugger. The core was then processed inside the refrigerated container/van by the science team. Routine processing included imaging by track-mounted and hand-held infrared cameras, void-gas sampling, measurement and archiving the core into1-meter sections, and collection of core material for headspace gas and pore water analysis.

The possibility of pressure build-up and explosive cores when breaking the piston from the barrel on the rig floor and when removing the cutting shoe prior to core removal was mitigated by use of safety measures. A “mud-bucket” type guard was used for removal of the piston, and a cylindrical shield was placed around the cutting shoe. A weep hole in the cutting shoe thread gave indications of excess pressure.

Coring and Wireline Logging at AT13 #2

The first cored hole was AT13 #2, 14 core barrels were deployed (9 FHPC, 3 HRC, 2 FPC) over the intervals 0-157 ft (0-48 m) and 387-502 ft (118-153 m). Full cores were generally recovered with the FHPC, but deeper cores were jammed in the core barrel because of collapsed liners. Apparently a vacuum was being pulled on a small area of the liner when the piston was firing. Only one FPC deployment (AT13 #2-5P) recovered a core under pressure at this site. Two HRC cores (AT13 #2-3P, 7P) recovered sediment, but not under pressure.

The hole was drilled down to 656 ft (200 m) to begin the wireline logging program. The dipole sonic/FMS (Formation Micro-Scanner) could not be run in AT13 #2 through the drill pipe as planned, because of hole collapse and clay build up inside the bit sub that did not allow the tool to pass through the bit. An attempt to lower the logging tool through open water and enter the hole through the sea bed frame was successful despite the loop current. However, the hole had collapsed and the tool only penetrated 75 ft (246 m) into the hole.

Coring Operations at Mound Sites ATM1, ATM2

Shallow coring operations on top of Mound F had been approved and were undertaken as scientific investigations outside the normal MMS permitting requirements for deeper holes. Coring started at about 18:00 CT on 3 May.

The depth interval 0-29 mbsf was cored at mound site ATM1 (27°56'11.62"N, 89°16'46.09"W) with three FHPC cores and three FPC or HRC pressure cores. The FHPC cores recovered a total of 21 meters of sediment. The pressure cores in some cases recovered sediment, but did not retain subsurface pressure.

The depth interval 0-29 mbsf was cored late Wednesday and early Thursday at mound site ATM2 (27°56'11.60"N, 89°16'47.00"W). Three FHPC cores were taken in the upper portion followed by two HRC pressure cores and a final FPC pressure core near the base of the cored section. The FHPC cores recovered sediment from the upper 24 meters beneath the seafloor. Core observations (IR scans, gas voids, salinities, sediment textures) were consistent with gas hydrate having been present in the sediment and decomposing prior to sampling. The two deeper HRC pressure cores did not recover any sediment. The FPC pressure core recovered sediment from 27-28 meters under pressure. This pressurized core (ATM2-5P) was successfully transferred to an aluminum storage chamber, and 2D X-ray images show discrete zones of low-density (about 1 g/cc) material in the core. Controlled degassing experiments on the pressure core indicated gas content in excess of that which could have been present as dissolved methane, consistent with gas hydrate cementation at levels on the order of 1-5 percent of the sediment pore space.

Keathley Canyon 151 #2 LWD Hole

After transiting from Atwater Valley to Keathley Canyon, KC 151 #2 was spudded at 01:31 on 7 May in water depth of 4337 ft (1321.9 m). The planned KC 151 #1 reference LWD hole that was previously approved and named by MMS was not drilled because of time constraints. The drilling objectives at the Keathley Canyon 151 site were to characterize the possible occurrence of gas hydrate in relation to a bottom simulating reflector (BSR) at a depth of about 385 mbml (Figure 3). The hole was spudded with 100 gpm and 50 rpm, but no GVR data were obtained due to exhausted battery life. After the NMR tool reached the mudline the rates were increased to 330 gpm and 75 rpm. The rate of penetration was maintained at less than 75 ft per hour. Each joint was backreamed three or four times, and 9.2 ppg gel sweeps and XCD sweeps were used every 3rd joint to aid in hole cleaning. Hole conditions were good while drilling, with no overtorque or stalling of the rotary. The BSR depth was control drilled, with a 15 bbl sweep and circulate out at each connection. The hole reached a total depth of 1549 ft bml (472.1 mbsf). The hole was displaced with 9.1 ppg mud, and the pick up of the drill string off the bottom required 20K lbs of pull while working the pipe. The weight on the drill string suddenly dropped off 20K lbs and the rig listed. The weight slowly came back after pumping was started. About 500 ft (152.4 m) of 12.2 ppg mud was spotted in the hole,

giving a mud column with an estimated mud weight of 9.8 ppg to the sea floor. At a depth of about 200 ft below the mudline the hole began to flow. Heavy mud (12.2 ppg) was pumped at 200 ft and stabilized the hole, but flow began again after 30 minutes.

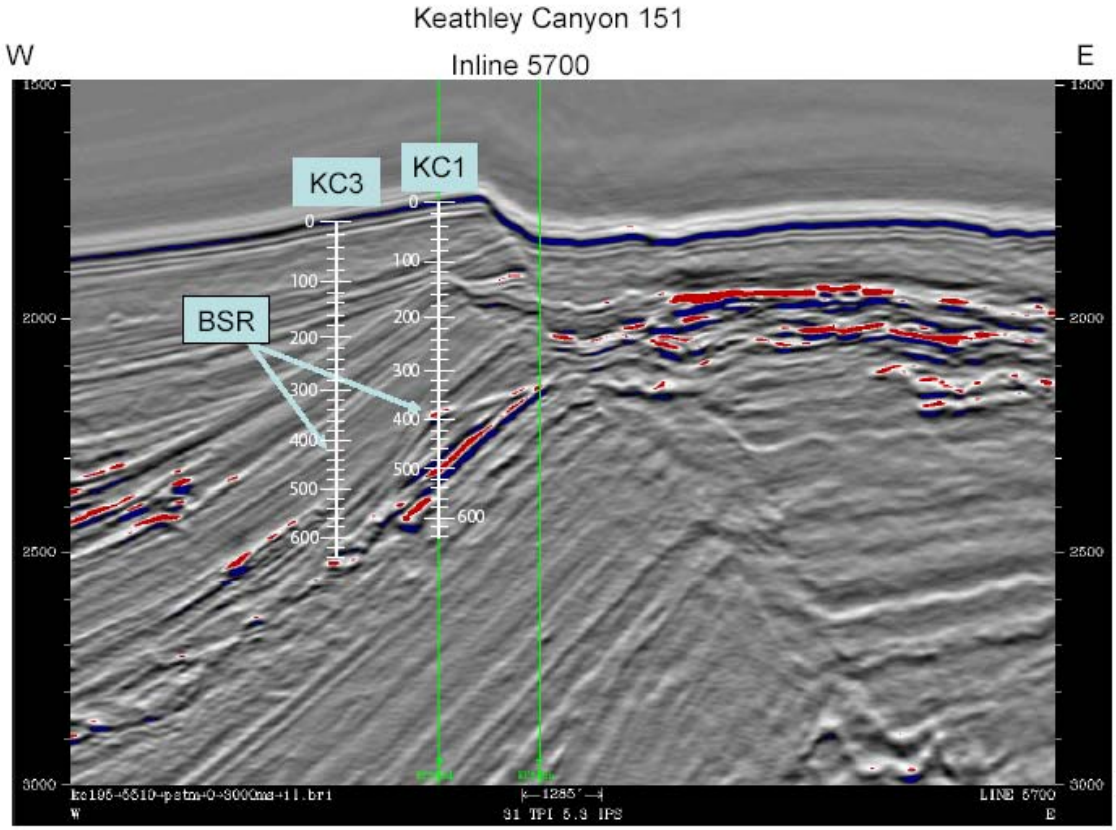

Figure 3.—Seismic line showing proposed drilling locations in the Keathley Canyon 151 block. KC1 indicates location of logging while drilling hole KC151#2 and coring hole KC151#3. KC3 is location of undrilled reference site. Arrows show depth of faintly imaged bottom simulation reflector.

Additional heavy mud (12.2 ppg) was pumped and did not get full returns at the sea floor. The drill pipe was lowered to 445 ft bml and 40 barrels of 10.4 ppg mud pumped into the hole. The hole continued to flow with moderate severity. The drill string with the LWD tools was pulled out of the hole to the surface at 19:00 CT on May 9. Hole KC 151 #1 was periodically monitored by ROV, and after about 20 hours the hole had collapsed and the flow had stopped. The hole was considered plugged and abandoned. No resumption of flow was observed during the drilling of KC 151 #3.

Coring and Wireline Logging at KC 151 #3

After removing the drill string and LWD tools from KC 151 #2, the sea bed frame and bottom hole assembly were made up and lowered to begin coring the KC 151 #3 hole, adjacent to the LWD hole. The first FHPC core arrived on deck at 15:20 CT on 11 May. The uppermost 147 ft (45 m) below the mudline were rapidly cored (5 FHPC cores in 7.5 hours). The hole was washed down without coring to a depth of 328 ft (100 m) and

coring resumed using the Fugro Corer (FC) corer, anticipating stiffer sediments. Pressure cores were spotted in intervals suspected to contain gas hydrate based on the LWD logs. No obvious gas hydrates were recovered, probably due to warm water and slow core barrel retrieval time. A few cores had residual cool spots and textures suggestive of dissociated gas hydrate. One core contained a significant cold spot, which was cut out and immediately placed in liquid N_2. Gas voids were not present in the FC cores, due to loss of gas from the space around the core inside the liner.

Failure to recover obvious hydrate raised concern of significant lateral variation between the LWD and coring holes, and led to abandonment of the coring program tied to the LWD logs. Spot coring based on random footage intervals replaced the original log-based coring plan. XCD sweeps were used instead of attapulgite for Fugro Corer operational concerns. A center bit was used to drill out between cores and was recovered prior to each core run. The coring system was switched from FC to FHPC at 840 ft (256 m). FHPC cores were collected down to a depth of 1022 ft (312 m), where difficulty with pull out (>25K lb over pull) required a switch back to FC. Coring continued every other pipe joint down to the depth of the BSR. A pressure core (26R) was successfully recovered just above the BSR. A total of three pressure cores (2 HRC, 1 FPC) in hole KC 151 #3 provided evidence for the occurrence of gas hydrates.

A wiper trip was done prior to logging. When running the drill pipe back in while the hole was filled with sea water, the hole began to flow and was killed with 12.0 ppg mud. The hole was washed and reamed with sea water, but the drill pipe could not work past the 1208 ft (368 m) depth. The hole was in good condition and was re-spotted with 12.0 ppg mug. Dipole Sonic/GR/GIPT logs were run through the drill pipe to 1118 ft (341 m).

Wireline logging and VSP programs were carried out in the KC151#3 hole over the 120-342 mbsf interval. Logs showed high velocity depth intervals that correlated with the high resistivity intervals in the KC151#2 LWD hole, indicating no significant lateral variation. The vertical seismic profile (VSP) shot 108 stations over about the same depth interval. The hole was abandoned with a cement plug and the drill string and sea bed frame were picked up and transit to Galveston begun.

Downtime and Major Operational Problems

For the 35-day drilling cruise we experienced 175 trouble hours or about 21% trouble time. The majority of the downtime was due to problems with the coring tools, sea bed frame, and drilling rig (48, 42, and 38 hours respectively). About 13 hours of downtime were due to logging problems; 9 hours were weather-related, 8 hours were spent on borehole-control issues associated with flows.

The FPC coring tool was left on the bottom once when an internal rod parted during pull out. The core barrel was fished out using an improvised tool constructed of stacked core catchers on the sand line. On another occasion the FPC barrel stuck in the bottom-hole assembly because of sand that back-flowed into the hole. This required a pipe trip and cutting of the sand line with each 30 ft (10 m) at each pipe connection. The sand-packed

BHA was flushed out, and with further deployments of the FPC barrel an XCD pill was spotted on the bottom and flushed with a second sweep prior to landing the core barrel.

The sea bed frame was dropped when the drill pipe was being retrieved at the AT 13 location. The latch was not fully engaged and the frame fell 60 ft to the sea floor, landing sideways, half-buried in mud. An improvised sheet metal plate clamp and a ring run down the outside diameter of the drill pipe recovered the frame.

The electrical system for the top drive periodically malfunctioned. Cal Dive brought out maintenance personnel from the manufacturer (National) to replace defective wiring and a circuit board.

Demobilization

The *Uncle John* demobilized from Keathley Canyon to Pier 10 in Galveston. Fugro organized the logistics for trucks and offloading. All personnel and equipment were offloaded and the rig was released after 12 hours of demobilization.

Final Results

Thirty-five days were spent at sea gathering data, cores and logs. A total of seven holes were drilled, and $7.2 million was spent on the offshore phase of the project.

Gulf of Mexico Gas Hydrate JIP Drilling Program
Downhole Logging Program

Timothy S. Collett, U.S. Geological Survey

May 21, 2005

-EXPLANATORY NOTES-

Introduction

The downhole logging while drilling (LWD) and conventional wireline (CWL) logging operations in the Gulf of Mexico Gas Hydrate JIP Drilling Program (GOM-JIP) was designed in part to obtain data needed to assess the occurrence and concentration of gas hydrates in several key sites within the Gulf of Mexico. LWD and CWL operations were conducted in two different offshore lease areas, Atwater Valley 13/14 and Keathley Canyon 151, in water depths ranging from 1280 to 1330 m. Proposed drilling and logging depths range from 307 to 553 m beneath the sea floor. Not all tool strings were run in each hole; refer to individual site chapters for details of tool strings deployed at each site.

Logging While Drilling (LWD/MWD) Operations

During the GOM-JIP program, five Anadrill LWD and measurement-while-drilling (MWD) tools were deployed at three deep drill sites in the Atwater Valley 13/14 and Keathley Canyon 151. These tools were provided by Schlumberger-Anadrill services.

LWD and MWD tools measure different parameters. LWD tools measure *in-situ* formation properties with instruments that are located in the drill collars immediately above the drill bit. MWD tools are also located in the drill collars and measure downhole drilling parameters (e.g., weight on bit, torque, etc.). The difference between LWD and MWD tools is that LWD data are recorded into downhole computer memory and retrieved when the tools reach the surface, whereas MWD data are transmitted through the drilling fluid within the drill pipe by means of a modulated pressure wave, or “mud pulsing”, and monitored in real time. However, MWD tools enable both LWD and MWD data to be transmitted uphole when the tools are used in conjunction. The term LWD is often used more generically to cover both LWD and MWD type measurements.

The LWD and MWD tools (on 6-3/4 inch collars) used during the GOM-JIP drilling program included the resistivity-at-the-bit GeoVision tool (GVR6), the EcoScope tool (DVD with APWD), the TeleScope MWD tool (TeleScope), a magnetic resonance while drilling tool (MWD-ProVision), and the azimuthal density neutron (VDN) tool. Figure-1 shows the configuration of the LWD/MWD bottom hole assembly (BHA). The BHA was changed for the Keathley Canyon 151-2 well, in which the TeleScope was replaced with the MWD Power Pulse tool and the DVD was replaced with the Array Resistivity Compensated tool (ARC).

LWD measurements are made shortly after the hole is drilled and before the adverse effects of continued drilling or coring operations. Fluid invasion into the borehole wall is also reduced relative to wireline logging because of the shorter elapsed time between drilling and taking measurements.

The LWD equipment is partially battery powered and uses erasable/programmable read-only memory chips to store logging data until they are downloaded. The LWD tools take measurements at evenly spaced time intervals and are synchronized with a system on the rig that monitors time and drilling depth. After drilling, the LWD tools are retrieved and the data downloaded from each tool through an RS232 serial link to a laptop computer. Synchronization of the uphole and downhole clocks allows merging of the time-depth data (from the surface system) and the downhole time-measurement data (from the tools) into depth-measurement data files. The resulting depth-measurement data were transferred to the processing systems in the Schlumberger-Anadrill logging unit onboard the Uncle John for reduction and interpretation.

To provide the highest quality LWD data, the target instantaneous ROP of the drill string was 30 m/hr, with a pump rate of 300 GPM, and a bit rotation target between 80-100 RPM. To improve the quality of the near surface data within the upper 25-35 mbsf at spud in, we tried to advanced the near surface portion of each hole very slowly, with pump rates at about 50-100 GPM (building to 300 GPM from 25 to 35 mbsf) and a bit rotation target of about 50 RPM.

GeoVision Tool

GeoVision tool (RAB or GVR6) provides resistivity measurements of the formation and electrical images of the borehole wall, similar to the Formation MicroScanner but with complete coverage of the borehole walls and lower vertical and horizontal resolution. In addition, the RAB tool contains a scintillation counter that provides a total gamma ray measurement.

The GVR6 is connected directly above the drill bit and it uses the lower portion of the tool and the bit as a measuring electrode. This allows the tool to provide a bit resistivity measurement with a vertical resolution just a few inches longer than the length of the bit. A 1-in (4 cm) electrode is located 3 ft (91 cm) from the bottom of the tool and provides a focused lateral resistivity measurement (*R*RING) with a vertical resolution of 2 in (5 cm). The characteristics of *R*RING are independent of where the RAB tool is placed in the BHA and its depth of investigation is ~7 in (18 cm). In addition, button electrodes provide shallow-, medium-, and deep-focused resistivity measurements as well as azimuthally oriented images. These images can then reveal information about formation structure and lithologic contacts. The button electrodes are ~1 in (2.5 cm) in diameter and reside on a clamp-on sleeve. The buttons are longitudinally spaced along the RAB tool to render staggered depths of investigation of ~1, 3, and 5 in (2.5, 7.6, and 12.7 cm). The tool's orientation system uses the Earth's magnetic field as a reference to determine the tool position with respect to the borehole as the drill string rotates, thus allowing both azimuthal resistivity and gamma ray measurements. Furthermore, these measurements are acquired with an ~6° resolution as the RAB tool rotates.

RAB Programming

For quality control reasons, the minimum data density is one sample per 6-in (15.2 cm) interval; hence, a balance must be determined between the rate of penetration (ROP) and the sampling rate. This relationship depends on the recording rate, the number of data channels to record, and the memory capacity (46 MB) of the LWD tool. During the GOM-JIP drilling program, we used a data acquisition sampling rate of 5 seconds for high-resolution GVR6 images. The maximum ROP allowed to produce one sample per 6-in interval is given by the equation: ROP(m/hr) = 548/sample rate. This relationship gives 110m/hr maximum ROP for the GVR6. For the GOM-JIP the, the target ROP is 30 m/hr, roughly 30% of the maximum allowable for the GVR6 tool. These reduced rates improve the vertical resolution of the resistivity images to 5-10 cm per rotation. Under this configuration the

GVR6 tool has enough memory to record up to six days of data. This is sufficient, under normal operating conditions, to complete the scheduled LWD operations at Atwater and Keathley Canyon.

Bit Resistivity Measurements
For the bit resistivity measurements, a lower transmitter (T2) produces a current and a monitoring electrode (M0) located directly below the ring electrode measures the current returning to the collar. When connected directly to the bit, the GVR6 tool uses the lower few inches of the tool as well as the bit as a measurement electrode. The resultant resistivity measurement is termed *R*BIT and its depth of investigation is ~12 in (30.48 cm).

Ring Resistivity Measurements
The upper and lower transmitters (T1 and T2) produce currents in the collar that meet at the ring electrode. The sum of these currents is then focused radially into the formation. These current patterns can become distorted depending on the strength of the fields produced by the transmitters and the formation around the collar. Therefore, the GVR6 tool uses a cylindrical focusing technique that takes measurements in the central (M0) and lower (M2) monitor coils to reduce distortion and create an improved ring response. The ring electrode is held at the same potential as the collar to prevent interference with the current pattern. The current required for maintaining the ring at the required potential is then measured and related to the resistivity of the formation. Because the ring electrode is narrow (~4 cm), the result is a measurement (*R*RING) with 5-cm vertical resolution.

Button Resistivity Measurements
The button electrodes function the same way as the ring electrode. Each button is electrically isolated from the body of the collar but is maintained at the same potential to avoid interference with the current field. The amount of current required to maintain the button at the same potential is related to the resistivity of the mud and formation. The buttons are 4 cm in diameter and the measurements (*R*BUTTON) can be acquired azimuthally as the tool rotates within 56 sectors to produce a borehole image.

Interpreting RAB Images
Structural data were determined from GeoVision or RAB images using Schlumberger's GeoFrame software. GeoFrame presents RAB data as a planar, "unwrapped" 360° resistivity image of the borehole with depth. The image orientation is referenced to north, which is measured by the magnetometers inside the tool, and the hole is assumed to be vertical. Horizontal features appear horizontal on the images, whereas planar, dipping features are sinusoidal in aspect. Sinusoids are interactively fitted to beds and fractures to determine their dip and azimuth, and the data are exported from GeoFrame for further analysis.

Methods of interpreting structure and bedding differ considerably between core analysis and wireline Formation MicroScanner (FMS) images and RAB image analysis. Resolution is considerably lower for RAB image interpretation (5-10 cm at best, compared with millimeters within cores and 0.5 cm for FMS images), and therefore identified features are likely to be different in scale. For example, microfaults ("small faults," <1 mm width) and shear bands (1-2 mm, up to 1 cm width) can only be identified in FMS data. This should be considered when directly comparing FMS and RAB images. RAB provides 360° coverage at a lower resolution, FMS provides higher resolution data but coverage is restricted to only ~35% of the borehole wall. Fractures were identified within RAB images by their anomalous resistivity or conductivity and from contrasting dip relative to surrounding bedding trends.

Differentiating between fractures and bedding planes can be problematic, particularly if both are steeply dipping and with similar orientations.

EcoScope Tool

The EcoScope service integrates a full suite of formation evaluation, well placement, and drilling optimization measurements in a single collar to increase operational efficiency, reduce risk, and increase confidence in data interpretation and calculations of production and reserves. This tool is designed around a pulsed neutron generator (PNG). In addition to the suite of resistivity, thermal neutron porosity, and azimuthal gamma ray and density measurements, it provides the first commercial LWD measurements of elemental capture spectroscopy, neutron gamma density, photoelectric factor, and sigma. The dual-frequency propagation resistivity array makes 10 phase and 10 attenuation measurements at several depths of investigation, providing invasion profiling and formation resistivity. Drilling optimization measurements include Annular Pressure While Drilling (APWD), caliper, and shock detection. The PNG used in the EcoScope allows generation of neutrons without a chemical source. The EcoScope service integrates multiple LWD sensors in a single collar. This compact design reduces the amount of rathole that must be drilled to provide comprehensive evaluation measurements.

Array Resistivity Compensated Tool

Because of equipment failure, the TeleScope MWD tool in the KC 151-2 well was swapped for the Power Pulse MWD tool; which also required the EcoScope to be swapped out for the Array Resistivity Compensated Tool (ARC). The ARC tool provides resistivity measurements for logging while drilling holes. The tool is battery powered and can be operated in memory mode. For real-time applications, the ARC tool can be combined with Power Pulse MWD tool for realtime data transmission capabilities. Multiple depth resistivity measurements are achieved with high frequency electromagnetic propagation. Three transmitters are placed above the receiver pair and two transmitters are placed below the receivers for a total of five transmitter/ receiver spacings. Each transmitter sequentially broadcasts a 2-MHz electromagnetic wave into the formation. The phase shift and attenuation difference is measured between the receiver pair. The result is five depths of investigation of borehole compensated resistivities. Borehole compensation is important because it significantly reduces the effects of borehole rugosity and precisely cancels measurement errors caused by differences in each receiver's electronics that change with temperature. Multiple depths of investigation are useful to differentiate between borehole effects, invasion, shoulder beds and anisotropy. Resistivity inversion processing is available to correct for shoulder bed and invasion effects to resolve true formation resistivity (*Rt*), flushed zone resistivity (*Rxo*) and diameter of invasion (*di*). Inversion processing may also resolve horizontal resistivity (*Rh*) and vertical resistivity (*Rv*) in anisotropic formations. The ARC tool also carries the standard APWD tool.

Measurement-while-Drilling (MWD) Tool

During the GOM-JIP project, two different MWD tools were deployed: the TeleScope (in the AT 13-1 and AT 14-1 wells) and Power Pulse (in the KC 151-2 well) measurement tools. The MWD data are transmitted by means of a pressure wave (mud pulsing) through the fluid within the drill pipe. Both of the MWD tools operate by generating a continuous mud-wave transmission within the drilling fluid and by changing the phase of this signal (frequency modulation) to convert relevant bit words representing information from various sensors. Two pressure sensors were attached to the standpipe

(one near the top and the second near the bottom) on the rig floor and was used to measure the pressure wave acting on the drilling fluid when information is transmitted up the drill pipe by the MWD tool (Table 1). With the MWD mud pulsing systems, pulse rates range from 1 to 6 bits/s, depending primarily on water depth and mud density. In contrast to the real-time data, the downhole memory in the LWD tools records data at a minimum rate of one sample per 15 cm.

LWD/MWD indications of gas

As discussed above, the LWD/MWD tools deployed on the GOM-JIP project allowed for the communication of real-time data to the surface to monitor both drilling performance and physical properties of the sediments penetrated by the drill bit. The data sent (pulsed) to the surface (Table 1), include formation resistivity, natural gamma ray, density-neutron-NMR porosity, APWD measured borehole pressures, and other drilling performance information. One of the primary goals of the LWD/MWD monitoring program during drilling will be to predict and detect the presence of sedimentary sections in the borehole that have the potential to release or flow gas into the borehole. Results of previous gas hydrate drilling programs, such as ODP Legs 146, 164, and 204, have shown that gas-hydrate-bearing sections do not represent a significant threat to drilling operations and that as long as the hole is advanced at relatively normal drilling rates with mud temperatures near that of the deeper water column we do not see significant gas flows from gas-hydrate-bearing formations. However, the real concern of the LWD/MWD monitoring program will be the recognition of free-gas intervals below the base of the gas hydrate stability zone (i.e., BSR) with the potential to flow. With the pulsed LWD/MWD data, it is possible to identify a set of downhole measurements to detect the occurrence of free-gas-bearing sedimentary sections below the base of the gas hydrate stability zone. The LWD/MWD responses considered in this well monitoring program are listed below:

(1) One of the most important criteria for identifying a potential free gas zone in a borehole with LWD/MWD data is the recognition of porous sand units that could host enough gas to actually enter the borehole. One of the best first indicators of “reservoir” quality sands would be the response of the natural gamma ray log on the GVR6 (resistivity-at-bit) LWD tool. The expected gamma ray response to a sand section, relative to a shale-base-line, will vary from one area to another; but a relative gamma ray increase over base-line of about 50 API units would be indicative of a possible “reservoir” quality sand section.

(2) Beyond the identification of potential “reservoir” quality sand sections it is also possible to use the pulsed LWD/MWD data to directly detect the presence of gas in the penetrated section. Within this project, MMS and the project partners have defined a set of LWD/MWD measurements indicative of gas-bearing sediments. A log identified sedimentary section more then 5-m-thick with resistivities more than five times over background has been defined as a gas-bearing sedimentary section with the potential to flow.

(3) In standard downhole log analysis, neutron-density porosity log data is often used to indicate the presence of gas-bearing zones. Neutron porosity logs image gas-bearing sediments by apparent reductions in measured porosities. A relative shift in recorded neutron porosities of about 10%, generally indicate the presence of a gas-bearing zone with the potential to flow.

(4) But it needs to be highlighted that the first most important indicator of fluid flow into the formation would likely be detected as a borehole pressure change recorded by the APWD tool.

During the GOM-JIP project, the above described downhole measured criteria were monitored to identify potential gas-bearing zones that may represent drilling hazards. No "significant" gas-bearing zones were encountered in this project. However, we did experience shallow water flows with limited gas in both the KC 151-2 and 151-3 wells. MMS required that if a free gas zone or shallow flow was encountered, the well will be filled with 12.0 ppg mud, drilling will be ceased for this particular well and an abandonment procedure will be initiated. In the case of the KC 151-3 well a cement plug was set near the surface.

Nuclear Magnetic Resonance While-Drilling (ProVision) Tool

The basic technology behind the ProVision nuclear magnetic resonance tool is similar to modern wireline nuclear magnetic resonance technology, based on measurement of the relaxation time of the magnetically induced precession of polarized protons. A combination of bar magnets and directional antennas are used to focus a pulsed, polarizing field into the formation. The ProVision tool measures the relaxation time of polarized molecules in the formation, which is suited to provide information related to the formation porosity. By exploiting the nature of the chemical bonds within pore-fluids, for hydrogen in particular, the ProVision tool can provide estimates of the total porosity and bound fluid volume, and thus be useful to determine whether water, gas, or gas hydrates are present in the formation.

During the GOM-JIP project, the ProVision tool acquired formation and engineering information in memory and transmitted some data to the surface via MWD. The relaxation time spectra was recorded downhole and total porosity estimates were be transmitted to the surface in real time. These spectra were stacked in post-processing to improve the measurement precision. The signal investigates a 15-cm cylindrical volume of the borehole, and for a 8-1/2" bit size, the depth of investigation of the measurement is ~5 cm into the formation. Lateral tool motion may reduce ProVision data quality in some circumstances. Therefore, accelerometers and magnetometers contained in the downhole tool are used to evaluate data quality and determine the maximum relaxation times that can be resolved.

Vision Density Neutron (VDN) Tool

The VDN tool is similar in principle to the Azimuthal density neutron (ADN) tool. The density section of the tool uses a 1.7-Ci 137Cs gamma ray source in conjunction with two gain-stabilized scintillation detectors to provide a borehole-compensated density measurement. The detectors are located 5 and 12 in (12.7 and 30.48 cm) below the source. The number of Compton scattering collisions (change in gamma ray energy by interaction with the formation electrons) is related to the formation density. Returns of low energy gamma rays are converted to a photoelectric effect value, measured in barns per electron. The photoelectric effect value depends on electron density and hence responds to bulk density and lithology. It is particularly sensitive to low-density, high-porosity zones.

The density source and detectors are positioned behind holes in the fin of a full gauge clamp-on stabilizer. This geometry forces the sensors against the borehole wall, thereby reducing the effects of borehole irregularities and drilling. The vertical resolution of the density and photoelectric effect measurements is about 15 and 5 cm, respectively. For measurement of tool standoff and estimated borehole size, a 670-kHz ultrasonic caliper is available on the VDN tool. The ultrasonic sensor is aligned with and located just below the density detectors. In this position the sensor can also be used as a quality control for the density measurements. Neutron porosity measurements are obtained using fast neutrons emitted from a 10-Ci americium oxide-beryllium (AmBe) source. Hydrogen quantities

in the formation largely control the rate at which the neutrons slow down to epithermal and thermal energies. The energy of the detected neutrons has an epithermal component because much of the incoming thermal neutron flux is absorbed as it passes through the 1-in drill collar. Neutrons are detected in near- and far-spacing detector banks, located 12 and 24 in (30.48 and 60.96 cm), respectively, above the source. The vertical resolution of the tool under optimum conditions is ~34 cm. The neutron logs are affected to some extent by the lithology of the matrix rock because the neutron porosity unit is calibrated for a 100% limestone environment. Neutron logs are processed to eliminate the effects of borehole diameter, tool size, temperature, drilling mud hydrogen index (dependent on mud weight, pressure, and temperature), mud and formation salinities, lithology, and other environmental factors.

In near-vertical drill holes, the VDN tool does not collect quadrant azimuthal data. Data output from the VDN tool includes apparent neutron porosity (i.e., the tool does not distinguish between pore water and lattice-bound water), formation bulk density, and photoelectric effect. In addition, the VDN tool outputs a differential caliper record based on the standard deviation of density measurements made at high sampling rates around the circumference of the borehole. The measured standard deviation is compared with that of an in gauge borehole, and the difference is converted to the amount of borehole enlargement. A standoff of <1 inch between the tool and the borehole wall indicates good borehole conditions, for which the density log values are considered to be accurate to ±0.015 g/cm^3.

Conventional Wireline Logging Operations

Conventional wireline (CWL) logging operations in the Gulf of Mexico Gas Hydrate JIP Drilling Program (GOM-JIP) was scheduled to include the deployment of a signal logging string (Figure 2) and a vertical seismic profiling (VSP) tool (Figure 3) in several of the Atwater Valley and Keathley Canyon drill sites. The only wireline logging tool deployed was the FMS-sonic tool string, which consisted of the Formation MicroScanner (FMS), a general purpose inclinometer tool (GPIT), and the dipole shear sonic imager tool (DSI). The FMS-sonic tool also included a natural gamma ray tool to provide a reference log to correlate depths between different log runs. The vertical seismic imager tool (VSI) was also deployed during the GOM-JIP drilling program. Neither the FMS-sonic tool string nor the VSI tool were run in each hole; refer to individual site chapters for details of which holes were logged. The wireline logging tools were provided by Schlumberger Technology Corporation.

Early in the planning phase for the GOM-JIP drilling project, considerable effort was made to assess the use of existing LWD acoustic logging technology for logging near-surface, relatively acoustically “slow”, formations. It was decided that emerging quadrapole acoustic LWD logging technology may theoretically yield both compressional- and shear-wave data form these slow formations, it could not be conclusively proven that we would acquire the needed acoustic data. Thus, it was decided to move ahead with plans for a conventional wireline logging program with the DSI, which has been used in the past to obtain both compressional- and shear-wave acoustic log data in very slow formations during ODP and IODP operations.

Dipole Shear Sonic Imager Tool

The DSI tool employs a combination of monopole and dipole transducers to make accurate measurements of sonic wave propagation in a wide variety of formations. In addition to a robust and high-quality measurement of compressional wave velocity, the DSI excites a flexural mode in the

borehole that can be used to estimate shear-wave velocity even in highly unconsolidated formations. When the formation shear velocity is less than the borehole fluid velocity, particularly in un-consolidated sediments, the flexural wave travels at the shear-wave velocity and is the most reliable way to estimate a shear velocity log. Meanwhile, the omni-directional source generates compressional, shear, and Stoneley waves into hard formations. The configuration of the DSI also allows recording of both in-line and cross-line dipole waveforms. In many cases the dipole sources can yield estimates of shear wave velocity in hard rocks better than or equivalent to the monopole source. These combined modes can be used to estimate shear-wave splitting caused by preferred mineral and/or structural orientation in consolidated formations. A low-frequency (80 Hz) source enables Stoneley waveforms to be acquired as well.

DSI measures the transit times between sonic transmitters and an array of eight receiver groups with 15-cm spacing, each consisting of four orthogonal elements that are aligned with the dipole transmitters. During acquisition, the output from these 32 individual elements are differenced or summed appropriately to produce in-line and cross-line dipole signals or monopole-equivalent (compressional and Stoneley) waveforms, depending on the operation modes. In the GOM-JIP drilling program we followed standard GOM practices and the DSI logs were recorded for Stoneley, monopole compressional- and shear-waves, and both crossed receivers (BCR) modes; with the main pass ran at “low” frequency and a second pass conducted at “standard” frequency.

Formation MicroScanner Tool
The FMS produces high-resolution images of borehole wall micro-resistivity that can be used for detailed sedimentologic or structural interpretation. This tool has four orthogonally oriented pads, each with 16 button electrodes that are pressed against the borehole walls. Good contact with the borehole wall is necessary for acquiring good-quality data. Approximately 30% of a borehole with a diameter of 25 cm is imaged during a single pass. The vertical resolution of FMS images is ~5 mm, allowing features such as burrows, thin beds, fractures, veins, and vesicles to be imaged. The resistivity measurements are converted to color or grayscale images for display. FMS images are oriented to magnetic north using the GPIT (General Purpose Inclinometer Tool). This allows the dip and strike of geological features intersecting the hole to be measured from processed FMS images. FMS images can be used to visually compare logs with the core to ascertain the orientations of bedding, fracture patterns, and sedimentary structures and to identify stacking patterns, and in some cases to identify gas-hydrate-bearing sedimentary sections.

Because of problems experienced trying to log out of the drill pipe in AT 13-2, the FMS was removed for the only other CWL run in KC 151-3.

General Purpose Inclinometer Tool
The GPIT is included in the FMS-sonic tool string to calculate tool acceleration and orientation during logging. The GPIT contains a triple-axis accelerometer and a triple-axis magnetometer. The GPIT records the orientation of the FMS images and allows more precise determination of log depths than can be determined from cable length, which may experience stretching and/or be affected by ship heave.

Vertical Seismic Imager (VSI)
The Vertical Seismic Imager (VSI-4) is a borehole seismic wireline tool optimized for obtaining vertical and walkaway seismic profiles (VSP; W-VSP) in both cased hole and open hole, vertical, and deviated wells. The VSI consists of mulitple three-axis geophones in series separated by "hard wired",

acoustically-isolating spacers. A schematic illustration of the tool is given in Figure 3. The tool diameter is 3 3/8 inches, with temperature and pressure ratings to 175 °C and 20,000 psi, respectively.

During the GOM-JIP drilling program, the VSI was configured using four geophone shuttles (approximately 7 ft (2.06 m) spacing with rigid interconnections) and combined with a natural gamma ray tool. Only one vertical incident or zero-offset VSP experiment was conducted during the GOM-JIP drilling program; in the KC 151-3 well. During the vertical incidence VSP operations in the KC 151-33 well, the shuttles were mechanically clamped against the borehole wall and the source (1520 cubic inch guns in a Dual Itaga Air Gun Array) on the *Uncle John* was fired between 6 and 10 times by control hardware in the Schlumberger logging unit. The VSI tool was then unclamped and pulled 28 ft (8.5 m) uphole, maintaining a 7 ft (2.06 m) receiver station depth spacing throughout the hole. The VSI records the full seismic waveform for each firing. These waveform data are stacked by the Schlumberger recording software and output in both LDF (internal Schlumberger format) and SEG-Y formats.

Logging Data Flow and Processing

Data for each LWD and CWL logging run were recorded and stored digitally and monitored in real time as the data was acquired. After logging was completed, the data were transferred first to Schlumberger Anadrill and wireline services for compilation and data quality check. The Provision NMR data was processed by Anadrill and returned to the ship during the cruise. The final and complete field data sets were than transferred to the LDEO-BRG for processing. Data processing at LDEO-BRG consists of (1) depth-shifting all logs relative to a common datum (i.e., mbsf), (2) corrections specific to individual tools, and (3) quality control and rejection of unrealistic or spurious values. Once processed at LDEO-BRG, log data will be made available to the JIP members and project scientist through either the JIP website or direct transfers via DVDs.

Logging data quality may be seriously degraded by changes in the hole diameter and in sections where the borehole diameter greatly decreases or is washed out. Deep-investigation measurements such as resistivity and sonic velocity are least sensitive to borehole conditions. Nuclear measurements (density and neutron porosity) are more sensitive because of their shallower depth of investigation and the effect of drilling fluid volume on neutron and gamma ray attenuation. Corrections can be applied to the original data in order to reduce these effects. The effects of very large washouts, however, cannot be corrected. Logs from the LWD and CWL tool strings will have minor depth mismatches caused by that fact that the data was obtained in two different holes at each site surveyed. A gamma ray log has been included in each tool run to correlate the log data between each at hole within a drill site. Because of technical difficulties, the CWL surveys were conducted without heave compensation. In the case of the Atwater Valley LWD holes, the drill-string heave compensator was not used during LWD operations.

Gas Hydrate Detection and Evaluation

With growing interest in natural gas hydrate, it is becoming increasingly important to be able to identify the occurrence of *in-situ* gas hydrate and accurately assess the volume of gas hydrate and included free gas within gas-hydrate accumulations. Numerous publications (Mathews, 1986; Collett, 1993, 1998a, 1998b, 2001; Goldberg, 1997; Guerin et al., 1999; Goldberg et al., 2000; Helgerud et al.,

2000) have shown that downhole geophysical logs can yield information about the occurrence of gas hydrate.

Since gas hydrates are characterized by unique chemical compositions and distinct electrical resistivities, physical and acoustic properties, it is possible to obtain gas-hydrate saturation (percent of pore space occupied by gas hydrate) and sediment porosity data by characterizing the electrical resistivity, acoustic properties, and chemical composition of the pore-filling constituents within gas-hydrate-bearing reservoirs. Two of the most difficult reservoir parameters to determine are porosity and the degree of gas-hydrate saturation. Downhole logs often serve as a source of porosity and hydrocarbon saturation data. Most of the existing gas hydrate log evaluation techniques are qualitative in nature and have been developed by the extrapolation of untested petroleum industry log evaluation procedures. To adequately test the utility of standard petroleum log evaluation techniques in gas-hydrate-bearing reservoirs would require numerous laboratory and field measurements. However, only a limited number of gas hydrate occurrences have been sampled and surveyed with open-hole logging devices.

Reviewed below are downhole log measurements that yield useful gas hydrate reservoir information. The downhole measurements considered include gamma-gamma density, neutron porosity, electrical resistivity, acoustic transit-time, and nuclear magnetic resonance.

Gamma-Gamma Density Logs
Density logs are primarily used to assess sediment porosities. The theoretical bulk-density of a Structure-I methane hydrate is about 0.9 g/cm^3 (Sloan, 1998). Gas hydrate can cause a small but measurable effect on density-derived porosities. At relatively high porosity (>40%) and high gas-hydrate saturation (>50%), the density-log-derived porosities need to be corrected for the presence of gas hydrate (Collett, 1998b).

Neutron Porosity Logs
Neutron logs are also used to determine sediment porosities. Since Structure-I methane hydrate and pure water have similar hydrogen concentrations it can be generally assumed that neutron porosity logs, which are calibrated to pure water, are not significantly affected by the presence of gas hydrates. At high reservoir porosities, however, the neutron porosity log could overestimate porosities (Collett, 1998b).

Electrical Resistivity
Water content and pore-water salinity are the most significant factors controlling the electrical resistivity of a formation. Other factors influencing resistivity of a formation include the concentration of hydrous and metallic minerals, volume of hydrocarbons including gas hydrates, and pore structure geometry. Gas-hydrate-bearing sediments exhibit relatively high electrical-resistivities in comparison to water-saturated units, which suggests that a downhole resistivity log can be used to identify and assess the concentration of gas hydrates in a sedimentary section. The relation between rock and pore-fluid resistivity has been studied in numerous laboratory and field experiments. From these studies, relations among porosity, pore-fluid resistivity, and rock resistivity have been found. Among these findings is the empirical relation established by Archie (Archie, 1942), which is used to estimate water saturations in gas-oil-water-matrix systems. Research has shown that the Archie relation also appears to yield useful gas-hydrate saturation data (reviewed by Collett, 2001).

Acoustic transit-time
The velocity of compressional and shear acoustic waves in a solid medium, such as gas-hydrate-bearing sediment, is usually several times greater than the velocity of compressional and shear acoustic waves in water or gas-bearing sediments. Studies of downhole acoustic log data from both marine and permafrost associated has hydrate accumulations have shown that the volume of gas hydrate in sediment can also be estimated by measuring interval velocities (Guerin et al., 1999; Helgerud et al., 2000; Collett, 2001; Guerin and Goldberg, 2002).

Nuclear Magnetic Resonance Logs
Nuclear magnetic resonance (NMR) logs use the electromagnetic properties of hydrogen molecules to analyze the nature of the chemical bonds within pore-fluids. Relative to other pore-filling constituents, gas hydrates exhibit unique chemical structures and hydrogen concentrations. In theory, therefore, it should be possible to develop NMR well-log evaluation techniques that would yield accurate reservoir porosities and water saturations in gas-hydrate-bearing sediments. Because of tool design limitations, gas hydrates cannot be directly detected with today's downhole NMR technology; however, they can be useful to yield very accurate gas-hydrate saturation estimates. Due to the short transverse magnetization relaxation times (*T2*) of the water molecules in the clathrate, gas hydrates are not "seen" by the NMR tool and may be assumed to be part of the solid matrix. Thus, the NMR-calculated total porosity in a gas-hydrate-bearing sediment should be lower than the actual porosity. With an independent source of accurate total porosity, such as density- or neutron-porosity-log measurements, it should be possible to accurately estimate gas-hydrate saturations by comparing the apparent NMR-derived porosity to the total density-derived porosity.

References

Archie, G.E., The electrical resistivity log as an aid in determining some reservoir characteristics. Journal of Petroleum Technology, v. 5, p. 1-8, 1942.

Collett, T.S., Natural gas hydrates of the Prudhoe Bay and Kuparuk River area, North Slope, Alaska: American Association of Petroleum Geologists Bulletin, v. 77, no. 5, p. 793-812, 1993.

Collett, T.S., Well log evaluation of gas hydrate saturations. Transactions of the Society of Professional Well Log Analysts, Thirty-Ninth Annual Logging Symposium, May 26-29, 1998, Keystone, Colorado, USA, Paper MM, 1998a.

Collett, T.S., Well log characterization of sediment porosities in gas-hydrate-bearing reservoirs. Proceedings of the 1998 Annual Technical Conference and Exhibition of the Society of Petroleum Engineers, September 27-30, 1998, New Orleans, Louisiana, USA, 12 p. (CD-ROM), 1998b.

Collett, T.S., A review of well-log analysis techniques used to assess gas-hydrate-bearing reservoirs: In Natural Gas Hydrates: Occurrence, Distribution, and Detection, American Geophysical Union, Geophysical Monograph 124, p. 189-210, 2001.

Goldberg, D., The role of downhole measurements in marine geology and geophysics. Review of Geophysics, v. 35, no. 3, p. 315-342, 1997.

Goldberg, D., Collett. T.S., and Hyndman, R.D., Ground truth: in-situ properties of hydrate. *in* Max, M.D., ed., Natural Gas Hydrate in Oceanic and Permafrost Environments, Kluwer Academic Publishers, The Netherlands, p. 295-310, 2000.

Guerin, G., Goldberg, D., and Melster, A., Characterization of in situ elastic properties of gas hydrate-bearing sediments on the Blake Ridge. Journal of Geophysical Research, v. 104, 17,781-17,795, 1999.

Guerin, G., and D. Goldberg, Sonic attenuation measurements in the Mallik 2L-38 gas hydrates research well, MacKenzie Delta, NWT Canada, Journal of Geophysical Research, v. 107, 2002.

Helgerud, M.B., Dvorkin, J., and Nur, A., Rock physics characterization for gas hydrate reservoirs, elastic properties. In Holder, G.D., and Bishnoi, P.R., eds., Gas Hydrates, Challenges for the Future, Annals of the New York Academy of Sciences, v. 912, p. 116-125, 2000.

Mathews, M., Logging characteristics of methane hydrate. The Log Analyst, v. 27, no. 3, p. 26-63, 1986.

Sloan, E.D., 1998. Clathrate hydrates of natural gases. Marcel Dekker Inc. Pub., New York, pp. 641.

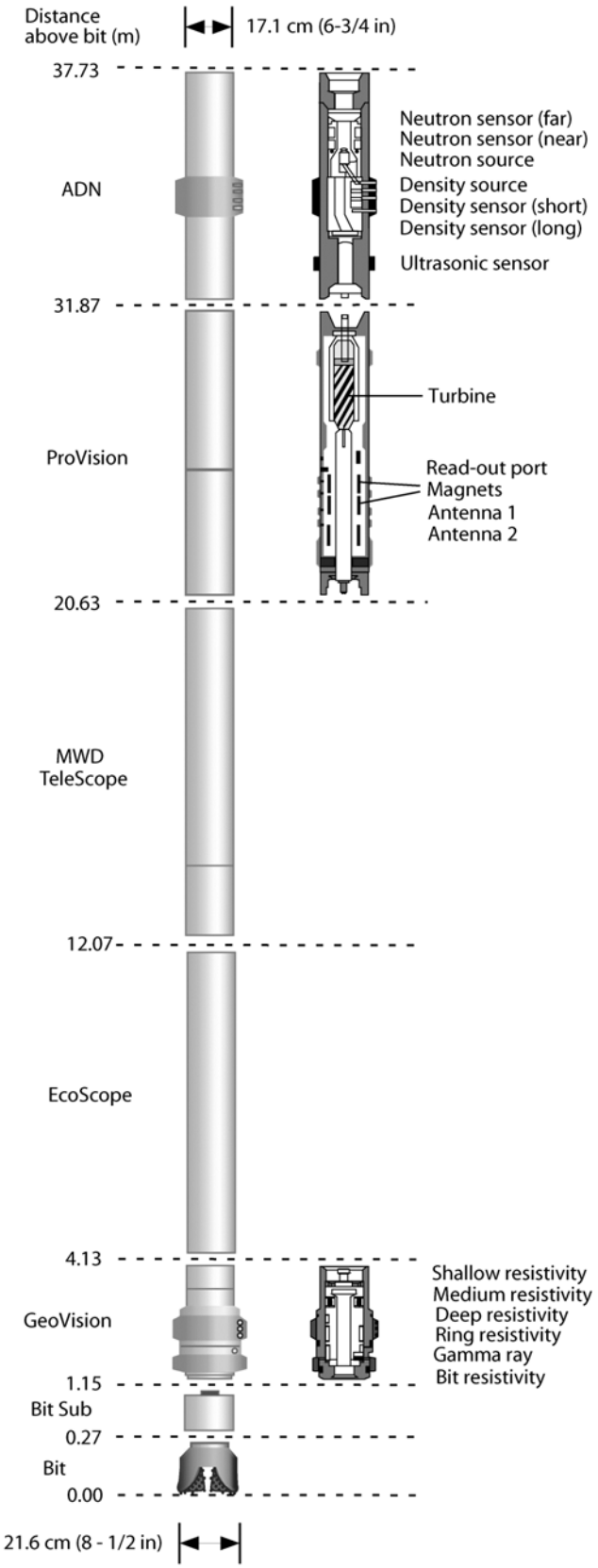

Figure 1. Configuration of the drill string used for LWD-MWD operations.

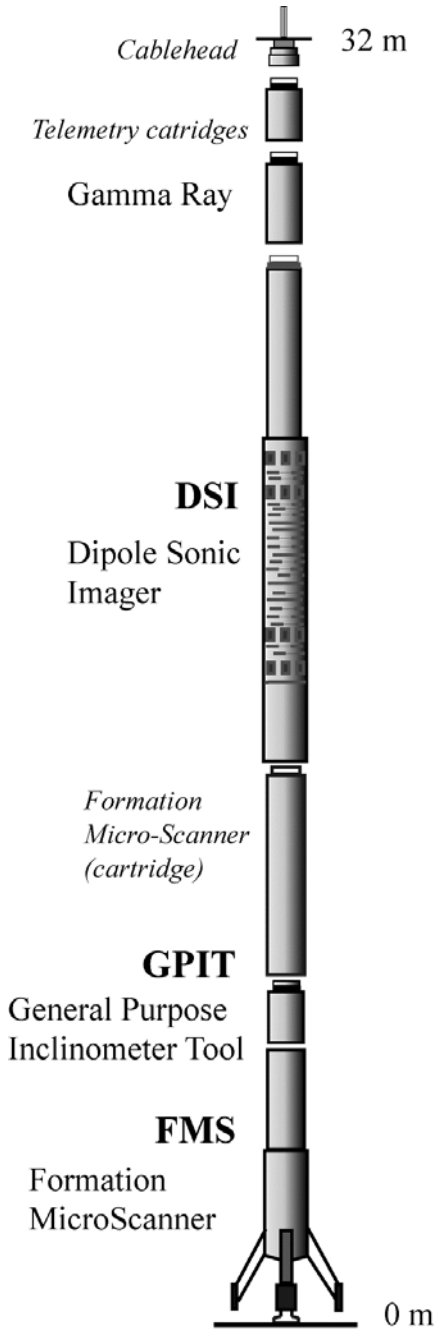

Figure 2. Configuration of the FMS-sonic CWL tool string.

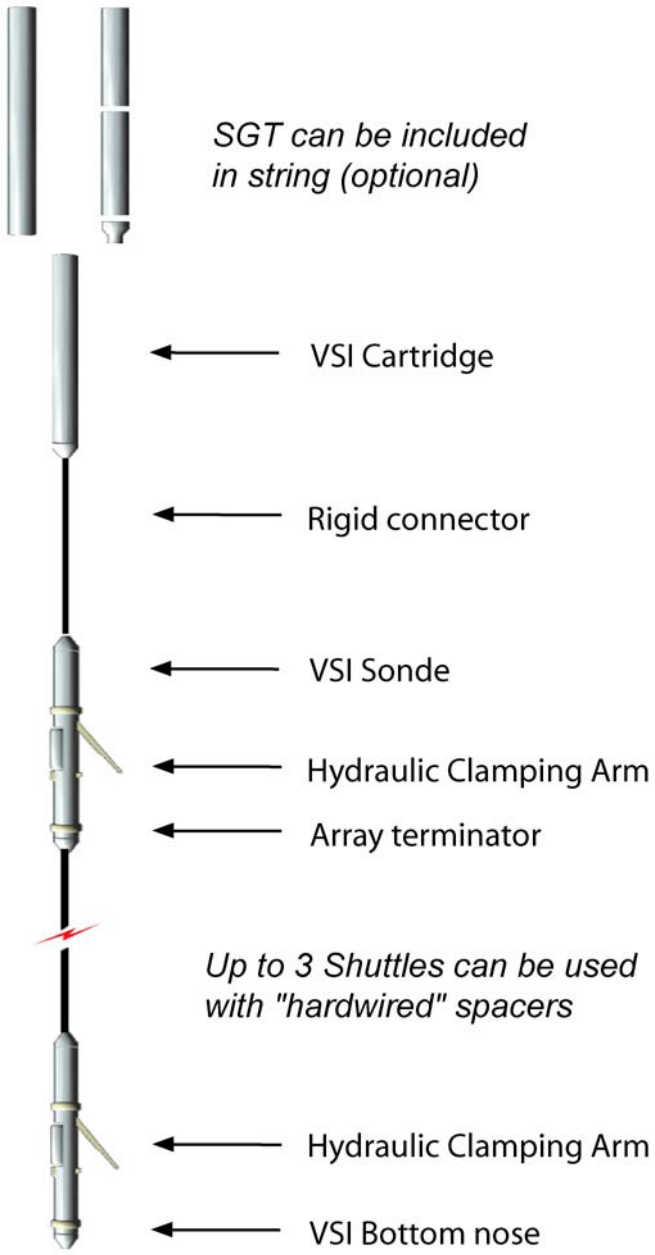

Figure 3. Configuration of the VSI wireline tool string.

Table 1. Frame Builder Power Frame listing of Data-Points (Dpoint) for pulsed real time data for both Atwater Valley LWD/MWD holes drilled during the GOM-JIP gas hydrate research drilling and coring leg (ROP 100 ft/hr; Bit rate 12.00 bps).

Mtfs
GRRA_r
APRS_v
RBIT_r
RING_r
RDBA_r
MON_v
IDRO_a
IDDR_a
TNRA_a
C_SPEC_v
RA40B_v
DCAV_a
Tur_rpm
BFV1C_m
MRP1C_m
MRTCRPM_m8
ATMP_v
GRRA_r
IDPE_a
RBIT_r
RING_r
RDBA_r
Shock_i
IDRO_a
IDDR_a
TNRA_a
SRFA_v
DCAV_a
Shkrsk
DCAV_v
IDRO_v
Itbrt
A_jam

Atwater Valley 13-1
OCS-G-24203

-LOGGING WHILE DRILLING-

Operations

LWD operations (Table 1) began at the Atwater Valley 13-1 (AT 13-1) drill site on April 19, 2005 at 00:28 CT with initial BHA make-up, tool initialization, and calibration. The LWD tools (6-3/4" collars) included the resistivity-at-the-bit GeoVision tool (GVR6) with a 8-1/8" button sleeve, the EcoScope tool (DVD with APWD), a MWD tool (Telescope), a magnetic resonance while drilling tool (MWD-ProVision), and the azimuthal density neutron (VDN) tool. Figure-1 in the *Explanatory Notes* shows the configuration of the LWD/MWD bottom hole assembly (BHA). Memory and battery life allowed for at least six days of continuous drilling. Atwater Valley 13-1 was spudded at 23:00 CT (April 19, 2005) at a drillers water depth of 1,303.7 mbrf to the northwest of the seismic inferred surface Mound F in Atwater Valley Block 14. The ROV from the *Uncle John* was used to position the BHA and monitor the drilling operations at the sea floor throughout the drilling of the AT 13-1 well. The drill-string heave compensator was not used during LWD operations at AT 13-1. For the most part the AT 13-1 well was drilled with only sea water as the drilling fluid, but as the hole was advanced periodic sweeps of Attapulgite based drilling mud was used to sweep and stabilize the hole.

In an attempt to acquire high quality resistivity-at-bit log and image data within the near-surface sedimentary section, we implemented a controlled spud in drilling protocol which consisted of drilling at a low mud flow rate of about 100 gpm (33 strokes per minute), a limited penetration rate of less than 30 m/hr (which was actually maintained at about 35 m/hr), and a spud in bit rotation rate of 50 RPM. It is important to note that the turbine powered tools on the BHA, including the DVD, MWD, ProVision, and the VDN do not operate at a flow rate of less than about 230 gallons per minute. At a depth about 25 mbsf the mud pump rates were increased to 240 GPM to turn-on the turbine powered tools in the BHA. However, in this case a flow rate of 300 GPM was required to activate the turbine powered tools, based on assumed pump efficiency of three gallons per pump stroke; which could not verified.

Below 25 mbsf, the hole was advanced at an instantaneous rate of approximately 20-30 m/hr to a TD at 246.3 mbsf without significant difficulty and real-time data were transmitted to the surface throughout the drilling of the well. The AT 13-1 well was TD early because of hole clearing problems and because all of our science objectives were achieved. Some extraneous pump noise affected the data transmission, but caused minimal real-time data loss. The BHA was pulled back to sea floor while running a sweep of heavy drilling mud. The tools were pulled out of the hole at 08:30 CT on April 21, 2005 and the recorded LWD data were retrieved at the rig floor at 14:30 CT on April 24, 2005 after drilling the AT 14-1 well.

Log Quality

After the completion of LWD operations in the AT 13-1 well, a highly reduced version of the "primary" set of downhole recorded well log data was transferred to the onboard science party for initial analysis. For this report, we have loaded this primary data set into Microsoft Excel and generated a series of well log displays; which has been included with this report (Figures 1-13).

The target rate-of-penetration (ROP) of 30 m/hr (± 5 m/hr) in the interval from the seafloor to total depth (TD) was generally achieved (Figure 1). Using slow drilling rates enhanced the quality of the NMR porosity data and RAB images. The quality of RAB images is quite high and no significant resolution loss is observed with variation in ROP in the AT 13-1 well.

The caliper log (DCAV), which provides a measurement of the diameter of the borehole as recorded by the VDN density tool is the best indicator of borehole conditions (Figure 4). The calculated differential caliper values (assuming a bit size of 8-1/2 inches) are <1 inch over 78% of the total section in AT 13-1. With the uppermost 25 mbsf of the hole showing the most sever washouts. The bulk density correction (IDDR), calculated from the difference between the short- and long-spaced density measurements, varies from -0.04 to +0.02 g/cm^3, which shows the high quality of the density measurements (Figure 6). The interval below 158 mbsf shows minor washouts due to borehole breakouts, with caliper measurements up to 13 inches. Reducing BIT and RING electrical resistivity values below 217 mbsf also indicate that the borehole is enlarged (Figures 10 and 11); which was do to a borehole cleaing problem and an increase in mud pump rates to 380 GPM.

The depths, relative to seafloor, for all of the LWD logs were fixed by using the *Uncle John* ROV to identify the actual BHA bit contact with the sea floor and shifting the log data to the appropriate depth as determined by the drillers' pipe tallies. For AT 13-1 it was determined that the seafloor was at a depth of 1303.7 mbrf. The rig floor logging datum was located 13.2 m above sea level for this hole.

Interpretation of LWD Logs

LWD logs along with core analyses reveals that both AT 13-1 and AT 13-2 penetrated mostly a fine-grained clay dominated sedimentary section with no apparent suitable sand reservoir sections. The higher electrical resistivities within the upper 40 m of the well are in part a product of bad borehole conditions, as is the section below 217 mbsf. The high resistivities within the interval 110-140 mbsf appears to be associated with increased formation densities and reductions in core derived pore-water salinities.

On ODP Leg 204, RAB images were proven to be a very useful tool with which to evaluate the occurrence of borehole breakouts, which are the product of differential horizontal stress acting on the borehole; similar breakout features were identified in the RAB image log from the AT 13-1 well.

Log Porosities

Sediment porosities can be determined from analyses of recovered cores and from numerous borehole measurements. Data from the LWD density, neutron, and nuclear magnetic resonance logs have been used to calculate sediment porosities in the AT 13-1 well. The VDN log-derived measurements of bulk-density (Figure 7) in AT 13-1 for the most part ranges from about 1.6 g/cm^3 to 1.8 g/cm^3, with values less than about 1.4 g/cm^3 near the seafloor. The density log measurements are degraded in the upper 25 mbsf, as discussed earlier in this report. The LWD log-derived bulk density measurements from AT 13-1 were used to calculate sediment porosities ($\varnothing$) using the standard density-porosity relation: $\varnothing=(\rho m-\rho b)/(\rho m-\rho w)$. Water densities ($\rho w$) were assumed to be constant and equal to 1.05 g/cm^3; while the grain/matrix densities (ρm) were assumed to be 2.65 g/cm^3 for each log density porosity calculation. The density-log derived porosities range from about 50 to 70 percent (Figure 8). However, the density log porosities near the top of the hole (above 35 mbsf), ranging from 60 to near 95 percent, is in part controlled by degraded borehole conditions. The LWD neutron porosity log (Figure 9) yielded sediment porosities ranging from an average value at the top of the logged section of about 65% to near 50% at the bottom of the hole. NMR data were transmitted to shore for

processing to estimate bound fluid volume and total free fluid porosity and for comparison with neutron, density, and core porosity estimates. The sediment porosities derived by the LWD NMR tool are very similar to the both the density and neutron log derived porosities.

Gas Hydrate

The presence of gas hydrates was not verified at the Atwater Valley 13 drill site by either sampling in the 13-2 well or in the LWD well log data from the 13-1 well. The LWD GVR6 resistivity tool, however, reveals several thin high-resistivity zones with depth in the 13-1 well, suggesting the possible occurrence of gas hydrate.

Resistivity log data have been used to quantify the amount of gas hydrate at AT 13-1. For the purpose of this discussion, it is assumed that any high resistivities measured in the 13-1 well are due to the presence of gas hydrate. The Archie relation ($S_w=(aR_w/\varnothing^m R_t)^{1/n}$) was used with resistivity data (R_t) from the LWD RAB tool and porosity data ($\varnothing$) from the VDN density tool to calculate water saturations. It should be noted that gas hydrate saturation (S_h) is the measurement of the percentage of pore space in a sediment occupied by gas hydrate, which is the mathematical complement of Archie derived water saturations (S_w), with S_h=1-S_w. For the Archie relation, the formation water resistivity (R_w) was calculated from recovered core water samples and assumed to range from 30 to 38 ppt. Because of the wide range of reported core derived pore water salinities from AT 13-2, a constant pore water salinity of 34.5 ppt (sea water salinity) was assumed to represent the in-situ R_w conditions. The Archie *a* and *m* variables were calculated using a cross plot technique (a= 0.44, m= 3.4), which compares the downhole log derived resistivities and density porosities (Figure 12). The APCT temperature data obtained from the AT 13-2 well revealed an equilibrium seabed temperature of 4.37°C and a geothermal gradient of 3.2°C/100m.

The Archie relation for the most part yielded water saturations near 100%, values less than 100% within the near-surface section (above 35 mbsf) are a product of degraded density porosity measurements. The plot of the Archie water saturations also reveal several thin stratigraphic sections with apparent reduced water saturations, which are likely do to the presence of gas hydrate. The most prominent of these zones is at a depth of about 125-128 mbsf. This interval was shown to contain pore-waters with relatively low salinities (near 30 ppt) in the cores from the AT 13-2 well, which could be a product of gas hydrate dissociation pore-water freshening in the recovered cores

A review of the well log data from AT 13-1 shows little evidence of any significant gas hydrate occurrences, other than several thin, possibly stratigrahically controlled, gas-hydrate-bearing intervals. The LWD logs from this site further suggests the presence of a complex pore water fluid regime, with variable well log inferred pore water salinities.

Borehole Temperature and Pressure Data

The APWD measured borehole pressures (DHAP) generally indicate a uniform pressure gradient with depth (Figure 3), with some pressure deviations associated with running heavy mud sweeps near the end of pipe connections. The DHAT temperature log indicates that the circulating fluids were cooled in their descent in the drill pipe to a relatively uniform temperature in the range of 3-7 degrees Celsius (Figure 2).

Table 1. Atwater 13-1 LWD/MWD Logging Program

Water depth: 1303.7m RKB
Drillers TD: 1550.0m RKB
RKB above sea level: 13.2m

Date	Time (CT)	Depth of drill bit (mbrf)*	Event
18-Apr-05	20:30	0.0	Move LWD/MWD tools to pipe rack
	22:20	0.0	Pre-spud and safety meeting
	22:30	0.0	Power check tools
19-Apr-05	0:28	0.0	Begin to pickup LWD/MWD tools
	4:45	0.0	Finish assembling the LWD/MWD BHA
	5:00	0.0	Run tools string to 120 mbrf
	9:00	120.0	Pump test LWD/MWD tool string and run to sea floor
	20:50	1303.7	LWD/MWD reached sea floor
	23:00	1303.7	Spud well, controlled drill 100 GPM, 35 m/hr ROP, 50 RPM
	23:50	1328.0	Bring pump rate up to 240 GPM, than to 300 GPM, MWD tool powered up
20-Apr-05	14:30	1456.0	Bring pump rate up to 380 GPM, for hole clearing
21-Apr-05	6:30	1550.0	Well reaches TD at 246.3 mbsf
	6:35	1550.0	Begin trip of BHA to sea floor, running heavy mud sweep
	8:30	1303.7	BHA clears sea floor

*1m = 3.28084ft

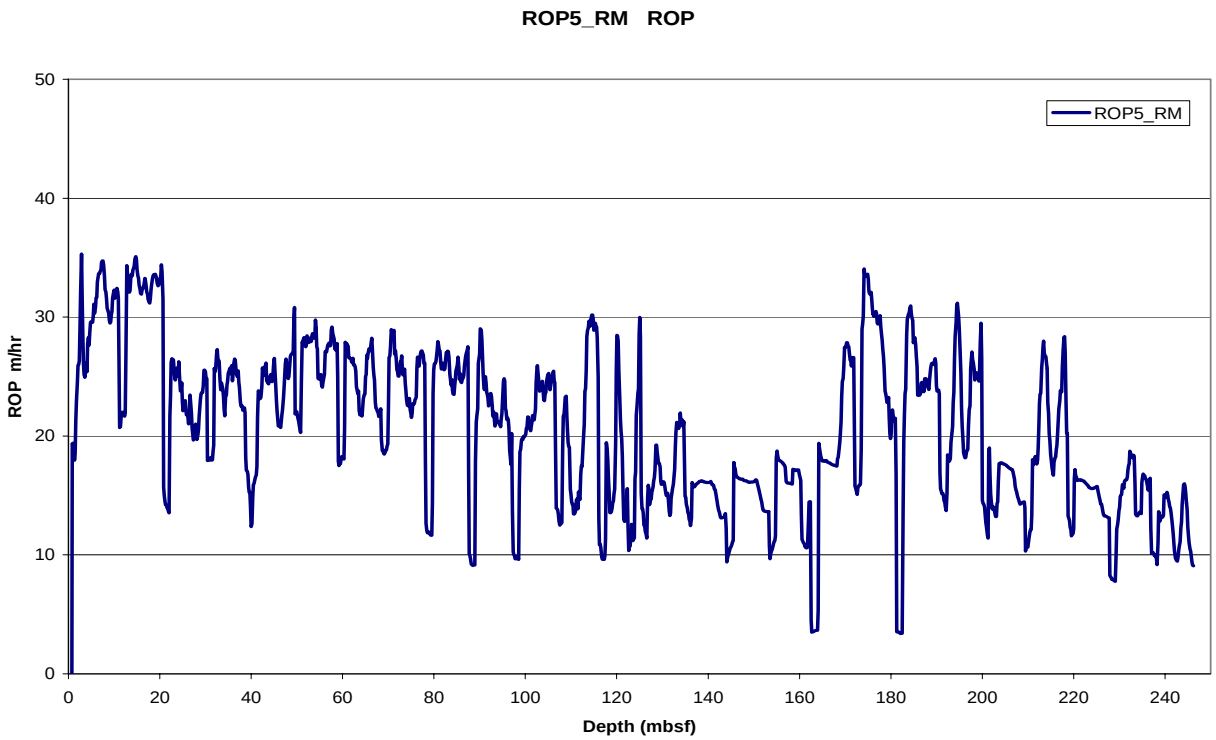

Figure 1. Rate of penetration (ROP) while drilling the AT 13-1 well (recorded data).

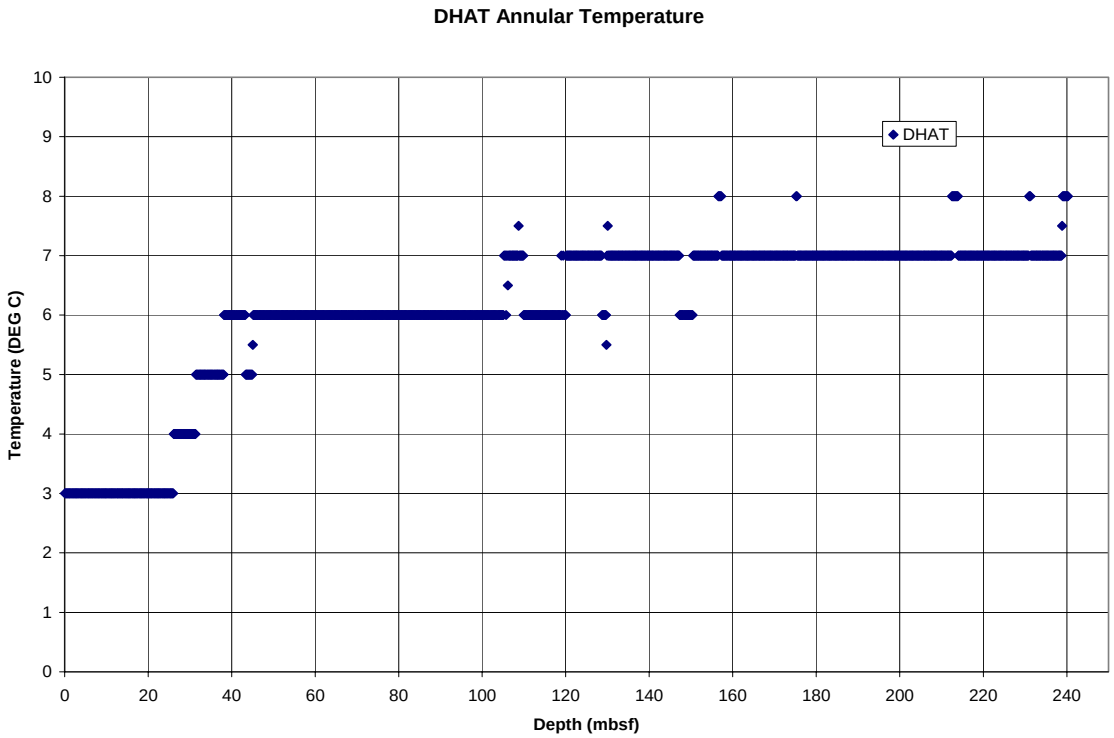

Figure 2. Annular temperature for AT 13-1 from the APWD tool (recorded data).

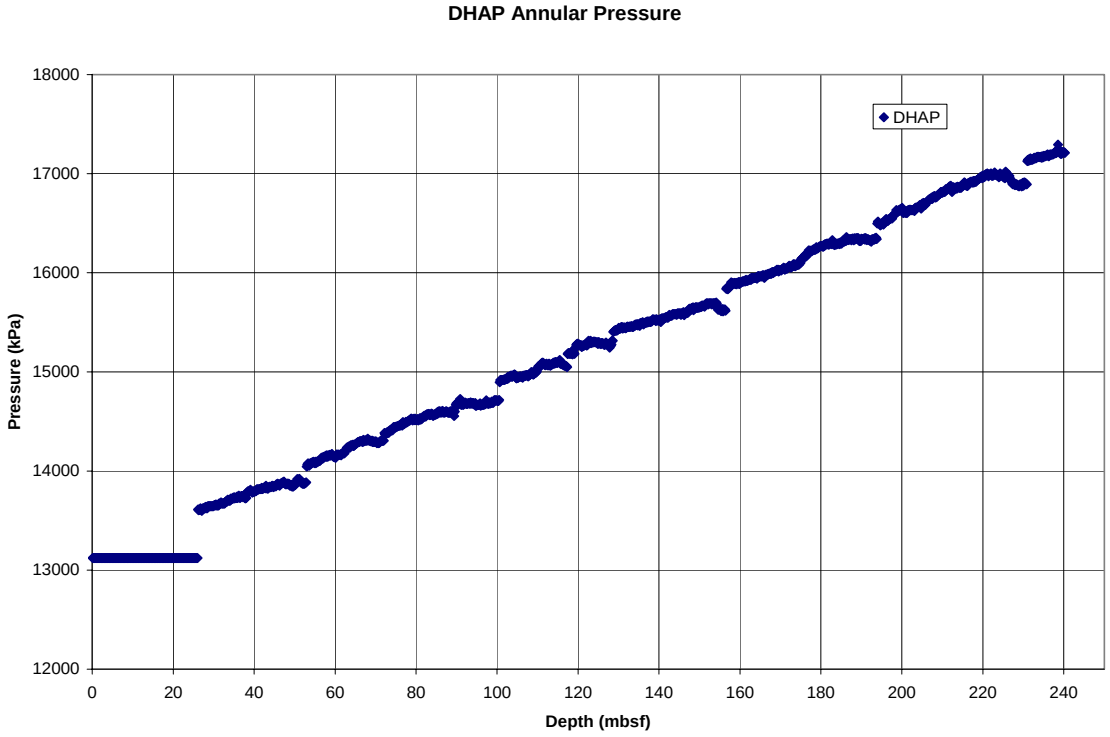

Figure 3. Annular pressure as recorded by the APWD tool in the AT 13-1 well (recorded data).

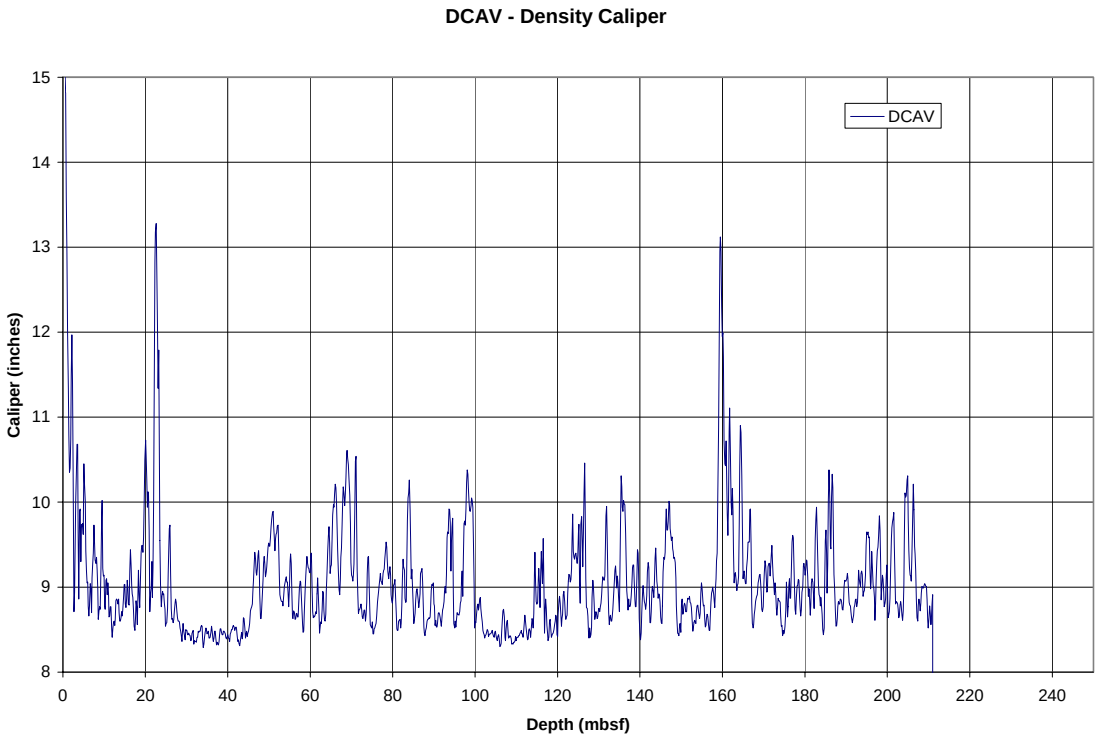

Figure 4. Borehole density caliper as measured by the VDN tool in the AT 13-1 well (recorded data).

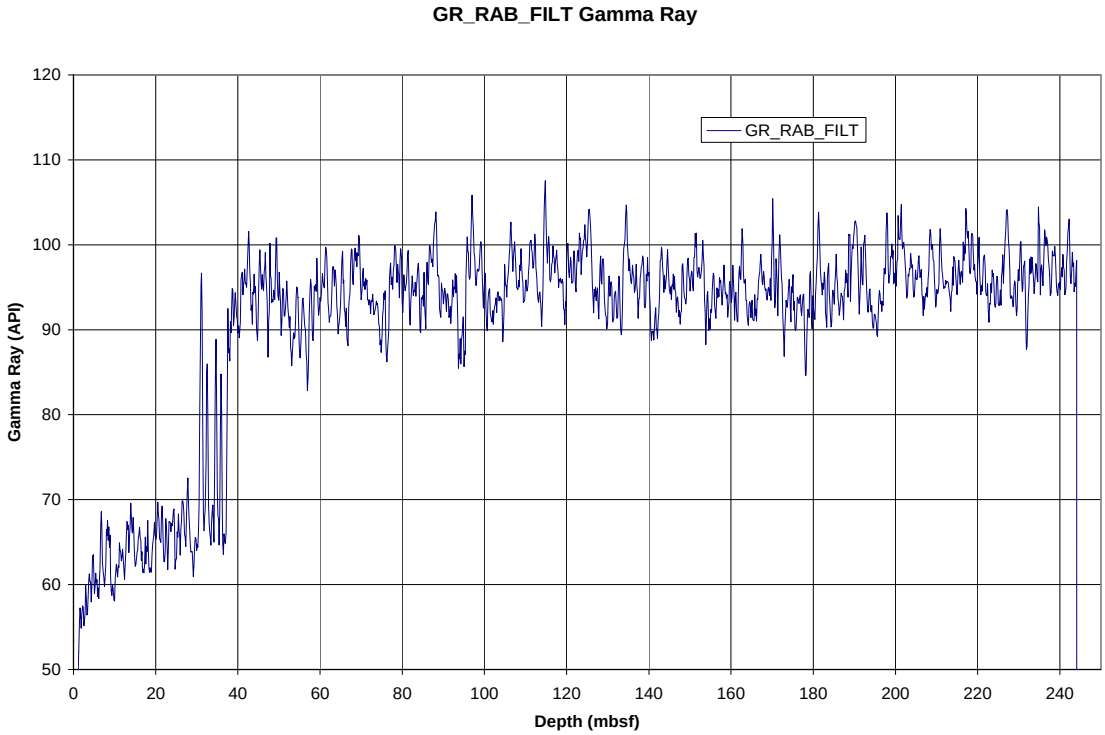

Figure 5. Gamma ray log as measured by GVR6 tool in the AT 13-1 well (recorded data).

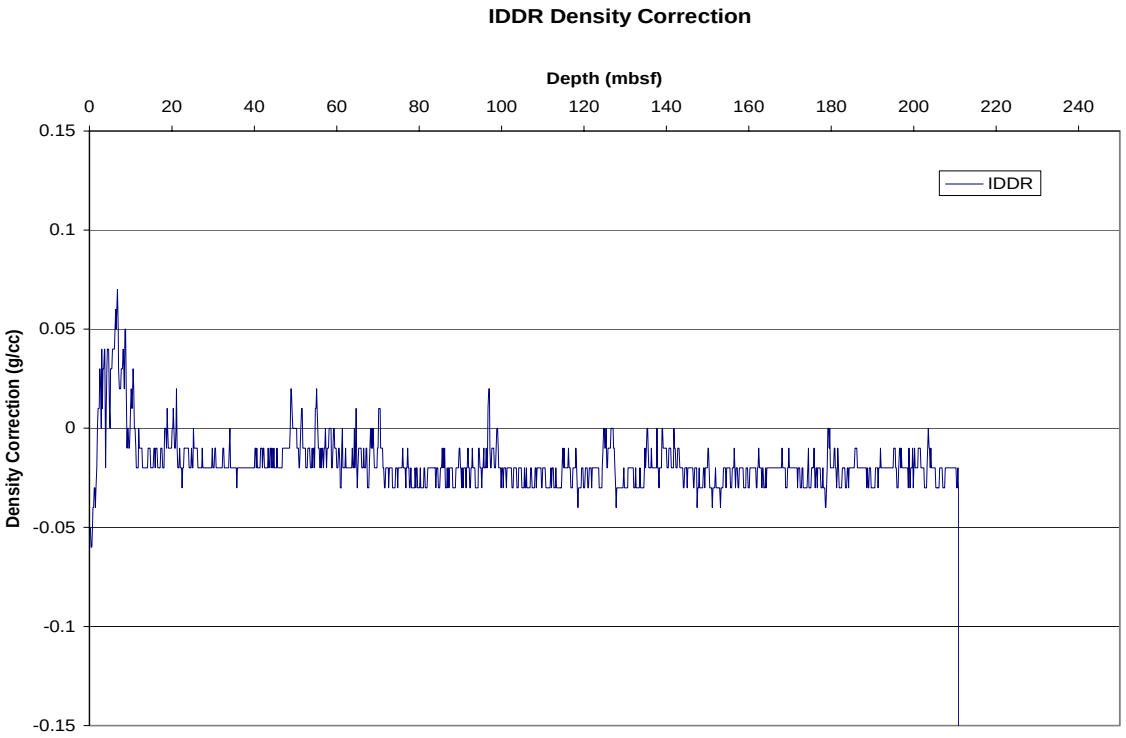

Figure 6. Density log correction for the density log as measured by the VDN tool in the AT 13-1 well (recorded data).

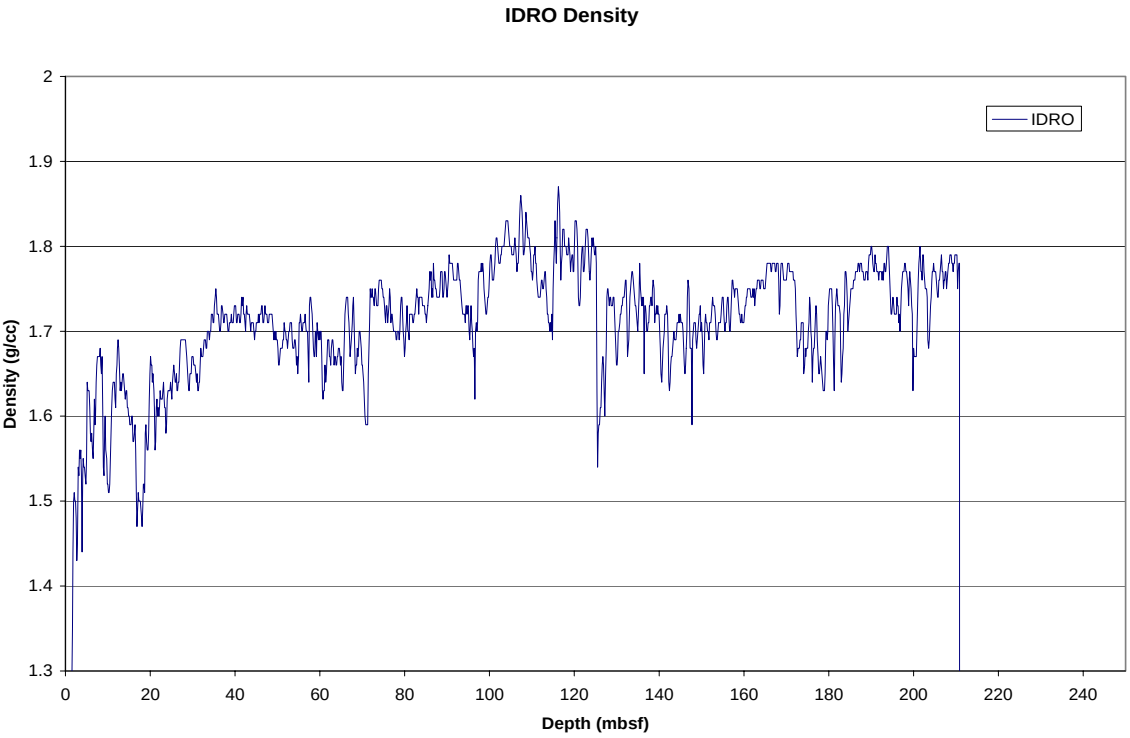

Figure 7. Density log as measured by the VDN tool in the AT 13-1 well (recorded data).

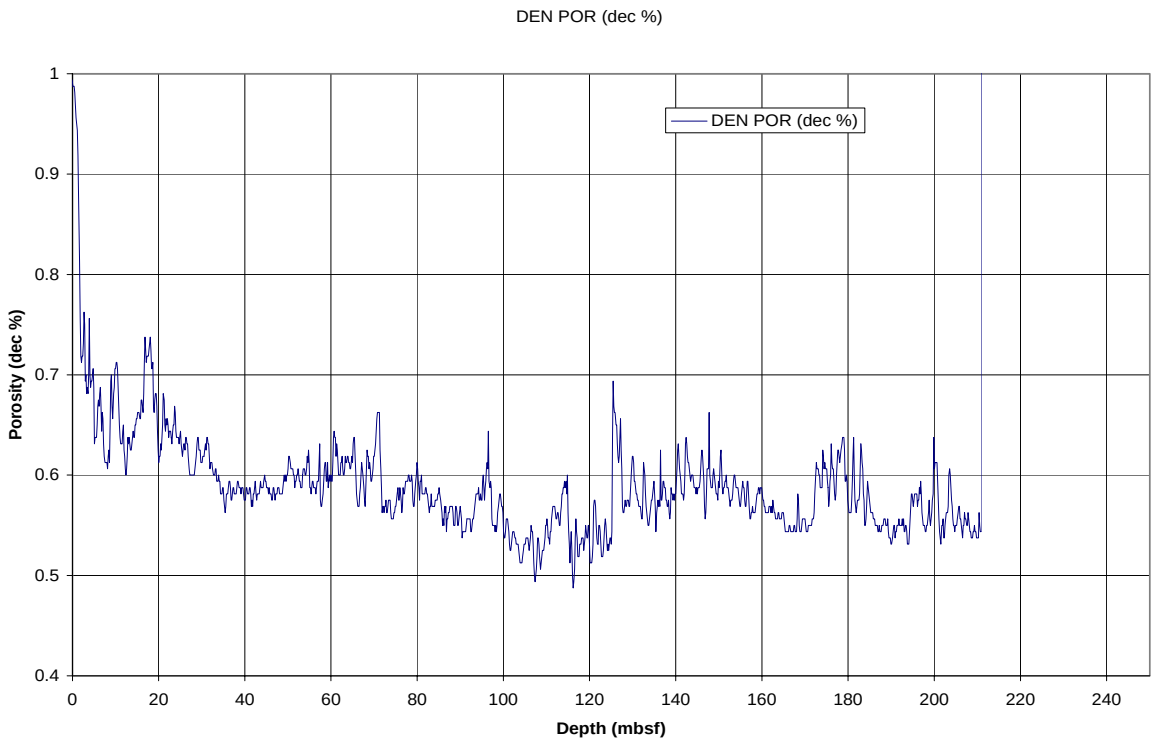

Figure 8. Density log derived porosities in the AT 13-1 well (recorded data).

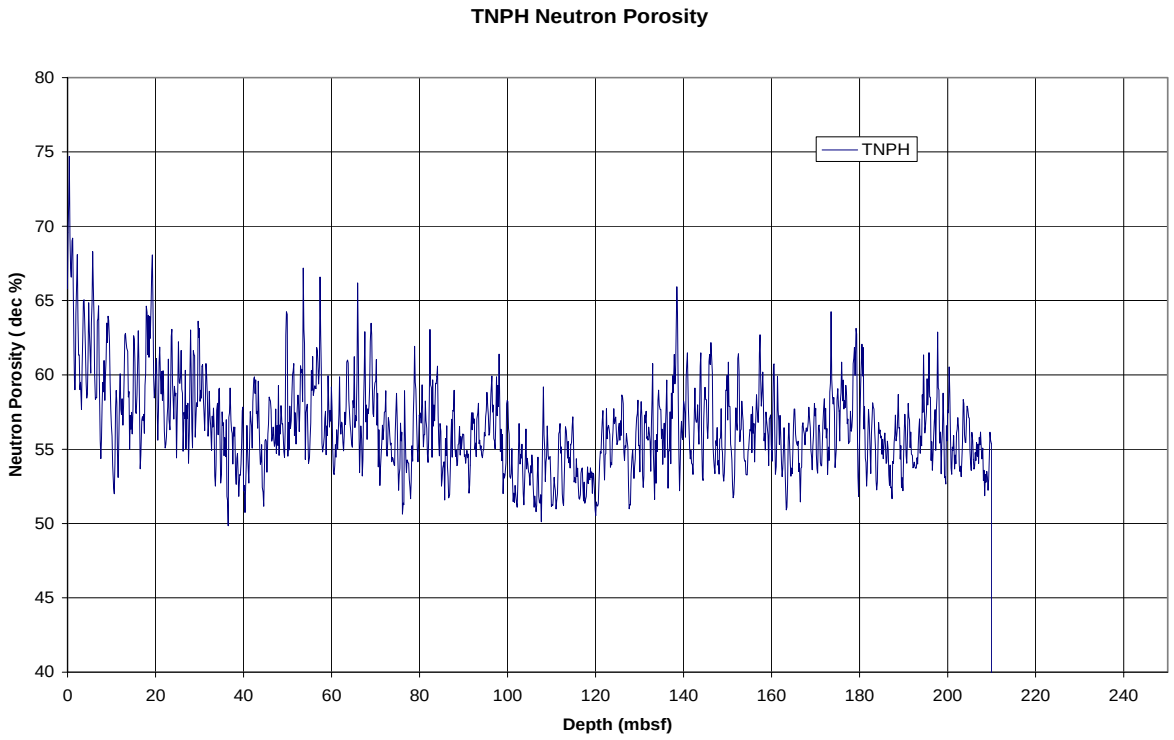

Figure 9. Neutron porosity log as measured by the VDN tool in the AT 13-1 well (recorded data).

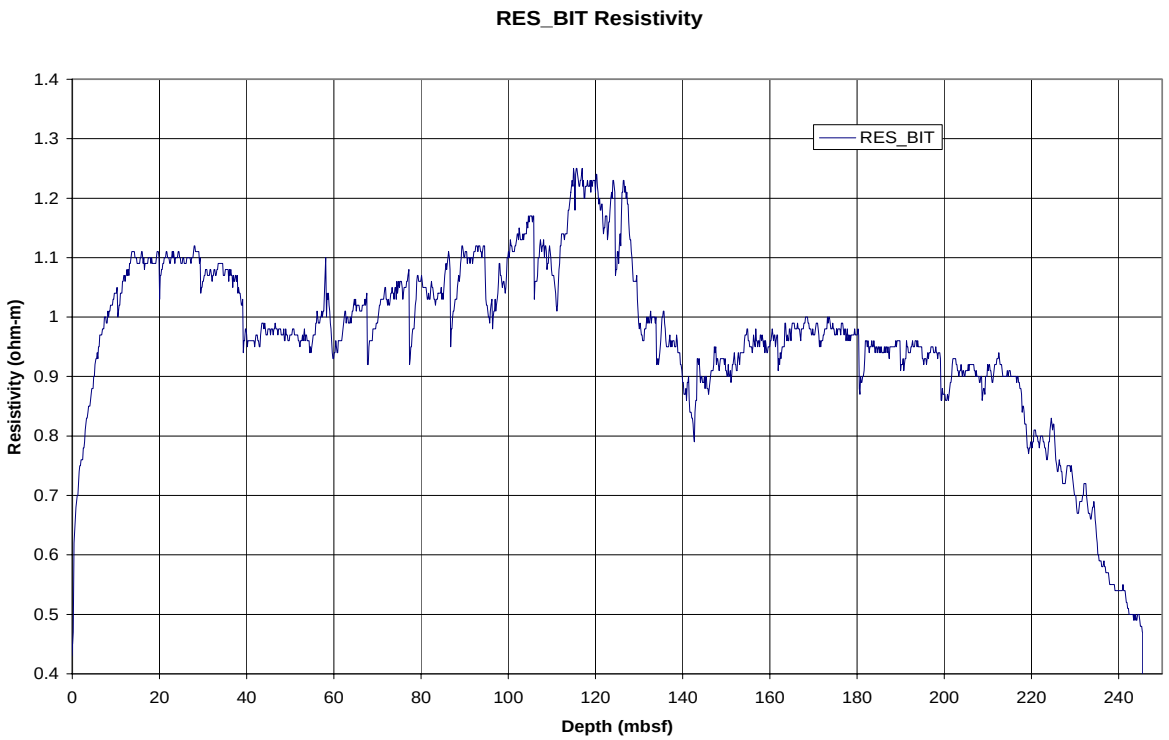

Figure 10. Bit resistivity log as measured by the GVR6 tool in the AT 13-1 well (recorded data).

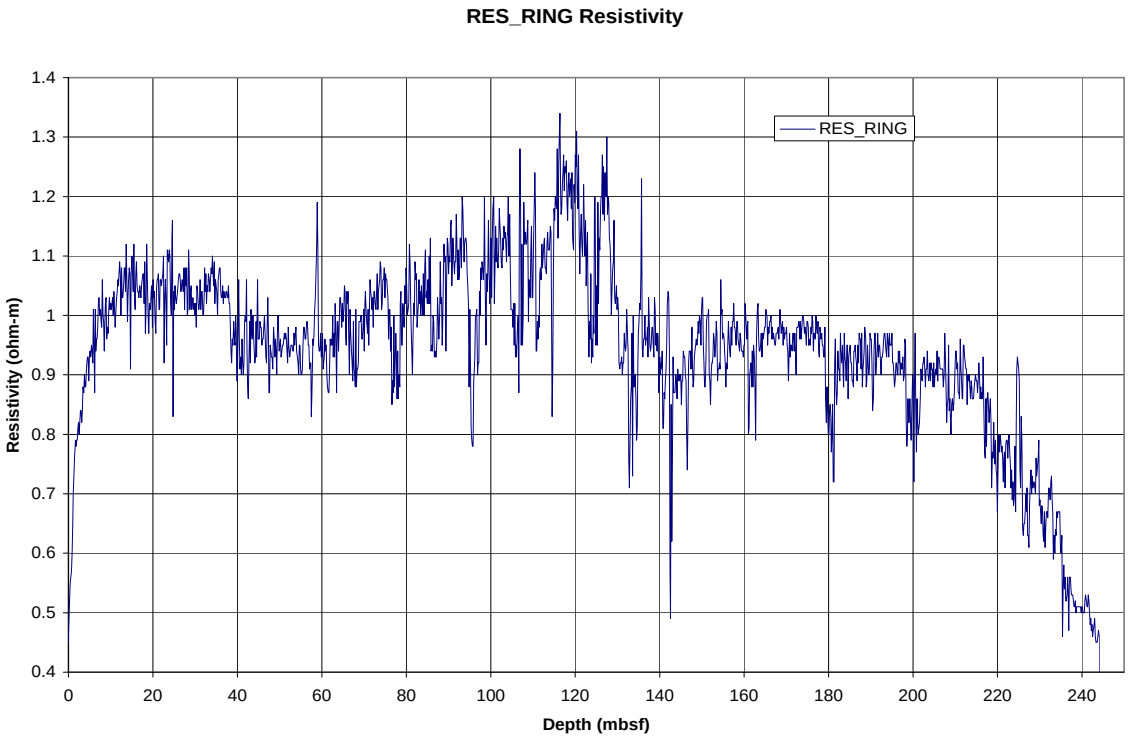

Figure 11. Ring resistivity log as measured by the GVR6 tool in the AT 13-1 well (recorded data).

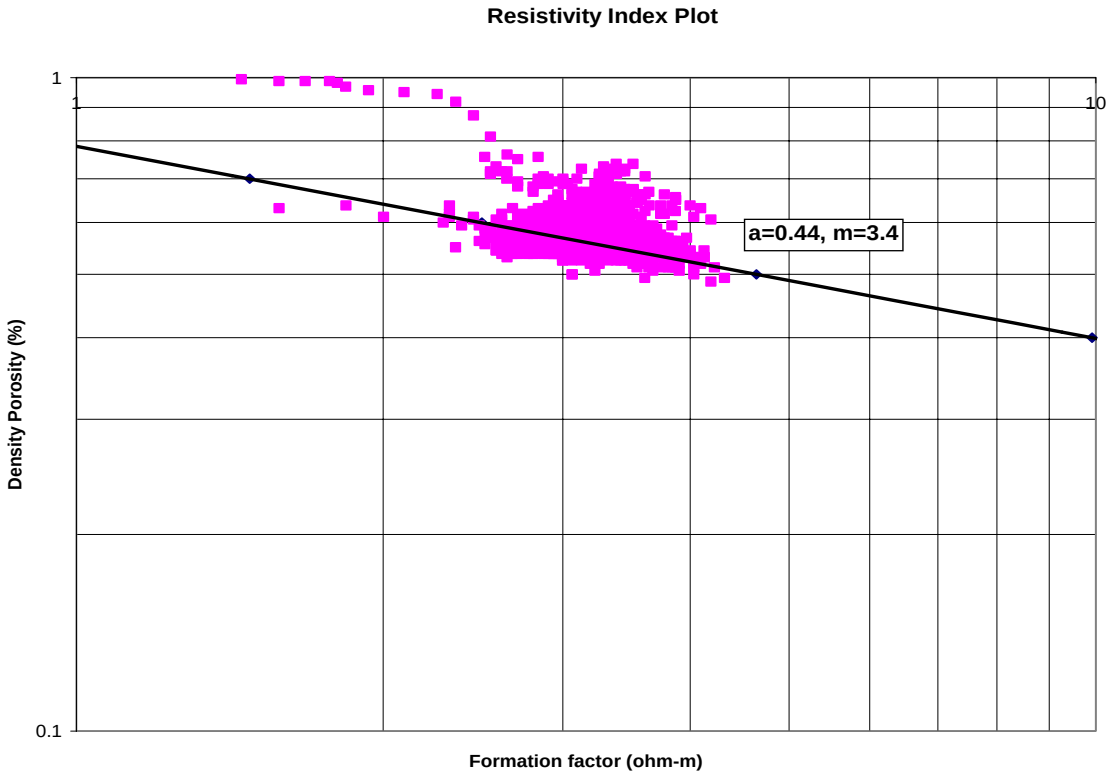

Figure 12. Resistivity index plot (formation factor vs. porosity) for the AT 13-1 well (recorded data).

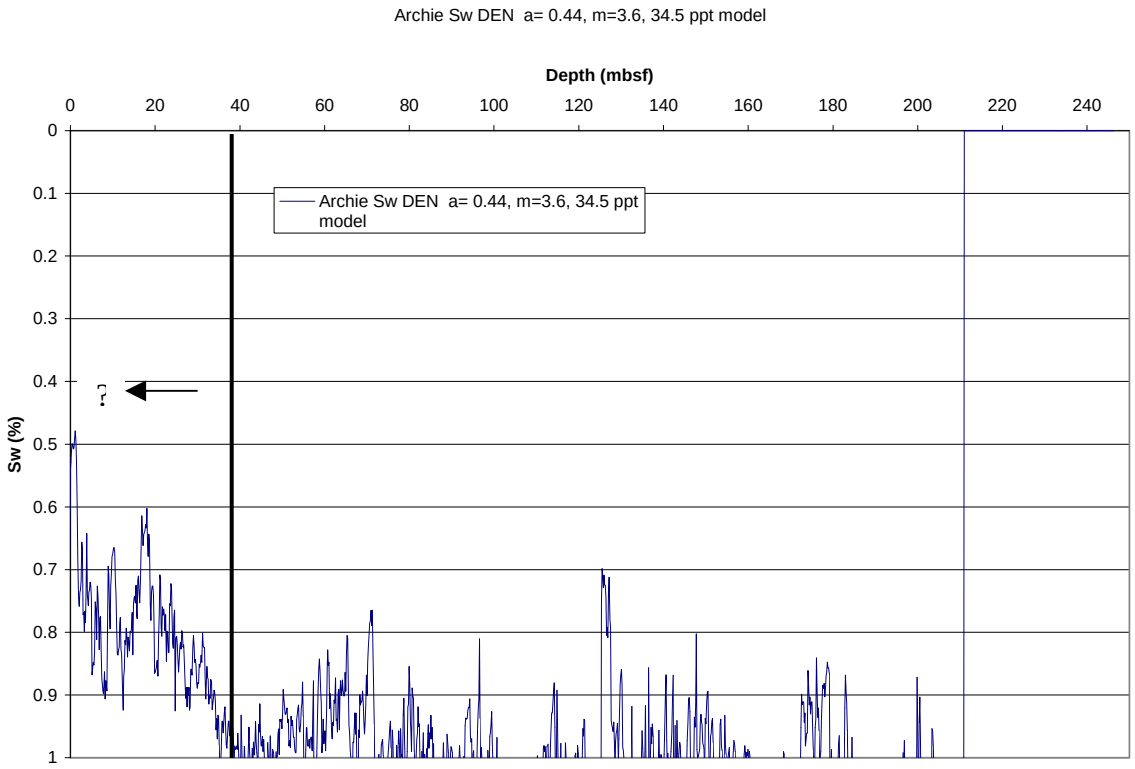

Figure 13. Archie derived water saturations for the AT 13-1 well (recorded data).

Atwater Valley 13-2
OCS-G-24203

-WIRELINE LOGGING-

Operations

Atwater Valley 13-2 (AT 13-2) was cored (FHPC, FC, HRC, FPC) and drilled to a total depth of 200.0 mbsf (drillers depth). Conventional wireline logging (CWL) operations began at 19:40 CT on April 30, 2005 with the makeup of the FMS-sonic tool string. See Table 1 for detailed information on the AT 13-2 CWL program. Figure 2 in the *Explanatory Notes* shows the configuration of the FMS-sonic tool string. For the most part the AT 13-2 well was drilled with only sea water as the drilling fluid, but as the hole was advanced periodic sweeps of Attapulgite based drilling mud was used to sweep and stabilize the hole. Because of concerns associated with severe weather conditions, it was decided to pull the drill string back to only 13.2 mbsf.

After the makeup of the FMS-sonic tool string, it was ran into the hole at 1830 m/hr. Upon encountering the drill bit at 13.2 mbsf (1317.4 mbrf), the FMS-sonic could not exit the drill pipe. It appears that we had swabbed drilling cuttings into the pipe and packed off the bit. We tried to wash the pipe clean by pumping on the drill string; however, we were still unable to exit the drill pipe. A drill pipe drift test at the surface later determined that the closed arms of the FMS caliper were a very tight fit through the bit used on the AT 13-2 well (with a drill bit ID of 3.78 inches and a maximum FMS tool OD of 3.66 inches), which likely contributed to the problems we experienced trying to get out of the pipe. After working for more than an hour to get out of the drill pipe, it was decided to abandon this logging attempt and move a ahead with a proposal to attempt an open water logging run.

At 0:20 CT on May 1, 2005 the FMS-sonic tool was deployed through one of the rigs mouse holes into the open ocean. The *Uncle John* ROV was used to monitor the decent of the FMS-sonic tool to the seafloor. While attempting to enter the hole, the logging cable became tangled around the drill string that had been pulled form the hole to about 10 m above the seafloor. After over two hours of labor, the ROV was able to remove the logging cable from the drill string. We were than able to spud the FMS-sonic tool into the open hole, but we encountered a bridge at only 26.8 mbsf. The FMS-sonic tool string was pulled from the hole and tripped back to the surface reaching the rig floor at 7:12 CT on May 1, 2005; without recording any data.

Table 1. Atwater 13-2 Wireline Logging Program

Water depth: 1304.2m RKB
Drillers TD: 1504.2 m RKB
RKB above sea level: 13.2 m

Date	Time (CT)	Depth of logging string (mbrf)	Event
30-Apr-05	9:00	0.0	Drilled well to total depth (200.0 mbsf)
	9:35	0.0	Begin wiper trip to 110 mbsf, return to bottom of hole
	12:20	0.0	Begin mud displacement run to 13.2 mbsf
	16:00	0.0	Weather hold and seafloor frame "repair"
	19:40	0.0	Begin picking up logging tools
	20:15	0.0	Running into hole at 1830 m/hr
	20:45	1317.4	Could not run out of pipe - pumped pipe (13.2 mbsf)
	22:20	0.0	Pulled logging tools to the derrick floor
	23:20	0.0	Rig up for open water logging run
1-May-05	0:20	0.0	Running in through open ocean at 1830 m/hr
	1:05	1304.2	Attempted open ocean entry, tangle cable
	3:30	1331.0	Spudded tool, bridge at 26.8 mbsf (2000 lb over pull)
	6:00	1304.2	Begin pulling logging tools from sea floor at 1200 m/hr
	7:12	0.0	Pulled tools to the derrick floor and laid down tools

*1m = 3.28084ft

Atwater Valley 14-1
OCS-G-25212

-LOGGING WHILE DRILLING-

Operations

Drilling at Atwater Valley 14 site was designed to penetrate the side of a seismic inferred intrusive feature that is capped by an amplitude anomaly believed to represent free gas. LWD operations (Table 1) began at the Atwater Valley 14-1 (AT 14-1) drill site on April 22, 2005 at 01:17 CT with the spudding of the well, following a short DP move from AT 13-1. The BHA was not tripped to the surface after completing AT 13-1. The LWD tools (6-3/4" collars) included the resistivity-at-the-bit GeoVision tool (GVR6) with a 8-1/8" button sleeve, the EcoScope tool (DVD with APWD), a MWD tool (Telescope), a magnetic resonance while drilling tool (MWD-ProVision), and the azimuthal density neutron (VDN) tool. Figure-1 in the *Explanatory Notes* shows the configuration of the LWD/MWD bottom hole assembly (BHA). Memory and battery life allowed for at least six days of continuous drilling. The initial BHA make-up and tool initialization started at 00:28 CT on April 19, 2005 before drilling AT 13-1. AT 14-1 was spudded at a drillers water depth of 1,313.4 mbrf near the crest of the seismic inferred surface Mound F in Atwater Valley Block 14. The ROV from the *Uncle John* was used to position the BHA and monitor the drilling operations at the sea floor throughout the drilling of the AT 14-1 well. The drill-string heave compensator was not used during LWD operations at AT 14-1. For the most part the AT 14-1 well was drilled with only sea water as the drilling fluid, but as the hole was advanced periodic sweeps of Attapulgite based drilling mud was used to sweep and stabilize the hole.

In an attempt to acquire high quality resistivity-at-bit log and image data within the near-surface sedimentary section, we implemented a controlled spud in drilling protocol which consisted of drilling at a low mud flow rate of about 90 GPM (30 strokes per minute), a limited penetration rate of less than 30 m/hr (which was actually maintained at about 28 m/hr), and a spud in bit rotation rate of 50 RPM. It is important to note that the turbine powered tools on the BHA, including the DVD, MWD, ProVision, and the VDN do not operate at a flow rate of less than about 230 gallons per minute. At a depth about 30 mbsf the mud pump rates were increased to 300 GPM to turn-on the turbine powered tools in the BHA. A flow rate of 300 GPM was required to activate the turbine powered tools, based on assumed pump efficiency of three gallons per pump stroke; which could not verified.

Below 30 mbsf, the hole was advanced at an instantaneous rate of approximately 20-28 m/hr to a TD at 286.6 mbsf without difficulty and real-time data were transmitted to the surface throughout the drilling of the well. Some extraneous pump noise affected the data transmission, but caused minimal real-time data loss. After completion, the BHA was pulled back to sea floor while running a sweep of heavy drilling mud. The tools were pulled out of the hole at 20:38 CT on April 23, 2005, the drill bit cleared the rig floor at 12:00 CT on April 24, 2005, and the recorded LWD data from AT 13-1 and AT 14-1 were retrieved at the rig floor at 14:30 CT on April 24, 2005.

Log Quality

After the completion of LWD operations in the AT 14-1 well, a highly reduced version of the "primary" set of downhole recorded well log data was transferred to the onboard science party for initial analysis. For this report, we have loaded this primary data set into Microsoft Excel and generated a series of well log displays; which has been included with this report (Figures 1-13).

The target rate-of-penetration (ROP) of 30 m/hr (± 5 m/hr) in the interval from the seafloor to total depth (TD) was generally approved upon with instantaneous ROPs ranging from about 20 m/hr to about 25 m/hr (Figure 1). Using slow drilling rates enhanced the quality of the NMR porosity data and RAB images. The quality of RAB images is quite high and no significant resolution loss is observed with variation in ROP in the AT 14-1 well.

The caliper log (DCAV), which provides a measurement of the diameter of the borehole as recorded by the VDN density tool is the best indicator of borehole conditions (Figure 4). The calculated differential caliper values (assuming a bit size of 8-1/2 inches) are <1 inch over 80% of the total section in AT 14-1. With the uppermost 25 mbsf of the hole characterized by significant washouts, as is the section from about 160 mbsf to near the bottom of the hole (286.6 mbsf). The bulk density correction (IDDR), calculated from the difference between the short- and long-spaced density measurements, varies from -0.03 to +0.02 g/cm^3, which shows the high quality of the density measurements (Figure 6).

The depths, relative to seafloor, for all of the LWD logs were fixed by using the *Uncle John* ROV to identify the actual BHA bit contact with the sea floor and shifting the log data to the appropriate depth as determined by the drillers' pipe tallies. For AT 14-1 it was determined that the seafloor was at a depth of 1313.4 mbrf. The rig floor logging datum was located 13.2 m above sea level for this hole.

Interpretation of LWD Logs

LWD gamma ray measurements suggests that the AT 14-1 penetrated mostly a fine-grained clay dominated sedimentary section with no apparent suitable sand reservoir units. The low gamma ray values and slightly elevated density porosity values within the upper 30 m of the well are in part a product of bad borehole conditions. A notable characteristic of the AT 14-1 site is the apparent uniform reduction in formation resistivity in comparison to the AT 13-1 well, which probably indicates an increase in the pore water salinity concentrations. The most significant well log response is the step wise shift with depth to lower formation densities and resistivities at a depth of about 180 mbsf, which probably corresponds to the depth of the BSR or "intrusion" like feature on the seismic surveys at this site.

Log Porosities

Sediment porosities can be determined from analyses of recovered cores and from numerous borehole measurements. Data from the LWD density, neutron, and nuclear magnetic resonance logs have been used to calculate sediment porosities in the AT 14-1 well. The VDN log-derived measurements of bulk-density (Figure 7) in AT 14-1 for the most part ranges from about 1.6 g/cm^3 to 1.8 g/cm^3, with values less than about 1.6 g/cm^3 near the seafloor. The density log measurements are degraded in the upper 25 mbsf, as discussed earlier in this report. The LWD log-derived bulk density measurements from AT 14-1 were used to calculate sediment porosities ($\varnothing$) using the standard density-porosity relation: $\varnothing=(\rho m-\rho b)/(\rho m-\rho w)$. Water densities ($\rho w$) were assumed to be constant and equal to 1.05 g/cm^3; while the grain/matrix densities (ρm) were assumed to be 2.65 g/cm^3 for each log density porosity calculation. The density-log derived porosities range from about 55 to 70 percent (Figure 8), with the most notable high porosity zone in the interval from 180 mbsf to 220 mbsf. However, the density log porosities near the top of the hole (above 10 mbsf), ranging from 60 to near 70 percent, are in part controlled by degraded borehole conditions. The LWD neutron porosity log (Figure 9) yielded sediment porosities ranging from an average value at the top of the logged section of about 58% to near 55% at the bottom of the hole. NMR data were transmitted to shore for processing to estimate bound fluid volume and total free fluid porosity and for comparison with neutron, density, and core porosity estimates. The sediment porosities derived by the LWD NMR tool are very similar to the both the density and neutron log derived porosities.

Gas Hydrate

The presence of gas hydrates was not verified at any of the Atwater Valley drill sites by either sampling in the AT 13-2 well or in the LWD well log data from the AT 13-1 or AT 14-1 wells. The LWD GVR6 resistivity tool, however, reveals several thin high-resistivity zones within the depth interval 18-78 mbsf in the AT 14-1 well, suggesting the possible occurrence of gas hydrate.

Resistivity log data have been used to quantify the amount of gas hydrate at AT 14-1. For the purpose of this discussion, it is assumed that any high resistivities measured in the AT 14-1 well are due to the presence of gas hydrate or possibly free-gas. The Archie relation ($S_w=(aR_w/\varnothing^m R_t)^{1/n}$) was used with resistivity data (R_t) from the LWD RAB tool and porosity data ($\varnothing$) from the VDN density tool to calculate water saturations. It should be noted that gas hydrate saturation (S_h) is the measurement of the percentage of pore space in a sediment occupied by gas hydrate, which is the mathematical complement of Archie derived water saturations (S_w), with S_h=1-S_w.

For the Archie relation, the formation water resistivity (R_w) was calculated from recovered core water samples in AT 13-2 and assumed to range from 30 to 38 ppt. However, both resistivity log data from AT 14-1 and the Mound cores obtained from the top of Mound F suggests that the porewater salinities in the AT 14-1 may be higher than those in AT 13-1. Because of the lack of any deep core data from the AT 14 site, a constant pore water salinity of 34.5 ppt (sea water salinity) was assumed to represent the in-situ R_w conditions. The Archie *a* and *m* variables were calculated using a cross plot technique (a= 0.40, m= 3.0), which compares the downhole log derived resistivities and density porosities (Figure 12). The APCT temperature data obtained from the AT 13-2 well revealed an equilibrium seabed temperature of 4.37°C and a geothermal gradient of 3.2°C/100m.

The Archie relation generally yielded water saturations near 100% for most the well. There is some indication of low gas hydrate saturations (percent of pore space occupied by gas hydrate) of less than 10-20% in the upper 0-65 mbsf of the AT 14-1 well. There is also some indication of low gas hydrate or free-gas saturations (i.e., reduced Archie derived water saturations), ranging from 10-20 %, within

the depth interval between 180-220 mbsf. But this section is closely associated with the apparent changes in formation resistivities and inferred pore water salinities at 180 mbsf, the affect of which needs to be further investigated.

It is possible that the BSR or "intrusion" like feature at 180 mbsf marks a fluid boundary between upwelling higher salinity brines in the seep feature and lower more normal salinities in the surrounding section. As noted above, the slight drop in the recorded BIT and RING resistivities within the interval 180-220 mbsf appears to be associated with low density values and elevated neutron porosities. However, lower formation densities are not compatible with the occurrence of a more dense brine intrusion. But the apparent drop in the Archie derived water saturations within the interval from 180 mbsf to 220 mbsf, which suggest the presence of free gas below the BSR like feature is compatible with an apparent reduction in log measured formation densities. Without acoustic log data, however, we cannot conclusively prove the occurrence of free gas within this feature.

The review of the well log data from AT 14-1 shows relatively little evidence for any significant gas hydrates at this site. The LWD logs from this site further suggests the presence of a complex pore water fluid regime, with variable well log inferred pore water salinities. It is important to highlight, however, that the well log and seismically inferred fluid salinity and possible free-gas feature associated with the Atwater 14-1 site is limited in spatial size and likely exhibits only local influence on gas hydrate stability conditions.

Borehole Temperature and Pressure Data
The APWD measured borehole pressures (DHAP) generally indicate a uniform pressure gradient with depth (Figure 3), with some pressure deviations associated with running heavy mud sweeps near the end of pipe connections. The DHAT temperature log indicates that the circulating fluids were cooled in their descent in the drill pipe to a relatively uniform temperature in the range of 4-8 degrees Celsius (Figure 2).

Table 1. Atwater 14-1 LWD/MWD Logging Program

Water depth: 1313.4 m RKB
Drillers TD: 1600.0 m RKB
RKB above sea level: 13.2 m

Date	Time (CT)	Depth of drill bit (mbrf)*	Event
22-Apr-05	1:17	1313.4	Spud well, controlled drill 90 GPM, 28 m/hr ROP, 50 RPM
	2:01	1343.0	Pump rate up to 300 GPM, 27 m/hr ROP, 90 RPM; MWD tool powered up
23-Apr-05	9:41	1600.0	Well reaches TD at 286.6 mbsf
	10:21	1600.0	Begin trip of BHA to sea floor, running heavy mud sweep
	13:35	1352.0	Hold at 38.6 mbsf for mud pump repairs
	18:30	1352.0	Pump-out logging as BHA pulled to sea floor, 300 GPM, 25 m/hr ROP
	20:38	1313.4	BHA clears sea floor
24-Apr-05	2:00	1313.4	Begin trip of BHA to the rig floor
	12:00	0.0	BHA clears rig floor and laid down tools
	14:30	0.0	LWD/MWD log data transfer completed

*1m = 3.28084ft

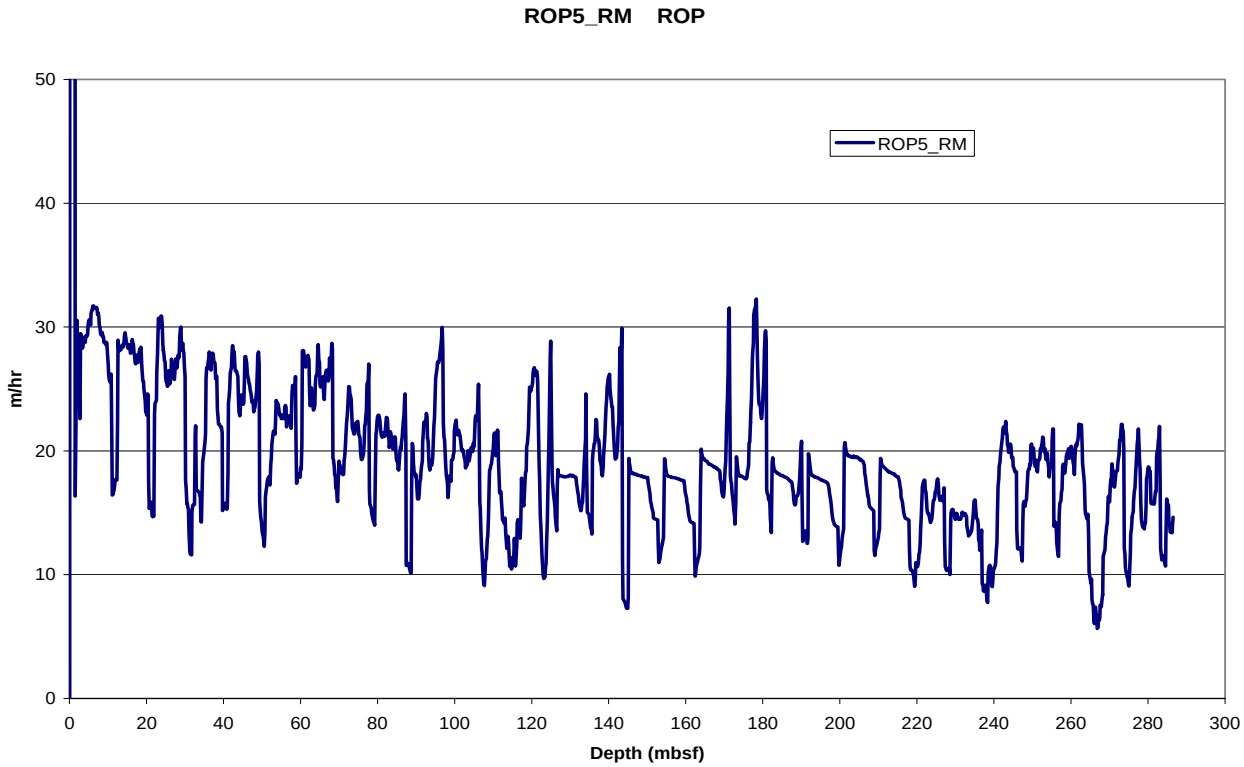

Figure 1. Rate of penetration (ROP) while drilling the AT 14-1 well (recorded data).

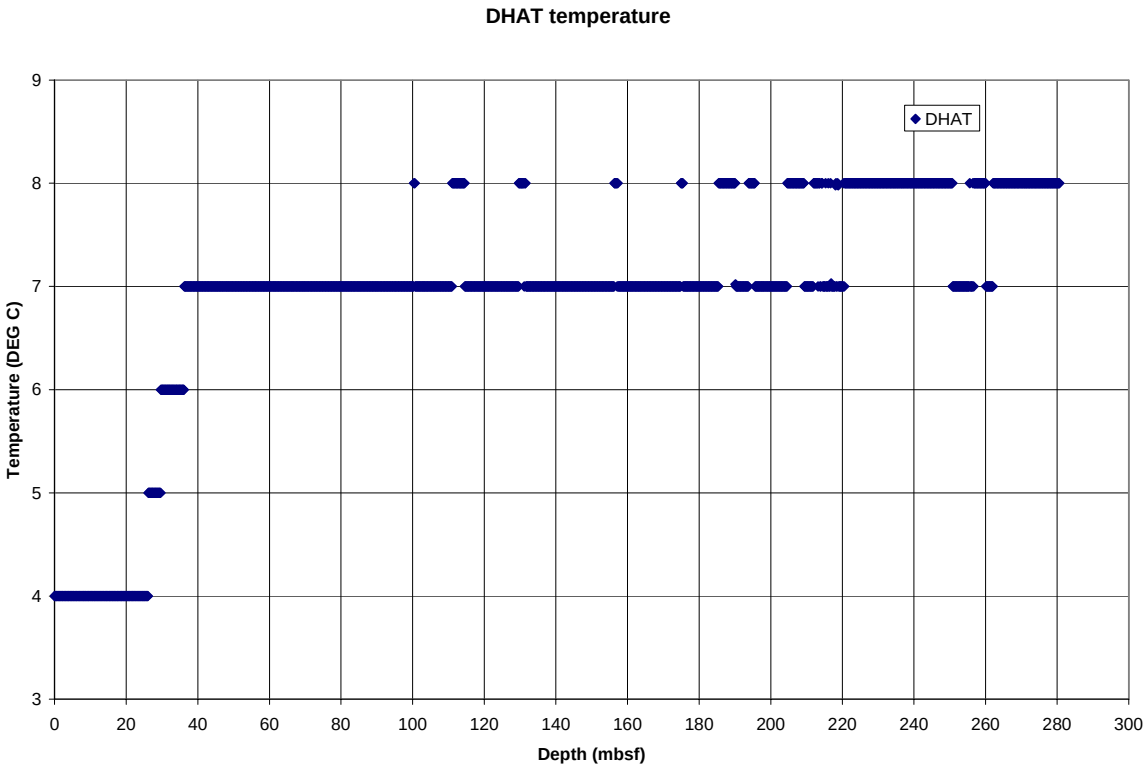

Figure 2. Annular temperature for AT 14-1 from the APWD tool (recorded data).

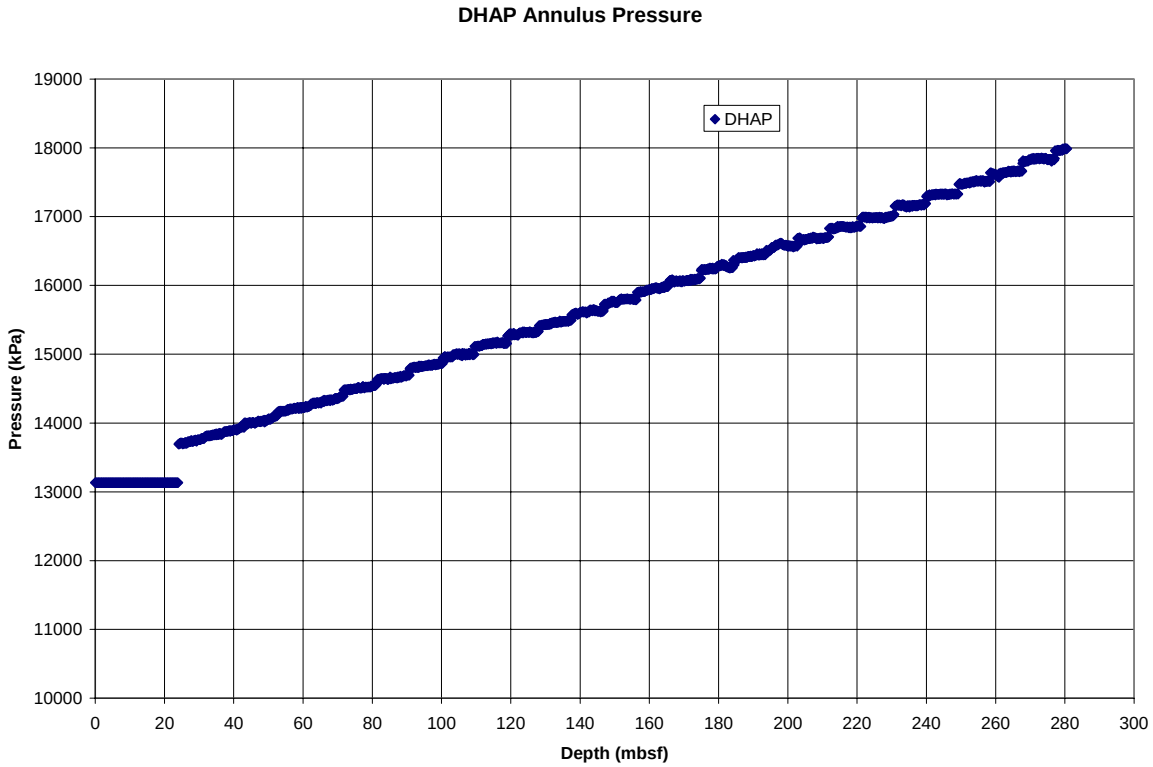

Figure 3. Annular pressure as recorded by the APWD tool in the AT 14-1 well (recorded data).

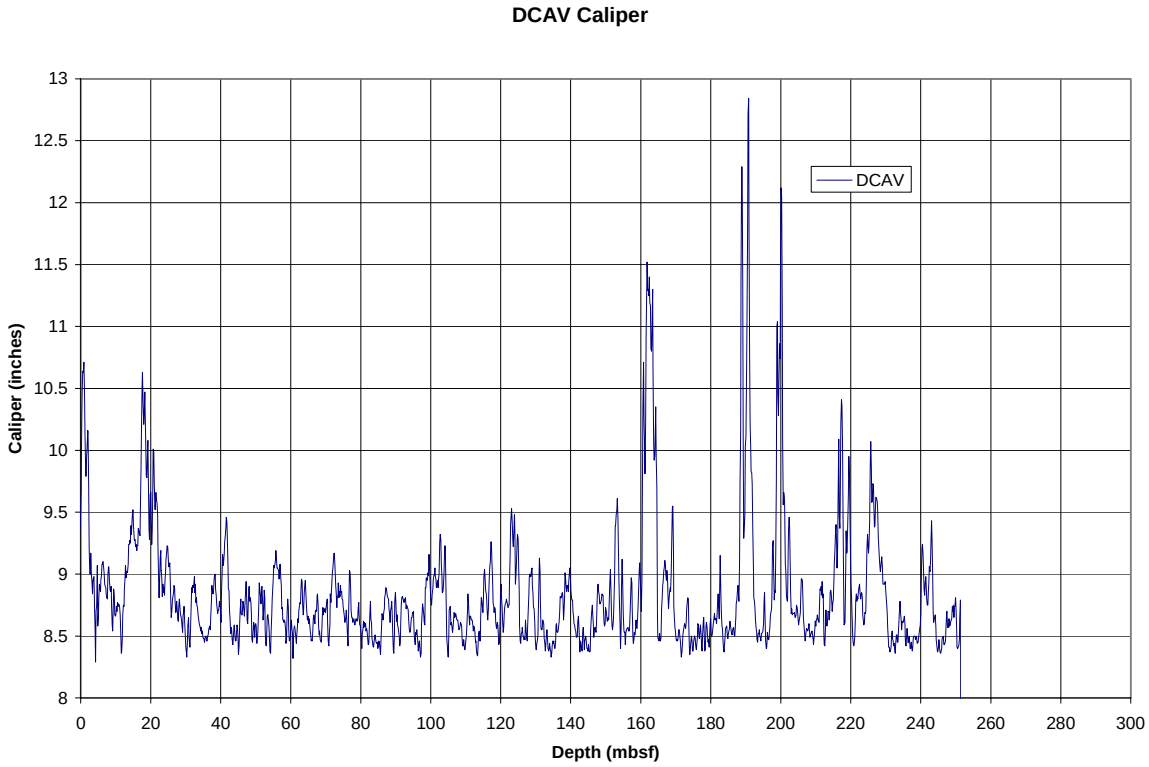

Figure 4. Borehole density caliper as measured by the VDN tool in the AT 14-1 well (recorded data).

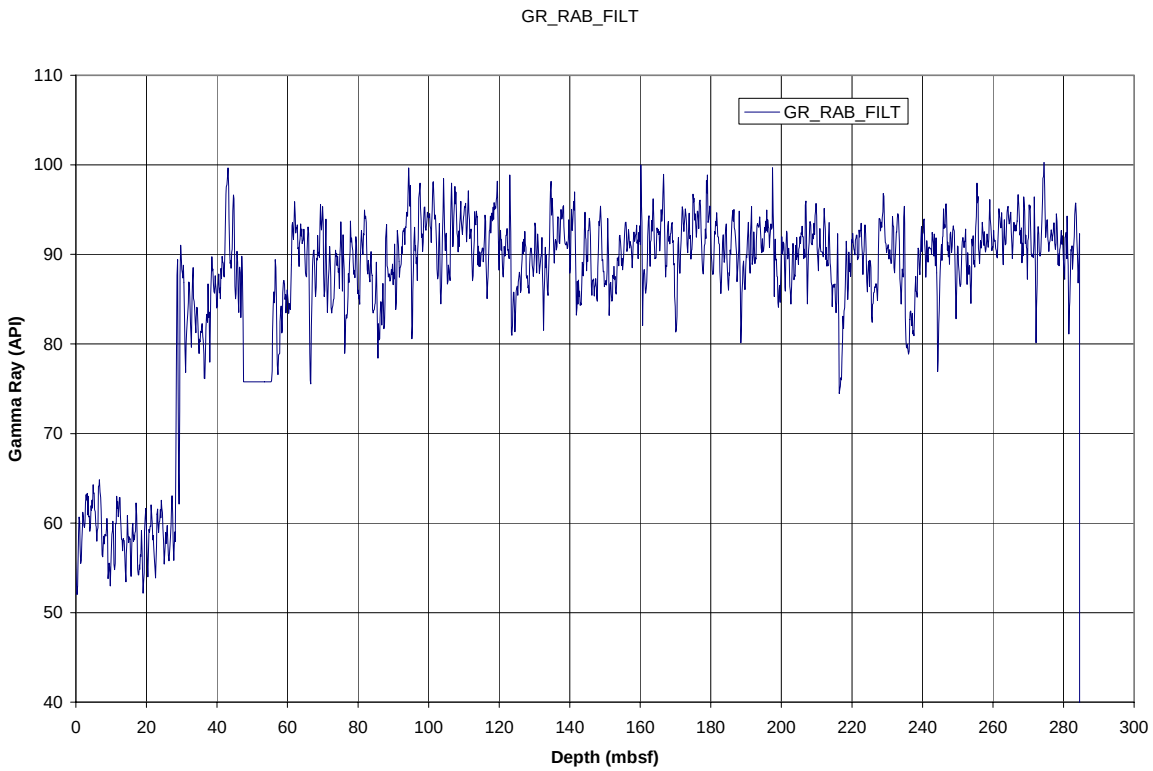

Figure 5. Gamma ray log as measured by GVR6 tool in the AT 14-1 well (recorded data).

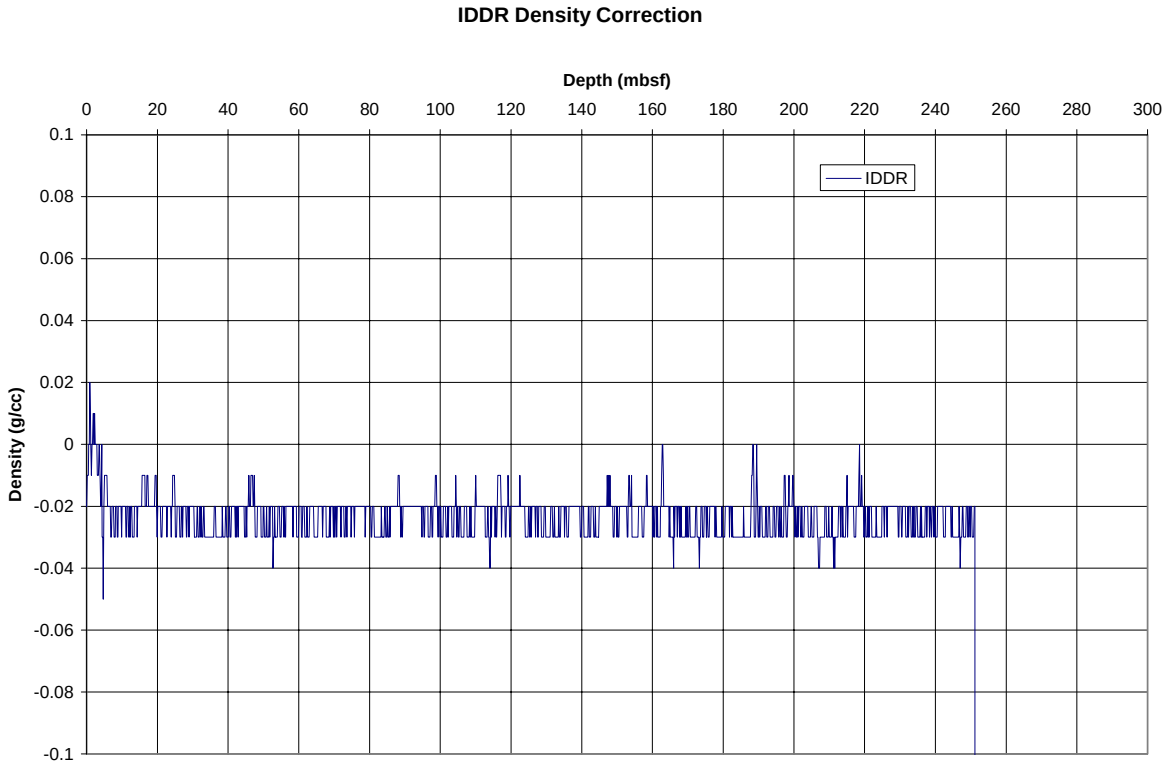

Figure 6. Density log correction for the density log as measured by the VDN tool in the AT 14-1 well (recorded data).

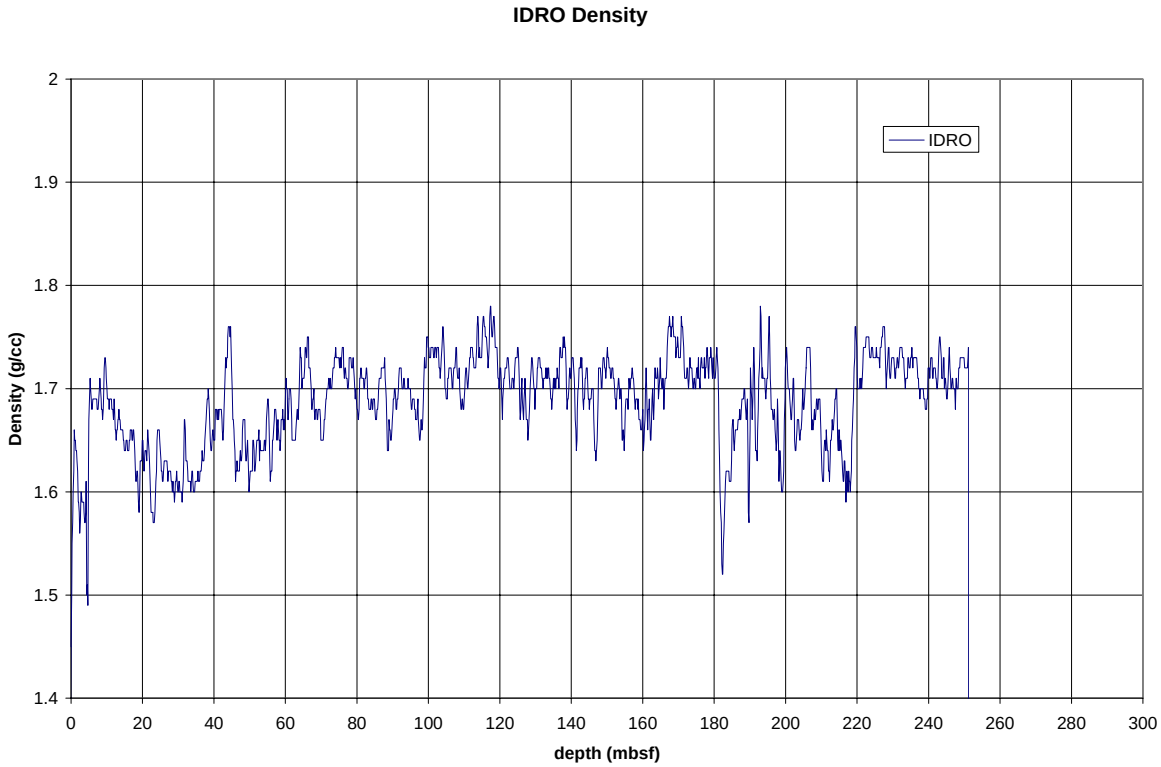

Figure 7. Density log as measured by the VDN tool in the AT 14-1 well (recorded data).

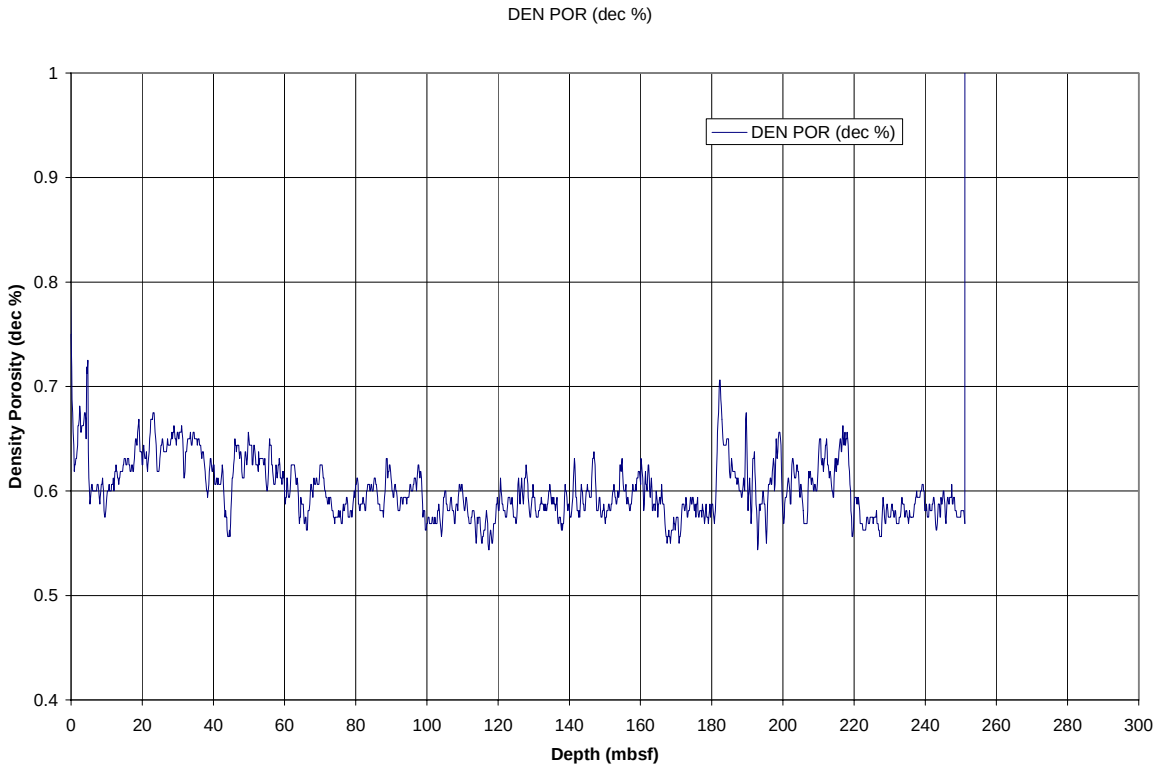

Figure 8. Density log derived porosities in the AT 14-1 well (recorded data).

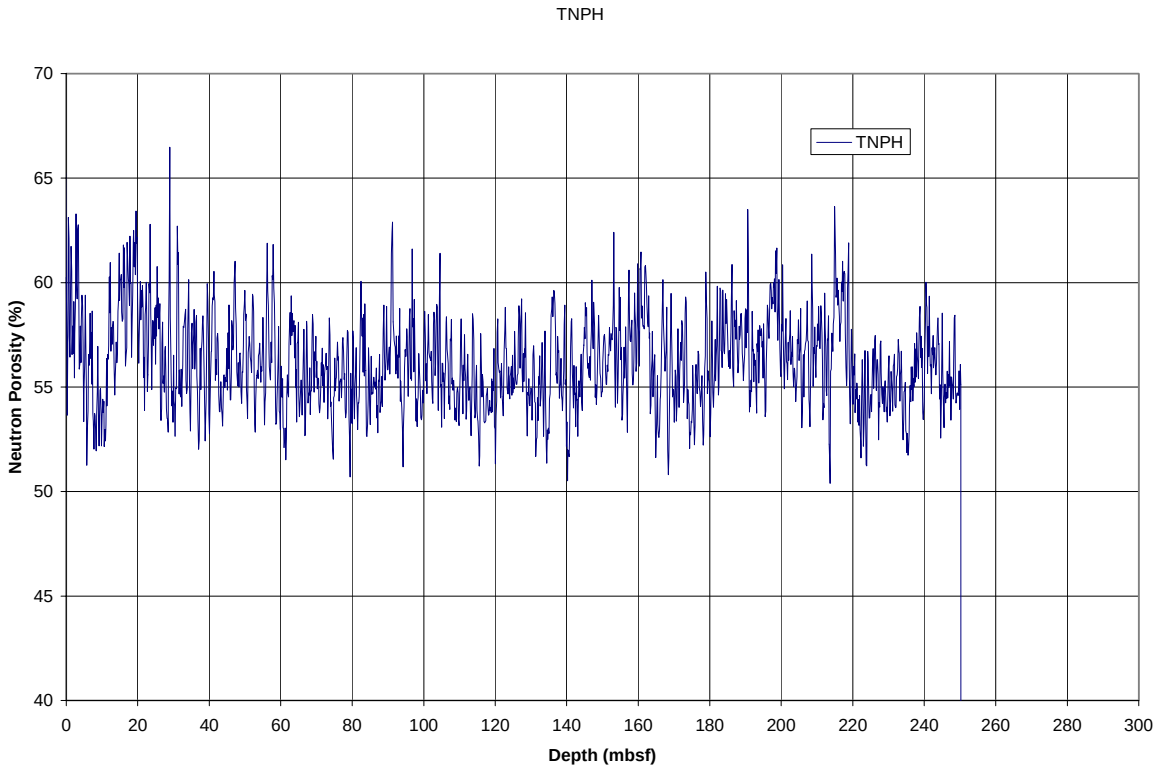

Figure 9. Neutron porosity log as measured by the VDN tool in the AT 14-1 well (recorded data).

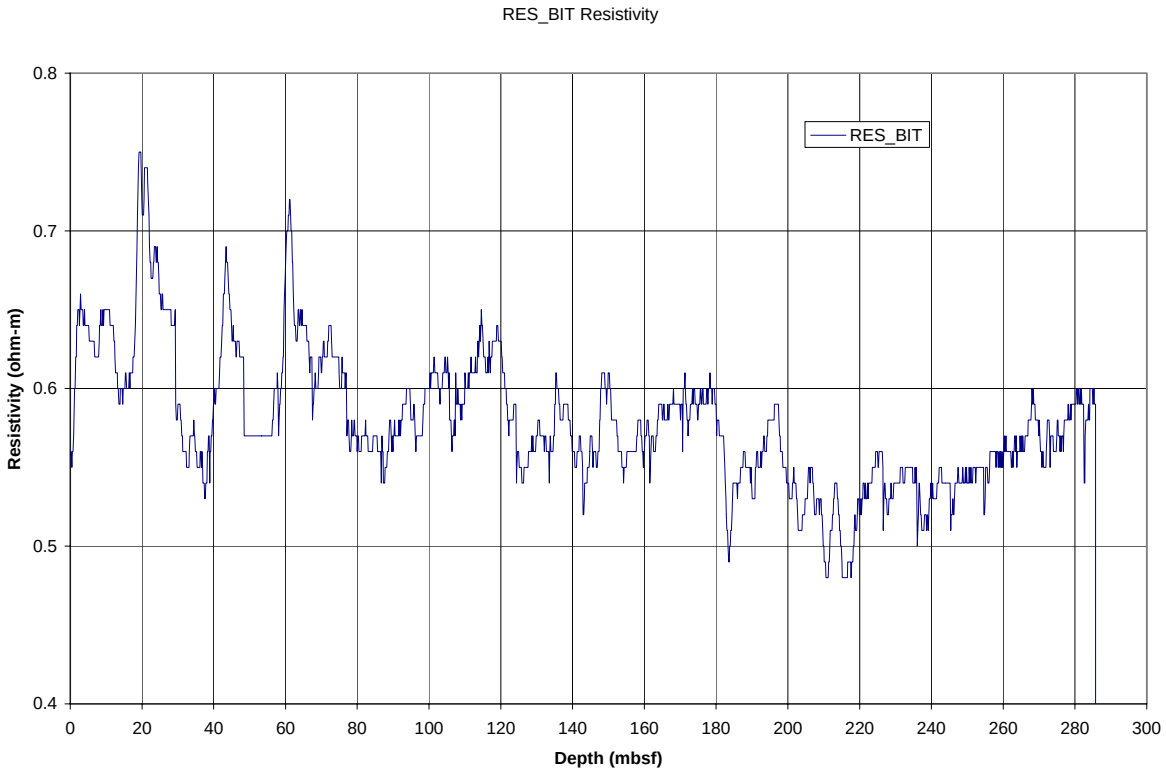

Figure 10. Bit resistivity log as measured by the GVR6 tool in the AT 14-1 well (recorded data).

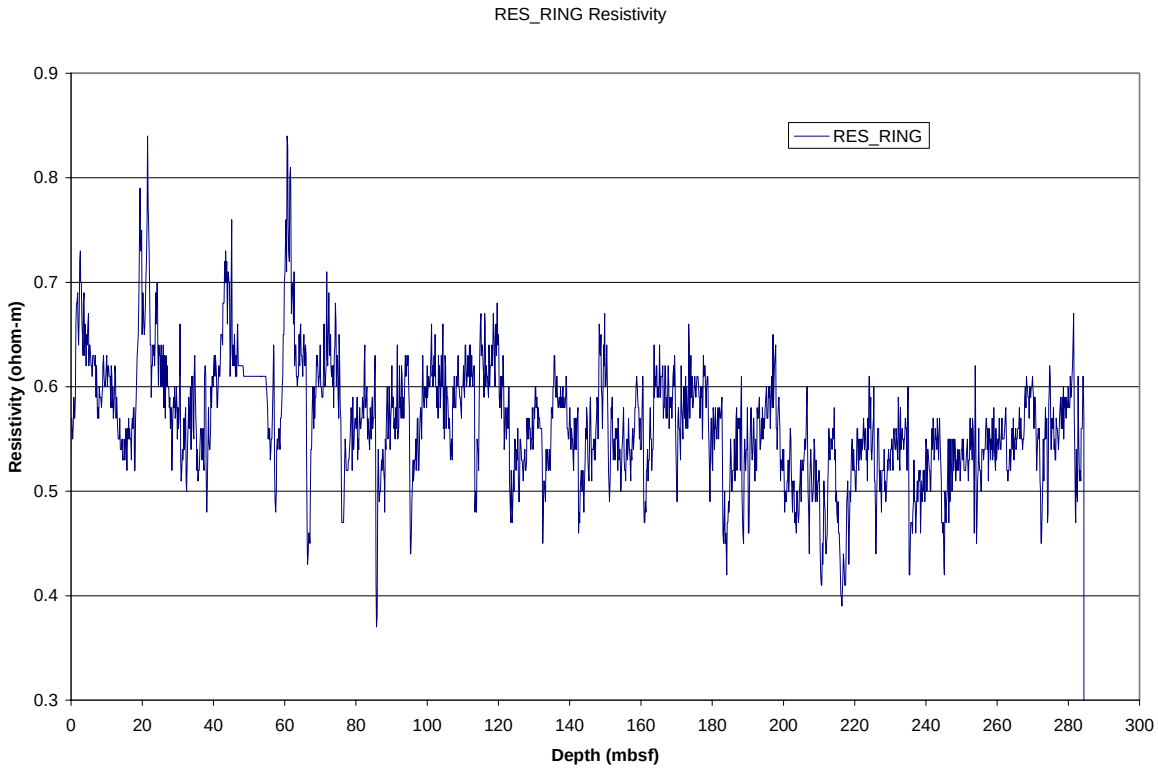

Figure 11. Ring resistivity log as measured by the GVR6 tool in the AT 14-1 well (recorded data).

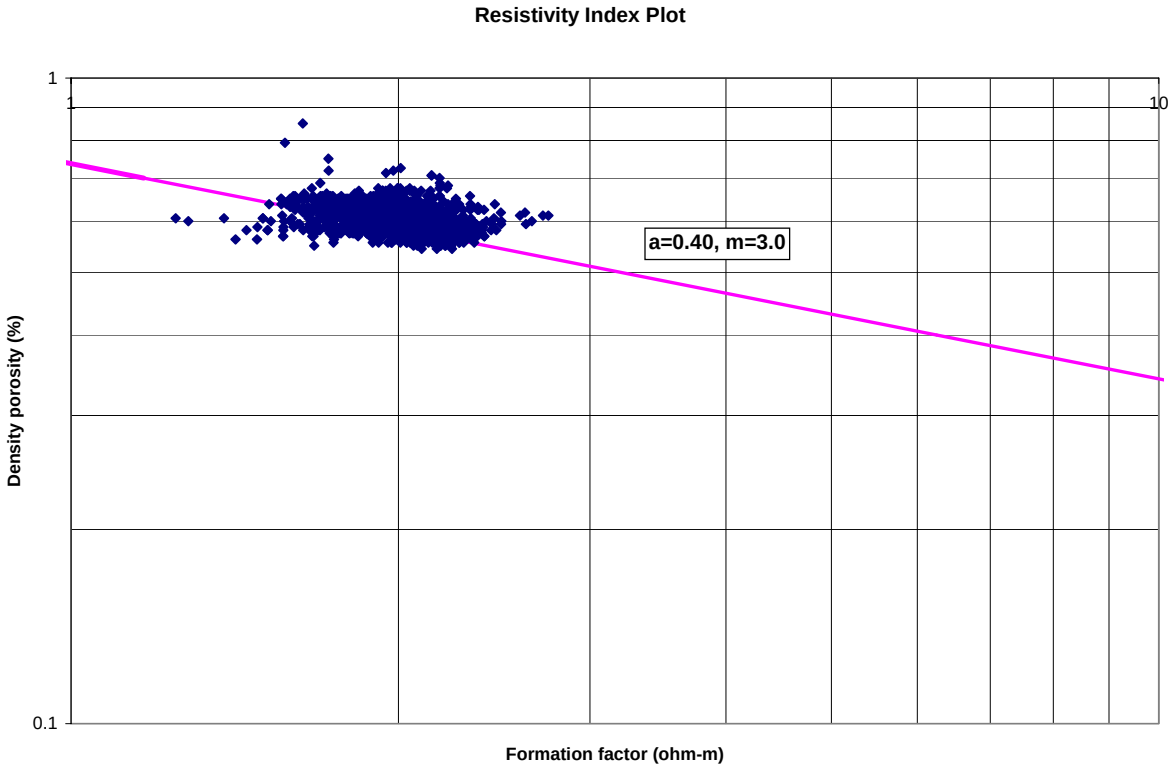

Figure 12. Resistivity index plot (formation factor vs. porosity) for the AT 14-1 well (recorded data).

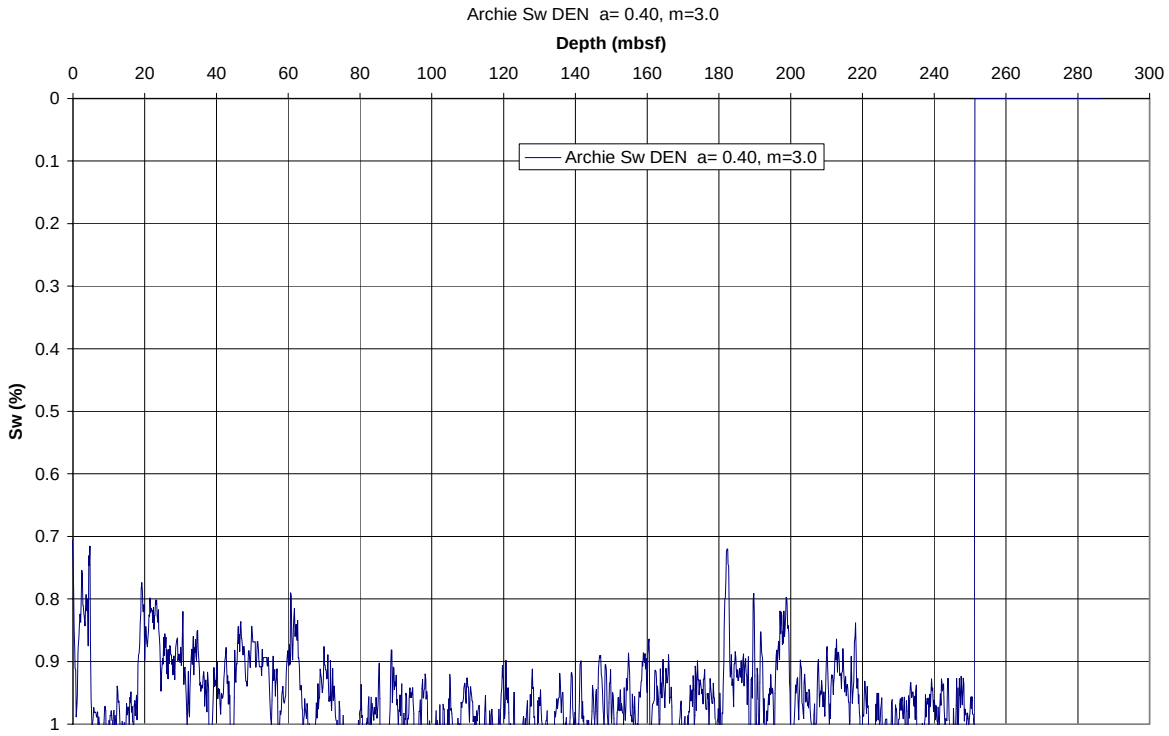

Figure 13. Archie derived water saturations for the AT 14-1 well (recorded data).

Keathley Canyon 151-2

-LOGGING WHILE DRILLING-

Operations

The drilling objectives at the Keathley Canyon 151 site was to characterize the possible occurrence of a gas hydrate related bottom simulating reflector (or BSR). Seismic lines from both high resolution research seismic surveys and from regional 3D surveys through the Keathley Canyon 151 proposed drill site reveal the presence of a BSR at a depth of about 385 mbsf. Thus, the Keathley Canyon 151 block contains one of the rare instances of a BSR in the Gulf of Mexico, and may indicate the occurrence of gas hydrates at depth.

LWD operations (Table 1) began at the Keathley Canyon 151-2 (KC 151-2) drill site on May 7, 2005 at 01:31 CT with initial BHA make-up, tool initialization, and calibration. The LWD tools (6-3/4" collars) included the resistivity-at-the-bit GeoVision tool (GVR6) with a 8-1/8" button sleeve, the EcoScope tool (DVD with APWD), a MWD tool (Telescope), a magnetic resonance while drilling tool (MWD-ProVision), and the azimuthal density neutron (VDN) tool. Figure-1 in the *Explanatory Notes* shows the configuration of the LWD/MWD bottom hole assembly (BHA). Memory and battery life allowed for at least six days of continuous drilling.

A pump test of the BHA (at a subsea depth of about 128.0 mbrf), indicated a power failure in the ProVision and GVR6 tools, which was linked to a possible problem in the Telescope MWD tool. The BHA was pulled back to the surface, and the backup ProVision and GVR6 tools were inserted into the BHA. Because of concerns associated with minor communication/power problems observed during the drilling of the AT 13-1 and AT 14-1 wells (mostly noticed in the ProVision tool) it was decided to also swap out the TeleScope MWD tool for the more conventional Power Pulse MWD tool; which also required the EcoScope to be swapped out for the Array Resistivity Compensated Tool (ARC). The new BHA was initialized, ran to the sea floor, and the KC 151-2 well was spudded at 06:35 CT on May 8, 2005 at a drillers water depth of 1,335.0 mbrf along the western flank of a subtle ridge feature in Keathley Canyon 151. The ROV from the *Uncle John* was used to monitor the drilling operations at the sea floor throughout the drilling of the KC 151-2 well. The active drill-string heave compensator on the *Uncle John* was used during LWD operations at KC 151-2. For the most part the KC 151-2 well was drilled with only sea water as the drilling fluid, but as the hole was advanced periodic sweeps of Attapulgite based drilling mud was used to sweep and stabilize the hole. A barite kill mud was also used to control a water/gas flow problem that developed after the well was drilled, thus the logs should not be affected by any of the normal barite mud affects.

In an attempt to acquire high quality resistivity-at-bit log and image data within the near-surface sedimentary section, we implemented a controlled spud in drilling protocol which consisted of drilling at a low mud flow rate of about 100 GPM (33 strokes per minute), a limited penetration rate of less than 25 m/hr, and a spud in bit rotation rate of 50 RPM. It is important to note that the turbine powered tools on the BHA, including the DVD (ARC), MWD, ProVision, and the VDN do not operate at a flow rate of less than about 230 gallons per minute. At a depth about 25 mbsf the mud pump rates were increased to 360 GPM to turn-on the turbine powered tools in the BHA. It was decided that a flow rate of 360 GPM was required to adequately clear the hole of drill cuttings, which did contribute to some borehole erosion problems.

Below 30 mbsf, the hole was advanced at an instantaneous rate (Figure 1) of approximately 15 to about 35 m/hr (with most of the well drilled at rates below 25 m/hr) to a TD at 459.8 mbsf without difficulty. The ROP in the KC 151-2 well was much more variable than what we experienced in either of the Atwater Valley wells, which was attributed to the more complex geologic conditions encountered at the Keathley Canyon site. Real-time data were transmitted to the surface throughout the drilling of the KC 151-2 well. Some extraneous pump noise affected the data transmission, but caused minimal real-time data loss. In comparison to the Atwater Valley wells, the quality of the pulsed ProVision data was vastly improved in the KC 151-2 well.

After completion, the BHA was pulled back to sea floor while running a sweep of heavy drilling mud. The tools were pulled out of the hole at 08:30 CT on May 9, 2005, the drill bit cleared the rig floor at 09:45 CT on May 9, 2005, and the recorded LWD data were retrieved at the rig floor at 11:45 CT on May 9, 2005. It was later determined that the ARC tool failed to record any data into the tool memory because of a software problem. Thus, we have only MWD pulsed (real time) data from ARC and APWD tools; which was limited to the ARC "blended" resistivity measurement (Figure 11) and the APWD temperature and pressure measurements (Figures 2 and 3).

It is also important to note that the KC 151-2 well began to flow water (probably a high salinity brine) and a small amount of gas while tripping the LWD BHA out of the hole. A barite kill mud was pumped through the LWD BHA to control the well. It was speculated that the source of the water flow was from a deep horizon near the TD of the hole. But a thick sand section at a depth of 100 mbsf, later determined to contain high salinity pore waters (also characterized by very low electrical resistivities), could have been the source of this shallow water flow. The shallow sand at 100 mbsf also exhibited a slight APWD measured annular pressure response of about a 300 kPa increase when originally drilled (Figure 3).

Log Quality

After the completion of LWD operations in the KC 151-2 well, a highly reduced version of the "primary" set of downhole recorded well log data was transferred to the onboard science party for initial analysis. For this report, we have loaded this primary data set into Microsoft Excel and generated a series of well log displays; which has been included with this report (Figures 1-13).

As noted earlier in this report, the target rate-of-penetration (ROP) of 30 m/hr (± 5 m/hr) in the interval from the seafloor to the total depth (TD) of the well was generally achieved, with instantaneous ROPs ranging from about 15 m/hr to about 35 m/hr (Figure 1). The quality of RAB images is quite high; however it appears that the RAB image in the first 10 m of the hole may have been degraded by low ROPs.

The caliper log (DCAV), which provides a measurement of the diameter of the borehole as recorded by the VDN density tool is the best indicator of borehole conditions (Figure 4). The calculated differential caliper values (assuming a bit size of 8-1/2 inches) are <1 inch over 75% of the total section in KC 151-2. With the uppermost 20 mbsf of the hole characterized by significant washouts, as is the section from about 25 mbsf to about 110 mbsf. This lower interval is dominated by a series of thin sand units and one thick sand section at 95-110 mbsf. The bulk density correction (IDDR), calculated from the difference between the short- and long-spaced density measurements, varies from 0 to as high as +0.1 g/cm^3, which shows some deterioration in the quality of the density measurements (Figure 6).

The depths, relative to seafloor, for all of the LWD logs were fixed by using the *Uncle John* ROV to identify the actual BHA bit contact with the sea floor and shifting the log data to the appropriate depth as determined by the drillers' pipe tallies. For KC 151-2 it was determined that the seafloor was at a depth of 1335.0 mbrf. The rig floor logging datum was located 13.2 m above sea level for this hole.

Interpretation of LWD Logs

LWD gamma ray measurements suggests that the KC 151-2 well penetrated mostly a fine-grained clay dominated sedimentary section, except for one thick sand section at 95-110 mbsf. There are also several notable sand rich sections deeper in the well near 140 and 150 mbsf. The low gamma ray values and slightly elevated density porosity values within the upper 35 m of the well are in part a product of bad borehole conditions. The most notable characteristic of the KC 151-2 well is a high resistivity interval (measured by both the GVR6 and the ARC tools) within the section from about 220 mbsf to 300 mbsf, which probably indicates the occurrence of gas hydrates (Figures 10 and 11). RAB images from this high resistivity interval, also reveals the presence of numerous steeply dipping (82 plus degrees) fractures throughout this section.

The other most significant well log response is the relatively subtle resistivity response within the interval 371-392 mbsf associated with the expected depth of the BSR (seismic inferred at 385mbsf). The comparison of the ARC measured resistivity data (blended resistivity) with that RING resistivities recorded by the GVR6 reveal that within the "high resistivity interval" from 220 mbsf to 300 mbsf, the ARC measured resistivities were significantly higher than those measured by the GVR6. The reason for this discrepancy is unclear at this time, but it may be related to the way these two tools function.

Log Porosities

Sediment porosities can be determined from analyses of recovered cores and from numerous borehole measurements. Data from the LWD density, neutron, and nuclear magnetic resonance logs have been used to calculate sediment porosities in the KC 151-2 well. The VDN log-derived measurements of bulk-density (Figure 7) in KC 151-2 for the most part ranges from about 1.7 g/cm^3 to 2.05 g/cm^3, with values less than about 1.5 g/cm^3 near the seafloor. The density log measurements are degraded in the upper 25 mbsf, as discussed earlier in this report. The LWD log-derived bulk density measurements from KC 151-2 were used to calculate sediment porosities ($\varnothing$) using the standard density-porosity relation: $\varnothing=(\rho m-\rho b)/(\rho m-\rho w)$. Water densities ($\rho w$) were assumed to be constant and equal to 1.05 g/cm^3; while the grain/matrix densities (ρm) were assumed to be 2.65 g/cm^3 for each log density porosity calculation. The density-log derived porosities for the most part range from about 37 to 60 percent (Figure 8), with the most notable high porosity zone in the interval from 88 mbsf to 107 mbsf. However, the density log porosities near the top of the hole (above 45 mbsf), ranging from 50 to near 80 percent, is in part controlled by degraded borehole conditions. The LWD neutron porosity log (Figure 9) yielded sediment porosities ranging from an average value at the top of the logged section of about 62% to near 50% at the bottom of the hole. NMR data were transmitted to shore for processing to estimate bound fluid volume and total free fluid porosity and for comparison with neutron, density, and core porosity estimates. The sediment porosities derived by the LWD NMR tool are very similar to the both the density and neutron log derived porosities.

Gas Hydrate

The presence of gas hydrates was not fully verified by coring in the KC 151-3 well. In several instances IR identified cold spots in cores, mousey sediment textures in the recovered cores, and anomalous low pore water salinity values inferred the presence of gas hydrate. Several, of the recovered pressure cores also indicated gas concentrations exceeding normal solubility, but no gas hydrate was physically observed. However, the conspicuous LWD measured high resistivity zone in the KC 151-2 well from 220 mbsf to 300 mbsf is indicative of a gas hydrate or free gas bearing sediments. It is also possible that very low pore water salinities could yield the high resistivity values observed in this anomalous section. Subsequent analysis of pore waters from cores in this interval, however, revealed elevated pore water salinities with values exceeding 50 ppt. Also since this anomalous section is well above the base of the BSR inferred gas hydrate stability field, it is unlikely that this interval contains free gas. It is also important to note that a portion of this interval from about 220 mbsf to 258 mbsf (plus other sections) are characterized by relatively low acoustic transit-times (high acoustic velocities) as recorded by the DSI wireline tool in the KC 151-3 well, which is also indicative of gas-hydrate-bearing sediment.

Both the GVR6 (Figure 10) and the ARC (Figure 11) resistivity logs also reveal a zone of elevated resistivities around depth of the expected BSR, between 371 mbsf and 392 mbsf. In this case we cannot easily differentiate between the occurrence gas hydrate or free gas; and since we failed to log this interval with the wireline DSI tool in the AT 151-3 well we are unable to conclusively identify the actual contact between gas hydrate and free gas section (i.e., the BSR) at this site.

Resistivity log data have been used to quantify the amount of gas hydrate at KC 151-2. For the purpose of this discussion, it is assumed that any high resistivities measured in the KC 151-2 well are due to the presence of gas hydrate or possibly free-gas at the depth of the BSR. The Archie relation ($S_w=(aR_w/\varnothing^m R_t)^{1/n}$) was used with resistivity data (R_t) from the LWD RAB tool and porosity data ($\varnothing$) from the VDN density tool to calculate water saturations. It should be noted that gas hydrate saturation (S_h) is the measurement of the percentage of pore space in a sediment occupied by gas

hydrate, which is the mathematical complement of Archie derived water saturations (S_w), with S_h=1-S_w.

For the Archie relation, the formation water resistivity (R_w) were calculated assuming a constant pore water salinity of 34.4 ppt (sea water salinity). However, pore water salinities calculated from recovered core water samples in KC 151-3 were often very high, exceeding 50 ppt. It was decided for now, to take a conservative approach and assume a sea water salinity, which would yield generally higher water saturations (or lower gas hydrate saturations). The Archie *a* and *m* variables were calculated using a cross plot technique (a=0.62, m=2.15), which compares the downhole log derived resistivities and density porosities (Figure 12). The APCT temperature data obtained from the KC 151-3 well revealed an equilibrium seabed temperature of 4.79°C and a geothermal gradient of about 3.0°C/100m.

The Archie relation generally yielded water saturations from 100% to as low as 60%. The low water saturations in the upper 110 mbsf of the well is likely in error and is a product of density log data that has been degraded by enlarged borehole conditions. In Figure 13, the previously identified high resistivity interval from 220 mbsf to 300 mbsf is characterized by relatively low water saturations or high gas hydrate saturations, with inferred peak gas hydrate saturations averaging about 30%. The BSR feature however is marked by only a very small reduction in water saturations at a depth of 388 mbsf.

The review of the well log data from KC 151-2 does suggests the presence of significant gas hydrate occurrences. As previously noted above, the RAB images in the high resistivity interval from 220 mbsf to 300 mbsf, reveals the presence of numerous steeply dipping fractures throughout this section. It is likely that the RAB imaged fractures are the “reservoir” or void space in which the deep reading resistivity inferred gas hydrates occur in the KC 151-2 well.

Borehole Temperature and Pressure Data
The APWD measured borehole pressures (DHAP) generally indicate a uniform pressure gradient with depth (Figure 3), with some pressure deviations associated with running heavy mud sweeps near the end of pipe connections. The anomalous APWD pressure response near 100 mbsf needs to be further examined. The DHAT temperature log indicates that the circulating fluids were cooled in their descent in the drill pipe to a relatively uniform temperature in the range of 6-9 degrees Celsius (Figure 2).

Table 1. Keathley Canyon 151-2 LWD/MWD Logging Program

Water depth: 1335.0 m RKB
Drillers TD: 1794.8 m RKB
RKB above sea level: 13.2 m

Date	Time (CT)	Depth of drill bit (mbrf)*	Event
7-May-05	1:31	0.0	Move LWD/MWD tools to pipe rack and initialize tools
	10:22	0.0	Begin to pickup LWD/MWD tools and run into hole
	12:00	128.0	Pump test LWD/MWD tool string, test fails, pull BHA to surface
	13:23	0.0	Swap in Power Pulse and ARC, re-initialize tools and RIH
	15:30	65.0	Pump test LWD/MWD tool string, past test
8-May-05	6:35	1335.0	Spud well, controlled drill 100 GPM, 25 m/hr ROP, 50 RPM
	8:10	1358.6	Bring pump rate up to 360 GPM, MWD powered up, problem with GVR6
9-May-05	20:40	1794.8	Well reached TD at 459.8 mbsf
	22:06	1794.8	Start trip of BHA to sea floor, running heavy mud sweep
	8:30	1335.0	BHA clears sea floor
	13:00	1335.0	Begin trip of BHA to the rig floor
	9:45	0.0	BHA clears rig floor and laid down tools
	11:45	0.0	LWD/MWD log data transfer completed

*1m = 3.28084ft

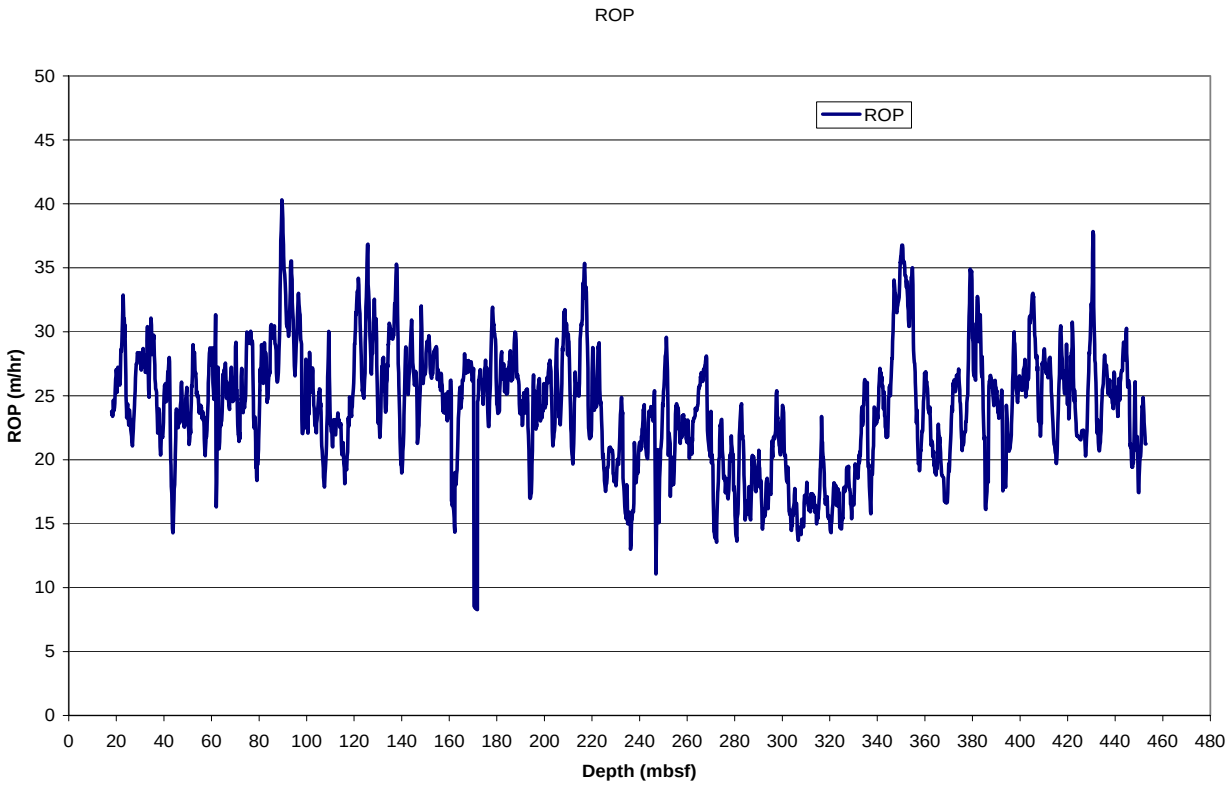

Figure 1. Rate of penetration (ROP) while drilling the KC 151-2 well (real time data).

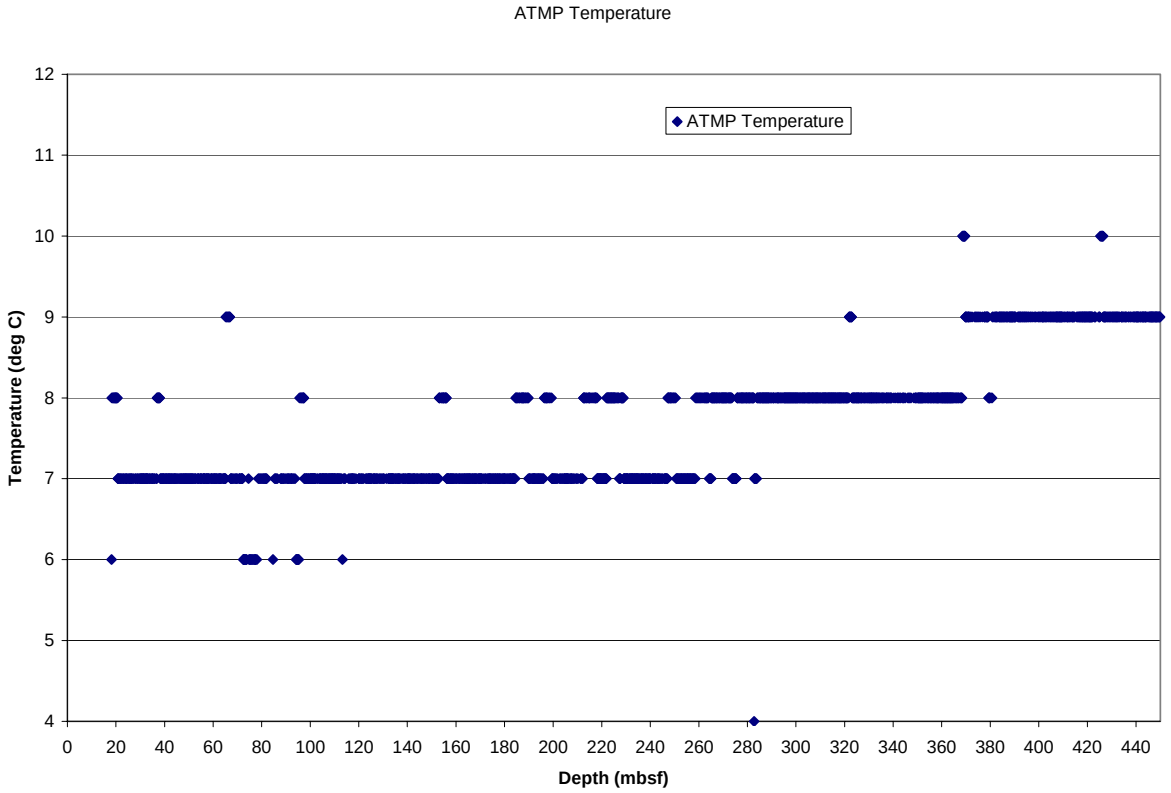

Figure 2. Annular temperature for KC 151-2 from the APWD tool (real time data).

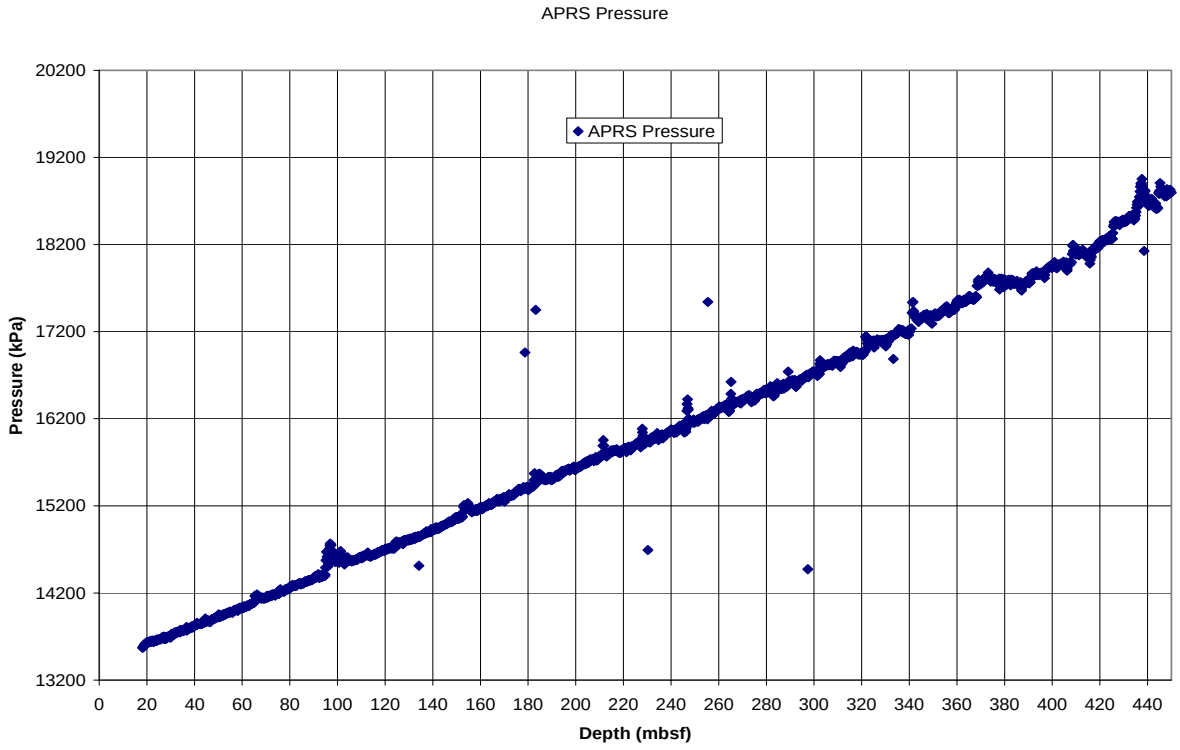

Figure 3. Annular pressures recorded (APWD tool) in the KC 151-2 well (real time data).

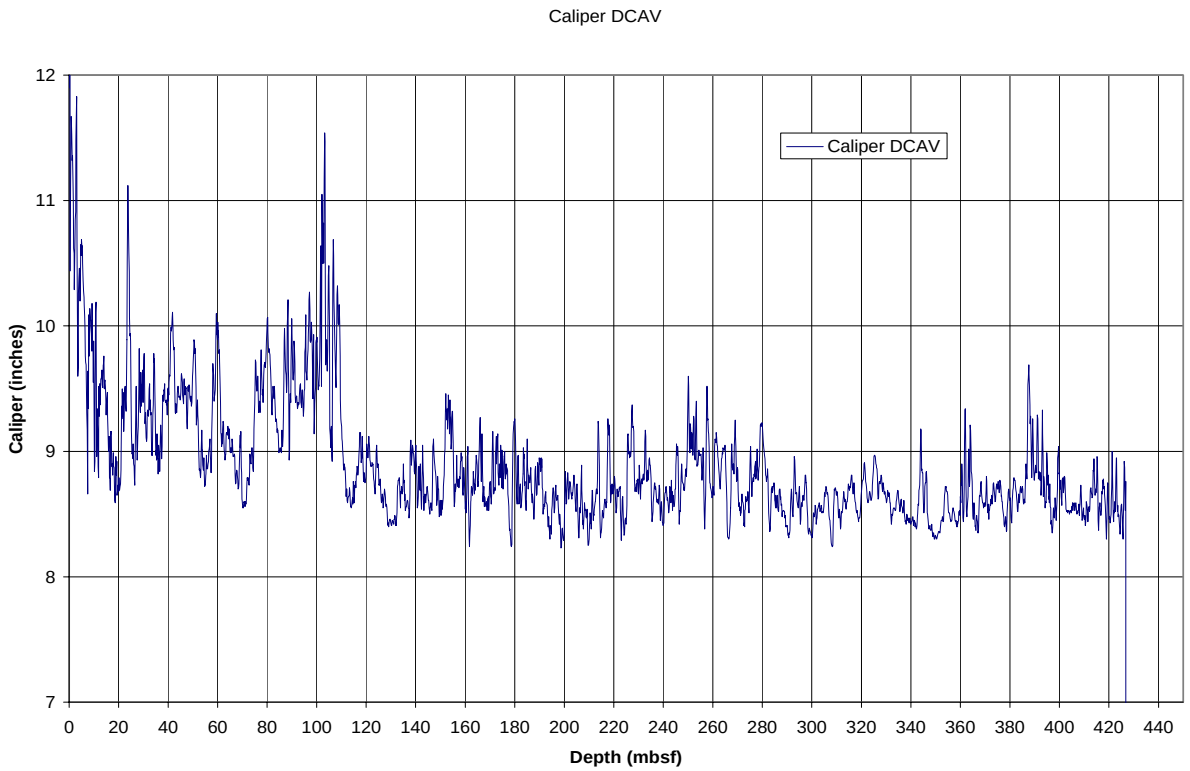

Figure 4. Borehole density caliper as measured by the VDN tool in the KC 151-2 well (recorded data).

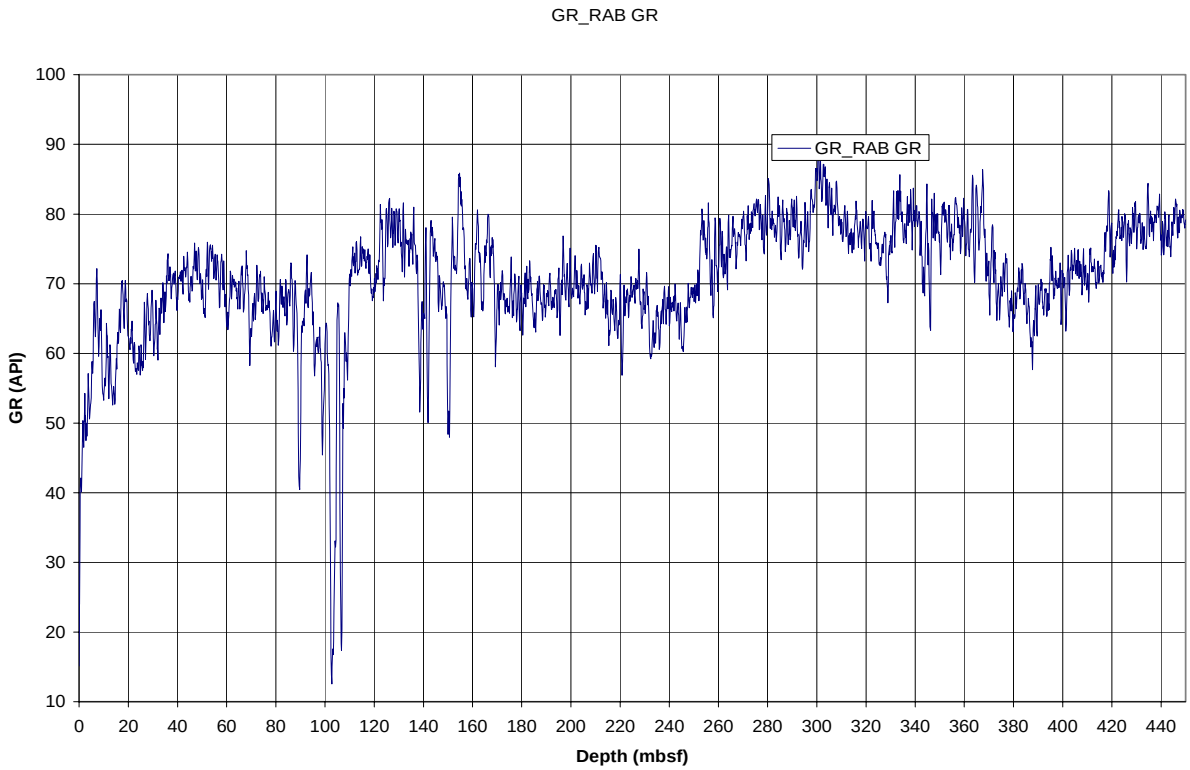

Figure 5. Gamma ray log as measured by the GVR6 tool in the KC 151-2 well (recorded data).

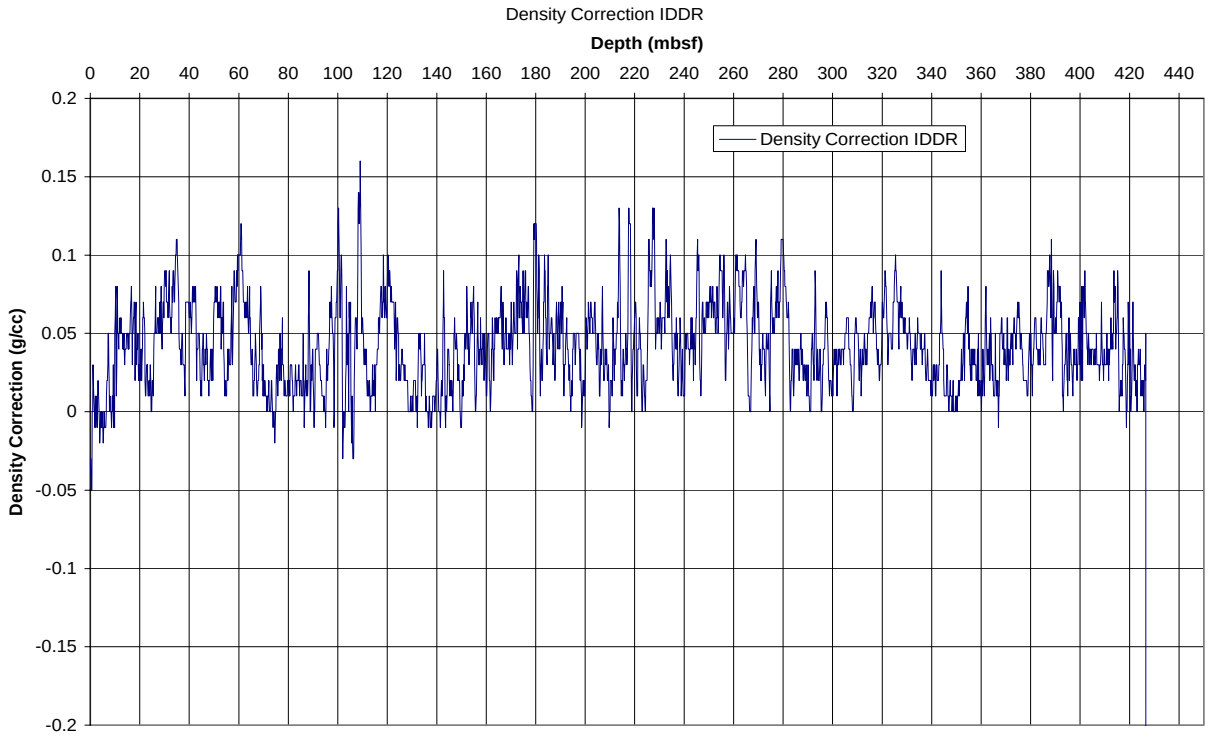

Figure 6. Density log correction for the density log as measured by the VDN tool in the KC 151-2 well (recorded data).

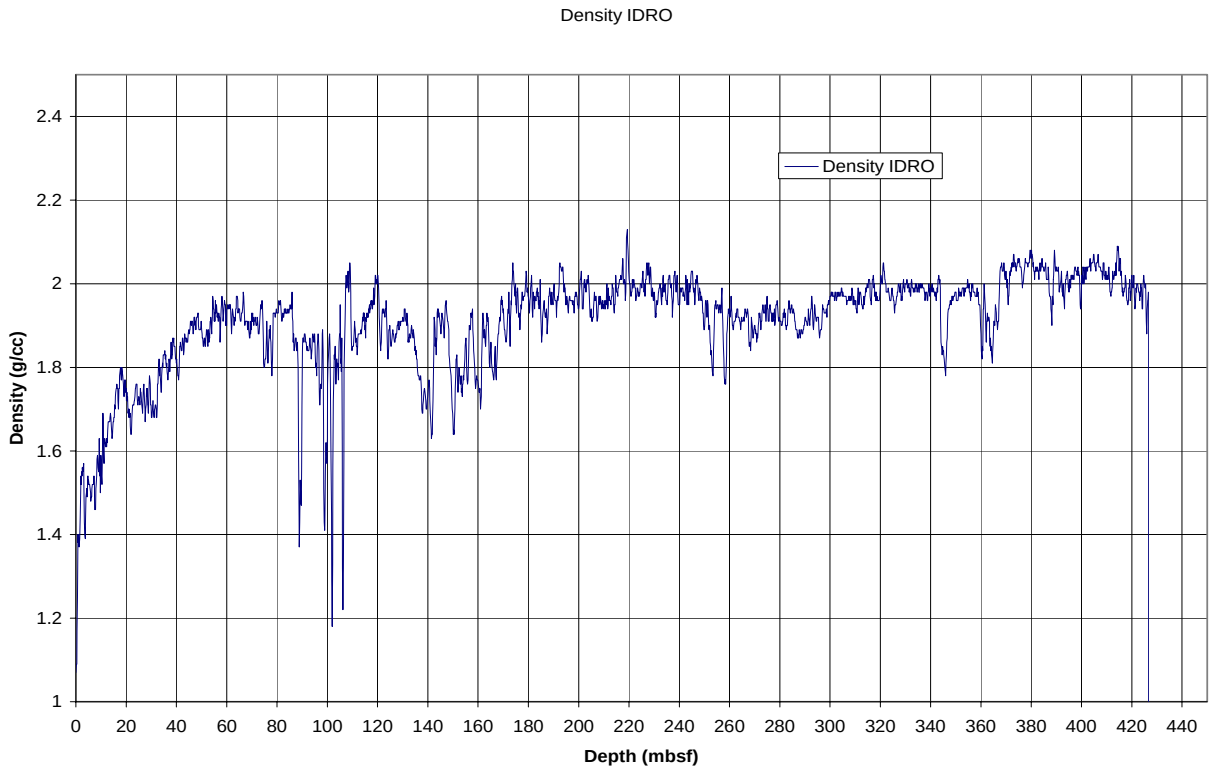

Figure 7. Density log as measured by the VDN tool in the KC 151-2 well (recorded data).

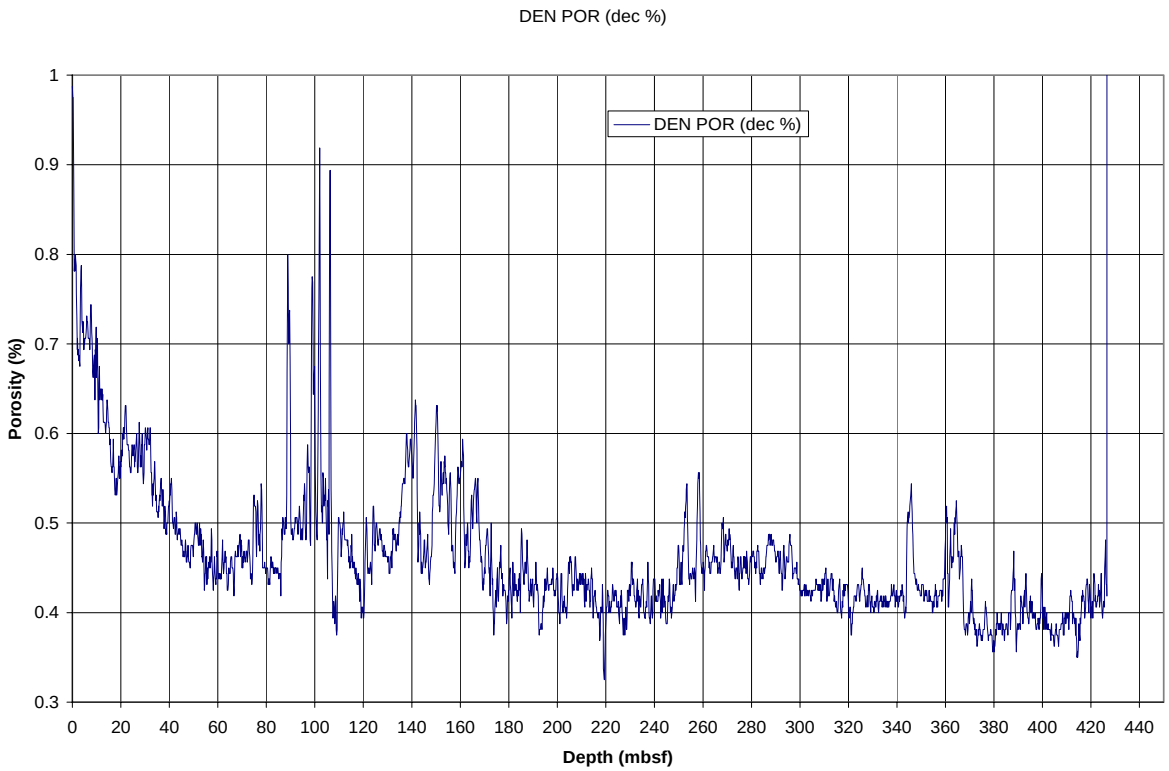

Figure 8. Density log derived porosities in the KC 151-2 well (recorded data).

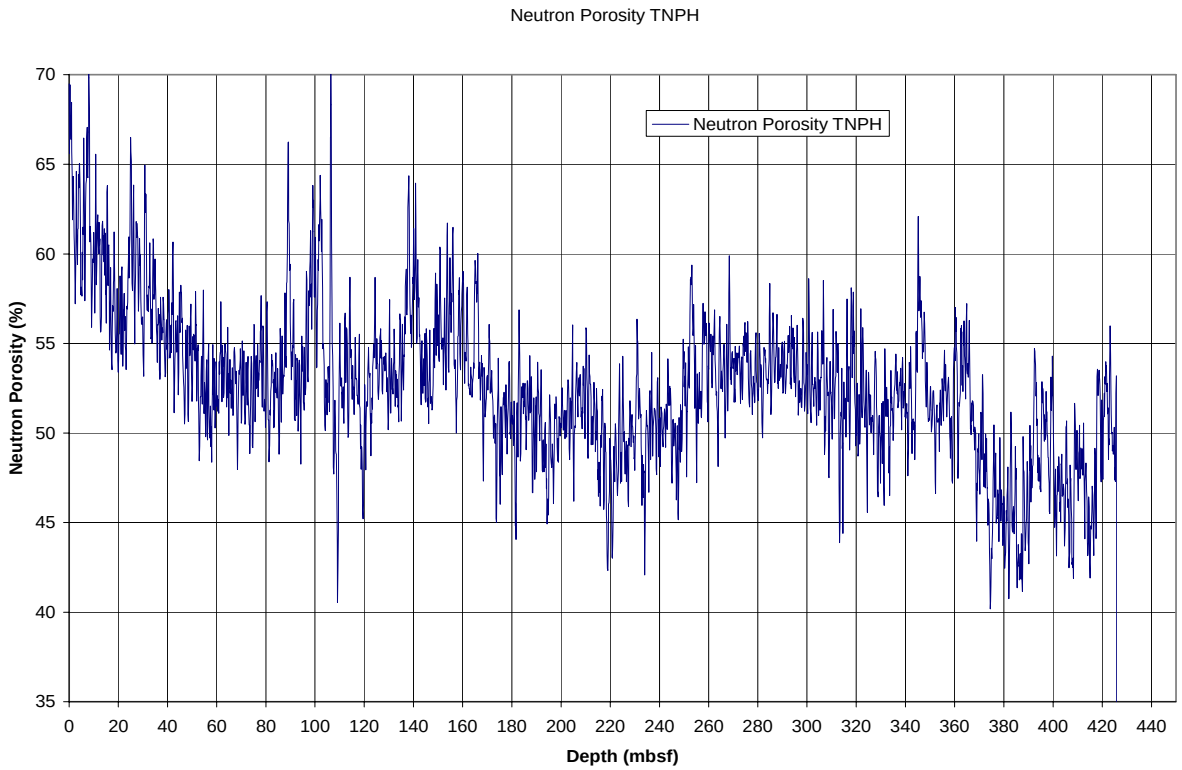

Figure 9. Neutron porosity log as measured by the VDN tool in the KC 151-2 well (recorded data).

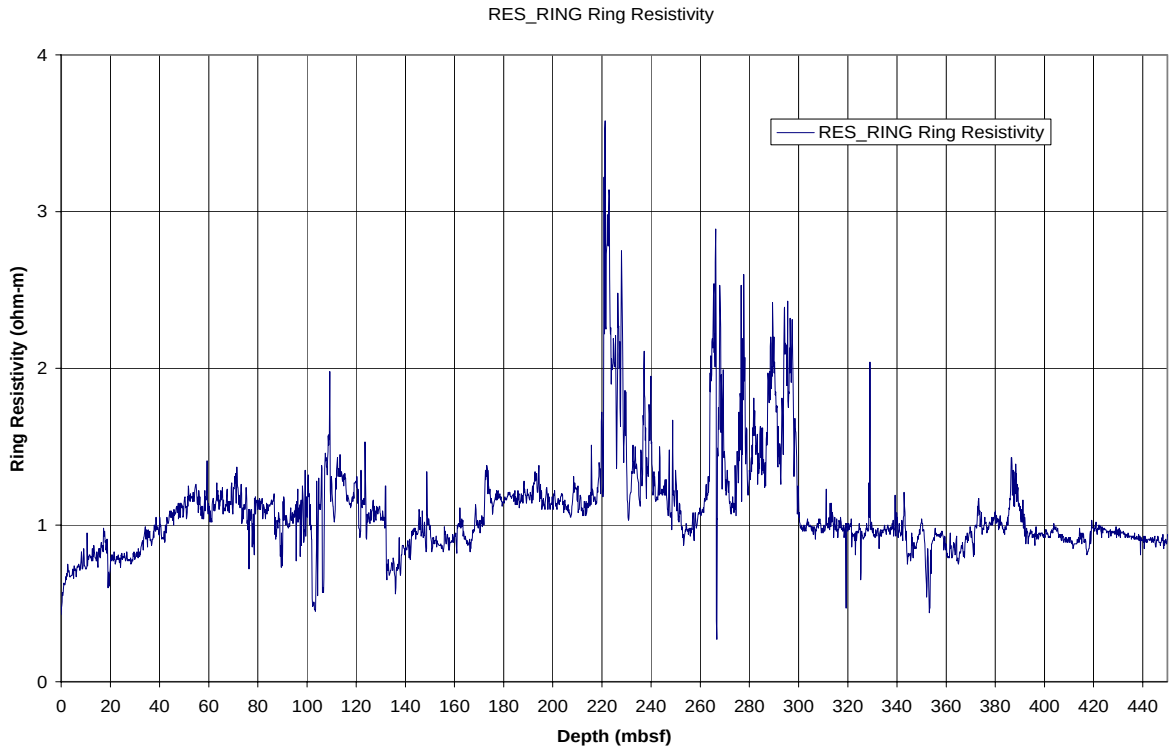

Figure 10. Ring resistivity log as measured by the GVR6 tool in the KC 151-2 well (recorded data).

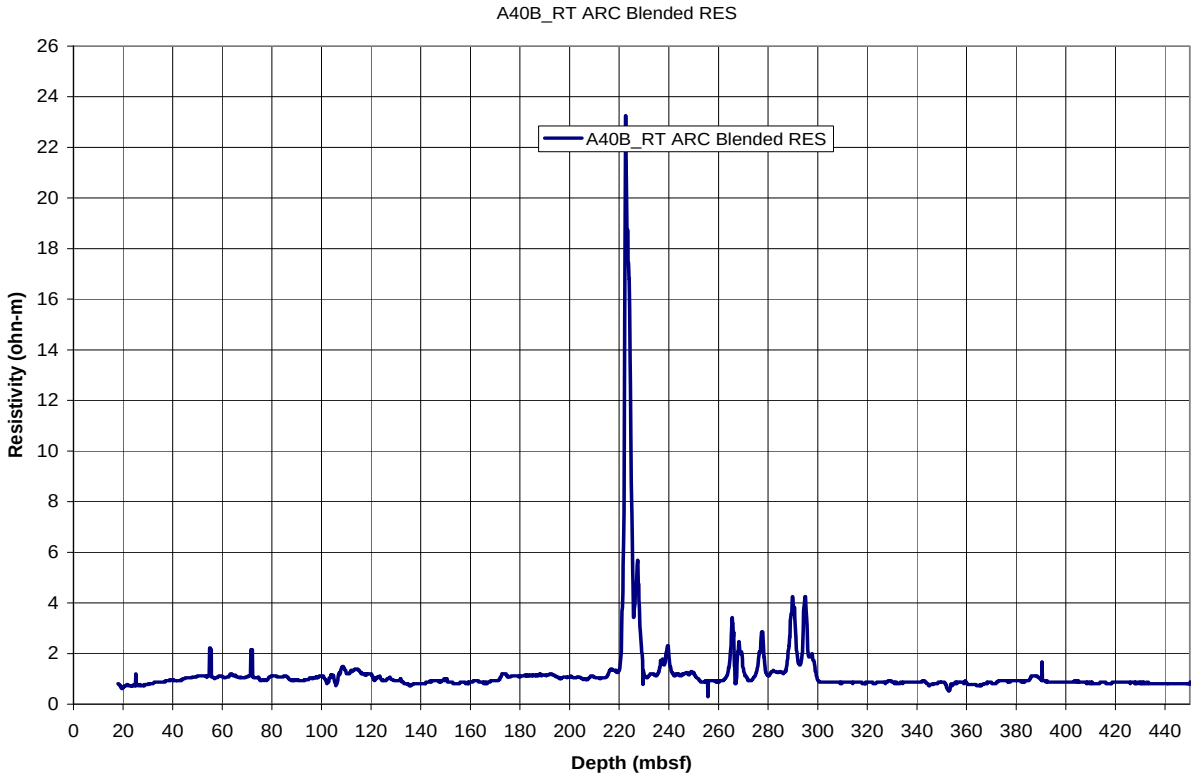

Figure 11. Deep blended resistivity log as measured by the ARC tool in the KC 151-2 well (recorded data).

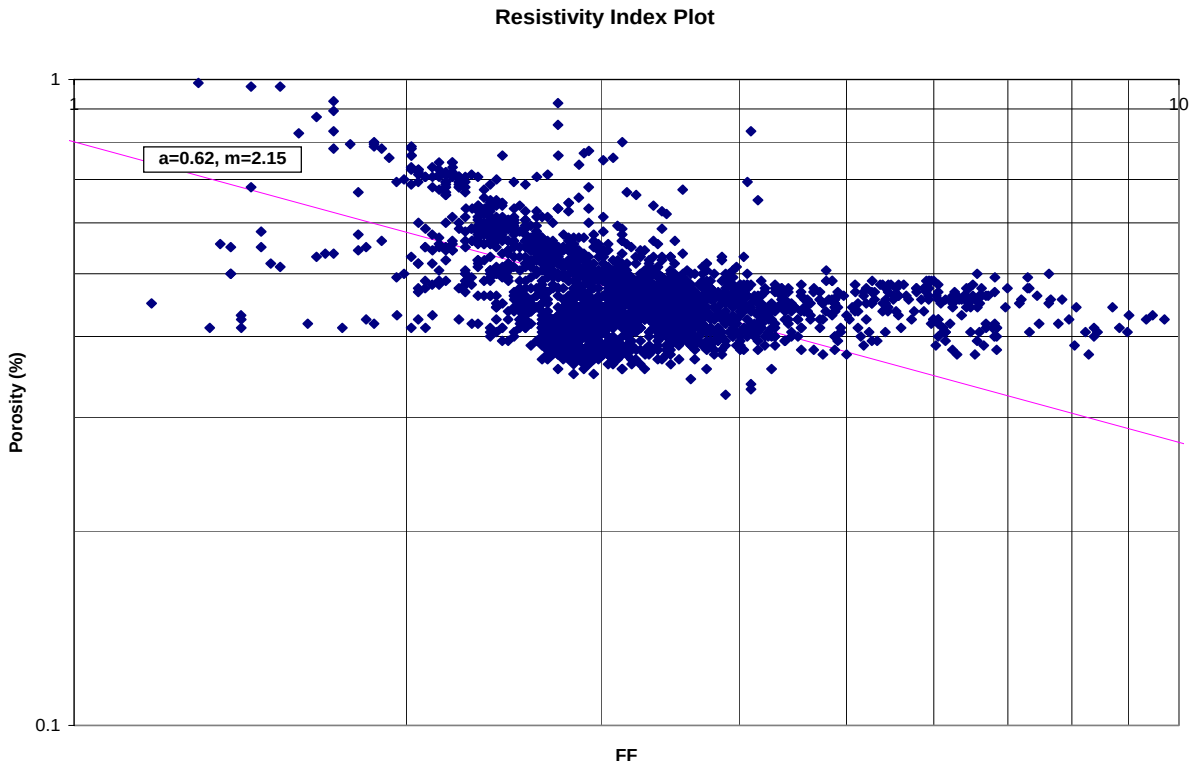

Figure 12. Resistivity index plot (formation factor vs. porosity) for the KC 151-2 well (recorded data).

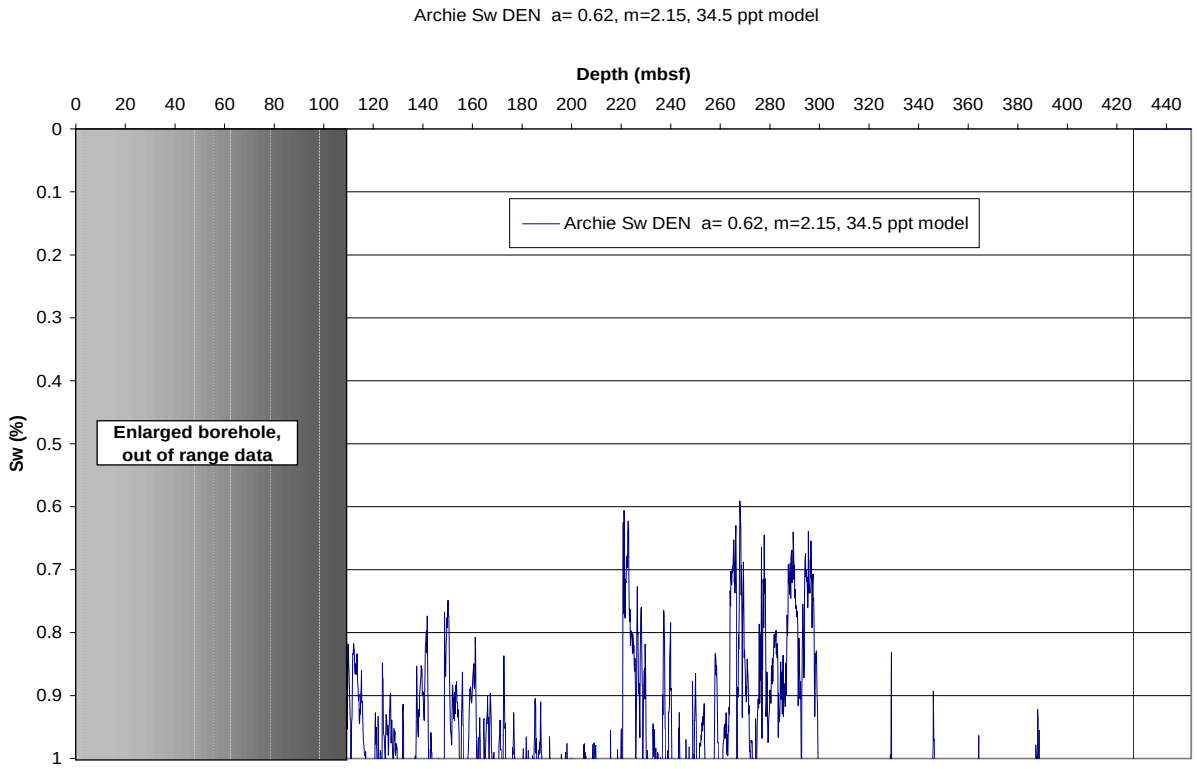

Figure 13. Archie derived water saturations for the KC 151-2 well (recorded data).

Keathley Canyon 151-3

-WIRELINE AND VSP LOGGING-

Operations

The drilling objectives at the Keathley Canyon 151 site was to further characterize the possible occurrence of gas hydrate related bottom simulating reflector (or BSR). Seismic lines from both high resolution research seismic surveys and from regional 3D surveys through the Keathley Canyon 151 proposed drill site reveal the presence of a BSR at a depth of about 380 mbsf. Thus, the Keathley Canyon 151 block contains one of the rare instances of a BSR in the Gulf of Mexico, and may indicate the occurrence of gas hydrates at depth.

Keathley Canyon 151-3 (KC 151-3) was cored (FHPC, FC, HRC, FPC) and drilled to a total depth of 444.1 mbsf (drillers depth). Conventional wireline logging (CWL) operations began at 03:00 CT on May 19, 2005 with makeup of the DSI-GR-GPIT tool string and ended with the final rig-down for the VSI tool at 15:15 CT on May 19, 2005. See Table 1 for detailed information on the KC 151-2 CWL program. Figures 2 and 3 in the *Explanatory Notes* shows the configuration of the FMS-sonic tool and the VSI tool. For the most part the KC 151-3 well was drilled with only sea water as the drilling fluid, but as the hole was advanced periodic sweeps of Attapulgite based drilling mud was used to sweep and stabilize the hole. Additional sweeps of a polymer based mud was used to clear the KC 151-3 well. A barite kill mud was also used to control a water flow problem that developed after the well was drilled and before the deployment of the CWL tools.

CWL operations in KC 151-3, began with the deployment of the FMS-sonic tool (GR-DSI-GPIT) without the FMS tool. After the drill pipe exiting problems experienced in the AT 13-2 well, it was decided remove the FMS tool from the CWL tool string deployed in the KC 151-3 well. In the KC 151-3 well, the GR-DSI-GPIT tool string exited the drill pipe without any problems; however, we did require several attempts to re-enter the drillpipe after the uphole main pass of the tool string.

The GR-DSI-GPIT tool string reached a depth of only 341 mbsf, some 103.1 m above the drillers TD of 444.1 mbsf and 44 m above the depth of the expected BSR (385 mbsf). Because of concerns associated with borehole stability problems, a down going log was collected while tripping in at 245 m/hr. Also the drillpipe was set at a relatively deep depth of 123 mbsf, to avoid expected borehole stability problems in the overlying section. The down going DSI survey was acquired in BCR mode, with the monopole source ran at a “standard central frequency” of 12.5 kHz. Excellent quality data were acquired during the main up hole pass, at a wireline speed of 245m/hr. During the uphole main pass the DSI survey was acquired in BCR mode, with the monopole source set at a lower frequency of 6 kHz. Without the FMS tool, we were unable to mechanically centralize the DSI tool. Also we had no caliper measurements to evaluate the hole conditions. The shuttle clamps from the VSI tool (acquired during the VSP survey), however, showed only a slightly enlarged borehole with the hole diameter seldom exceeding 11 inches (bit size was 8.75 inches). The sonic waveforms recorded from the two DSI log runs (downhole and uphole passes) suggests that we acquired generally high quality compressional wave acoustic data, but the shear wave coherence plot revealed only a faint shear-wave coherence. The very low velocity of the formation made it difficult for the automatic slowness/time coherence (STC) picking program to select accurate compressional- or shear-wave velocities. Some adjustment of the STC parameters allowed for improved compressional- and shear-wave picking, but still further reprocessing will be required.

After completing the GR-DSI-GPIT log run, the VSI tool (VSP logging tool) was assembled and lowered to a depth of 337.3 mbsf (Tables 1 and 2). The VSI was configured using four geophone shuttles (approximately 2.06 m spacing with rigid interconnections) and combined with a natural gamma ray tool. One uphole vertical incident or zero-offset VSP experiment was conducted in the KC 151-3 well. During the vertical incidence VSP operations in the KC 151-3 well, the shuttles were mechanically clamped against the borehole wall and the source (1520 cubic inch guns in a Dual Itaga Air Gun Array) on the *Uncle John* was fired between 6 and 10 times by control hardware in the Schlumberger logging unit. The VSI tool was then unclamped and pulled 8.5 m uphole, maintaining a 2.06 m receiver station depth spacing throughout the hole. The VSI recorded the full seismic waveform for each firing. These waveform data were stacked by the Schlumberger recording software and output in both LDF (internal Schlumberger format) and SEG-Y formats. The VSP survey in the KC 151-3 well was conducted in the interval from 334 mbsf to 124 mbsf, with 26 open hole stations and 104 individual shuttle clampings.

The depths, relative to seafloor, for the GR-DSI-GPIT log runs and the VSP survey were fixed by using the *Uncle John* ROV to identify the actual BHA bit contact with the sea floor and shifting the log data to the appropriate depth as determined by the drillers' pipe tallies. For KC 151-3 it was determined that the seafloor was at a depth of 1335.0 mbrf. The rig floor logging datum was located 13.1 m above sea level for this hole. The absolute logger's depth, relative to seafloor, will be further analyzed post cruise by identifying the gamma ray signal associated with the seafloor and depth shifting the log data appropriately.

Interpretation of Wireline Logs

After the completion of CWL operations in the KC 151-3 well, a highly reduced version of the "primary" set of the GR-DSI-GPIT well log data was transferred to the onboard science party for initial analysis. For this report, we have loaded this primary data set into Microsoft Excel and generated two well log displays (Figures 1 and 2). The well log data plots of compressional- and shear-wave transit times for KC 151-3 show relatively high quality CWL logs.

Gamma ray measurements from the GR-DSI-GPIT tool string also indicates that the KC 151-3 well penetrated mostly a fine-grained clay dominated sedimentary section, except for one thick sand section at 95-110 mbsf. There are also several notable sand rich sections deeper in the well near 139-143 mbsf and 150-165 mbsf (similar to those observed in the LWD gamma ray data from the KC 151-2 well).

As discussed in the LWD logging report for KC 151-2, the presence of gas hydrates was not fully verified by coring in the KC 151-3 well. In several instances cold spots, mousey sediment textures in the recovered cores, and anomalous low pore water salinity values inferred the presence of gas hydrate. Several, of the recovered pressure cores also indicated gas concentrations exceeding normal solubility, but no gas hydrate was physically observed. However, the conspicuous LWD measured high resistivity zone in the KC 151-2 well from 220 mbsf to 300 mbsf is indicative of a gas hydrate bearing sediment. It is also important to note that a portion of this interval from about 220 mbsf to 258 mbsf (plus other sections) are characterized by relatively low acoustic transit-times (high acoustic velocities) as recorded by the DSI wireline tool in the KC 151-3 well, which is also indicative of gas-hydrate-bearing sediment.

It is important to highlight, that portions of the CWL and LWD logged sections in both of the Keathley Canyon wells are characterized by zones of distinct high resistivities and high acoustic velocities (low acoustic travel-times), with the resistivity in one relatively thin zone exceeding 22.0 ohm-m and compressional-wave transit-times as low as 155 msec/ft. As previously discussed in the Explanatory Notes, gas hydrate occurrences are generally characterized by increases in log measured electrical resistivities and acoustic velocities.

Table 1. Keathley Canyon 151-3 Wireline Logging Program

Water depth: 1335.0 m RKB
Drillers TD: 1776.1 m RKB
RKB above sea level: 13.1 m

Date	Time (CT)	Depth of logging string (mbrf)	Event
18-May-05	14:30	0.0	Drilled well to total depth (441.1 mbsf)
	16:25	0.0	Begin wiper trip to 306.1 mbsf, return to bottom of hole
	17:15	0.0	Well flowed during wiper trip, killed with 12lb/g mud
	20:45	0.0	Begin mud displacement run to 123.0 mbsf
19-May-05	3:00	0.0	Begin picking up logging tools
	3:35	0.0	Running into hole at 1200 m/hr
	4:40	1458.0	DSI tool exits drillpipe, 123.0 mbsf
	4:40	1458.0	Logging down at 245 m/hr, DSI medium frequency
	5:32	1676.0	Reached loggers TD at 341 mbsf
	5:32	1676.0	Logging up at 245 m/hr, DSI low frequency
	6:14	1458.0	DSI tool entered drillpipe
	8:10	0.0	Pulled logging tools to the derrick floor, 1200 m/hr
	8:15	0.0	Rig up for VSP survey and RIH at 1200 m/hr
	9:45	1421.8	Conduct air gun and tool check
	9:58	1458.0	VSP tool exits pipe, RIH at 245 m/hr
	10:35	1672.3	Reach loggers new TD at 337.3 mbsf
	10:40	1669.0	Begin up logging at 8.4m stations w/ 4 shuttles
	13:28	1459.0	Complete up log VSP, 26 stations w/ 4 shuttles
	13:30	1458.0	VSP tool entered drillpipe, POH 1200 m/hr
	15:15	0.0	Pulled tools to the derrick floor and laid down tools

*1m = 3.28084ft

Table 2. Keathley Canyon 151-3 VSP stations and shots, four shuttle VSI tool at 2.06 m spacing.

Water depth: 1335.0 m RKB
Drillers TD: 1776.1 m RKB
RKB above sea level: 13.1 m

Station Number	Depth of deepest shuttle (mbrf)	Shot numbers
1 (pipe)	1429.1	xx
2	1669.0	28-31
3	1660.9	32-35
4	1652.7	36-40
5	1644.5	41-48
6	1636.3	49-53
7	1628.0	54-58
8	1619.7	59-63
9	1611.4	64-69
10	1603.2	70-76
11	1595.0	77-82
12	1586.6	83-91
13	1578.4	92-97
14	1570.2	98-103
15	1562.0	104-110
16	1553.6	111-116
17	1545.4	117-123
18	1537.1	124-129
19	1528.9	130-136
20	1520.7	137-143
21	1512.5	144-150
22	1504.1	151-161
23	1495.8	162-172
24	1487.6	173-179
25	1479.3	180-186
26	1471.2	187-193
27	1462.8	194-201
28 (pipe)	1429.1	202-208

*1m = 3.28084ft

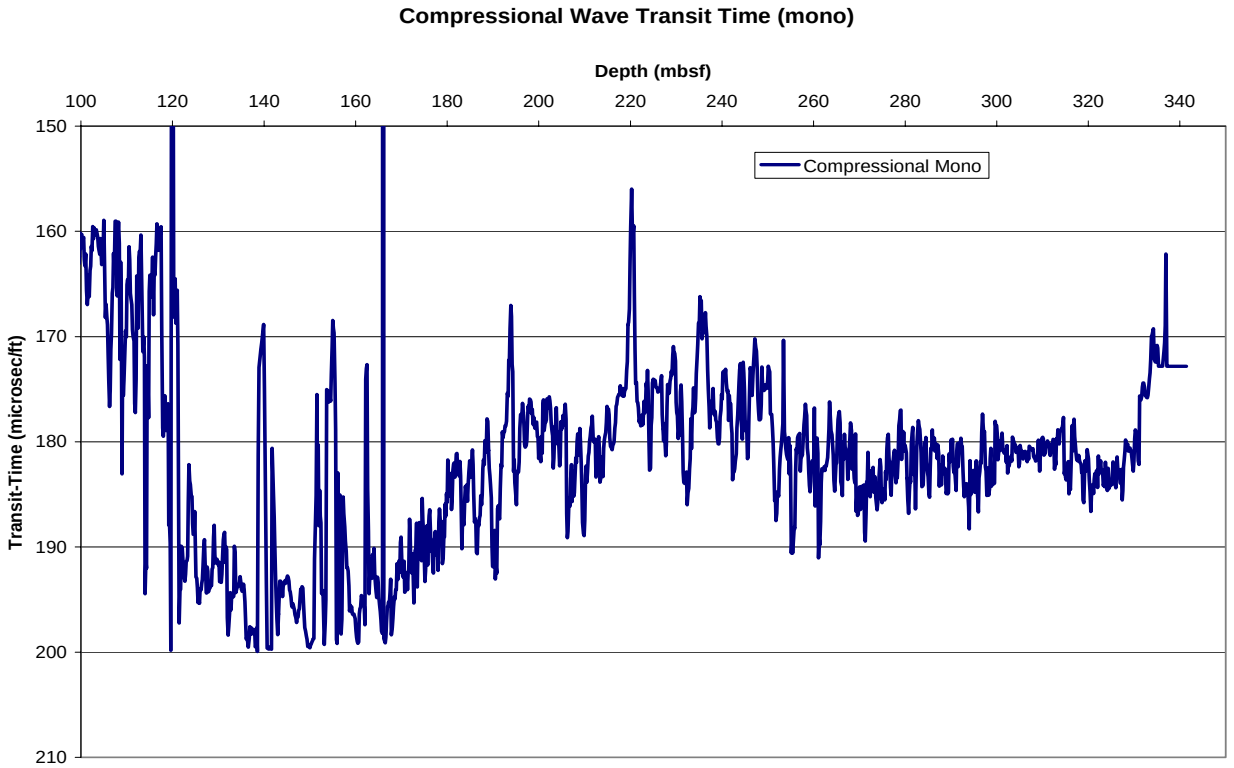

Figure 1. Compressional-wave acoustic transit-time log data from the DSI tool run in the KC 151-3 well.

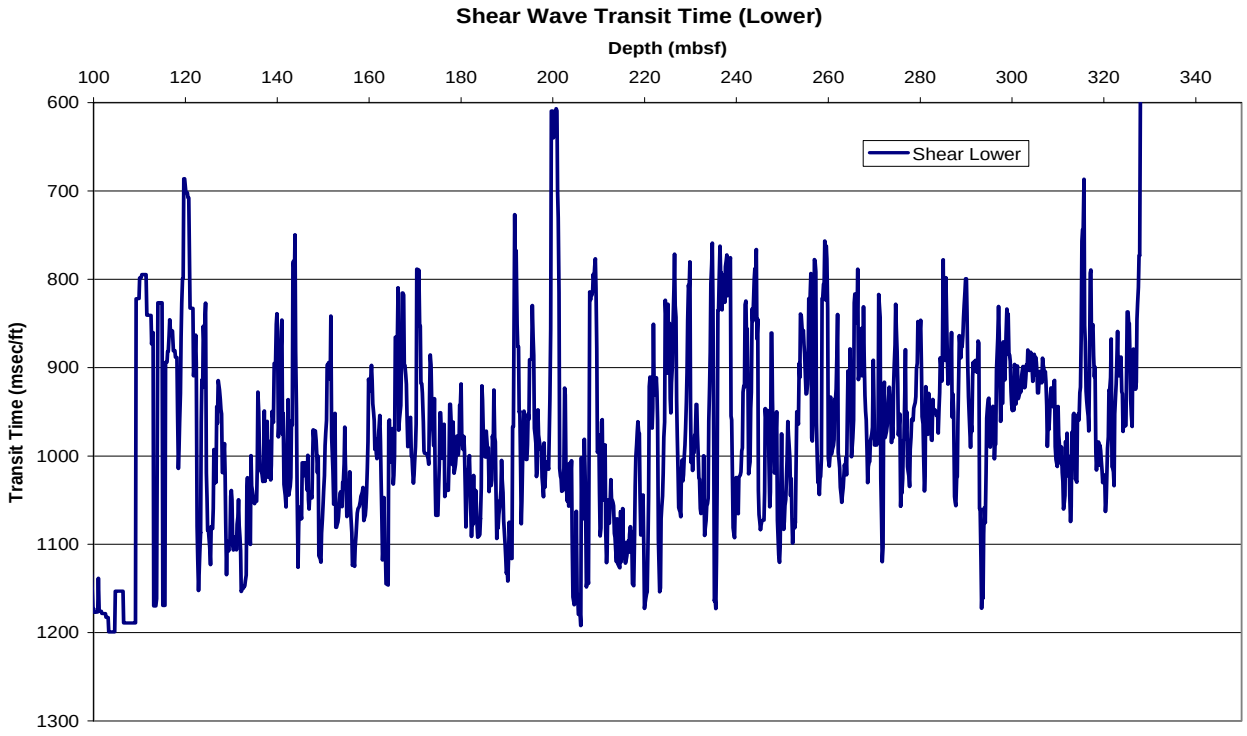

Figure 2. Shear-wave acoustic transit-time log data from the DSI tool run in the KC 151-3 well.

Natural Gas Geochemistry—2005 Gulf of Mexico JIP Cruise

Tom Lorenson, Jennifer Dougherty
U.S. Geological Survey
Menlo Park, CA
and
George Claypool
Lakewood, CO

Introduction

Natural gas components in sediment cores were monitored during the cruise for the presence or absence of and for the general level of hydrocarbon abundance. When gas was present in sufficient amounts, samples were collected for more detailed chemical and isotopic analyses post-cruise in shore-based laboratories. Gas was monitored to determine if sediments contained sufficient gas concentration and composition to support the presence of gas hydrate, and to determine the origin of the gas. Possible gas sources evaluated are those produced locally by sedimentary microbial processes or thermogenic gas from underlying petroleum accumulations.

The two areas selected for coring and logging, Atwater Valley and Keathley Canyon, were evaluated in previous cruises by analysis of near-surface sediments recovered by gravity and piston cores. Gas hydrates have previously been recovered in shallow coring operations (unpublished JIP data), and are widespread on the continental slope of the northern Gulf of Mexico (Milkov and Sassen, 2001).

Methods

The shipboard organic geochemistry program for JIP Gulf of Mexico gas hydrate program included three routine sets of analyses: (1) analysis for volatile hydrocarbons in sediment by the headspace method including methane, ethane, and propane (C_1–C_4) and fixed natural gases (i.e., O_2, CO_2, and N_2+Ar); (2) measurement of free gas or gas voids in cores (VG) for C_1–C_4 and fixed natural gases; and (3) analysis of gas collected from the FPC or HPC cores also for C_1–C_4 and fixed natural gases. These samples were augmented by the onshore analysis of void gas and PCS/HRC gas samples for C_1-C_5 hydrocarbons and fixed natural gases. Selected samples of void gas or pressure core gas were analyzed for the carbon isotopic composition of C_1, C_2, and CO_2.

Procedures used during the JIP are adapted from Ocean Drilling Program standard methods described by Pimmel and Claypool (2001). Comments on routine sampling and deviations from standard practice are noted below.

Gas Sampling. Samples for headspace (HS) analysis were collected next to the interstitial water sample to integrate the interstitial water and gas datasets. The sampling frequency was increased in the uppermost 10-m of sediment to achieve high-resolution sampling at the sulfate-methane interface (SMI). Upon core retrieval, a 5-mL sediment

sample was collected with a 5-mL cut-off plastic syringe from a freshly exposed end of a core section and was extruded into a 21-mL glass serum vial. The samples were immediately sealed with a 20-mm thick septum and metal crimp cap and heated to 60°C for 20 min. Air blanks incubated with septum fragments inside confirmed that no hydrocarbons (C_1-C_3) were released by the septum. Sediment volume was estimated from weight, recorded to nearest 0.1 gm using density as determined by logs or physical properties. Methane concentration was estimated as millimoles per liter (mM) of pore water, using the expression

CH_4 (mM) = CH_4 (ppmv) x (21/[sample weight/density] – 1) x (1/[porosity x 24,300]).

In most cases, density and fractional porosity were assumed to be 1.65 gm/cc and 0.6 respectively.

Gas samples from expansion voids were collected by piercing the core liner with a penetration tool equipped with a 3-way valve and allowing gas to expand into a 60 or 140 ml syringe. Excess gas was stored in pre-evacuated 30-ml serum vials capped with butyl-rubber stoppers and over-pressured by injecting about 60-ml of sample gas into a vial for shore-based analyses.

Gas samples from pressure (FPC or HPC) cores were trapped in large water-filled collection chambers and sub-sampled by syringe. Samples were drawn at various times from successive increments from the start to the end of core degassing. Gas samples were injected onto the GC shortly after collection. Excess gas was injected into an evacuated 30-ml serum vial for shore-based analyses.

Onboard gas analyses were preformed on an Agilent 3000-micro gas chromatograph equipped with 2 independent columns. Column 1 is a 8-m x .32 mm PLOT U column that separates C_1-C_4 hydrocarbons, air gases (O_2 + N_2+ Ar – one peak), H_2S and CO_2. Column 2 is a 10-m x .32 mm MolSieve 5A PLOT column that separates O_2, N_2+Ar, CO_2, and CO. Detection limits vary but at best are about 15 ppmv for methane and increase for higher molecular weight gases such that the detection limit for butane is about 100 ppmv. Precision of the measurements varies from 0.5 to 2%. The GC is controlled by Ezchrom software run from a Windows operating system laptop computer.

In all analyses, the gas composition is expressed as parts per million by volume (ppmv) of gas component relative to the standard volume of gas injected. Major variation in the C1 ppmv results for gas samples mainly reflects dilution of the gas samples with air. Only the HS results were recalculated to reflect gas content relative to a volume of sediment pore water.

Gas taken directly from gas voids in 60 or 140-ml syringes were injected directly on to the GC for analysis. Gas concentrations are expressed in ppmv and normalized to methane. Gas samples taken from the FPC and HPC cores were treated in the same manner.

Shore based analyses. A Shimadzu GC-14A gas chromatograph equipped with a Chemipack C-18, 6 ft. x 1/8 in. 80/100 mesh stainless steel column was used to measure C_1-C_8 hydrocarbon gases. The GC-14A is configured with a 1-mL, valve-actuated, sample loop for injection, and a flame ionization detector (FID) for gas detection. Samples were introduced by syringe at atmospheric pressure, and a minimum of 10 mL of gas was used to flush the injection loop. Run conditions were 35° C for 1.5 minutes ramping up at 20°/minute to 150°C , and held. Helium was used as the carrier gas at a constant mass flow rate of 3 kg/cm^2. FID temperature was held at 150°C.

Gas concentration data are reported for a series of hydrocarbons given in order of elution methane (C_1), ethane (C_2), propane (C_3), isobutane (iC_4), normal butane (nC_4), neopentane ($neoC_5$), isopentane (iC_5), and normal pentane (nC_5). Approximate detection limits for all hydrocarbon compounds are 0.05 parts per million by volume (ppmv).

Carbon isotopic ratio determination. Stable carbon isotope ratio determinations of C_1, C_2, and CO_2 were made on a Continuous Flow–Isotope Ratio Mass Spectrometer (Finnigan MAT 252 GC-C-IRMS) at the School of Earth and Ocean Sciences (SOES), University of Victoria, Canada. Samples are introduced by syringe into a SRI gas chromatograph (GC) via a gas sample valve (loop volumes: 10, 100 or 200 μL). Analytes are separated at 40°C on a 30 m GS-Q column (0.32 mm ID) with a carrier gas flow of 1.8 mL/min ultra-high purity helium. After gas partitioning on the GC, the gas then passes through a CuO/Pt microcombustion oven at 850^{o}C. This oven quantitatively converts the hydrocarbon gases to carbon dioxide and water. The combusted sample products are then passed through a Nafion™ tube to remove water from the combustion and any that may be in the carrier gas. The purified CO_2/He pulse is scaled by an open-split interface, and then transferred into the GC-C-IRMS. Isotope ratios are referenced to the conventional PDB standard through a known CO_2 isotope standard that is added at the open split to the sample runs several times during the analysis.

For stable carbon isotope ratio measurements on the sample CO_2, the gas was partitioned on the GC as above. The microcombustion oven was bypassed for the CO_2 measurements, but the gas stream was dried, split and measured by CF-IRMS in a manner similar to the light hydrocarbons.

Results

Headspace gas. The results for headspace gas analyses are presented in Table 1. Headspace gas analyses were performed on 67 samples from cores collected at the AT13-2, AT14-1, ATM-1, ATM-2, and KC151-3 sites. Core number, core type, and section number within the core designate samples from each site. The H designation indicates a sample from an FHPC core, C indicates FC cores, and PC indicates push cores deployed by the ROV. Samples range in depth from 0.2 to 379.21 meters below seafloor (mbsf). The cored sediments contained residual methane calculated as dissolved in pore water at concentrations ranging from zero or non-detectable near the surface to 14.9 mM at 23.75 mbsf in hole ATM-2 (Table 1).

Table 1.--Headspace gas (air-free) and residual dissolved methane content.

Hole-Core-sect.	Depth mbsf	C1 ppmv	C2 ppmv	C3 ppmv	C1 mM
AT13-2-					
PC1-1	0.2	0	0	0	0.0
PC4-1	0.2	0	0	0	0.0
1H-2	1.00	580	0	0	0.8
1H-5	4.00	310	0	0	0.4
1H-7	6.00	220	0	0	0.2
2H-2	8.01	1,375	0	0	5.2
2H-5	11.01	4,690	0	0	1.5
2H-7	13.01	7,350	0	0	2.0
4H-2	19.54	1,680	0	0	1.0
4H-6	23.44	6,970	0	0	1.8
6H-2	29.65	1,790	0	0	0.7
6H-5	32.65	5,790	0	0	1.8
8H-3	41.62	8,310	0	0	2.5
8H-5	44.35	6,710	0	0	2.3
9H-4	121.26	12,050	0	0	3.6
9H-7	124.26	10,460	0	0	3.8
11H-4	129.80	12,900	0	0	3.5
11H-6	131.80	16,410	0	0	4.1
13H-3	143.12	8,290	10	0	2.7
13H-6	148.62	20,760	10	0	5.2
14H-2	158.89	15,840	10	0	4.0
AT14-1-					
PC2-1	0.2	7,480	0	0	1.7
PC5-1	0.2	12,770	10	0	5.2
PC7-1	0.2	29,150	0	0	9.1
ATM1-					
1H-2	1.00	14,990	0	0	4.0
1H-3	2.00	4,290	0	0	1.5
2H-2	8.94	4,660	0	0	1.4
2H-3	10.89	5,930	0	0	2.1
2H-6	12.94	2,630	0	0	0.6
5H-3	20.90	3,130	0	0	1.2
5H-6	23.90	10,040	0	0	4.8
5H-8	25.90	350	0	0	0.1

Table 1.--Continued.

Hole-Core-sect.	Depth mbsf	C1 ppmv	C2 ppmv	C3 ppmv	C1 mM
ATM2-					
1H-2	1.00	8,220	0	0	3.1
1H-3	2.25	9,600	0	0	3.9
2H-4	11.87	6,490	0	0	2.4
2H-6	12.92	5,320	0	0	1.8
3H-4	20.74	7,090	0	0	1.6
3H-4	23.75	31,870	0	0	14.9
KC151-3-					
PC1-1	0.20	540	0	0	0.2
1H-2	1.00	0	0	0	0.0
1H-4	3.00	0	0	0	0.0
1H-6	5.00	0	0	0	0.0
2H-2	10.45	38,800	0	0	10.3
2H-4	12.45	53,690	0	0	13.8
2H-6	14.45	48,620	10	0	12.7
3H-4	21.59	15,360	0	0	4.0
3H-6	23.59	10,260	0	0	3.2
4H-6	32.74	7,760	0	0	1.9
4H-8	34.74	4,300	0	0	1.3
5H-4	40.19	5,590	0	0	2.0
7C-1	213.58	3,990	0	0	1.0
8C-3	216.73	7,940	0	0	2.8
10C-3	225.11	2,950	0	0	1.7
12C-1	231.07	4,700	0	0	1.6
12C-3	232.12	3,410	0	0	1.9
14C-3	244.01	5,280	0	0	1.8
15C-3	253.35	3,070	0	0	1.3
17H-2	257.73	3,380	0	0	1.5
17H-4	259.98	4,720	0	0	2.2
19H-3	276.62	8,650	0	0	4.9
19H-7	280.62	8,580	0	0	4.4
20H-3	294.91	3,420	0	0	1.4
21H-2	312.51	8,680	0	0	3.3
22C-3	332.40	8,850	0	0	3.2
23C-1	350.57	7,560	0	0	2.7
24C-2	370.42	6,570	20	1.6	2.3
25C-1	379.21	4,100	0	0	1.5

Table 2.--Composition of gas from expansion voids in cores, normalized to air-free basis.

Hole- Core	Depth	C1	C2	C3	iC4	nC4	neoC5	iC5	nC5	H2S	CO2	C1/C2	$\delta^{13}C$ (‰)		
Section (cm)	mbsf	ppmv	ppmv	ppmv	ppmv	ppmv	ppmv	ppmv	ppmv	ppmv	ppmv		CO2	C1	C2
AT13-2-															
2H-4 (100)	11.01	923,000	23.1	7.1	3.9	1.7	183.3	0.0	0.0	77,100	0	40,000			
2H-9 (0)	15.01	973,000	70.1	0.0	0.0	0.0	0.0	0.0	0.0	0	27,800	13,900		-76.3	
4H-3 (98)	21.52	990,000	99.4	1.9	0.8	0.2	1.5	0.2	0.1	0	10,400	10,000			
4H-6 (50)	24.04	992,000	141.6	2.0	0.4	3.5	0.0	0.0	0.0	0	8,400	7,100			
4H-8 (39)	25.93	989,000	133.1	1.6	0.3	0.8	0.0	0.0	0.0	0	11,300	7,500		-75.5	
6H-2 (76)	30.41	985,000	173.6	4.0	0.5	0.2	0.9	0.2	0.1	0	15,600	5,700	-5.7	-75.1	
6H-4 (44)	31.85	991,000	175.9	2.0	0.2	6.2	0.0	0.0	0.0	0	9,200	5,700		-75.0	
6H-8 (26)	35.91	989,000	170.8	3.0	0.5	0.2	0.9	0.2	0.1	0	10,900	5,800		-75.5	
8H-3 (97)	42.59	994,000	158.6	0.8	0.1	15.3	0.0	0.0	0.0	0	6,200	6,300	-5.6	-75.2	
8H-6 (16)	44.81	998,000	884.9	0.4	0.1	73.4	0.0	0.0	0.0	0	1,600	1,200			
8H-8 (72)	46.53	991,000	221.4	2.3	0.3	50.9	0.0	0.0	0.0	0	9,500	4,500			
13H-6 (0)	140.21	962,000	242.0	8.6	3.1	0.8	5.6	0.8	0.2	0	38,500	4,000		-84.3	
13H-7 (18)	141.12	972,000	182.3	0.0	0.0	0.0	0.0	0.0	0.0	0	28,300	5,400			
14H-1 (0)	149.27	909,000	323.9	9.9	20.6	1.1	70.6	1.5	2.4	0	90,700	2,900		-82.1	
ATM-1-															
1H-2 (18)	1.20	988,000	34.9	2.2	0.3	0.2	1.6	0.1	0.1	0	12,200	28,400			
2H-1 (78)	8.70	987,000	166.4	2.5	0.2	0.1	0.9	0.0	0.0	0	13,600	6,000	-2.0	-71.5	
2H-2 (72)	9.67	987,000	167.3	2.1	0.2	0.1	0.8	0.0	0.0	0	13,200	5,900		-71.7	
2H-3 (60)	10.54	990,000	192.7	2.0	0.2	0.1	0.8	0.0	0.0	0	10,300	5,200			
5H-5 (50)	23.40	991,000	34.1	0.0	0.0	0.0	0.0	0.0	0.0	0	9,500	29,100			
5H-8 (22)	26.12	981,000	147.3	3.8	0.4	0.2	1.1	0.0	0.0	0	19,200	6,700		-71.7	
ATM-2-															
1H-2 (15)	1.15	991,000	41.8	2.5	0.2	0.1	0.9	0.0	0.0	0	9,100	23,800	-7.3	-71.6	
1H-2 (95)	1.95	991,000	42.1	2.8	0.2	0.1	0.9	0.0	0.0	0	9,100	23,600			
2H-2 (19)	9.12	989,000	116.2	2.2	0.3	0.2	1.3	0.0	0.0	0	11,700	8,600		-71.7	
3H-5 (2)	21.39	989,000	141.6	1.8	0.2	0.2	0.9	0.0	0.0	0	11,700	7,000	-5.6	-71.8	-48.4
3H-5 (35)	21.72	988,000	370.8	2.7	0.3	0.1	1.2	0.0	0.0	0	12,100	2,700			
3H-5 (92)	22.30	990,000	202.2	1.9	0.3	0.1	1.2	0.0	0.0	0	10,800	4,900			
3H-6 (94)	22.31	991,000	163.0	1.9	0.2	0.1	0.9	0.0	0.0	0	9,800	6,100			
3H-8 (60)	24.97	991,000	169.3	1.9	0.2	0.0	1.2	0.0	0.0	0	8,900	5,900		-72.0	
KC151-3-															
2H-7 (93)	16.38	998,000	80.4	7.6	17.8	1.1	0.0	0.3	0.1	1,310	1,000	12,500		-78.2	
3H-1 (98)	19.57	996,000	65.9	3.1	0.8	1.0	0.5	0.1	0.0	0	4,000	15,200	-12.8	-77.3	
3H-4 (19)	21.78	997,000	53.4	5.0	8.9	0.9	0.0	0.2	0.0	0	3,600	18,700		-76.1	
3H-5 (12)	22.71	998,000	48.1	3.1	0.4	0.8	0.4	0.1	0.1	0	2,300	20,800		-76.6	
3H-7 (64)	25.23	998,000	65.3	3.3	0.8	0.9	0.9	0.1	0.1	0	2,600	15,300		-76.4	
3H-8 (32)	25.91	996,000	55.0	4.7	9.4	1.0	0.0	0.2	0.1	0	4,100	18,200		-75.2	
4H-1 (47)	28.21	997,000	119.8	5.4	7.9	0.9	0.0	0.2	0.1	0	3,600	8,400	-9.6	-74.6	
4H-2 (71)	29.45	999,000	49.3	0.0	0.0	0.0	0.0	0.0	0.0	0	1,800	20,300			
4H-8 (4)	34.78	996,000	90.0	5.0	6.8	0.9	0.0	0.2	0.1	0	4,600	11,100		-74.0	
4H-8 (58)	35.32	997,000	61.5	5.9	9.1	0.9	0.0	0.2	0.1	0	3,300	16,300		-74.0	
5H-3 (52)	39.81	998,000	64.0	5.6	6.2	0.9	0.0	0.2	0.1	0	2,400	15,600		-73.8	
5H-5 (30)	41.49	998,000	66.8	5.2	6.7	0.7	0.0	0.2	0.1	0	2,100	15,000		-73.7	
5H-7 (70)	43.96	998,000	53.5	5.3	6.0	0.6	0.0	0.2	0.0	0	2,300	18,700		-73.8	
6C-2 (29)	101.27	996,000	156.2	1.0	5.6	0.1	0.0	0.1	0.0	0	4,400	6,400		-72.5	
6C-2 (70)	101.67	996,000	48.4	1.3	6.9	0.1	0.0	0.1	0.0	0	5,000	20,600		-72.2	
6C-3 (98)	102.97	994,000	18.6	1.8	6.4	0.1	0.1	0.1	0.0	0	6,600	53,500	-3.0	-72.1	
17H-2 (36)	257.39	994,000	38.7	7.6	9.1	1.6	0.0	0.5	0.3	0	6,400	25,700		-72.4	
17H-3 (11)	258.13	996,000	91.8	6.5	7.3	1.4	0.0	0.3	0.1	0	4,500	10,900	-8.9	-72.6	
17H-5 (63)	260.66	997,000	53.2	7.7	8.1	1.5	0.0	0.4	0.2	0	3,600	18,800		-72.6	
19H-3 (54)	277.16	997,000	79.1	15.3	13.7	2.7	0.0	0.7	0.4	0	3,800	12,600		-72.4	
19H-3 (73)	277.35	996,000	88.2	13.1	14.4	2.3	0.1	0.6	0.3	0	4,600	11,300		-72.5	
19H-4 (8)	277.70	997,000	52.9	9.3	8.9	1.7	0.0	0.4	0.2	0	3,600	18,900		-72.3	
19H-8 (34)	281.96	998,000	63.5	7.8	7.5	1.4	0.0	0.4	0.1	0	2,500	15,800		-72.4	
20H-3 (65)	295.56	991,000	740.9	2.4	7.7	0.4	0.0	0.2	0.1	0	9,000	1,400		-72.6	-65.3
20H-5 (50)	297.50	998,000	104.6	3.7	9.3	0.6	0.0	0.3	0.0	0	2,500	9,600		-72.5	
20H-8 (52)	300.43	997,000	46.8	18.3	25.7	3.6	0.0	1.4	0.6	0	3,300	21,400		-72.3	
21H-1 (71)	312.22	995,000	51.9	8.6	14.3	1.3	0.0	0.5	0.2	0	5,400	19,200	-11.3	-72.1	
21H-2 (56)	313.07	991,000	70.0	14.2	43.5	1.4	0.2	0.1	0.0	0	9,200	14,200		-71.7	

Theoretical dissolved methane saturation in pore water ranges from about 50 mM at the seafloor to ~130 mM at depth of 400 mbsf in KC151-3, whereas equilibrium saturation under shipboard atmospheric conditions is on the order of 1-2 mM. Residual concentrations estimated in all headspace samples were far less than the solubility of methane for a given depth, mainly because of gas loss during core recovery. $\delta^{13}C$ values of headspace gas samples were not measured because of incomplete recovery and potential for fractionation.

Expansion Void gas. The results for analyses of gas from expansion voids in the cores are given in Table 2. Expansion void gases are primarily from FHPC (H) cores taken at the two deep coring sites (AT 13-2, KC 151-3) and the two Mound sites (ATM-1, ATM-2). Free gas or void gas samples were collected from 56 different intervals and range in depth from 1.2 to 313.1 mbsf (Table 2). The void gas samples primarily contained methane, although C_2-C_5 hydrocarbons were also detected in nearly all samples with increasing concentration with depth. Carbon dioxide concentrations ranged from below detection to 90,693 parts per million by volume (ppmv), with both the minimum and maximum concentrations found in hole AT13-2, and are tabulated with other gas data in Table 2. Hydrogen sulfide gas (7.7% and 0.13%) was observed only in the shallowest void gas samples from holes AT13-2 and KC151-3, respectively. Carbon isotopic composition of methane from void gas samples ranged from –84.3 to –71.5 ‰. All of the methane in expansion void gas samples from the mound sites (ATM-1, ATM-2) has very uniform isotopic composition ($\delta^{13}C = -71.8 \pm 0.3$‰). Expansion void gas samples from AT13-2 have heavier methane (-76.3 to –75.0 ‰) in samples from shallow depth intervals (15.1 to 42.6 mbsf), and the lightest methane observed (-84.3, -82.1 ‰) in the deepest samples from this site (140.2, 149.3 mbsf). The carbon isotopic composition of expansion void gas from the KC151-3 hole shows a more regular pattern, with the $\delta^{13}C$ of methane decreasing monotonically from –78.2 to –73.8 ‰ over the depth interval from 16.4 to 42.6 mbsf. Deeper samples (101 to 313 mbsf) at KC151-3 are fairly uniform in isotopic composition with methane $\delta^{13}C$ in the range of –72.6 to –71.7 ‰. The carbon isotopic composition of carbon dioxide was determined for ten samples, and for ethane in two samples of the expansion void gas samples. $\delta^{13}C$ of CO_2 ranged from –12.8 to –3‰, while the ethane values were –48.4 and –65.3‰.

Pressure Core Gas. Gas was collected from four pressure core samples (2 FPC, 2 HRC) from well ATM-2 and KC151-3 (Table 3). Gas composition of pressure cores was consistent with that of void gas at comparable depths, however CO_2 concentrations were approximately 1 order of magnitude lower. The decrease in concentration may be related to the sample collection method, whereby gas must first pass through the water-filled PCS chamber and into a water-filled inverted graduated cylinder. An exception to diminished CO_2 contents occurred in KC151-3-11P with the first 5 sampling intervals with normalized CO_2 values are up to 943,000 ppmv. Because these samples were more contaminated with air, these concentrations somewhat are suspect. Pressure core gases also confirmed the presence of C_2-C_5 hydrocarbons, with concentrations ranging from below detection to 678 ppmv. Values for C_1/C_2 ratio of pressure core gases ranged from ~1,900 to ~11,900 with indication that C1 is relatively enriched in the initial gas given off in the degassing procedure. The methane $\delta^{13}C$ values for pressure core gases are

Table 3.--Composition of gas from pressure core, normalized to air-free basis.

Hole-Core	Depth mbsf	Time Sampled	C1 ppmv	C2 ppmv	C3 ppmv	iC4 ppmv	nC4 ppmv	neoC5 ppmv	iC5 ppmv	nC5 ppmv	CO2 ppmv	C1/C2	$\delta^{13}C$ (‰) CO2	C1	C2
ATM-2 -															
5P	26.8	3:30 PM	997,000	87.1	0.0	0.0	0.0	0.0	0.0	0.0	3,900	11,500			
5P	26.8	3:48 PM	997,000	110.1	5.8	2.1	6.5	7.3	0.2	0.6	3,000	9,100		-71.9	
5P	26.8	4:17 PM	997,000	84.7	4.0	1.0	3.3	2.7	0.1	0.3	3,700	11,800		-72	
5P	26.8	7:07 PM	999,000	255.4	1.1	0.3	0.7	1.1	0.0	0.0	1,000	4,000			
5P	26.8	7:43 PM	999,000	279.1	1.9	8.6	0.1	0.0	0.1	0.0	1,700	3,600		-71	
5P	26.8	8:20 PM	998,000	296.0	1.5	7.7	0.1	0.0	0.1	0.0	2,100	3,400		-71.0	
5P	26.8	8:56 PM	999,000	294.6	1.2	5.8	0.1	0.0	0.1	0.0	1,400	3,400		-71.0	
5P	26.8	9:00 PM	999,000	302.3	1.3	6.8	0.1	0.0	0.1	0.0	800	3,400		-71.0	
5P	26.8	9:17 PM	1,000,000	306.7	1.2	5.6	0.1	0.0	0.1	0.0	200	3,300		-70.8	
5P	26.8	9:36 PM	990,000	487.6	43.0	13.1	13.6	211.6	6.9	7.0	9,500	2,100			
*KC151-3-															
11P	227.0	5:26 PM	79,000	0.0	256.7	603.0	58.1	251.9	46.0	19.4	920,300				
11P	227.0	5:34 PM	109,000	0.0	261.1	534.1	38.6	329.4	35.6	14.8	890,200		-20.1	-74.3	
11P	227.0	6:30 PM	61,000	0.0	200.2	318.8	61.8	182.9	22.2	19.8	939,200		-19.7	-73.7	
11P	227.0	6:40 PM	56,000	0.0	76.4	211.3	0.0	89.9	0.0	0.0	943,900				
11P	227.0	6:54 PM	167,000	0.0	37.6	53.3	35.9	42.3	10.4	8.7	833,700		-23.5	-73.7	
11P	227.0	7:01 PM	994,000	2.4	1.5	341.5	0.0	1.4	0.4	0.0	6,400	420,200			
11P	227.0	7:09 PM	988,000	0.0	7.9	4.7	1.8	3.2	1.1	0.8	12,900				
11P	227.0	7:18 PM	980,000	2.7	6.0	2.2	2.2	0.8	1.0	0.2	20,700	360,200	-21	-73.4	
13R	235.0	7:46 PM	1,000,000	84.1	0.8	0.1	0.2	0.1	0.1	0.0	600	11,900		-74.2	
13R	235.0	8:04 PM	1,000,000	85.1	1.0	0.1	0.2	0.0	0.1	0.0	500	11,800		-74.1	
13R	235.0	8:17 PM	1,000,000	118.9	1.0	0.1	0.2	0.0	0.1	0.0	300	8,500		-74.4	
13R	235.0	8:24 PM	1,000,000	94.2	0.9	0.1	0.2	0.0	0.1	0.0	800	10,700		-74.3	
13R	235.0	8:49 PM	1,000,000	94.7	0.8	0.2	0.2	0.1	0.1	0.0	600	10,600		-74.4	
13R	235.0	8:53 PM	1,000,000	89.7	0.9	0.2	0.2	0.1	0.1	0.0	500	11,200		-74.4	
13R	235.0	9:14 PM	1,000,000	89.7	1.0	0.2	0.3	0.1	0.1	0.0	500	11,200		-74	
13R	235.0	9:20 PM	1,000,000	73.0	1.0	0.2	0.2	0.1	0.1	0.0	500	13,700		-74.4	
13R	235.0	9:26 PM	1,000,000	87.3	1.2	0.3	0.2	0.1	0.1	0.0	700	11,500		-74.2	
13R	235.0	9:31 PM	1,000,000	91.1	1.2	0.3	0.3	0.0	0.2	0.0	800	11,000		-74.4	
13R	235.0	9:36 PM	998,000	87.3	1.4	0.3	0.4	0.1	0.2	0.0	2,300	11,500		-74.3	
13R	235.0	9:51 PM	999,000	102.0	1.4	0.3	0.4	0.1	0.2	0.0	1,100	9,800		-74.7	
13R	235.0	9:59 PM	999,000	98.3	1.5	0.3	0.5	0.0	0.3	0.0	1,700	10,200		-74.4	
13R	235.0	11:39 PM	997,000	104.6	1.6	0.5	0.9	0.1	0.3	0.1	3,400	9,600	-16.3	-74.3	
13R	235.0	11:55 PM	996,000	123.6	6.6	4.6	4.6	101.0	2.1	3.0	4,700	8,100			
26R	383.0	3:55 PM	1,000,000	0.0	0.0	0.0	0.0	0.0	0.0	0.0	0			-72	
26R	383.0	4:08 PM	998,000	413.0	41.2	8.9	12.1	96.0	5.7	3.3	2,400	2,500			
26R	383.0	4:09 PM	1,000,000	0.0	0.0	0.0	0.0	0.0	0.0	0.0	0				
26R	383.0	4:24 PM	999,000	677.7	35.8	15.9	6.7	0.3	6.1	0.6	600	1,500		-70.9	-46.8
26R	383.0	4:26 PM	998,000	548.4	27.9	19.8	4.3	0.2	4.3	0.4	2,400	1,900			
26R	383.0	4:27 PM	999,000	542.7	22.2	9.9	3.6	0.2	3.5	0.3	1,400	1,900			
26R	383.0	4:41 PM	997,000	557.1	12.0	6.9	1.8	0.1	1.8	0.2	3,200	1,800			
26R	383.0	4:43 PM	998,000	537.2	24.8	13.8	4.2	0.2	3.6	1.0	2,100	1,900			
26R	383.0	5:07 PM	999,000	580.6	23.9	10.5	4.0	0.3	3.8	0.3	1,200	1,800		-71.1	-47.0
26R	383.0	5:09 PM	997,000	559.1	19.7	9.2	3.2	0.2	3.0	0.3	2,700	1,800			
26R	383.0	5:11 PM	998,000	540.6	21.5	12.8	3.3	0.2	3.0	0.2	1,700	1,900			
26R	383.0	5:12 PM	999,000	544.6	18.8	9.6	3.0	0.2	2.6	0.3	1,300	1,900			
26R	383.0	6:32 PM	997,000	532.4	23.8	20.8	3.2	0.2	3.0	0.4	2,700	1,900		-70.9	
26R	383.0	6:35 PM	999,000	536.3	17.9	9.0	2.5	0.0	2.2	0.3	1,300	1,900			
26R	383.0	6:38 PM	999,000	528.0	18.2	4.0	4.5	51.4	1.9	1.2	1,300	1,900			
26R	383.0	6:39 PM	998,000	501.6	18.4	10.5	2.4	0.2	2.0	0.2	1,700	2,000			
26R	383.0	7:04 PM	999,000	506.7	17.0	1.9	2.6	0.5	1.9	0.1	500	2,000			
26R	383.0	7:06 PM	998,000	536.7	17.7	1.8	2.5	0.8	2.1	0.2	2,000	1,900			
26R	383.0	7:08 PM	999,000	507.8	17.6	2.0	2.7	0.5	2.0	0.1	600	2,000			
26R	383.0	7:10 PM	999,000	507.9	17.5	1.9	2.5	0.3	1.9	0.1	700	2,000			
26R	383.0	7:31 PM	999,000	502.1	18.1	2.1	3.1	0.5	2.1	0.1	1,000	2,000		-71.9	-48.3
26R	383.0	7:32 PM	999,000	519.4	19.8	2.5	3.5	0.9	2.1	0.1	800	2,000			

*KC 151-3-11P samples had high air contents, which influence the calculated air-free concentrations but should not affect isotopic compositions.

consistent with the expansion void gas at comparable depth levels. The CO_2 in pressure core gas appears to be isotopically lighter than that in the expansion void gas, possibly related to CO_2 exchange with the water during the offgassing process.

Discussion

In general, the predominant hydrocarbon found in the all cores at these JIP sites was isotopically light (–84.3 to -71.5‰) methane; however C_2-C_5 hydrocarbons were measurable in almost all void gas and pressure core samples, suggesting that a portion of the dissolved gas content has a deeper thermogenic source. However the predominant source of methane appears to be from sedimentary microbial processes, based on the standard interpretation of the chemical and isotopic evidence (Figure 1).

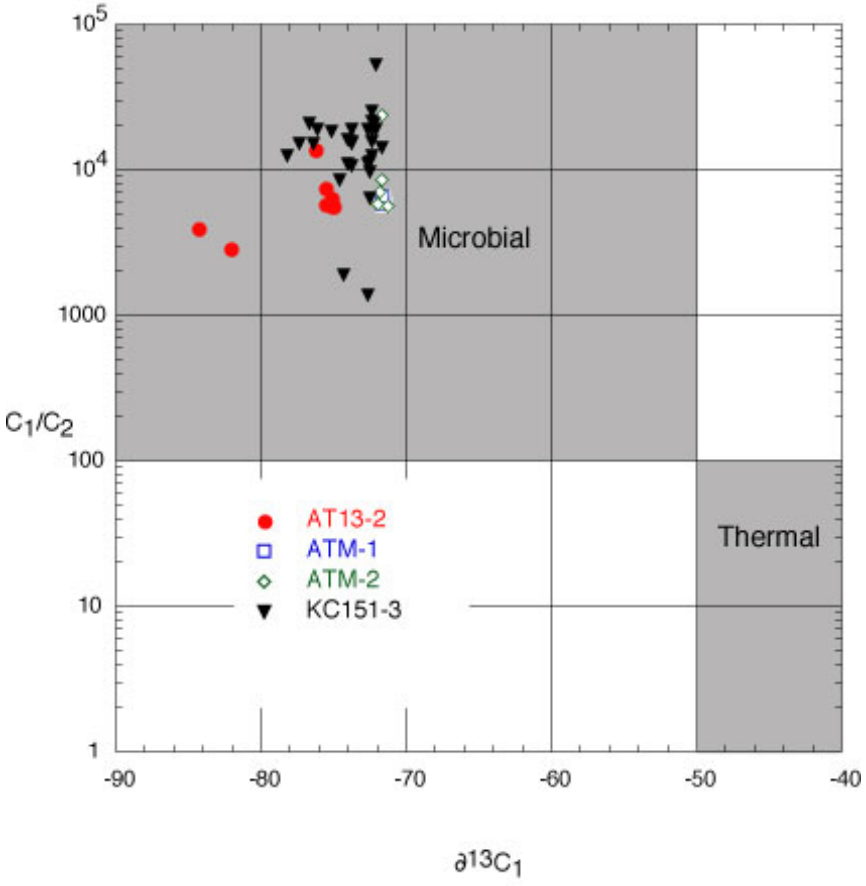

Figure 1. Plot of the methane to ethane ratio of void gas and PCS gas vs. the carbon isotopic composition of methane. Traditional microbial and thermal gas source fields after Bernard et al., 1978. All data are consistent with a microbial source of methane in cores at all depths. The similarity of the gas at each site suggests a similar process of microbial methane production.

The headspace gas analyses are consistent with an upward methane flux of variable intensity. Significant amount of dissolved methane are present in even the shallowest (20-100 cm beneath the sea floor) core samples from the mound sites in Atwater Valley block 14 (AT14-1, ATM1, ATM2) shown in Figure 2.

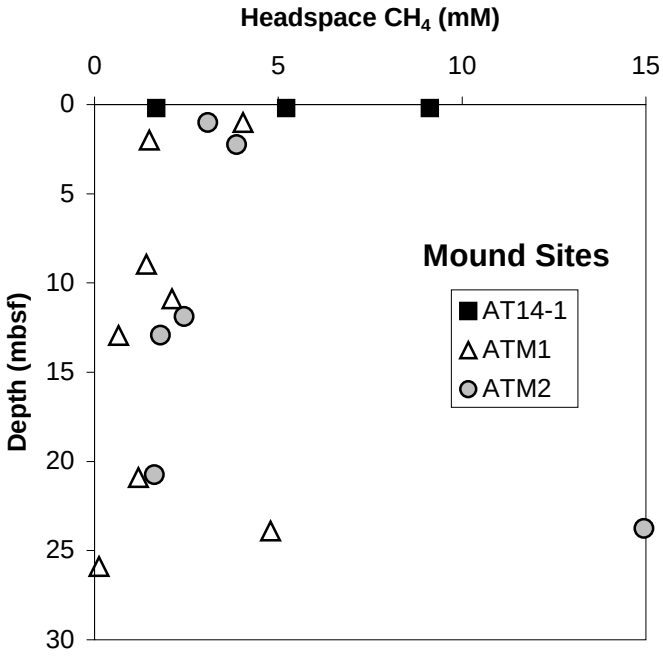

Figure 2. Dissolved residual methane in cores as estimated from headspace gas analysis. Samples are from shallow cores on top of (ATM1, ATM2) and ROV deployed push cores adjacent to (AT14-1) Mound F in Atwater Valley block 14.

Measurable methane contents at the mound site are consistent with the absence of dissolved sulfate in near surface sediments (see section on pore water geochemistry), and indicate that the rate of upward methane flux is sufficient to overcome the downward flux of dissolved sulfate from the overlying seawater. These mound sites are above a seismically imaged diapiric feature with an amplitude anomaly suggesting the presence of free gas at a depth of about 30 mbsf.

The headspace gas analyses in shallow sediments of the deeper coring sites are consistent with a well-defined sulfate-methane interface at a depth of about 6 mbsf at AT13-2, and a depth of about 9 mbsf at KC151-3, as best indicated by pore water chemistry and the first appearance of dissolved gas separations in some of the core logging (e.g., gamma density, P-wave velocity). Sample spacing is not adequate to completely define dissolved methane concentration gradients, but a sample at depth of 6 mbsf in hole AT13-2 has residual methane of only 0.2 mM while the next sample in the core at a depth of 8 mbsf has methane content of 5.2 mM. In similar fashion at hole KC151-3 a sample at 5 mbsf has 0 mM while the next sample down the core at 10.4 mbsf has 10.3 mM of methane (Figure 3).

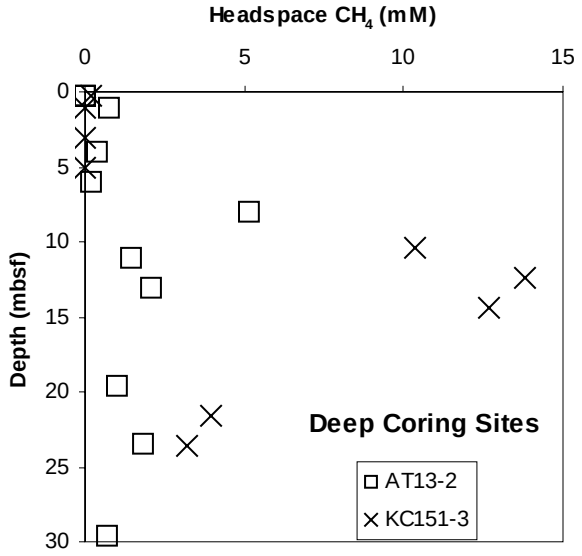

Figure 3. Dissolved residual methane in cores as estimated from headspace gas analysis. Samples are from the uppermost 30 m beneath the sea floor at the deeper coring sites (AT13-2, KC151-3).

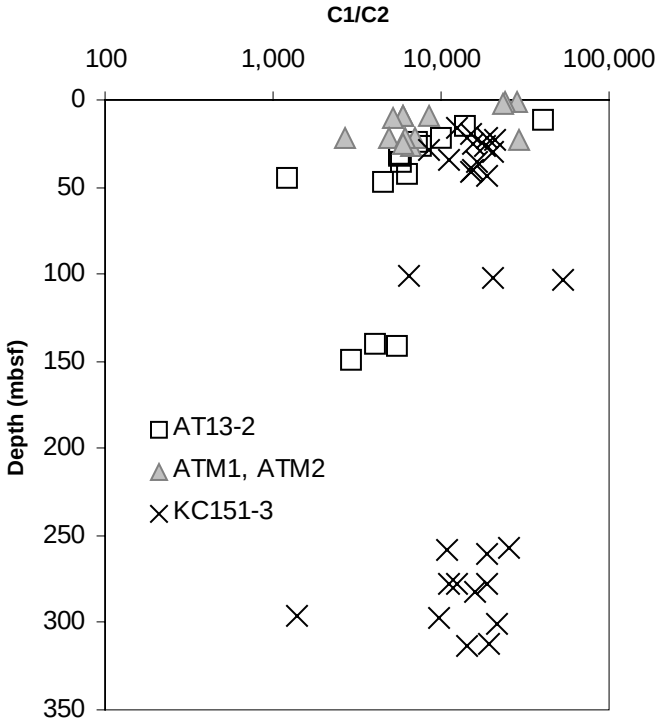

Figure 4. Plot of C_1/C_2 of void gas vs. depth. There is general trend of increasing C_2 content with depth in the Atwater Valley sites, but fairly uniform C_1/C_2 composition with depth at Keathley Canyon.

There is some evidence of an increase in thermogenic gas with depth for the Atwater Valley sites as evidenced by a decrease in the C_1/C_2 ratio with depth (Figure 4). There was no similar depth trend in C_1/C_2 values for the Keathley Canyon 151-3 well, indicating that there is very little thermogenic gas present and suggesting an unusually deep microbial methane source and upward advection of gas at this location. Each site had trace amounts of increasing concentrations of propane, isobutane, and normal butane with depth indicating that small concentrations of thermogenic gas are present, however the majority of the gas is microbially derived methane.

The trends in carbon isotopic ratio of methane with depth are plotted in Figure 5.

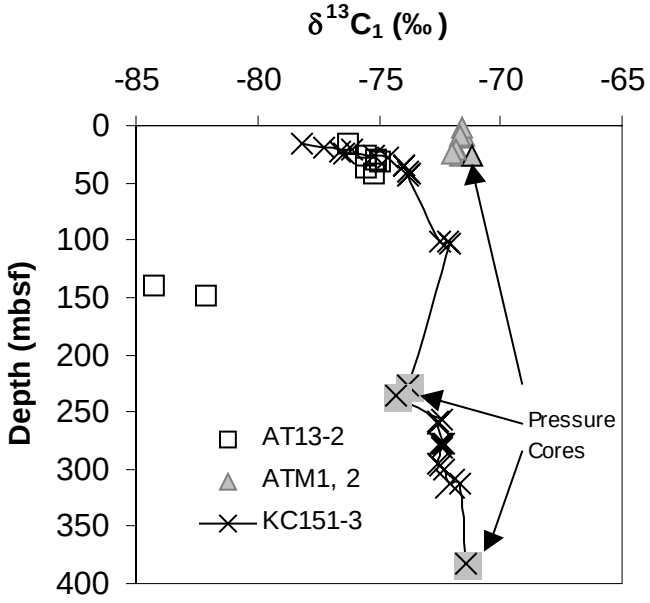

Figure 5. $\delta^{13}C$ of methane vs. depth of burial, void gas and pressure core samples from Atwater Valley 13/14 and Keathley Canyon 151.

There is significant variation in the isotopic composition of methane at the Atwater Valley sites. The mound sites (ATM1, ATM2) are tightly clustered in the range of –72 to –71.5‰, but there is a slight trend suggesting that (upwardly migrating) methane gets heavier as it approaches the sea floor. This is a possible effect of methane oxidation near the sea floor, with ^{12}C-enriched methane being preferentially oxidized.

At the AT13-2 reference site, the samples between 11 and 42.6 mbsf show the reverse trend, with methane getting lighter in sample depths approaching the sulfate-methane interface at a depth of about 6 mbsf. This trend is more consistent with some dilution (~20%) of the migrating methane flux with locally generated microbial methane relative to the mound sites. The shallowest void gas sample at AT13-2 is at a depth of 11 mbsf, which is probably deep enough to minimize effects of methane oxidation resulting in a misleading heavy methane isotopic composition. The methane in the deeper cored

sediments at depths of 140.2 and 149.3 mbsf in hole AT13-2 is even more negative, with $\delta^{13}C$ values of –84.3 and –82.1‰, respectively. This most negative observed methane at depth is inconsistent with a regional vertical flux of methane of the isotopic composition (–70 to –72‰) as observed at the mound sites, and suggests that there may be some lateral migration or *insitu* production of lighter, microbially sourced methane relative to the main flux regions represented by the mounds on either side of site AT13-2.

The $\delta^{13}C$ of methane in the 100-313 m interval at KC151-3 is about the same (-72.6 to –71.7‰) as that venting at the mound sites in Atwater Valley block 14. The methane in the shallow (16.4-44 mbsf) sediments may show a similar effect as that observed in the AT13-2 hole, with an overprint of methane locally generated in sediments just below the sulfate reduction zone.

The limited number of void gas samples (12) with measurement of $\delta^{13}C$ on coexisting CH_4 and CO_2 can be evaluated for an isotopic relation that is consistent with the process of methanogenesis by CO_2 reduction (Figure 6). The labeled diagonal lines on Figure 6 represent constant $\delta^{13}C$ separations of 70 and 65‰. Microbial methanogenesis by CO_2 reduction in marine sediments proceeds with instantaneous ^{13}C fractionation of about 75‰ (Claypool and Kaplan, 1974). The observed isotopic separation between coexisting microbial CH_4 and CO_2 is initially about 75‰, and diminishes as CO_2 reduction progresses, generally leveling off in the range of 60-70‰ depending on relative rates of CO_2 addition and removal. The limited data on $\delta^{13}C$ of coexisting CH_4 and CO_2 in the Gulf of Mexico JIP boreholes is reasonably consistent with origin of the isotopically light methane by CO_2 reduction.

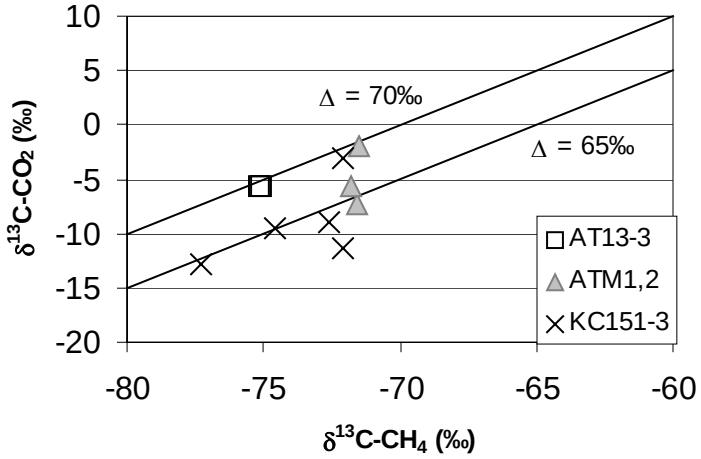

Figure 6. $\delta^{13}C$ of coexisting CH_4 and CO_2 in void gas samples from JIP boreholes.

The $\delta^{13}C$ of ethane was measured on two samples of void gas (ATM2-3H-5, KC151-3-20H-3) and on one of the pressure core samples (KC151-3-26R). The $\delta^{13}C$ of coexisting CH_4 and C_2H_5 is plotted in Figure 7. The diagonal line in Figure 7 represents the equation:

$$\delta C_2 = -0.5(\delta Co - \delta C_1) + \delta Co$$

where δC_2 and δC_1 are $\delta^{13}C$ values of ethane and methane, and δCo is the $\delta^{13}C$ of the gas-producing organic matter (assumed to be –27.5‰). This line shows the expected relationship between methane and ethane for the earliest stages of thermogenic gas production, according to the interpretation of Chung and others (1989). Although isotopically light methane is generally assumed to be of microbial origin, examples of low temperature thermogenic gas with extremely light methane $\delta^{13}C$ values have been reported by Rowe and Muehlenbachs (1999) and by Coleman (2001). With only three samples, the results are extremely limited and provide mixed evidence for the origin of the gas. The ethane in the void gas sample from KC151-3-20H-3 has $\delta^{13}C$ of –65.3‰, which is more consistent with a microbial origin. The other two samples (ATM2-3H-5, KC151-3-26R) have ethane $\delta^{13}C$ of –47.6±0.8‰, which is more consistent with and early thermogenic origin.

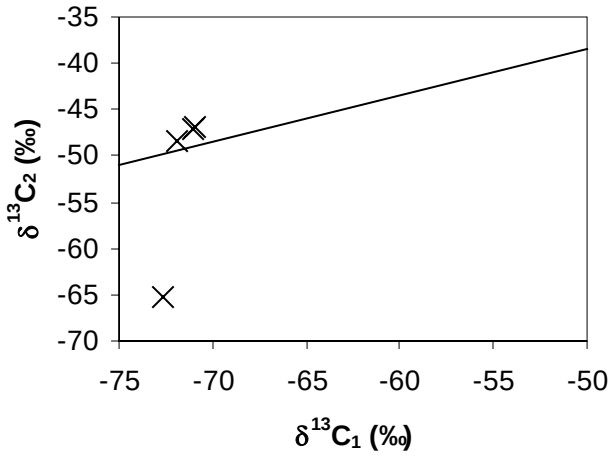

Figure 7. $\delta^{13}C$ of coexisting methane and ethane in gas samples from ATM2 and KC151-3 boreholes.

The predominance of isotopically light methane in sampled sediment cores to depths of 380 mbsf, and the absence or minor amounts of obvious petroleum-related thermogenic gas is somewhat surprising given the widespread occurrence of thermogenic gas in the northern Gulf of Mexico. However, this is consistent with previous observations of gas in near surface sediments over a broad area of the upper continental slope in this region. Sassen and others (2002) measured the $\delta^{13}C$ of methane at 160 high-flux gas seeps in the region and presented the histogram shown in Figure 8.

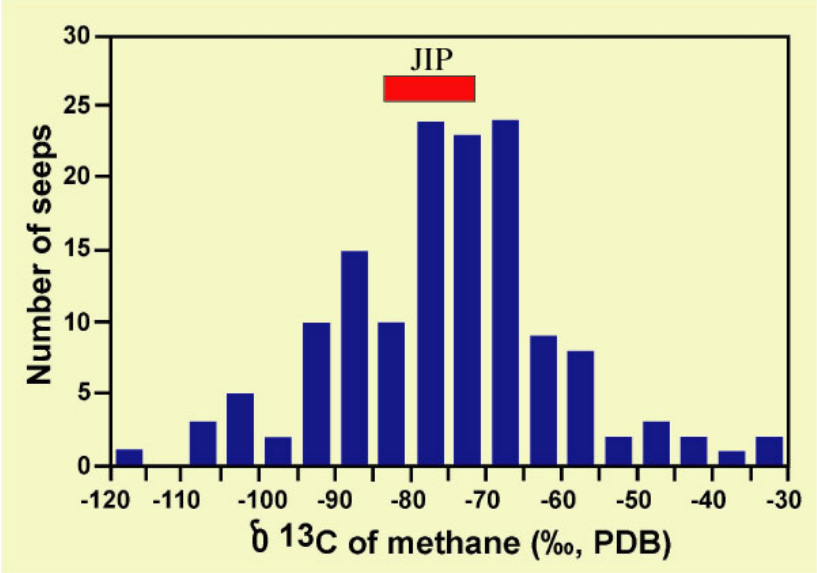

Figure 8. Histogram of the $\delta^{13}C$ of methane from the northern Gulf of Mexico as complied by Sassen and others (2002). The red bar labeled "JIP" is the $\delta^{13}C$ range of void gas methane and pressure core methane from boreholes in Atwater Valley 13/14 and Keathley Canyon 151.

High-flux gas seeps imply a supply of gas from depth, and the JIP sites are associated with known seafloor seeps. Figure 8 shows the mean methane carbon isotopic range in the northern Gulf of Mexico to be centered around –65 to –80‰. The methane samples from the JIP wells have a mean $\delta^{13}C$ of 74‰ for gas void samples and –73.9‰ for pressure core methane samples. Thus, the $\delta^{13}C$ of methane from JIP boreholes falls well within the predominant seep gas composition of the northern Gulf of Mexico and are consistent with a widespread, deeper source of gas containing isotopically light methane.

Conclusion

Microbial methane is the predominant gas present at both the Atwater Valley and Keathley Canyon sites as evidenced by isotopically light methane and very small concentrations of thermogenic C_2-C_5 hydrocarbons. Upward flux of methane is apparent from many lines of evidence including seafloor mounds, seismic anomalies consistent with upward gas migration, a shallow methane/sulfate interface, and similar gas compositions observed near the seafloor relative to the gas sampled from depth.

The exact origin of this deeper gas source is uncertain. Possibilities include: (1) microbial methane that was generated at shallow depths and buried with rapidly subsiding sediments, (2) microbial methane associated with biodegradation of migrating petroleum that originates in more deeply buried sediments, or (3) upwardly migrating gas of early, low-temperature thermogenic origin. More information on gases and the nature of organic matter in the sediments of the upper 2-3 km of sediment will be required to understand the relative importance of gas-generating mechanisms operating in the Gulf of Mexico.

References

Bernard, B. B., Brooks, J. M., and Sackett, W. M., 1978, Light hydrocarbons in recent Texas continental shelf and slope sediments. Journal of Geophysical Research; v. 83, p. 4053-4061.

Chung, H.M., Gormly J.R., and Squires, R.M., 1988, Origin of gaseous hydrocarbons in subsurface environments: Theoretical considerations of carbon isotope distribution: Chemical Geology, v. 71, p. 97-104.

Claypool, G.E., and Kaplan, I.R., 1974, The origin and distribution of methane in marine sediments: in I.R. Kaplan (ed.), Natural gases in marine sediments, Plenum Press, New York, p. 99-139.

Coleman, D.D., 2001, -70‰ methane, is it biogenic or thermogenic?: AAPG Bulletin, v. 85 (Supplement).

Kvenvolden, K. A., and Lorenson, T. D., 2000, Methane and other hydrocarbon gases in sediment from the southeastern North American continental margin; proceedings of the ocean drilling program; v. 164; Scientific results; gas hydrate sampling on the Blake Ridge and Carolina Rise; Proceedings of the Ocean Drilling Program, Scientific Results; 164, 29-36.

Rowe, D. and Muehlenbachs, K., 1999, Low-temperature thermal generation of hydrocarbon gases in shallow shales: Nature, v. 398, p. 61-63.

Sassen, R., Milkov, A.V., de Freitas, D.A., and Sweet. S.T., 2002, Molecular and isotopic properties of high-flux gas seeps, northwestern Gulf of Mexico; AAPG annual convention with SEPM. Annual Meeting Expanded Abstracts - American Association of Petroleum Geologists; v. 155.

Pore Water Geochemistry--2005 Gulf of Mexico JIP Cruise

Miriam Kastner, George Claypool, and Gretchen Robertson
Scripps Institution of Oceanography, La Jolla, CA

Introduction

The objectives of the geochemistry program are to document the pore-water chemical and isotopic compositions at drill sites in the Atwater Valley (AT) and Keathley Canyon (KC) protraction areas. The analytical emphasis, especially at sea is on key components that provide information on: (1) the depth and spatial distribution and concentration of gas hydrates and the relation to lithology and other physical properties, of which the latter will be acquired by other scientists involved in the project; (2) the nature and rates of the key microbial reactions responsible for gas generation *in situ* by microbial processes versus upward advection of methane (and other gases) from deeper sources; and (3) the subsurface hydrology that controls the pore water chemistry, thus the gas hydrate distribution, concentration, and potential dissociation.

The key components are pH, salinity, Cl, alkalinity, sulfate, sulfide, Ca and Mg concentrations, and δ^{13}DIC. The salinity and Cl concentration provide information on dilution or concentration of the pore water by *in situ* dissociation or formation of gas hydrate, respectively, or by mixing with fresh water or a saline fluid, respectively. Resolving between these possibilities is achievable by additional shore-based chemical and isotopic analyses. Alkalinity is produced both by microbial sulfate reduction at a molar ratio of 1:2, and by anaerobic methane oxidation (AMO) at a molar ratio of 1:1. Shore-based analysis of the δ^{13}C –DIC will provide a clear distinction between these two reactions. In addition, the relative contribution of alkalinity production by the two processes can be determined by the sulfate reduction profile, after correcting the alkalinity for Ca and Mg concentrations; moderate to high alkalinities induce authigenic carbonate precipitation that reduces seawater Ca and Mg concentrations. At greater depth, below the AMO zone, CO_2 is produced by fermentation reactions, and this CO_2 (with H^+) is converted microbially to CH_4; therefore, alkalinity concentrations are low to moderate. Calcium and Mg concentrations reflect the amount of authigenic carbonate formation.

Methods

Samples for pore waters were chosen from FHPC (Fugro Hydraulic Piston Corer) cores at intervals shown in Table 1. Infra-red images of the cores were helpful in guiding core sub-sampling, in cores in which gas hydrate was present. After careful cleaning, the sediment sample was placed in titanium squeezers and subjected to pressures ranging from 800 to 40,000 lbs, depending on the consistency of the sediment, using a Carver "Auto" Series automatic hydraulic press. The pore waters derived from squeezing were filtered and analyzed shipboard for salinity by refractometry, and for the transient species alkalinity and sulfate, by the Gran-titration and spectrophotometry, respectively. Because time and personnel constraints did not allow us to analyze ship-board immediately for

Table 1. Scheme for frequency and volume/length of core required for pore water samples.

Section	1	2	3	4	5	6	7	8
Core								
1	10-15 cm	10-15 cm	10-15 cm	10-15 cm	10-15 cm	10-15 cm	10-15 cm	10-15 cm
2	10-15 cm		10-15 cm		10-15 cm		10-15 cm	
3		15-20 cm			15-20 cm		15-20 cm	
4*			15-30 cm*			15-30 cm*		
etc.*								

*Depends on porosity and volume of water recovered, may require adjustments.

**If gas hydrates observed, collect 10-20 cm whole round core adjacent to hydrates, and at cold zones indicated by IR. Also sub-sample hydrate (~3 cc foil-wrapped, bagged and in LN2) for water analysis.

both sulfate and sulfide concentrations, the upper sections of the cores were analyzed for sulfate concentrations in order to determine the depth of the sulfate methane boundary. Following the alkalinity and sulfate analyses, the remaining volume of the squeezed pore water was subdivided according to the scheme shown in Table 2. The various aliquots were fixed or preserved for shore-based analyses at SIO, USGS Menlo Park, and Rice University, as indicated in Table 2.

Table 2. Pore water sub-sample and aliquot schedule.

		Pore Water Volume Available						
Sample Code	Analysis	50 mL	40 mL	30 mL	20 mL	10 mL	5 mL	Addition
Shipboard & Scripps								
Cd	H_2S	0.5	0.5	0.5	0.5	0.5	0.5	0.5 mL $Cd(NO_3)_2$
Cl	major ions, Cl	10.5	8.5	6	2.5	2	2.5	
Alk	Alkalinity	3	3	3	3	3		
DIC	DIC-$\delta^{13}C$	3	3	3	3			0.5 mL $HgCl_2$
Ba	Ba, Si, Sr, Li	4	4	4	4	2		30 mL HNO_3 (Ultra Pure)
SS	Sulfide/S	0.5	0.5	0.5	0.5			
Lorenson-USGS								
TL	Organic Acids	0.5	0.5	0.5	0.5	0.5	0.5	
Rice University								
Ac	Ba, P	5	5	5	3	2	1.5	30 mL HNO_3 (Ultra Pure)
Ha	Halides	3		7.5	3			
Io	^{129}I	20	15					

Push cores recovered with the ROV were sectioned, sampled and analyzed following the same protocol as above. Bottom water samples obtained with the ROV at three sites

(AT13#1, AT13#2, KC151#1) were filtered and analyzed shipboard for salinity and alkalinity, and additional aliquots were fixed for shore-based analyses of δ^{13}C-DIC, Ca and Mg concentrations.

During the first few days at sea, the chemistry laboratory was set-up and the various procedures were calibrated. Detailed protocols for using the hydraulic pump for pore water squeezing and for alkalinity titration and calculation, were established and clearly documented.

Pore water Chemistry at Atwater Valley, Sites AT13#1 and AT13#2

At **AT13 #1** the ROV recovered bottom water with the Scripps and Fugro Niskin bottles, conductivity-temperature-depth (CTD) data were obtained, and two push cores were taken. One of them, a 42 cm long core devoted to pore water chemistry, was cut into three sections. The sections were cleaned, squeezed, and immediately analyzed on board ship for salinity and alkalinity. The remaining pore water was subdivided, following the pore water sampling scheme outlined in Table 2. The sediment is fine-grained with borrows filled with coarser sediment, and ranged in color from a ~2cm soft brownish layer at the top to greenish clay at the bottom. All samples have average seawater salinity of 35 parts per thousand (ppt). The bottom water sample has average seawater alkalinity (2.4 mM). However, already in the first pore water sample, from 0-12 cmbs, the alkalinity concentration is ~ 3 x higher than the bottom water value, indicating intense microbial activity near the seafloor; the alkalinity increases with depth. The core exuded no sulfide 'smell', however the sulfate content was lower (24 mM) than the seawater value (29 mM) already in the first sample. Extrapolating the few data points with depth suggested that zero sulfate level should be at a shallow sub-surface depth of ≤8 m. (The 2nd push core recovered was sampled for gas analysis and the remaining sediment section was stored). Results of pore water analyses of push core samples from AT13 #1 are shown in Table 3.

Table 3. Pore water analyses, AT13 #1 Push Cores.

Hole-Core-section	top depth mbsf	bot. Depth mbsf	Salinity ppt	Alkalinity (mM)	Sulfate (mM)
AT13 #1-					
Bottom Water				2.44	
1PC-1	0	0.12	35	6.24	24.5
1PC-2	0.12	0.27	35	6.5	24.5
1PC-3	0.27	0.43	35	7.18	23.7

At **AT13 #2** nine FHPC cores were recovered and sampled for pore waters from the seafloor to 159 mbsf. The interval between 48-118mbsf was washed down. The sediment consists of a soft, fine-grained and homogeneous green-gray clayey-silt. The first few cores had gas voids, but the deeper ones did not have 'obvious' visible gas voids. Extensive gas expansion and separation features were, however, observed in each sediment sample that was squeezed for pore water, even in the cores without gas voids. In addition, gas bubbles were evident in most pore water samples, and some of the pore waters had a characteristic yellowish color, from dissolved organic matter and/or Fe.

Alkalinity rose steadily and steeply in the first core, from about twice seawater value in the first sample analyzed, at ~ 0.9 mbsf, to 19.47 mM at 5.9 mbsf (Table 3b, Figure 1a), indicating intense microbial sulfate reduction (Table 4). Measured sulfate data are not reported in Table 4 because of interference by sulfide oxidation, a problem that was later corrected.

Table 4. Hole AT13 #2 Shipboard Pore Water Chemistry

Hole	Top Depth	Bottom Depth	Salinity	Alkalinity	Sulfate
Core-section (cm interval)	(mbsf)	(mbsf)	(ppt)	(mM)	(mM)
AT13 #2					
1H-1 (85-100)	0.85	1.00	34.5	5.39	23.7
1H-2 (85-100)	1.85	2.00	34.5	6.70	22.8
1H-3 (85-100)	2.85	3.00	34.0	7.36	22.0
1H-4 (85-100)	3.85	4.00	34.0	9.64	18.0
1H-5 (85-100)	4.85	5.00	34.0	8.54	19.7
1H-6 (85-100)	5.85	6.00	33.0	19.47	10.5
2H-1 (85-100)	7.86	8.01	33.0	19.71	2.7
2H-3 (85-100)	9.86	10.01	32.0	11.88	0.5
2H-5 (85-100)	12.20	12.35	32.0	9.43	0.6
2H-7 (85-100)	14.20	14.35	32.0	9.37	0.4
4H-2 (85-100)	20.14	20.29	32.0	9.70	
4H-5 (0-17)	22.29	22.46	32.0	8.82	
6H-1 (85-100)	29.50	29.65	33.5	7.30	
6H-4 (83-100)	32.48	32.65	33.5	9.28	0.8
8H-2 (84-100)	41.46	41.62	36.5	8.74	0.3
8H-5 (78-100)	44.40	44.62	37.5	8.43	0.0
9H-3 (0-20)	120.26	120.46	31.5	11.11	0.2
9H-6 (80-100)	124.06	124.26	31.0	9.38	
11H-3 (80-100)	129.60	129.80	30.5	7.52	0.1
11H-5 (80-100)	131.60	131.80	31.0	6.93	
13H-2 (80-100)	142.92	143.12	32.5	8.81	
13H-5 (80-100)	148.42	148.62	32.5	9.23	
14H-1 (80-100)	158.69	158.89	33.0	8.43	0.0

A strong odor of H_2S and yellowish pore water filtrate were encountered in the two bottom sections of core 1 and in the first section of core 2, between 4.9-7.9 mbsf. In these cores gas expansion features were especially pervasive in the sediments sub-sampled for pore water squeezing, and gas bubbles were abundant in the pore waters. The sulfate/methane boundary occurs at a depth of 7-8 mbsf, just above the measured alkalinity maximum depth (Figure 1).

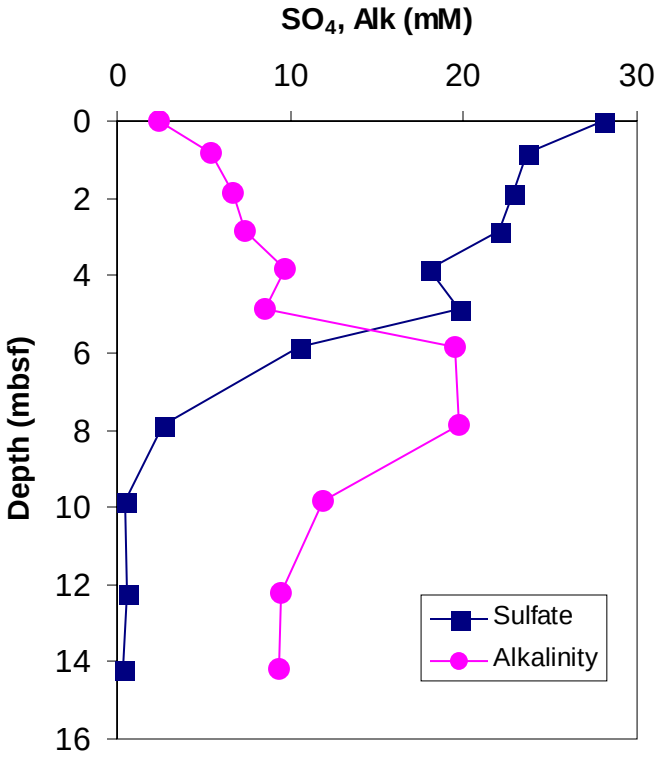

Figure 1. Alkalinity and sulfate, Hole AT13#2.

Below the maximum value alkalinity gradually decreases, from ~8 mbsf, down-hole to 8.43 mM at 44.5 mbsf (Table 4). Below the 70 m coring gap, at 120.3 mbsf, alkalinity is somewhat higher, 11.11 mM; it steadily decreases with depth to a minimum value of 6.93 mM at 131.7 mbsf, and slightly rises again to ~9 mM at the bottom of the hole (Table 4). The lowest salinities of 30.5-31.0 were measured in the minimum alkalinity horizon, where the sediments are sandier than in the rest of the recovered sections at this site.

At this site salinity varies between a minimum of 30.5 at 12.97 mbsf to 37.5 at 44.5mbsf, respectively (Table 4, Figure 2). In the uppermost ~40 mbsf, a distinct low salinity zone is observed; it is bounded by about seawater salinity near the seafloor and at ~ 40 mbsf, with a minimum salinity of 32 between 9.9-22.3 mbsf (Figure 2). The coldest areas observed by IR scanning were concentrated within this low salinity horizon. Gas hydrate dissociation, at a concentration of approximately 4% pore-space filling, or a lateral flow of low-salinity water may be responsible for the observed freshening of the pore fluid between the seafloor and 40 mbsf. Shore-based analyses will be able to distinguish between these two possible origins. Below this zone, between ~40-44.4 mbsf, salinity rises sharply to 37.5 (Table 4, Figure 2). It suggests the existence of a high salinity fluid in the washed out depth interval. The minimum salinity at 129-130 mbsf, in the more sandy horizon, discussed above, as well suggests lateral flow of low-salinity water. It seems that at this site the hydrology is characterized by lateral flow systems.

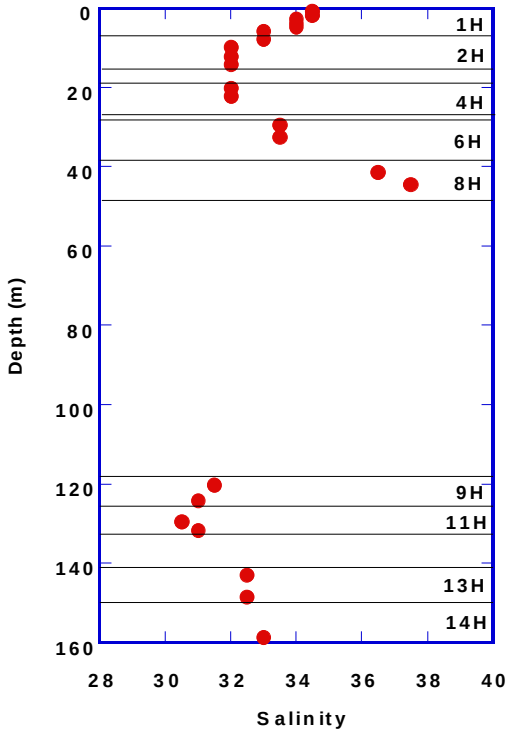

Figure 2. Hole AT13 #2 Salinity plotted versus depth of burial. Horizontal lines indicate top and bottom of FHPC cored intervals.

Pore Water Chemistry at Mound Sites, AT14#1, ATM1 and ATM2

Site AT14 #1 is located on the flank of Mound F. Before the LWD hole the ROV was deployed at AT14 #1 to collect CTD data, bottom water samples with the SIO and Fugro Niskin bottles, and push cores. The bottom water sample was filtered, analyzed for salinity and alkalinity, and sub-sampled for shore-based analyses, following the procedure in Table 2. The salinity and alkalinity of the bottom water is equal to the seawater values. One of the push cores, 35 cm long, was sub-divided into three sections, as indicated in the pore water data Table 5. The sections were immediately cleaned, squeezed, and analyzed shipboard for salinity, alkalinity, and sulfate concentrations. The data are summarized in Table 5.

Table 5. Site AT14 #1, Shipboard Pore Water Chemistry.

Hole-core-section	Depth (mbsf)	Salinity (ppt)	Alkalinity (mM)	Sulfate (mM)
AT14 #1				
Bottom Water			2.39	
1PC-1	0.0-0.10	44.5	16.43	4.7
1PC-2	0.10-0.20	47.5	9.60	2.9
1PC-3	0.20-0.35	50.0	10.23	0.2

The sediment in the AT14 #1 push core is a fine-grained, gray-green silty-clay. At the surface of the core a thin, ~1 cm, lithified layer, cemented by authigenic carbonate was recovered. H_2S odor was pervasive throughout the core and the pore water had a yellowish-green color. The salinity increases with depth from 44.5 to 50.0. Already in the first sample, between 0-10 cmbsf the alkalinity value is high, 16.43 mM and is lower in the two deeper samples (Table 5). Sulfate reduction gradient is steep, the concentration at 0-10 cmbs is 4.74, just ~16% of seawater value, and at 20-35 cmbsf the concentration is 0.21 mM; thus, the sulfate-methane boundary is at ~0.3 - 0.4 mbsf.

At ATM1 three FHPC cores were recovered and sampled for pore water from the seafloor to 25.8 mbsf. Fugro Pressure Cores were recovered between FHPC cores 1, 2, and 5. The sediment consists of soft moussy and somewhat soupy dark-gray silty-clay. In addition to the pore water core sampling scheme (Table 1), guided by infra-red, five extra samples of the coldest intervals and intervals adjacent to them were as well taken, squeezed and analyzed. Gas bubbles were evident in each pore water sample. At both mound Sites (ATM1 and ATM2) already in the first samples, at 0.9 mbsf, sulfate concentration was zero, alkalinity concentrations were moderate and only vary with depth by just 2 mM, between 6.57-8.43 mM, throughout the depth interval cored (Figure 3); an overall trend of decreasing alkalinity with depth is observed (Figure 3).

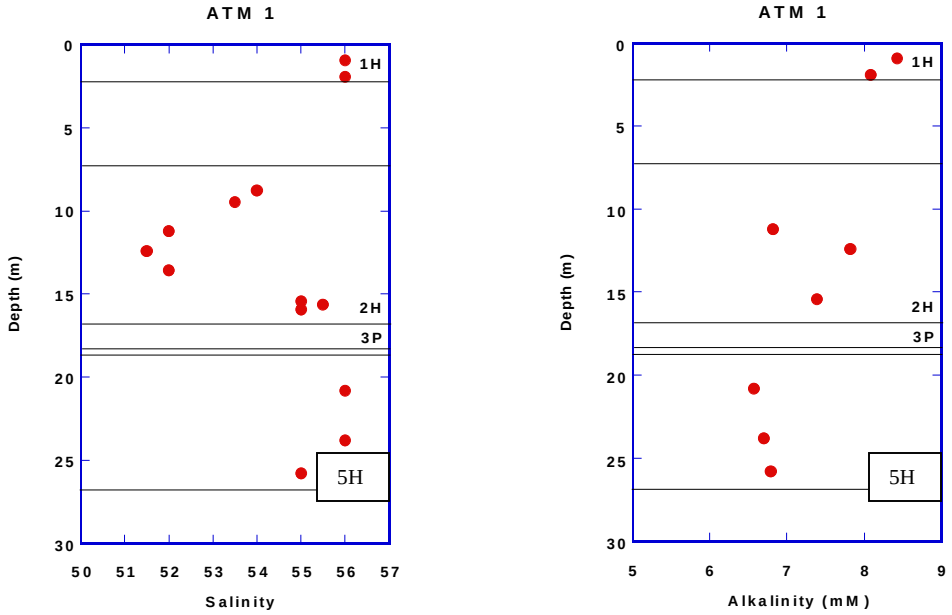

Figure 3. Mound Site ATM1, Salinity and Alkalinity versus depth of burial. Horizontal lines indicate upper and lower depths of cores.

The backround salinity at this site is high (56) as seen in FHPC cores 1 and 5 (Figure 3). In the second core salinity varies from between 55.5 – 51.5. The minimum salinity value of 51.5 at 12.4 mbsf (Figure 3), corresponds with the coldest interval observed with the infra-red camera. The salinity-depth profile (Figure 3) indicates that gas hydrate was present only in FHPC 2H at a concentration of about 4-5% pore space filling. At the

bottom of core 5H, at 25.7 mbsf, which is close to the seismic reflector, salinity started to decrease. The pore water analyses for Hole ATM1 are given in Table 6.

Table 6. Shipboard pore water chemistry, Hole ATM1.

Hole-core section (cm)	Depth (mbsf)	Salinity	Alkalinity (mM)
ATM1			
1H-1 (85-100)	0.85-1.00	56.0	8.43
1H-2 (85-100)	1.85-2.00	56.0	8.09
2H-2 (40-50)	8.74-8.84	54.0	
2H-2 (85-100)	9.14-9.34		
2H-3 (8-20)	9.42-9.54	53.5	
2H-4 (80-100)	11.14-11.34	52.0	6.82
2H-6 (0-20)	12.34-12.54	51.5	7.82
2H-7 (20-30)	13.54-13.64	52.0	
2H-9 (0-20)	15.34-15.54	55.0	7.39
2H-9 (20-40)	15.54-15.74	55.5	
2H-9 (50-70)	15.84-16.04	55.0	
5H-2 (80-100)	20.70-20.90	56.0	6.57
5H-5 (80-100)	23.70-23.90	56.0	6.70
5H-7 (80-100)	25.70-25.90	55.0	6.79

At ATM2 (as at ATM1) only three FHPC core were recovered from the seafloor to 23.7 mbsf. The cores were sampled for pore water following the scheme in Table 1. This mound site is just ~22 meters northwest of ATM1 mound site. Thus, both sites consist of the same moussy dark-gray silty-clay sediment, and gas bubbles were evident in the pore waters. As at ATM1 sulfate concentration is zero already in the first pore water sample, at 0.9 mbsf. Alkalinity concentrations are also similar to those at the ATM1 mound, and range from 6.07-8.04 mM (Table 7, Figure 4), lower by just ~ 1mM, than the alkalinity values at the adjacent ATM1 mound site. A minor alkalinity maximum seems to exist between 14-20 mbsf (Figure 4). The background salinity at this site is 56 as at ATM1, and most salinity values range between 55-56 (Table 7, Figure 4). Only two samples have lower salinity values, the deepest FHPC sample cored at the site, with salinity of 54, at 23.7 mbsf, and the sample at 20.65 mbsf has a considerably lower salinity of 51. The latter sample was chosen based on IR scanning; it was the coldest spot in the core as identified by infra-red scanning. The positive correlation between the lowest salinity value and coldest area in the core suggests that gas hydrate, filling ~5% of the pore space, was present at this depth-interval but dissociated during core processing.

Table 7. Shipboard pore water chemistry, Hole ATM2.

Hole-core section (cm)	Depth (mbsf)	Salinity (ppt)	Alkalinity (mM)
ATM1			
1H-1 (75-100)	0.75-1.00	56.0	7.96
1H-3 (0-25)	2.00-2.25	55.5	8.04
2H-4 (0-20)	10.93-11.13	55.0	6.12
2H-5 (80-100)	12.73-12.93	55.0	6.75
3H-4 (0-26)	20.38-20.64	55.5	7.04
3H-4 (26-37)	20.64-20.75	51.0	7.04
3H-7 (0-27)	23.37-23.64	55.0	6.58
3H-7 (27-38)	23.64-23.75	54.0	6.07

One FPC, 6P, was recovered at 29.0 mbsf. An X-ray scan of the core indicated that 49 cm were recovered; a low density interval was mapped in this core. During transfer under pressure ~10cm of the core were lost. After depressurization a ~16 cm section of the core

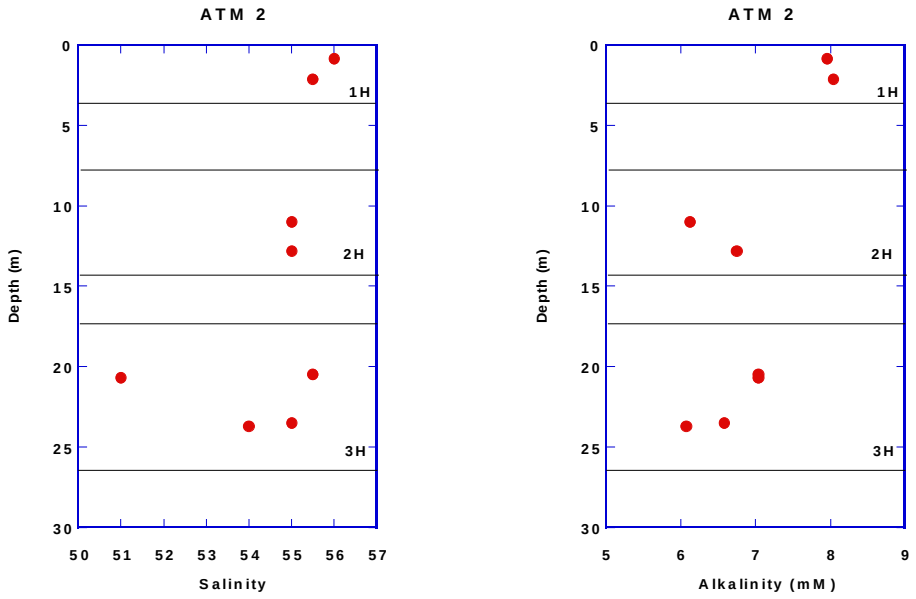

Figure 4. Mound Site ATM2, Salinity and Alkalinity versus depth of burial. Horizontal lines indicate upper and lower depths of cores.

that included the low-density interval was sub-sectioned into 5 samples. Each was squeezed and the pore fluid analyzed for salinity and sulfate. The sulfate data indicate the extent of contamination by seawater, because the pristine pore waters at the two mounds have no sulfate. Each of the pore waters contained sulfate that indicated some seawater contamination throughout the core. Based on the salinity and sulfate data the amount of hydrate in the low density interval was calculated. The calculations suggest a maximum of 6-8% of fresh water in the pore water or the low-density interval.

Pore water Chemistry at Keathley Canyon, Sites KC151 #2 and #3

At KC151 #2**,** the LWD borehole, the ROV recovered bottom water samples with the SIO and Fugro Niskin bottles, CTD data were obtained, and two push cores were taken. One of them, 43 cm long, was devoted to pore water chemistry. The push core was cut into three sections, immediately cleaned, squeezed, and analyzed shipboard for salinity, alkalinity, and sulfate as summarized in Table 5. The remaining pore water was subdivided, following the scheme in Table 2. The soft sediment is silty with some sand and brownish-tan in color. The bottom water sample has average seawater alkalinity and sulfate. All pore water samples from the push core have average seawater salinity of 35 ppt, with slightly elevated alkalinity and slightly diminished sulfate.

Table 5. Hole KC151-2 Shipboard Pore Water Chemistry.

Hole-core-section	Depth (mbsf)	Salinity (ppt)	Alkalinity (mM)	Sulfate (mM)
KC151-2				
Bottom Water			2.37	27.8
1PC-1	0-0.12	35	2.80	28.6
1PC-2	0.12-0.27	35	2.89	28.6
1PC-3	0.27-0.43	35	2.87	28.2

At KC151 #3 nine FHPC cores and nine FC cores were recovered and sampled for pore waters from the seafloor to 380 mbsf. The interval between 45-100 mbsf was drilled without coring. The uppermost few meters of sediment consists of a soft, fine-grained and tan-brown clayey-silt, changing to tan-gray at the base of core 1H. The FHPC cores had gas voids, but the deeper FC cores did not have ‘obvious’ gas voids.. Alkalinity rose gradually over the uppermost 5-6 mbsf, then more rapidly to the base of core 1H. The first sample in core 2H at 10.3 mbsf contained the maximum measured alkalinity at 16.1 mM. The sulfate profile showed degrees of depletion that were more or less proportional to the alkalinity increase. Examination of the core logging and imaging for evidence of the onset of methane expansion cracks indicated that the depth of the sulfate-methane interface occurs within the 2.3 meter coring gap between cores 1H and 2H. The shipboard pore water analyses are given in Table 6. The projected depth of the SMI based on the sulfate and alkalinity gradients is about 8 mbsf. The alkalinity and sulfate data for the uppermost 44 meters of sediment in Hole KC151 #3 are shown in Figure 5.

Table 6. Hole KC151 #3 Shipboard Pore Water Chemistry.

Hole Core-section (cm interval)	Top Depth (mbsf)	Salinity (ppt)	Alkalinity (mM)	Sulfate (mM)
KC151 #3				
1H-1 (85-100)	0.85	35.0	3.01	27.9
1H-2 (85-100)	1.85	35.0	2.87	26.6
1H-3 (85-100)	2.85	35.0	2.86	26.3
1H-4 (85-100)	3.85	35.0	3.84	26.3
1H-5 (85-100)	4.85	35.0	4.55	25.6
1H-6 (85-100)	5.85	35.3	6.73	24.1
1H-7 (85-100)	6.85	35.5	10.57	18.7
2H-1 (85-100)	10.30	38.0	16.06	0.7
2H-2 (85-100)	11.30	38.0	14.89	0
2H-3 (85-100)	12.30	38.5	13.42	0.7
2H-4 (85-100)	13.30	39.5	12.29	0
2H-5 (85-100)	14.30	40.0	10.82	0
2H-6 (85-100)	15.30	40.0	9.63	0
2H-7 (85-100)	16.25	40.5	8.53	0
3H-1 (82-100)	19.41	42.5	5.09	
3H-3 (77-100)	21.36	44.0	4.42	
3H-5 (83-100)	23.42	44.5	3.69	
3H-7 (77-100)	25.36	44.5	3.44	
4H-2 (80-100)	29.54	44.5	3.20	
4H-5 (80-100)	32.54	45.0	3.08	
4H-7 (80-100)	34.54	45.0	3.06	
5H-3 (78-100)	39.97	45.0	3.35	
5H-6 (82-100)	43.01	45.0	3.20	
6C-2 (80-100)	101.77	36.0	7.50	0
8C-2 (80-100)	216.53	49.5	5.99	0
8C-3 (80-100)	217.53	50.0	5.12	0
10C-2 (75-100)	224.86	50.0	5.51	0
12C-2 (0-25)	231.12	51.0	5.22	0
12C-3 (75-100)	231.87	50.0	4.34	1.1
14C-2 (80-100)	243.81	50.0	4.82	0
14C-3 (80-100)	244.81	51.0	4.06	0
15C-2 (39-64)	253.46	52.0	3.85	0
15C-3 (75-100)	254.82	52.0	3.29	0
17H-2 (75-100)	257.78	52.5	4.73	0
17H-5 (0-25)	260.03	51.0	4.12	0
19H-2 (57-65)	276.19	51.0	3.27	0
19H-2 (80-100)	276.62	53.0	2.40	0
19H-6 (65-100)	280.27	50.0	3.50	0
20H-2 (75-100)	294.66	52.0	2.48	0
20H-6 (75-100)	298.66	53.5	2.34	0
21H-1 (71-100)	312.22	54.0	2.53	0
22C-2 (75-100)	332.15	50.0	3.09	3.1
24C-1 (76-100)	370.18	55.0	3.89	0
25C-1 (75-100)	379.31	54.0	3.43	0

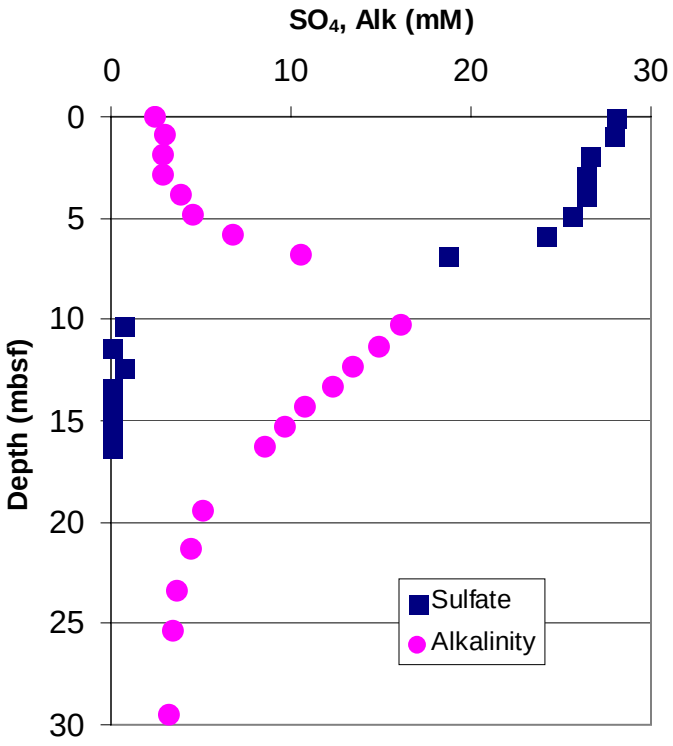

Figure 4. Alkalinity and sulfate, Hole KC151 #3.

Alkalinity in Hole KC151 #3 decreases rapidly beneath the maximum of 16.1 mM at 10.3 mbsf to about 3 mM at 44 mbsf, increases to 7.5 mM in the single sample at 101.2 mbsf, then diminishes regularly from 6 mM at 217 mbsf down to 2.5-3.9 mM in the deepest cored sediments at 380 mbsf. In this interval of low alkalinity, carbonate appears in sediment cores as disseminated flecks to thin beds. Sulfate was absent from the pore water in all cores below a depth of about 11 mbsf, except in cores 12C-3 and 14C-2, where the FC cores may have contained a small amount of seawater contamination. Salinity shows the only significant variation with depth as illustrated in Figure 5.

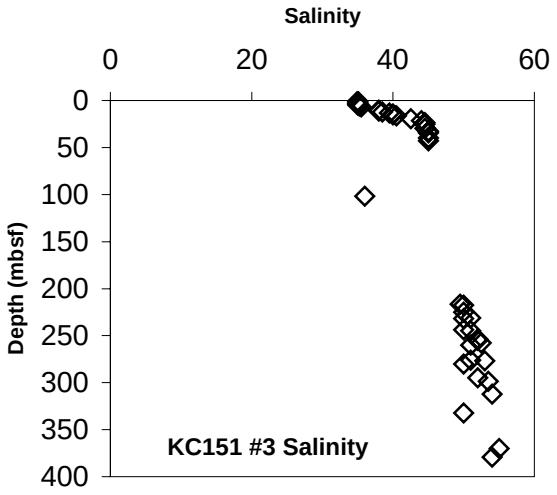

Figure 4. Salinity vs depth, Hole KC151 #3.

Salinity increases rapidly from seawater values (35 ppt) near the seafloor to about 44 ppt at depth of 24 mbsf, then appears to increase fairly linearly with depth to 55 ppt at depth of 380 mbsf, with the exception of the low salinity (36 ppt) in a core of a sand layer that appears on seismic records to intersect the seafloor. The variation in the salinity profile is small down to a depth of about 250 mbsf, and then shows increasing scatter from 250 to 380 mbsf. Some of this variation in salinity may be due to decomposition of gas hydrates, which were indicated in the LWD records and confirmed by pressure cores.

Conclusions

The shipboard pore water geochemistry program on the April-May 2005 Gulf of Mexico JIP cruise provided information on near seafloor gradients in some of the microbial metabolites and on the salinity of formation waters encountered in the cores. The sulfate and alkalinity gradients primarily reflect the upward flux of methane. Sulfate reduction is driven almost exclusively by oxidation of methane, as indicated by the 1:1 stoichiometric ratio of sulfate depletion relative to alkalinity addition, as shown in Figure 5.

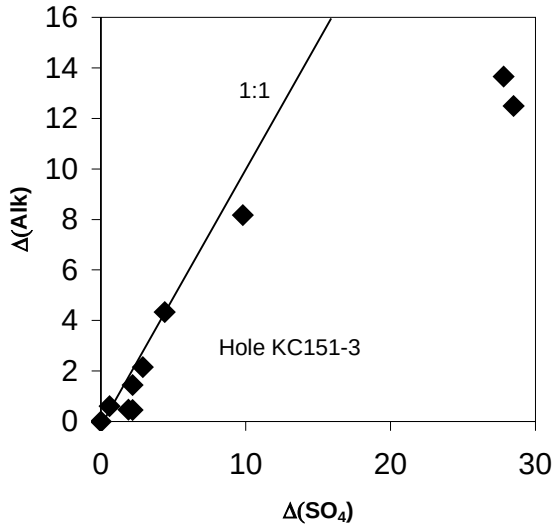

Figure 5. Plot of alkalinity added versus sulfate removed (relative to seawater concentrations). Diagonal line indicates 1:1 ratio, consistent with methane oxidation being the electron-generating process that fuels sulfate reduction.

The deviation of deeper samples from the 1:1 ratio probably indicates some degree of alkalinity removal associated with precipitation of authigenic carbonate. The importance of methane oxidation was confirmed by post-cruise analyses of the $\delta^{13}C$ of DIC, with values as negative as –50‰.

Elevated pore water salinities (up to 55-56 ppt) were observed in cores from the Atwater Valley Mound sites and Keathley Canyon. Both sites are underlain by salt structures, but more detailed work on the ionic composition of the pore waters indicates that the observed high salinities are not the product of simple dissolution of halite, but instead reflect the regional influence on pore water of a diagenetically modified basinal brine.

Total iodine, bromine, and barium concentrations in pore waters from the Atwater Valley area, Gulf of Mexico: Preliminary results from the Gas Hydrates JIP Cruise.

Glen Snyder*, L. Ashley Hubbard, Brandon Dugan, Gerald Dickens
Rice University
Earth Science Department
6100 Main Street, MS-126
Houston, TX 77005

*gsnyder@rice.edu

1. Introduction

The halogens iodine and bromine are both concentrated in marine organic matter and deposited on the sea floor. Long—term removal of iodine from the oceans has led to extremely low seawater concentrations, averaging only 0.44 μM (Broecker and Peng, 1982). In contrast, pore water concentrations of iodine in marine sediments may exceed 1200 μM (Egeberg and Dickens, 1998). The diagenetic release of iodine from organic matter in shallow sediments as water-soluble iodide is largely a microbial processes (Amachi et al., 2005a,b), although the degree to which this process is coupled with microbial methanogenesis is poorly known. Accumulations of iodine in shallow marine sediment have been observed (Kennedy and Elderfield, 1987) and appear to be a function of not only the deposition rate of organic matter (Martin et al., 1993) but also of the duration of deposition of organic matter in continental margin settings (Snyder et al., 2006). Bromine, on the other hand, is less effectively scavenged from the oceans in organic matter. Seawater concentrations average 840 μM (Broecker and Peng, 1982). In addition, sediment pore fluids have bromine concentrations which increase only modestly during diagenetic release (You et al., 1993; Egeberg and Dickens, 1998).

Barium cycling in the shallow subsurface is a complicated process that can help provide constraints on fluid flux. Authogenic barite fronts have been used in gas hydrate provinces to evaluate past fluxes of hydrocarbons through the hydrate stability zone (Dickens, 2001). Interstitial porewater analyses can be used to document mixing of shallow fluids and fluids advected from greater depths (Castellini et al., 2006). Integration of porewater barium analyses and sediment barite studies can constrain where fluids are rapidly migrating and how that relates to the distribution of hydrate.

In this investigation we determined the relative abundances of iodine, bromine, and barium in pore fluids and sediment from the Gulf of Mexico, and discuss their relationship to the migration of methane-charged fluids and the accumulation of gas hydrates. Iodine—isotopic measurements will be carried out in the near future with some of the pore fluids. Previous studies of ^{129}I have been carried out with brines from production wells in the Gulf of Mexico (Moran et al., 1995). Our investigation will be the first in the Gulf of Mexico to look at the systematic changes in iodine isotopic composition which occur with increasing sediment depth, as well as spatial changes related to proximity of active fluid venting sites.

This report provides the preliminary results for the Atwater Valley and Keathley Canyon field sites sampled on the JIP Gas Hydrates Cruse. Seismic data of the Atwater area prior to the cruise indicated the presence of mound structures on the seafloor, underlain by seismic "wipeout" indicating the presence of free gas in the subsurface. Drill cores recovered soupy mud and moussy dark grey mud from two sites near one of the Atwater mounds (ATM-1 and ATM-2). Further away from the mound, drilling recovered mud with some authigenic nodules (AT14). Samples were also recovered at some distance from the mounds (AT13-1 and AT13-2), yielding moussy dark gray and green/gray mud. In both cases, the AT13 cores yielded some gas and bubbles.

2. Methods

Interstitial pore fluids were squeezed from marine sediment samples onboard the ship. For iodine and bromine analyses, the samples were centrifuged and diluted in 18 megohm water. Rhodium was added as an internal drift standard and tetramethylammonium hydroxide (0.1%w/v) was added as a reducing agent and matrix solution to both samples and standards (Schnetger and Muramatsu, 1996). Iodine and bromine were analized at masses 79 and 127, respectively, on a Finnegan Element II ICP-MS in the Rice Laboratory Facility of Cin-Ty Lee. Iodine was scanned at low resolution, and bromine at medium resolution. While iodine was probably present in the fluids as iodide, iodate, and organically bound iodine, no attempt was made to determine speciation. Both the iodine and bromine referred to in this paper are total values, regardless of speciation. Given that iodine in reducing conditions exists primarily as aqueous iodide (e.g. Snyder et al., 2006; Kennedy and Elderfield, 1987), one would assume that this is the predominant species in the deeper samples.

Pore water samples splits for barium (Ba^{2+}) analyses were also prepared in the Rice University Geochemistry Laboratory. In order to minimize contamination, an aliquot of the HNO_3-treated pore water was transferred from its original, shipboard-sealed vial to an acid-washed micro-centrifuge tube under a laminar flow hood. All sub samples used for Ba^{2+} concentration analysis were taken from this fraction. Pore water was allowed to equilibrate to room temperature before any transfers were made. This was done to reduce contamination from condensate on the vial. A 1:10 dilution was prepared for each sample by combining 1 mL of pore water sample with 9.0 mL of 18Ω water and 100 µl of ultrapure HNO_3 in an acid washed 15 mL centrifuge tube. 100 µl of Yitrium was also added to each sample as an internal standard to monitor instrumental drift. Samples were

analyzed with a wavelength of 455.403 nm on a Varian Vista Pro ICP-AES in the Rice Geochemistry Laboratory. Ba^{2+} concentrations were determined by comparing the peak areas of the sample to those of a standard with similar and known NaCl and Ba^{2+} concentrations.

3. Discussion and preliminary conclusions

Iodine and bromine concentrations were greatest in the mound samples, ATM-1 and ATM-2 (Fig. 1), and actually decreased slightly with depth.

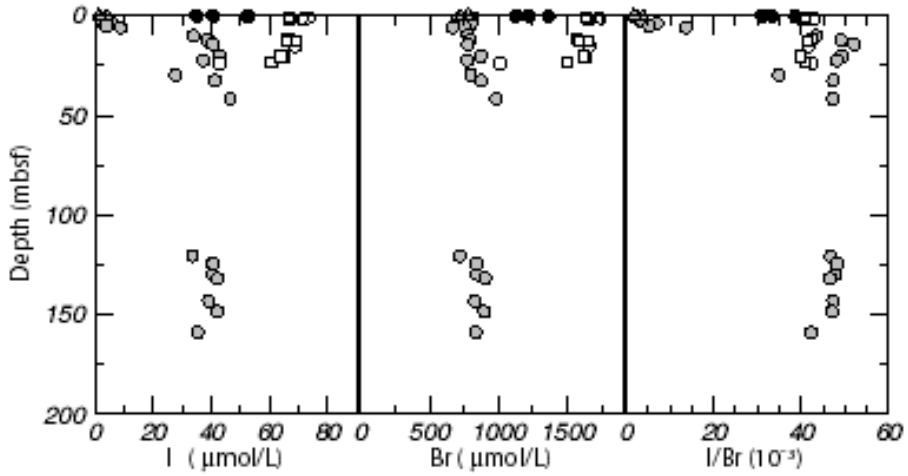

Figure 1: Depth profiles for iodine and bromine in interstitial pore fluids at Atwater Valley. White symbols=mounds, Gray symbols=samples collected away from the mounds, Black symbols=samples collected just off the mound. Gray triangle=AT13-1, gray circle=AT13-2, black circle=AT14, white circle=ATM-1, and white square=ATM-2.

In contrast, the site furthest from the mounds, AT13, had shallow pore fluids that were similar to seawater in terms of bromine and chlorine concentrations. Iodine concentrations at AT13 increase in depth over the first 25 meters to ~40 µM. Bromine concentrations are slightly less than seawater in the shallow sediments, and then remain fairly constant with depth. Shallow pore fluid samples collected close to the mound (AT14) have iodine concentrations which are between those of AT13 and those of the mounds. Ratios of I/Br are actually greater at site AT13 than at the mound sites. Apparently the deep fluids from the mound site are highly enriched in bromine as well as iodine, perhaps representing an ancient, residual brine.

Mixing relationships between different end-members is represented in Figure 2, and appears to be influenced by redox changes occurring near the sulfate methane transition (SMT).

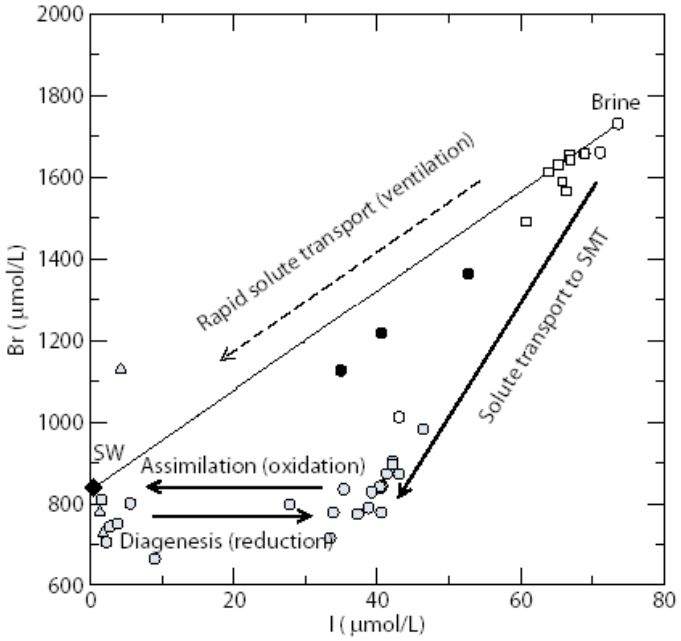

Figure 2: Relative amount of bromine and iodine in pore fluids. Symbols as in figure 1.

Where deep brines are rapidly brought to the surface by advection at the mound sites, they retain high iodine and bromine concentrations all the way to the sediment-water interface. AT14 also shows relatively high bromine concentrations in the three samples analyzed, and appears to show mixing of the deep brine with varying amounts of seawater in the shallow sediments. Site AT13 which is most distant to the mounds, indicates mixing of a deep brine component, presumably through upward diffusion of iodine and bromine, where it combines with shallow fluids that have near-seawater Br concentrations. Although bromine concentrations remain essentially constant at depths shallower than 25m (Fig. 1), iodine concentrations continue to decrease until they reach seawater values in very shallow sediments. Presumably, iodine is released diagenetically as the sediments are buried over the first 25 meters, and then reassimilated through microbial oxidation as it diffuses upward towards shallower intervals.

Pore water Ba^{2+} concentrations range from 13.255 - 18.201 µM in Atwater Valley mound samples and 0.060 - 3.178 µM in the remainder of the Atwater Valley samples (Fig. 3). In Keathley Canyon, Ba^{2+} varies from 0.022 to 6.659 µM (Fig. 4).

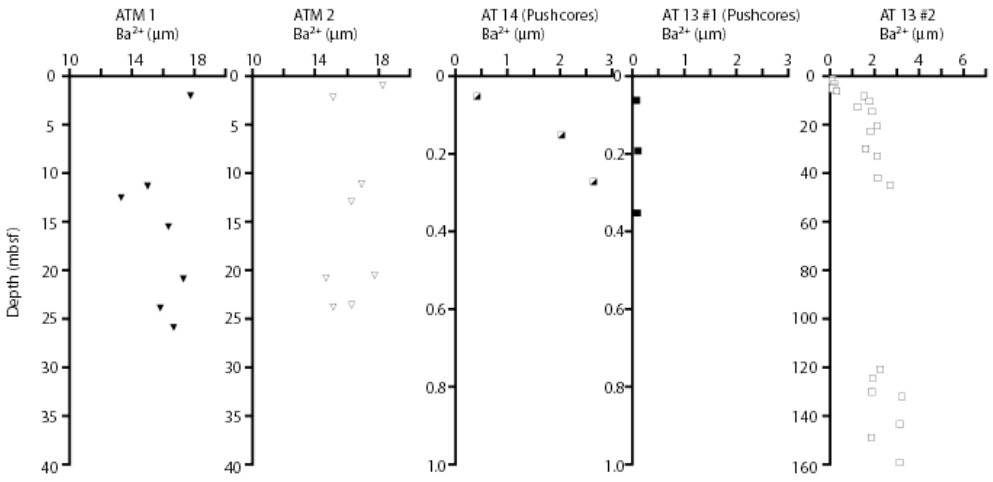

Figure 3: Ba^{2+} porewater concentrations for samples from Atwater Valley sites.

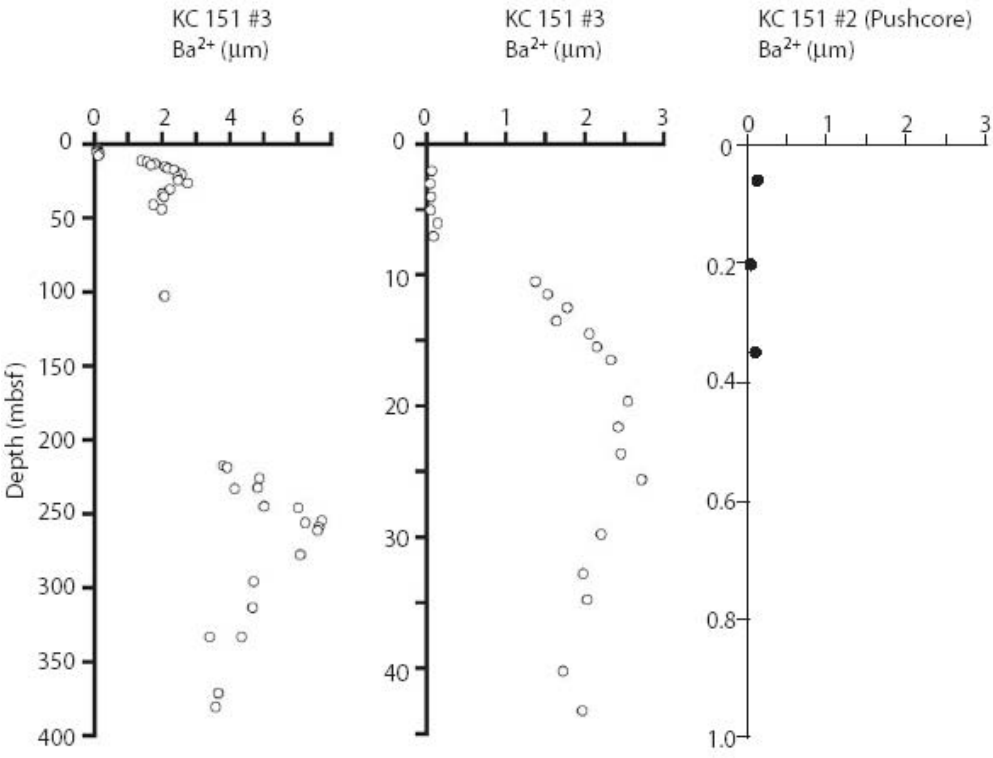

Figure 4: Ba^{2+} porewater concentrations for samples from Keathley Canyon sites.

The mean detection level (MDL) calculated for these analyses is 0.006 µM. Measured concentrations that fall below this value are not considered. Samples from KC151 #3 display peaks at approximately 25 and 254 mbsf. Samples from AT13 #2 increase in concentration between approximately 6-8 mbsf and remain at these higher concentrations down core. The Atwater Valley mound sites (ATM 1 and 2) are similar in concentration and show little down-core variation. The AT14 pushcore exhibits an increasing trend in concentration with depth whereas the KC151 #2 and AT13 #1 pushcores show little

variation with depth. In general, samples from Atwater Valley document and increase in pore water Ba^{2+} concentration with increasing proximity to the mound sites.

4. Further research

Iodine and bromine analyses will be carried out on pore waters from the Keathley Canyon site, where bottom simulating reflectors (BSRs) suggest the presence of free gas below a gas hydrate layer. Sediment samples will be analyzed for barite fronts at Atwater Valley and Keathley Canyon to determine the barium cycle at these two independent settings. In addition, halogens will be determined in the sediment samples (Schnetger and Muramatsu, 1996) from both Atwater Valley and Keathley Canyon, in order to find out if iodine accumulation has occurred in the shallow sediments. Although pore fluid iodine concentrations are significantly lower than other continental margin sites (e.g. Egeberg and Dickens, 1996) samples will be combined from similar depths in each core in order to carry out ^{129}iodine analyses, and derive an age for the deeply--sourced brines (Moran et al., 1995).

References

Amachi, S., Fugii, T., Muramatsu, Y., 2005a. Iodide oxidation and iodate reduction by marine bacteria. Geochim. Cosmochim. Acta, 69, A711.

Amachi, S., Muramatsu, Y., Akiyama, Y., Miyazaki, K., Hanada, S., Kamagata, Y., Shinoyama, H., Bannai, T., and Fujii, T., 2005b. Isolation of iodide-oxidizing bacteria from iodide-rich natural gas brines and seawater, Microbial Ecol., 49, 547-557.

Broecker, W.S., Peng, T.H., 1982. Tracers in the Sea. Eldigio Press, Columbia Univ., 690 pp.

Castellini, D.G., Dickens, G.R., Snyder, G.T., Ruppel, C.D., 2006. Barium cycling in shallow sediment above active mud volcanoes in the Gulf of Mexico, Chemical Geology, 226, 1-30.

Dickens, G.R., 2001. Sulfate profiles and barium fronts in sediment on the Blake Ridge: present and past methane fluxes through a large gas hydrate reservoir. Geochim. Cosmochim. Acta, 65, 529-543.

Egeberg, P.Kr., and Dickens, G.R., 1999. Thermodynamic and halogen pore water constraints on gas hydrate distribution at ODP Site 997 (Blake Ridge). Chem. Geol., 153, 53-79.

Kennedy, H.A., Elderfield, H., 1987. Iodine diagenesis in pelagic deep-sea sediments, Geochim. Cosmochim. Acta, 51, 2489-2504.

Martin, J.B., Gieskes, J.M., Torres, M., and Kastner, M., 1993. Bromine and iodine in Peru margin sediments and pore fluids: Implications for fluid origins. Geochim. Cosmochim. Acta, 57, 4377-4389.

Moran, J.E., Fehn, U., Hanor, J.S., 1995. Determination of source ages and migration of brines from the U.S. Gulf Coast basin using 129I, Geochim. Cosmochim. Acta, 59, 5055-5069.

Schnetger, B., Muramatsu, Y., 1996. Determination of the halogens, with special reference to iodidne, in geological and biological samples using pyrohydrolysis for preparation of inductively coupled plasma mass spectrometry and ion chromatography for measurement. Analyst, 121, 1627-1631.

Snyder, G., Fehn, U., Dickens, G., 2006. Iodine in open ocean and continental margin sedimentary sequences: Dynamic cycling and accumulation on the sea floor. Earth Planet. Sci. Lett., submitted.

You, C.F., Gieskes, J.M., Chen, R.F., Spivak, A., Gamo, T., 1993. Iodide, bromide, manganese, boron, and dissolved organic carbon in interstitial waters of organic carbon-rich marine sediments: Observations in the Nankai Accretionary Prison. In: Hill, I.A, Taira, A., Firth, J.V., et al. (Eds.), Proc. ODP Sci. Results, 131, College Station, 185-174.

Geomechanical Characteristics of Sediments from Atwater Valley and Keathley Canyon, Northern Gulf of Mexico

Brandon Dugan
Department of Earth Science
Rice University
6100 Main Street, MS-126
Houston, TX 77005
Phone: 713.348.5088
Email: dugan@rice.edu

Introduction

Geomechanical properties impact the strength of sedimentary sequences and the transport of fluid, heat, and chemicals through these sequences. We present shore-based, laboratory measurements of deformation and flow properties of sediments from Keathley Canyon and Atwater Valley. These properties are constrained at vertical effective stresses less than 3.0 MPa which are similar to the in situ values assuming hydrostatic fluid pressure. All experiments are conducted at 100% water saturation and room temperature and thus represent base-line conditions in the absence of free gas or gas hydrate. These physical properties can be incorporated into basin models that evaluate fluid flow, heat and chemical transport, and deformation in Keathley Canyon and Atwater Valley. These non-hydrate-bearing properties can be compared to estimates on hydrate-bearing properties to evaluate how hydrate saturation influences flow and strength properties of fine-grained sediments.

Methods

Constant-rate-of-strain consolidation (CRSC) experiments were performed to evaluate the elastic and plastic deformation behavior and the permeability on whole-core samples collected during JIP drilling in Atwater Valley and Keathley Canyon of the northern Gulf of Mexico. All samples analyzed were collected with the Fugro Hydraulic Piston Corer (FHPC) or the Fugro Corer (FC) (Table 1). Whole round sub-samples were cut from core sections based on visual inspection and MSCL data. End-caps were sealed on the whole-round sub-samples to help maintain the natural saturation of the samples. Samples were refrigerated during transport and storage. All experiments were conducted in the Rice University Geotechnical Lab.

For each CRSC experiment, a specimen was cut from the whole-round sample and trimmed directly into the fixed-wall consolidation ring. This consolidation ring ensures uniaxial strain (i.e., no lateral strain) conditions throughout the experiment. Each specimen was trimmed to be a right cylinder [5.09 cm (diameter) by 2.41 cm (height)].

Table 1: Summary of Core Specimens and Experimental Conditions

Expt	Boring	Core-Section	mbsf	w_c	f_i	e_i	r_b (g/cm^3)	S_i (%)	u_b (kPa)	s'_s (kPa)	e_i (%)	de/dt (%/hr)
CRS001	AT13#2	11H-5	131.88	51.7	59.1	1.447	1.674	96.4	586	3.8	-0.03	0.5
CRS002	KC151#3	1H-5	5.05	94.5	73.2	2.731	1.449	99.1	586	3.6	-0.04	0.5-0.7
CRS003	KC151#3	2H-8	17.27	49.5	59.8	1.490	1.629	91.0	586	1.7	-0.03	0.5-0.6
CRS004	KC151#3	4H-3	31.19	41.6	56.6	1.303	1.686	90.8	586	4.3	-0.03	0.50
CRS005	KC151#3	3H-5	22.61	51.7	59.8	1.485	1.643	93.0	586	0.8	-0.02	0.60
CRS006	KC151#3	10C-3	226.53	28.4	44.7	0.809	1.935	98.9	586	5.2	-0.04	0.50
CRS007	KC151#3	14C-1	243.13	29.3	45.6	0.840	1.903	95.3	586	3.4	-0.20	0.50
CRS008	KC151#3	20H-5	298.31	31.1	51.1	1.045	1.753	84.7	586	31.5	-0.22	0.50
CRS009	KC151#3	19H-5	280.01	32.3	51.1	1.044	1.769	87.8	586	31.7	-0.07	0.50
CRS010	KC151#3	21H-2	313.72	27.2	47.5	0.906	1.809	82.5	586	26.6	-0.03	0.50
CRS016	AT13#2	14H-1	158.35	44.1	53.7	1.160	1.800	100.0	386	7.7	-0.05	0.35
CRS017	AT13#2	14H-1	158.4	44.6	57.0	1.327	1.726	99.2	386	5.6	-0.08	0.50

Table 2: Geotechnical Properties Interpretted from CRSC Experiments and Log Data

Expt	Boring	Core-Section	mbsf	P_h (kPa)	s_v (kPa)	s_{vh}' (kPa)	e_o	C_c	C_e	K @ e_i (cm/s)
CRS001	AT13#2	11H-5	131.875	14295	15156	861	1.788	0.344	0.068	$1.1x10^{-5}$
CRS002	KC151#3	1H-5	5.05	13336	13356	20	3.341	0.605	0.065	$7.3x10^{-6}$
CRS003	KC151#3	2H-8	17.27	13459	13549	91	1.693	0.257	0.038	$6.2x10^{-7}$
CRS004	KC151#3	4H-3	31.19	13599	13785	187	1.491	0.203	0.035	$9.8x10^{-7}$
CRS005	KC151#3	3H-5	22.61	13513	13640	128	1.660	0.229	0.041	$6.3x10^{-6}$
CRS006	KC151#3	10C-3	226.53	15561	17402	1841	1.169	0.184	0.025	$2.2x10^{-7}$
CRS007	KC151#3	14C-1	243.13	15728	17725	1998	1.041	0.146	0.024	$3.3x10^{-7}$
CRS008	KC151#3	20H-5	298.31	16282	18764	2482	1.481	0.241	0.060	$3.0x10^{-7}$
CRS009	KC151#3	19H-5	280.005	16098	18421	2323	1.544	0.255	0.042	$5.5x10^{-8}$
CRS010	KC151#3	21H-2	313.72	16437	19061	2625	1.187	0.172	0.046	-
CRS016	AT13#2	14H-1	158.35	14561	15600	1039	1.980	0.431	0.091	$3.4x10^{-6}$
CRS017	AT13#2	14H-1	158.4	14561	15601	1040	2.219	0.472	0.112	$2.5x10^{-7}$

The CRSC experiment methodology was based upon the guidelines presented in ASTM D4186 (ASTM International, 2003).

The specimen-containing consolidation ring was placed in a consolidation cell with porous stones on the top and bottom of the specimen to facilitate fluid drainage. The specimen was then subject to a back pressure (u_b) (Table 1) while maintaining the initial height of the specimen. After maintaining height and backpressure on the specimen for at least 8 hours, uniaxial deformation proceeded at a constant rate of strain. The vertical effective stress prior to the start of consolidation (σ_s') and the initial strain (ε_i) on the specimen were documented for each experiment to evaluate any disturbance that may have occurred during set-up and applying backpressure (Table 1). During consolidation, the back pressure (top of specimen) was held constant; the pore pressure (base of specimen) and the axial load required to maintain the strain rate were monitored and measured. The strain rate ($d\varepsilon/dt$) for each experiment is provided in Table 1.

The initial properties of each specimen (Table 1) were evaluated from measurements on the individual specimen. For each specimen, we define the initial water content (ω_c), porosity (ϕ_i), void ratio (e_i), bulk density (ρ_b), and saturation (S_i) (Table 1). These properties are calculated from Equations [1]-[5] and assume a constant grain density (ρ_g) of 2.7 g/cm^3.

$$\omega_c = \frac{m_w}{m_s} \quad [1]$$

$$\phi_i = \frac{e_i}{1+e_i} \quad [2]$$

$$e_i = \frac{V_t - V_s}{V_s} \quad [3]$$

$$\rho_b = \frac{m_w}{V_t} \quad [4]$$

$$S_i = \frac{w_c}{e_i}\rho_g \quad [5]$$

From the consolidation phase of the experiment, we determined the primary compression behavior for each specimen by constraining the compression index (C_c) and reference void ratio (e_o) (Figure 1; Table 2). The compression index, Equation [6], characterizes primary consolidation on the linear portion of the *e*-log(σ_v') plot,

$$C_c = \frac{e_{\sigma_v'} - e_{\sigma_v'+\Delta\sigma_v'}}{\log\left[\left(\sigma_v'+\Delta\sigma_v'\right)/\sigma_v'\right]} \quad [6]$$

The reference void ratio defines the void ratio of the specimen at effective vertical stress equal to 1 kPa. C_c and e_o were determined by defining a best-fit line through the primary compression data.

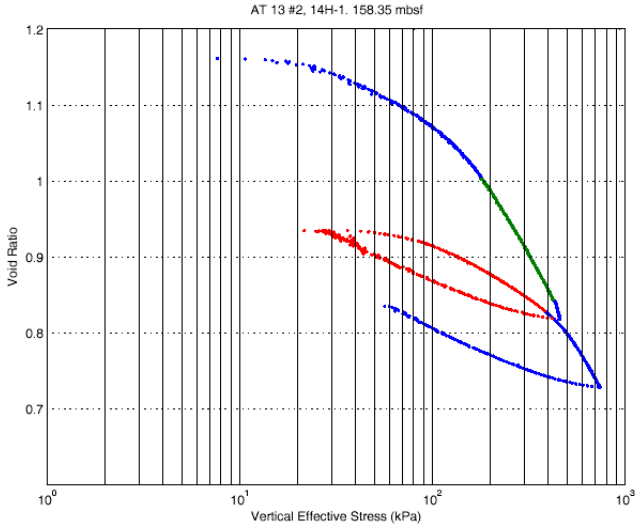

Figure 1: Example of CRSC data from AT 13#2, Core 14, Section 1. Specimen was from 158.35 mbsf. Green data were used to constrain the compression index (C_c) and reference void ratio (e_o) for primary consolidation and were used for the hydraulic conductivity (K) analyses. Red data are controlled unload-reload data used to evaluate the elastic, recompression index (C_e).

The recompression/expansion index, Equation [7], describes the elastic portion of the *e*-log(σ_v') plot. It is defined along the unloading/reloading curve,

$$C_e = \frac{e_{\sigma_v'} - e_{\sigma_v'+\Delta\sigma_v'}}{\log\left[\left(\sigma_v'+\Delta\sigma_v'\right)/\sigma_v'\right]} \qquad [7]$$

Hydrostatic fluid pressure (P_h), total vertical stress (σ_v'), and hydrostatic effective vertical stress ($\sigma_{vh}' = \sigma_v - P_h$) are provided as reference stresses for each specimen. These stresses represent that state of stress for hydrostatic fluid pressure at each specimen depth. Hydrostatic fluid pressure is calculated assuming an average water density of 1.024 g/cm^3. Total vertical stress is determined by integrating the LWD-measured bulk density.

The pore pressure response during CRSC experiments was used to evaluate the hydraulic conductivity (K) of the specimen during consolidation. Hydraulic conductivity was estimated following the approach presented by Tan et al. (2006). Hydraulic conductivity was determined during primary consolidation to establish a void ratio-hydraulic conductivity trendline (Figure 2).

This trendline was then used to estimate the hydraulic conductivity of each specimen at in situ conditions (Table 2). This approach assumes a log-linear relationship between hydraulic conductivity and void ratio (e.g., Lambe and Whitman, 1969) and that the initial specimen void ratio (e_i) represents in situ void ratio.

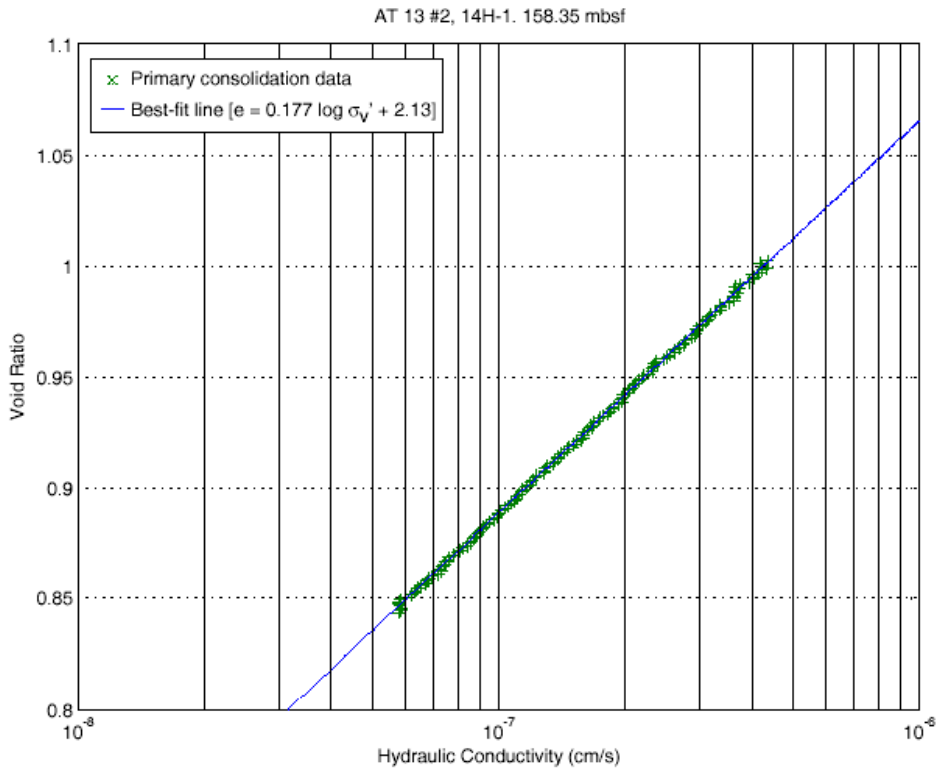

Figure 2: Void ratio-hydraulic conductivity data (green x) during primary consolidation of specimen from AT 13 #2, Core 14, Section 1, 158.35 mbsf. A best fit line of the data (blue line) is used to define a hydraulic conductivity function which is used to estimate the in situ hydraulic conductivity of the specimen.

Results

The initial conditions of the experimental specimens show general trends with depth (Figure 3). As depth increases downhole, the overburden pressure increases and the effective vertical stress also increases assuming hydrostatic conditions (Table 2). The downhole-decrease in pore volume of these specimens is consistent with increasing vertical effective stress with depth (Table 2). This behavior is manifested as decreasing water content (ω_c), initial specimen porosity (ϕ_i), and initial specimen void ratio (e_i) and as increasing bulk density (ρ_b). Saturation indices show that some of the specimens were slightly dehydrated prior to the experimental program. This may have resulted from air or gas voids sealed in the core liners or from air transfer through the sealed end-caps. Back pressure saturation prior to each experiment was completed to create 100% water saturation prior to each experiment.

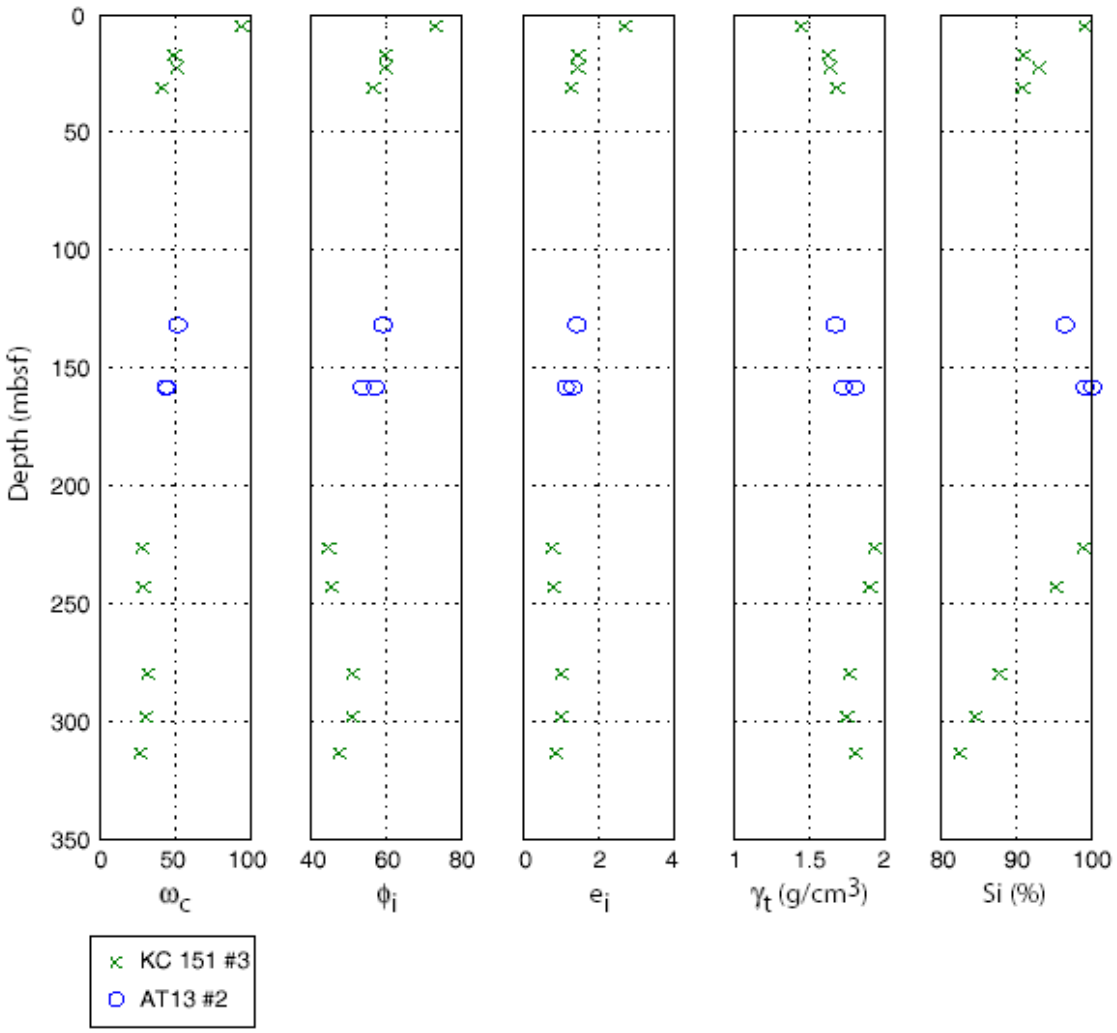

Figure 3: Initial conditions for experimental specimens used in CRSC experiments plotted versus depth in meters below sea floor (mbsf). Water content (ω_c), initial porosity (ϕ_i), initial void ratio (e_i), bulk density (ρ_b), and saturation index (Si) were determined for each specimen following Equations [1]-[5]. Data presented for KC 151 #3 (green x) and for AT 13 #2 (blue o).

Experimentally constrained deformation and flow properties do not separate into site- or depth-trends (Figure 4). Compression indices range from 0.146-0.605 and expansion recompression indices are approximately 10% of the compression indices (Table 2, Figure 4). The interpreted hydraulic conductivity does not exhibit a depth trend or relation with in situ void ratio (Figures 4, 5). The lack of depth or void ratio trends for compaction and flow properties may be the result of grain size and lithology changes between the specimens. Additional analyses of grain size and mineralogy should be completed on these specimens to help define what causes the difference in geomechanical properties of the sediments at AT 13 and KC 151.

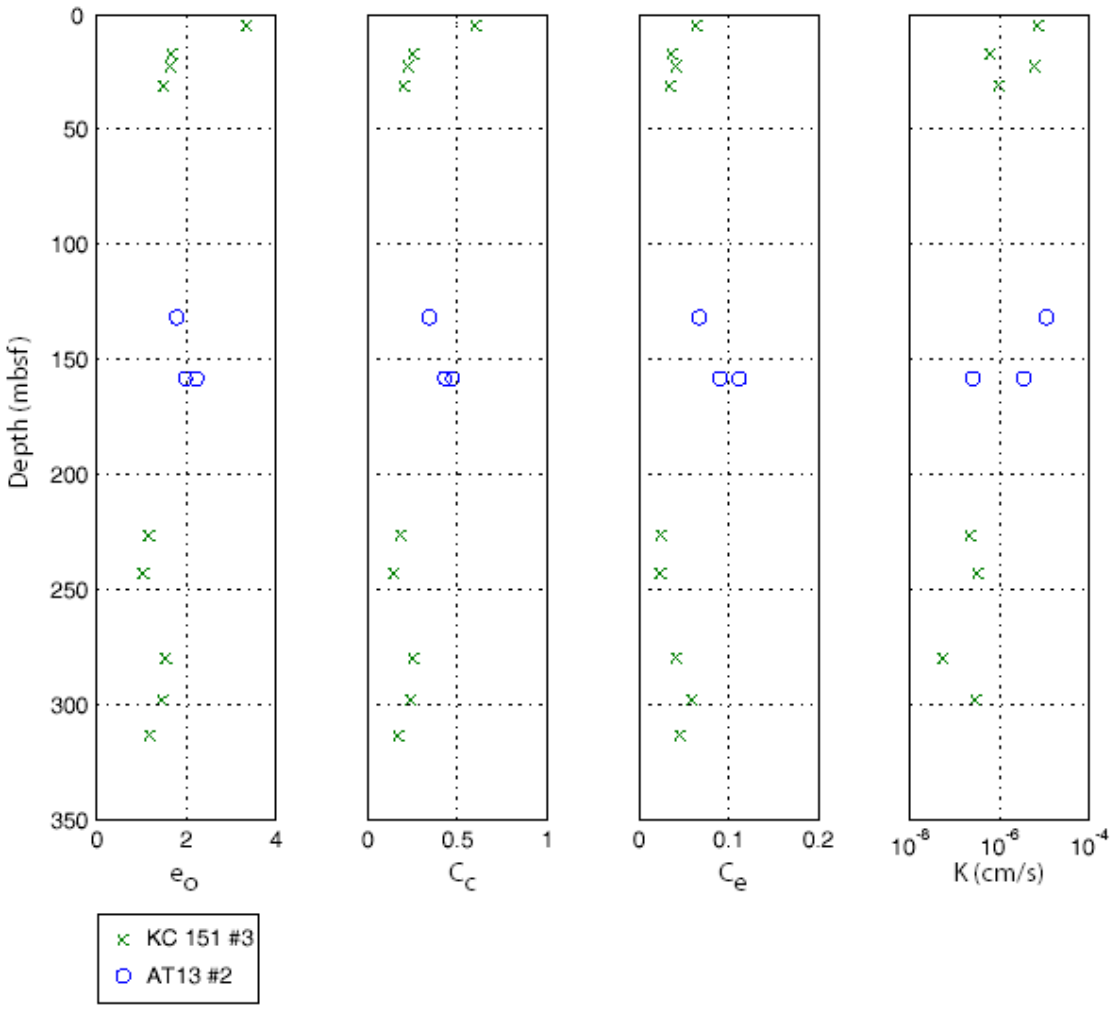

Figure 4: Consolidation and flow parameters determined from CRSC experiments at KC 151 #3 (green x) and AT 13 #2 (blue o). e_o and C_c define primary consolidation behavior. C_e defines expansion, recompression behavior. K is the hydraulic conductivity estimated for in situ void ratio.

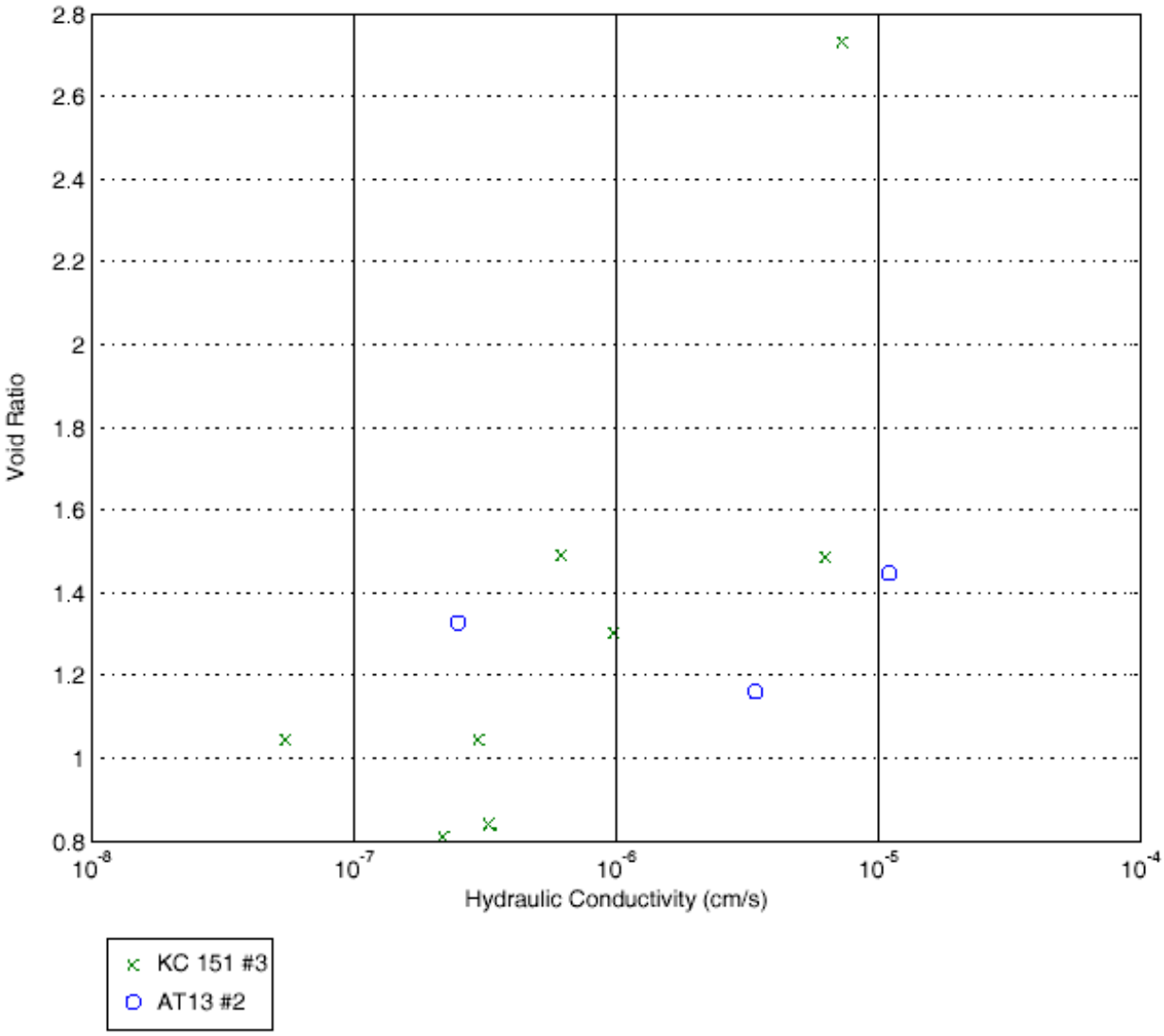

Figure 5: Summary of in situ void ratio and hydraulic conductivity data for specimens from KC 151 #3 (green x) and AT 13 #2 (blue o).

References

ASTM International, 2003, Standard test method for one-dimensional consolidation properties of soils using controlled-strain loading (Standard D4186-89[1998]); In Annual Book of ASTM Standards (Vol. 04.08): Soil and Rock (I): West Conshohocken, PA (Am. Soc. Testing and Mater.), 530–535.

Craig, R.F., 1992, Soil Mechanics, Chapman & Hall, London, 427pp.

Lambe, T.W. and Whitman, R.V., 1969, Soil Mechanics, John Wiley & Sons, New York, 553pp.

Tan, B., Germaine, J.T., and Flemings, P.B., 2006. Data report: Consolidation and strength characteristics of sediments from ODP Site 1244, Hydrate Ridge, Cascadia continental margin, In Tréhu, A.M., Bohrmann, G., Torres, M.E., and Colwell, F.S. (Eds.), Proc. ODP, Sci. Results, 204 [Online]. Available from World Wide Web: <http://www-odp.tamu.edu/publications/204_SR/102/102.htm>. [Cited 2006-07-10].

Gulf of Mexico Gas Hydrates Joint Industry Project
Pressure Coring and Core Logging

Peter Schultheiss, Melanie Holland, and John Roberts
Geotek Ltd., Daventry, UK
info@geotek.co.uk

Introduction

One of the goals of the US Department of Energy's Gulf of Mexico Joint Industry Project (GOM-JIP) is to "develop technology & data to assist in the characterization of naturally occurring gas hydrates." To help achieve this goal on the 2005 expedition on the D/V *Uncle John*, Geotek, Ltd., was contracted to mobilize the HYACINTH pressure coring system and to make non-destructive geophysical measurements to determine hydrate presence and sediment properties on all recovered cores, both conventional (non-pressure) cores and pressure cores.

The HYACINTH pressure coring system (Schultheiss et al., 2005) is designed to recover cores under *in situ* pressure and allow measurements to be made (e.g., gamma density, acoustic velocity, radiographs) and sub-samples to be taken from these cores while still maintaining pressure. Without pressure maintenance, sediment cores containing any significant amount of hydrate can suffer dramatic disturbance during core retrieval (Figure 1)–if they are retrieved at all! Not only does methane hydrate begin to dissociate during recovery, causing the cores to become soupy, but because methane hydrate only forms when pore waters are saturated with methane, cores also become disturbed by methane exsolution from porewater and subsequent gas expansion. Pressure coring obviates disturbance caused by gas expansion and retards methane hydrate dissociation. Pressure coring is particularly important for hydrate recovery in the warm waters of the Gulf of Mexico where core temperatures rise significantly during retrieval, which can result in the complete dissociation of hydrate in conventional cores before they are extracted from the core barrel.

Infrared thermal imaging was used to detect the existence of hydrate in conventional cores on the GOM-JIP Expedition. Hydrate dissociation within a core creates cold spots. Negative thermal anomalies attributable to methane hydrate were measured on Ocean Drilling Program (ODP) Leg 201 (Ford et al., 2003), and this work was expanded upon during ODP Leg 204, where massive and disseminated methane hydrate was identified by thermal anomalies (Shipboard Scientific Party, 2003). During the GOM-JIP Expedition, the temperatures of the cores were monitored primarily to identify negative thermal anomalies in a qualitative fashion, either for immediate hydrate identification and preservation or documentation of where hydrate may have existed.

Other non-destructive measurements made shipboard on most cores included gamma density, acoustic velocity, magnetic susceptibility, and electrical resistivity, using the Geotek MSCL-S. While most of these measurements are affected by the presence of methane hydrate, their primary purpose is to characterize the geological formation that hosts the hydrate and to provide a link to the downhole log data. Further measurements were made on shore using the Geotek MSCL-XYZ after the cores were split, which included RGB linescan imaging, color spectrophotometry, high-resolution magnetic susceptibility, and selective measurements of natural gamma activity.

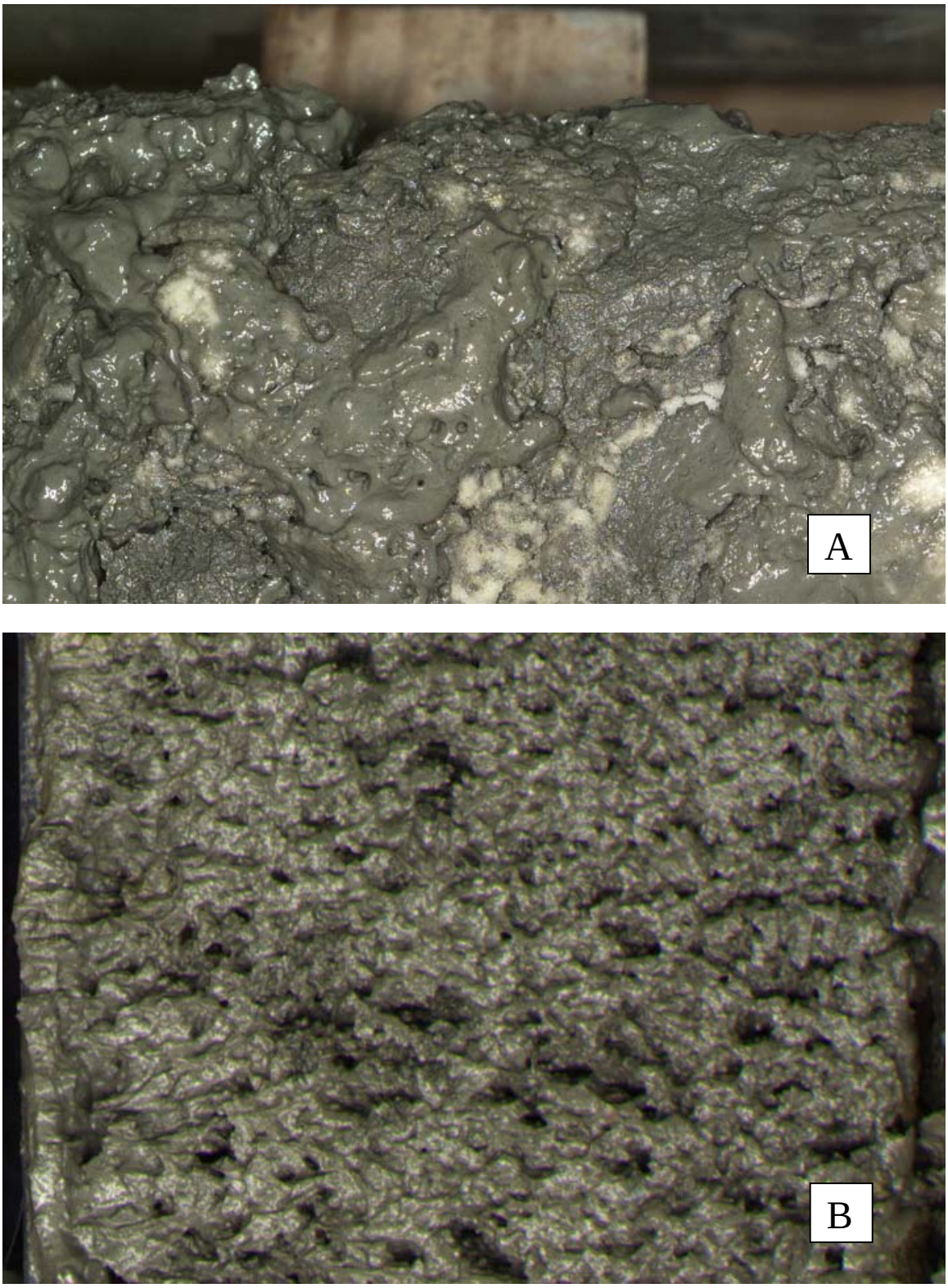

Figure 1. Moussy core, showing frothy, wet texture indicitave of hydrate dissociation. A. Core at top, containing gas hydrate is from ODP Leg 204. B. Core at bottom is from the GOM-JIP, Hole ATM1, Core 5H-2 (70-75 cm).

Explanatory Notes

These Explanatory Notes contain descriptions of techniques used on the GOM-JIP Expedition, and also address general issues encountered while performing measurements on cores from this Expedition.

HYACINTH Pressure Coring System

The HYACINTH pressure coring system is designed to recover cores at in situ pressure and transfer those cores, under pressure, into other pressure vessels or analytical equipment. The system consists of pressure coring tools and equipment to move the core from the coring autoclave into secondary pressure equipment. Analytical equipment used with these pressure cores on the GOM-JIP included the MSCL-V, the MSCL-P, and the X-ray computed tomography (CT) scanner.

HYACINTH Downhole Tools

Two types of wireline pressure coring tools have been developed: a percussion corer and a rotary corer, which were designed to cut and recover core in a wide range of lithologies where gas hydrate bearing formations might exist. Although the tools are quite different they include a number of important common features: they recover lined cores and mate to a common transfer system, use 'flapper valve' sealing mechanisms rather than ball valves to maximize the core diameter, and incorporate downhole drive mechanisms to ensure high core quality.

The percussion corer was developed by Fugro Engineers BV and is known as the Fugro Pressure Corer or FPC (Figure 2). The FPC uses a water hammer, driven by the circulating fluid pumped down the drill pipe, to drive the core barrel into the sediment up to 1 m ahead of the drill bit. The core diameter is 57 mm (liner outer diameter is 63 mm). On completion of coring, the recovery of the corer with the wireline pulls the core barrel into the autoclave, in which the pressure is sealed by a specially designed flapper valve. The FPC is designed to retain a pressure of up to 250 bar (25 MPa). It is suitable for use with unlithified sediments ranging from stiff clays to sandy or gravelly material. In soft sediments it acts like a push corer prior to the hammer mechanism becoming active.

The rotary corer was developed by the Technical University of Berlin and the Technical University of Clausthal, and is known as the HYACE Rotary Corer or HRC (Figure 3). The HRC uses an Inverse Moineau Motor driven by the circulating fluid pumped down the drill pipe to rotate the cutting shoe up to 1 m ahead of the roller cone bit. The cutting shoe of the HRC uses a narrow kerf, dry auger design with polycrystalline diamond (PCD) cutting elements. This design allows the core to enter into the inner barrel before any flushing fluid can contaminate the material being cored. The core diameter is 51 mm (liner outer diameter is 56 mm). On completion of coring, the recovery of the corer with the wireline pulls the core barrel into the autoclave in a similar manner to the FPC, and the pressure is sealed by a specially designed flapper valve. The HRC is designed to retain a pressure of up to 250 bar (25 MPa) and is primarily designed for use in sampling lithified sediment or rock. The HRC has also sampled softer formations effectively, though in “sticky” clay the flushing holes can become clogged with cuttings.

Figure 2. Fugro Pressure Corer (FPC) being deployed on the *Uncle John* during the GOM-JIP Expedition.

Figure 3. HYACE Rotary Corer (HRC) being deployed on the *Uncle John* during the GOM-JIP Expedition.

Transfer and Chamber Systems

The ability to manipulate cores, take sub-samples, and make measurements, all at *in situ* pressures, are major features of the HYACINTH system. To this end a series of interconnecting chambers and manipulator mechanisms have been developed to enable cores to be transferred, not only initially from the corer autoclaves, but subsequently between different chambers to enable a variety of measurements and sub-sampling tasks to be performed at full pressure. When the core is recovered on deck in the autoclave it is first cooled in an ice bath before being moved into a cold processing container. The autoclave is connected to a shear transfer chamber where the core is withdrawn and the core liner is cut to separate the geological part of the core from the remaining technical components which were inside the autoclave.

The pressure core in the FPC or HRC autoclave is similar to a conventional piston core in that the piston remains within the top of the liner; however, this pressure core piston assembly contains many more technical components than a conventional piston. The core and piston/sensor mechanism (referred to as the Catch Assembly, approx. 1.6 m long) consists of a "technical portion" (approx. 0.6 m long) and a "geological portion" (approx. 1.0 m long). The first transfer is designed to extract the Catch Assembly from the autoclave and to separate it into its 2 components (technical and geological). To achieve this, the autoclave is connected in series to a Shear Transfer Chamber (STC) and a Manipulator (Figure 4). After equalizing the pressures, the Manipulator is extended through the STC and mates to the Catch Assembly in the autoclave. The core is withdrawn into the STC where the technical and geologic parts of the Catch Assembly are separated by shearing the liner between them. At this stage the corer autoclave is isolated, removed, and replaced by another chamber (logging or storage). The pressures are again equalized and the Manipulator pushes the geological portion of the core into the logging or storage chamber. The technical portion of the core (still attached to the Manipulator) is pulled back into the STC. The ball valve on the logging or storage chamber is closed and the chamber, containing the geological portion of the core, removed for scientific measurements. The technical portion of the core is recycled for subsequent coring operations. Since the FPC and the HRC cores have slightly different diameters, the STC is supplied with two cutting boxes adapted to the specific core dimensions. The cutting boxes can be quickly interchanged by means of quick-fit flange clamp connections.

To move a core under pressure from one chamber to another, the chambers are connected, a Manipulator is attached to the end of the appropriate chamber (pushing vs. pulling), and the empty chambers are filled with water and pressurized until the pressure is equal to that in the chamber containing the core. The ball valves are opened and the core is moved from one chamber to the other with the Manipulator, which is retracted before closing all valves and depressurizing the empty chambers.

Logging / Storage Chambers

Once the core has been isolated in a sealed chamber, it can be examined by geophysical logging. Detailed structural information is necessary for many types of scientific study, as well as to provide information to guide sub-sampling. The Storage Chamber (Figure 5) is a simple cylindrical pressure vessel, sealed at one end with a ball valve and at the other with the conical seal fitting to which the Manipulator can be attached for making transfers. The cylindrical part of the Storage Chamber is manufactured from stainless steel or high-strength aluminum alloy. The Storage Chamber is designed to preserve a core under pressure for periods of hours, days, or possibly months. While in either steel or aluminum Storage Chambers, density profiles can be

Figure 4. HYACINTH Storage Chamber, connected to the Shear Transfer Chamber and Manipulator (top) and MSCL-P (bottom) in the 40-ft refrigerated core processing container on the *Uncle John* during the GOM-JIP Expedition.

Figure 5. HYACINTH Storage Chamber in placeand ready to be logged in the MSCL-V, inside the 20-ft refrigerated logging container on the *Uncle John* during the GOM-JIP Expedition.

obtained using a gamma attenuation densitometer (see MSCL-V below). The aluminum Storage Chambers are suited to X-ray scanning for either 2-D radiographs or 3-D computed tomography (CT) as well as gamma densitometry, and these chambers can be manufactured at different thicknesses (different maximum working pressures) to maximize the X-ray transmissivity. While still under pressure the core can be transferred from the storage chamber into the to MSCL-P to make other geophysical measurements (see MSCL-P below), or into the HYACINTH sub-sampling system.

Pressure Core Depressurization Experiments

Pressure cores not only preserve the properties of a sediment/hydrate core under near-*in-situ* conditions, they also seal a volume of porewater, sediment, hydrate, and gas such that mass-balance calculations can be used to determine whether hydrate was present in the sediment. Depressurizing a core, collecting the gas, and analyzing the composition of the gas are integral components of this mass balance process.

Cores recovered under full pressure were subjected to non-destructive measurements to characterize the core and any hydrate potentially captured. After all measurements were made, the cores were incrementally depressurized, sometimes with non-destructive measurements at intervals in the depressurization. When the cores were depressurized in the MSCL-V, the gas rose to the ball valve end of the chamber where it was easily collected. The total volume of evolved gas and the composition of this gas was measured by the on-board gas geochemists. Water forced out of the chamber was also measured; the volume of water corresponded to a volume of gas left at the end of depressurization (at 1 bar) inside the storage chamber. This gas was assigned the composition of the final gas sample for purposes of calculation. Total methane volume is reported as methane from gas (just the measured gas) and methane from gas & liquid, which includes the estimate of gas remaining in the storage chamber.

Hydrate volume was calculated by determining the amount of evolved methane that could have been dissolved *in situ* and assigning the remaining methane as hydrate (see Hydrate Calculation spreadsheet under Data Files, Pressure Cores). *In situ* methane saturations were calculated using the Xu methane saturation calculation spreadsheet. Total evolved methane was divided by the pore volume (from core volume and core porosity) to calculate a total methane "concentration" which was compared to the saturated concentration at *in situ* conditions. If the total concentration was over saturation, the excess methane above saturation was assumed to be hydrate and converted to a volume of hydrate.

Non-Destructive Measurements on Cores

Four different Geotek core logging techniques were used during the field program and a fifth was used when the cores were split and described on shore. An Infrared core logger was used to log the long FHPC (Fugro Hydraulic Piston Corer) and the shorter FC (Fugro Corer) cores immediately after they were recovered and removed from the core barrel. A standard Multi Sensor Core Logger (MSCL) was used to make a suite of non-destructive measurements on all non-pressure cores (mainly FHPC and FC cores). A vertically-oriented MSCL (MSCL-V) was used to obtain accurate density profiles of pressure cores in aluminum and/or stainless steel storage chambers. A pressure MSCL (MSCL-P) was used to measure P-wave velocity on pressure cores at *in situ* pressures and temperatures. The same mechanical device was used by Georgia Tech to pass the cores through their Central Measurement Chamber (CMC) to make other measurements

by drilling through the core liner (see separate Georgia Tech Report). The final core logging system (used on the split cores) was an MSCL-XYZ that acquires images and other data from the split core surface. All the core logging carried out by Geotek was complemented by both linear X-ray scans and X-ray CT scans of both the non-pressure cores and the pressure cores recovered (see separate Lawrence Berkeley X-ray Report).

Infrared Logging: Measurement of Core Temperature

The external temperature of the core liner was measured using two ThermaCam SC2000 infrared cameras (FLIR Systems), one of which was mounted on a motorized, computer-controlled track (Figure 6) and the other used in a handheld mode. The FLIR Systems cameras detect infrared radiation with wavelengths of 7-13.5 cm and provide temperature-calibrated images over a temperature range from –40° to 1500°C. For shipboard measurements, the cameras were set to Temperature Range 1 to record environmentally relevant temperatures (-40° to 120°C). The motorized camera was mounted and focused 33 cm above the core and this constant distance from the core was maintained by a wheeled "skate" that moved along the core (Figure 7). To minimize reflections from local infrared sources (Figure 8), the skate was covered in black felt. The skate wheels were out of the field of view of the camera and had no adverse effect on the infrared image. The camera's field of view at this distance from the core was 14 cm wide (along the core) and images were collected every 5 cm using the Geotek Infrared Imaging software in conjunction with ThermaCam Researcher software (FLIR Sytems). Using the Geotek Infrared Imaging software, 5 cm from the center of every image (Figure 9) was used to create a composite false-color thermal image of the entire core (Figure 10) with an accurate length scale in real time, which was valuable in identifying cold spots. The handheld camera was used to follow up on any cold anomalies and aid in marking and cutting these sections.

Infrared images were processed to obtain downcore temperature profiles using the ThermaCam Researcher software (FLIR Systems). All images were corrected for core liner emissivity and ambient temperature. The emissivity of the core liner was measured at 0.95, as was found on ODP Legs 201 & 204 (Ford et al., 2003; Shipboard Scientific Party, 2003). The ambient temperature of the core processing container was monitored with TMC20-HD soil/water temperature probes & HOBO U12 temperature loggers (both from Onset Corp.). The infrared images of the core had a bright streak down the center, which is a reflection off the warm camera. Temperature data was extracted from the sides of the core, away from this reflection. A ThermaCam Researcher session was created with four squares in a line down the side of the core, at 1 cm spacing (Figure 11). The average temperature of each square was logged to a file; when a set of images from a core was loaded into Researcher, this data was extracted by "playing" the images like a movie. If cores were loaded sequentially into Researcher in time order, all data could be collected in the same text file.

Core section end temperatures were collected as soon as the core was cut using 8 soil/water temperature probes (TMC20-HD, Onset Corp.) and 2 HOBO U12 temperature loggers (Onset Corp.). The manufacturer's documentation says this probe/logger combination has an accuracy of plus or minus 0.25˚C and a resolution of 0.03˚C over the temperature range 0-20˚C. Temperature probes were checked for consistency by placing them together in water over a temperature range of 0-25˚C. All probes were within 0.1˚C of each other. Data was collected continuously every 10 seconds and core section end temperatures were picked from the extrema in the records (Figure 12).

Figure 6. The infrared imaging track (red arrows) set up above the core rack along the length of the 40-ft core-processing container. The track was driven and the data acquired and displayed by the Geotek Infrared Imaging software.

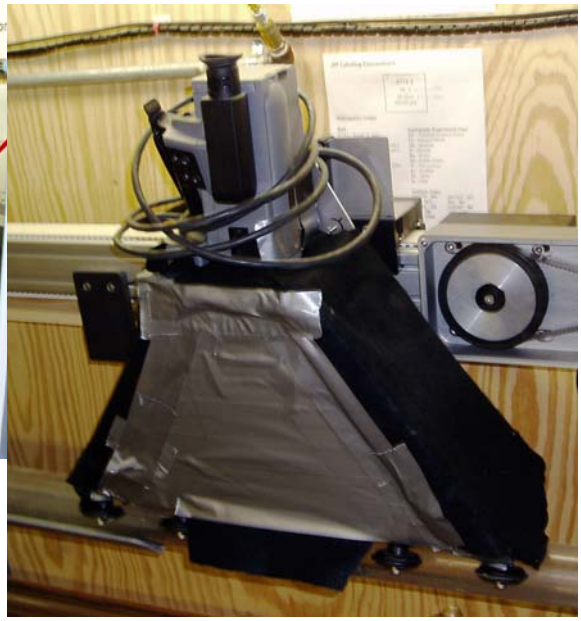

Figure 7. The FLIR ThermaCam SC2000 camera, mounted on its wheeled skate and covered with black felt to cut out reflected infrared radiation.

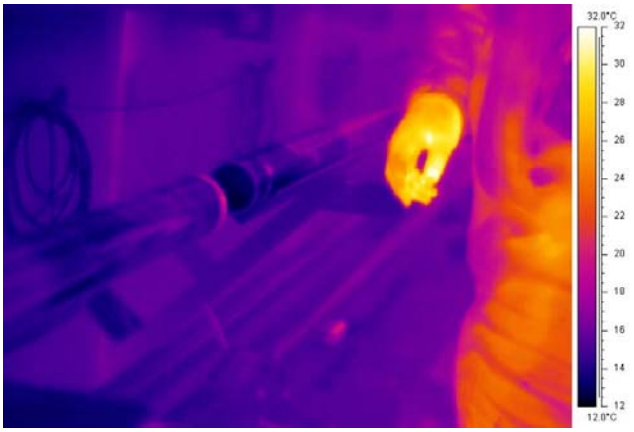

Figure 8. Scientists were the largest source of extraneous thermal radiation in the core processing container.

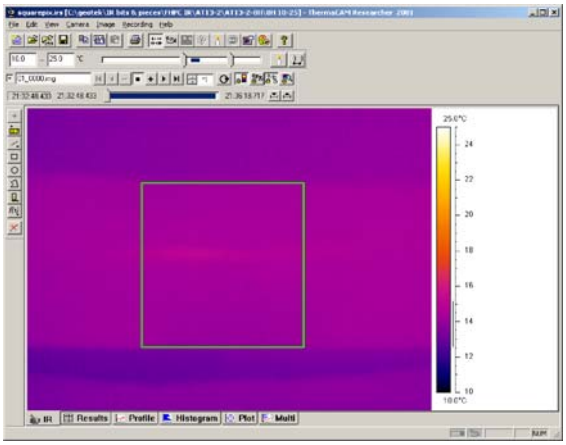

Figure 9. Sample infrared image, viewed in ThermaCam Researcher, collected automatically by the Geotek Infrared Imaging Software in conjunction with ThermaCam Rsearcher Software (FLIR Systems). The portion of the image in the central box was used to generate the composite image.

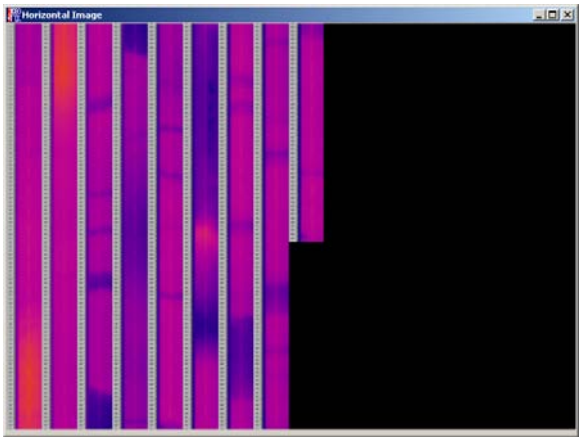

Figure 10. Composite infrared image of entire core, with ruler, generated by the Geotek Infrared Imaging system in real time.

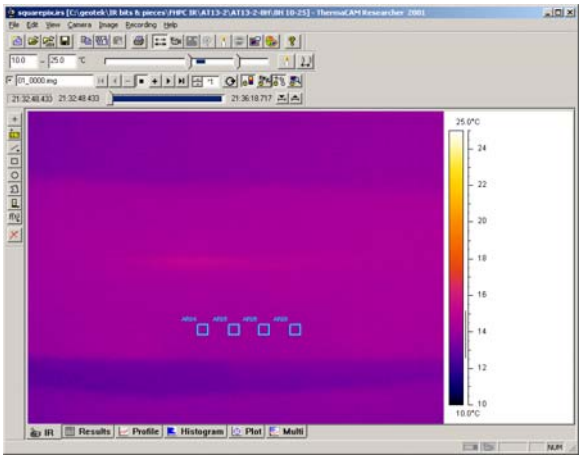

Figure 11. Screenshot of ThermaCam Researcher session used to extract data from the core image. The location of the squares is offset from the center of the cores to avoid reflections, which raise temperature ~0.5ºC.

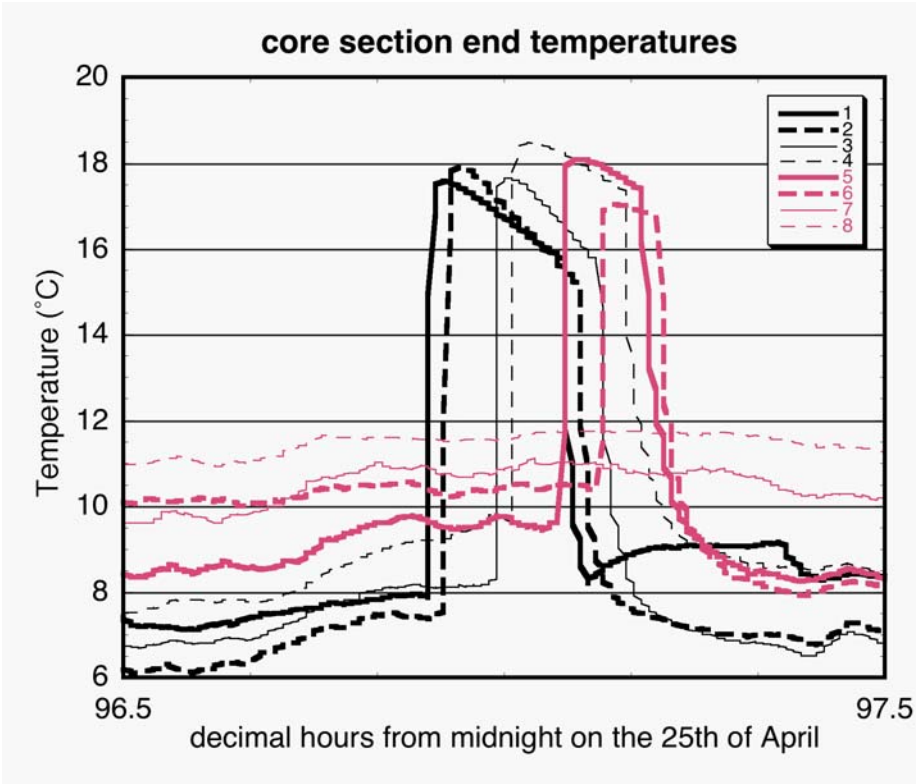

Figure 12. Sample data from temperature probes inserted routinely into core section ends. Temperatures were picked from maxima in data.

Thermal Anomalies & the GOM-JIP Core Recovery Protocols

Identification of cold spots or cold cores requires that the core handling be uniform, so that the thermal history between and along cores is similar. To this end, the curators monitored the core handling in an attempt to identify and eliminate sources of thermal "contamination." They attempted to record important times on the core log sheet: the time the core was pulled off the bottom, the time the core reached the drill floor, the time the core was brought to the ice trough, and the time the core was pulled into the core processing van. Other than simple warming in the water column and on deck, the three largest sources of thermal insult to the core were ice in the ice trough, frictional heating of stuck liner, and direct handling of the core by people (Figure 13). Ice in the ice trough was noted by the curators, including the length of the corer that is affected by the ice and whether the ice covers the top surface of the corer. Direct handling of the core with bare hands was discouraged but happened often and was not recorded.

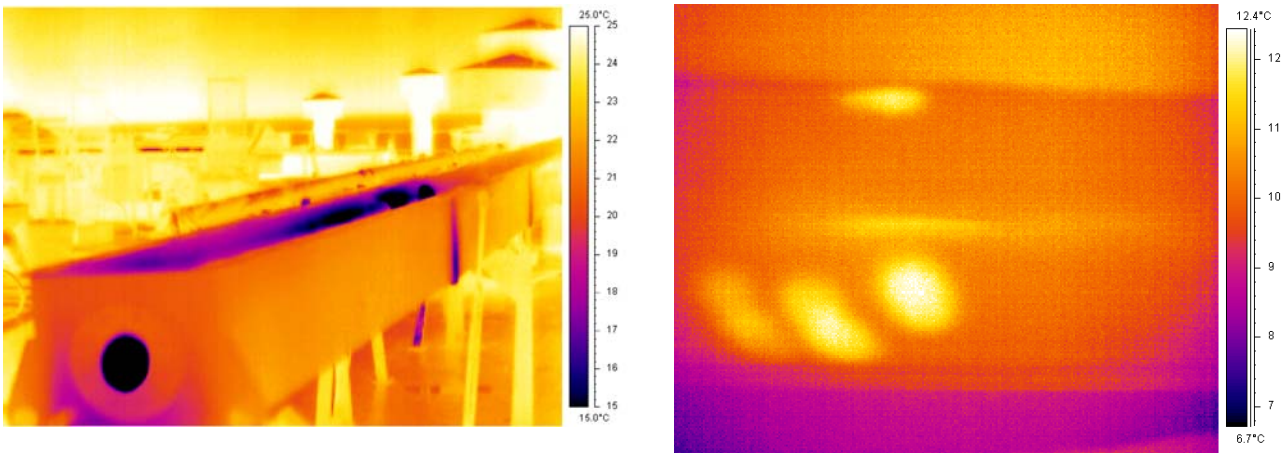

Figure 13. Infrared thermal images of (left) the ice trough, half-filled with ice and (right) a core that was recently handled by a gloveless individual. Both ice and people can change the temperature of cores and potentially disturb remnant thermal anomalies from gas hydrate dissociation.

If gas hydrate dissociates within a core, its only signature may be salinity anomalies and fading thermal anomalies. Cooling the core with ice could erase thermal anomalies from dissociated hydrate. Therefore there was a dilemma associated with cooling these unpressurized cores: cooling the core would preserve any remaining hydrate but would damp the negative thermal anomalies, making existing hydrate more difficult to find and destroying the record of already-dissociated hydrate. A decision was made partway through the cruise by the science party to place all cores on ice to preserve potential massive hydrate.

Quantification of hydrate from negative thermal anomalies requires extremely consistent core handling operations and was therefore beyond the scope of this work.

Standard Multi Sensor Core Logger (MSCL-S) Measurements

Whole-core Multi Sensor Core Logger measurements using a 'Standard' Geotek system (MSCL-S) are non-destructive to sediment fabric and can be used to provide intrinsic sediment properties

and as proxies for other data. These data can facilitate core-to-core correlation between adjacent holes at the same site or among different sites as well as providing base data to help formulate a core sub-sampling program. The MSCL-S (Figure 14) was configured to measure a suite of non-destructive parameters on whole FHPC or FC core in its plastic liner: gamma density, P-wave velocity, electrical resistivity and magnetic susceptibility. These measurements were also made on push cores taken in fiberglass liner. Each measurement device has an intrinsic down-core spatial resolution determined by its design specification and the physics of operation (see discussion of each measurement below). Data quality is a function of both core quality and sensor precision. Optimal MSCL measurements require a completely filled core liner with minimal drilling disturbance. Precision is a function of measurement time for magnetic susceptibility and gamma density but not for P-wave velocity or resistivity. Generally the spatial interval used for all sensors was set at 2 cm, although some core sections were logged at 1 cm. The rail and pusher system automatically measures the length of each core section using a laser and pushes them through the stationary sensor array.

Figure 14. MSCL-S inside the 20-ft unrefrigerated logging logging container on the *Uncle John* during the GOM-JIP Expedition.

MSCL-S Sensor Descriptions and Operating Principles

Gamma Density: Gamma density is measured through the center of the core using a 370 MBq 137Cs source and a NaI scintillation detector. The detection energy window is set to measure

only primary (unscattered) gamma photons (0.662 MeV), providing raw gamma attenuation data in counts per second. Gamma density is derived from gamma attenuation (see Sensor Calibration), and is reported as g/cc. The gamma beam is collimated through a 5 mm hole providing a down-core spatial resolution of around 1 cm. The precision is a direct function of total counts and hence is dependent upon the count times used (see Core Logging Protocols) and the core thickness and density. The data is reported as gamma density to differentiate it from bulk density, which is calculated directly from weights and volume measurements. Under most normal circumstances with the calibration protocols used here, the correlation between gamma density and bulk density should be excellent. Although the empirical calibration procedure for gamma density is based on bulk density measurements (i.e., of a known graduated aluminum and water standard), the measurements can vary from true gravimetric bulk density because of variations in mineralogy. Gamma attenuation coefficients for different materials vary as a function of atomic number. Fortuitously, most earth-forming minerals have similar and low atomic numbers (similar to aluminum). Consequently, the correlation of gamma density and bulk density is usually excellent.

Ultrasonic P-Wave Velocity: Ultrasonic P-wave velocity (V_P) is measured using a pair of Acoustic Rolling Contact Transducers. The travel time for pulse propagation through the core is measured with a precision of 50 ns. At the same time, the core diameter is measured using a set of displacement transducers (precision 0.02 mm) that are mechanically coupled to the ultrasonic transducers. Combined with the calibration, this produces an ultrasonic velocity with a precision of +/- 1.5 m/sec and a likely accuracy of around 5 m/sec. Core temperatures are obtained with a platinum resistance temperature probe (precision 0.05˚C) and the measured velocity is corrected to a velocity at a reference temperature (20˚C). Ultrasonic velocity is reported in m/sec has a typical down-core resolution of about 2 cm.

Electrical Resistivity: The Non Contact Resistivity sensor operates by inducing a primary high-frequency magnetic field in the core from a transmitter coil, which in turn induces electrical currents in the core that are inversely proportional to the resistivity. A receiver coil measures very small secondary magnetic fields that are regenerated by the electrical current. To measure these very small magnetic fields accurately, a difference technique has been developed that compares the readings generated from the measuring coils to the readings from an identical set of coils operating in air. This technique provides the accuracy and stability required. Resistivities between 0.1 and 10 Ω•m can be measured at spatial resolutions along the core of about 4 cm. As with other parameters, the measurements are sensitive to core temperature and should be obtained in a stable temperature environment for best results.

Magnetic Susceptibility: Whole core volume magnetic susceptibility was measured with a 80 mm diameter Bartington loop sensor operating at 513 Hz (note this is a slightly lower frequency than a standard Bartington loop sensor, but corrections to the data ensure there is no net effect). The frequency of the low-intensity, alternating magnetic field produced by the sensor is sensitive to changes in the magnetic susceptibility of material within and near the loop. The instrument has two fixed integration periods of ~1 and 10 s. During the GOM-JIP, magnetic susceptibility was normally measured at a spacing of 2 cm, using the 10 s integration time (because the susceptibilities were generally low). The instrument automatically zeroes at the beginning of each core. Magnetic susceptibility integrates over a core length of approximately 5 cm, with exponentially decreasing sensitivity with distance from the sensor. Magnetic susceptibility, a dimensionless

number, is reported as corrected volume susceptibility in SI units with an accuracy typically around +/- 4%.

Sensor Calibration

All sensors were calibrated to ensure that measurements were accurate and comparable throughout the GOM-JIP Expedition and to account for the effects of the core liner. Sections of core liner were cut to make calibration and check pieces for all the sensors as described below.

Gamma Density: Calibration of the gamma density measurement is performed by measuring the intensity of the gamma beam through a stepped aluminum bar of varying thickness sitting centrally in a short length of core liner filled with distilled water. This calibration procedure, using aluminum and water, provides a good approximation for a water-saturated sediment (minerals and water) and has proven to be an excellent calibration protocol for determining density from the attenuation of gamma rays.

Ultrasonic P-Wave Velocity: Calibration of the ultrasonic velocity is performed by measuring the total travel time of an ultrasonic pulse through a core liner filled with distilled water at a known temperature. The velocity of water at the calibration temperature is calculated theoretically and the difference between the actual travel time of the pulse and the theoretical time is calculated. This difference is then used to correct subsequent calculations of sediment velocity.

Electrical Resistivity: Calibration of the electrical resistivity was performed using a number of different salt water solutions, made using pure sodium chloride and distilled water, capped in short lengths of core liner. Dilutions corresponding to salinities of 35 ppt (parts per thousand by weight), 17.5 ppt, 3.5 ppt, and 1.75 ppt were used to construct a calibration profile.

Magnetic Susceptibility: The magnetic susceptibility sensor system is pre-calibrated by the manufacturer who provides a check piece to ensure the calibration is accurate.

Core Logging Protocols

Prior to each core being logged, 3 short “check” pieces were logged to ensure that the sensor systems were operating correctly. These check pieces were assigned negative sub-bottom depths and are easy to identify in the raw data. Core sections were logged at 2 cm spatial intervals, with 10 second integration times for the gamma density and magnetic susceptibility. With this sampling regime, each 1 m core section took about 13 minutes to log and a 9 m long core (with 9 core sections and a “check” section at the top) took a total of about 2.5 hours to log. With these logging speeds we easily kept up with the rate at which core was being recovered.

Butt error distance (the distance between one section and the beginning of the next, mainly taken up by end-caps) was automatically removed during data processing. P-wave velocity and gamma density measurements taken within 1 cm of core section ends were removed from the data set.

Gas Expansion Effects & GOM-JIP Cores

Most of the cores recovered during the GOM-JIP expedition suffered significant disturbance caused by gas-expansion effects. Expansion of free gas, exsolution of dissolved gas, and dissociation of hydrate all cause gas expansion effect that will disturb recovered cores. It is worth noting here that a unit volume of free gas at 1000 m below the sea surface will expand by a factor of 100 by the time it reaches the surface (ignoring any temperature expansion or further exsolution). Another way of visualizing the expansion of gas during the core recovery process is to

consider that a 0.1-mm-diameter free gas bubble in the sediment matrix at a depth of 1000 m will become a 4.5-mm-diameter gas bubble at the sea surface. If a sediment core (taken from around 1300 m) has pore waters that are saturated in methane, then at the surface the change in temperature and pressure can typically cause the core to expand by at least 1½ times its original volume. When relatively low volumes of gas exsolve from pore fluids during core recovery, small bubbles will form in the sediment matrix with only minor amounts of core volume expansion. As the gas volumes become greater, the sediment structure begins to fracture and a large amount of core expansion occurs, forming a series of large gas voids in the core. This process takes some time but is readily visible in the processing van. When core expansion occurred on GOM-JIP cores (e.g., Figure 15), the core was not pushed back together prior to sectioning, and hence the voids were curated and logged in the MSCL.

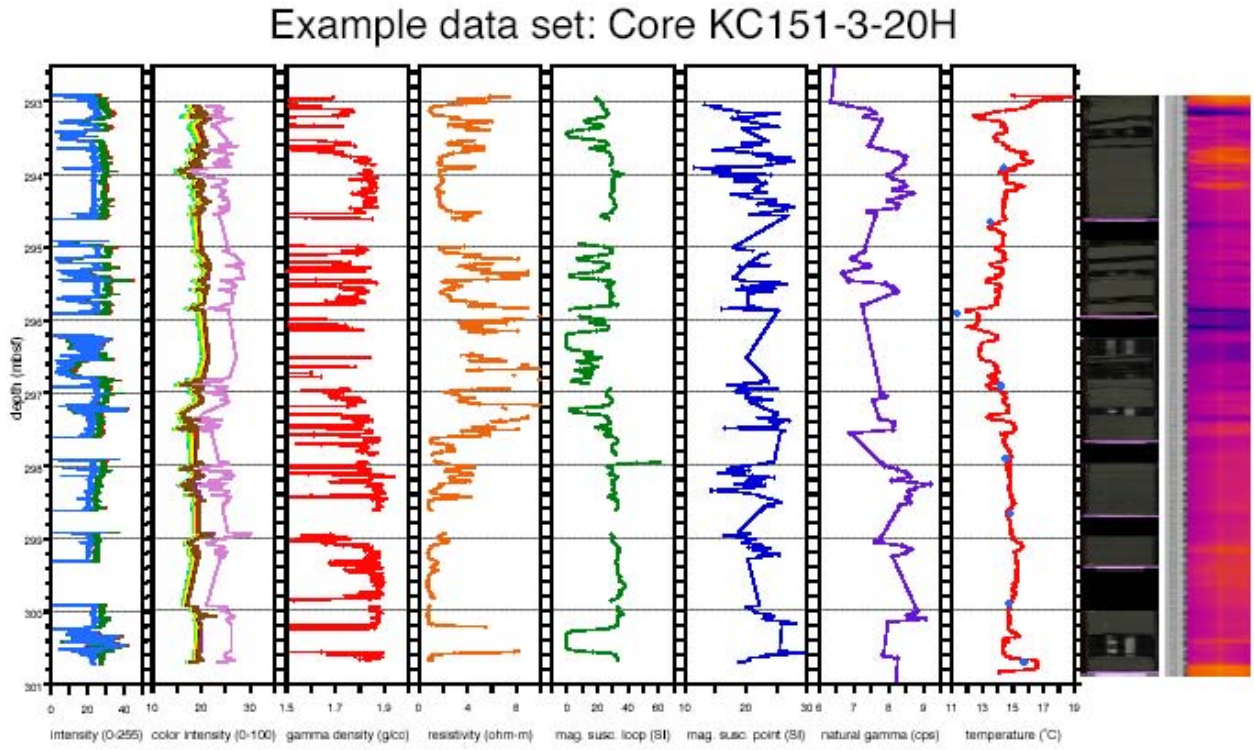

Figure 15. Complete data set for Core KC151-3-20H, showing influence of gas expansion on data. From left, RGB data from linescan image, spectral color data from Minolta color spectrophotometer, gamma density, resistivity, magnetic susceptibility (loop sensor), magnetic susceptibility (point sensor), natural gamma radioactivity, temperature, linescan image, and infrared image.

The expansion of gases inside the sediment matrix and the voids had a noticeable effect on all the parameters measured by the MSCL-S. Magnetic susceptibility (loop sensor) measurements were probably the least affected by core expansion, as these measurements depend only on the sediment/mineral volume. However, significant lowering of the magnetic susceptibility value was seen where there were clear gas gaps (greater than ~0.5 cm).

Gamma density measurements can be significantly affected by gas voids and sediment cracks. The downcore spatial resolution is ~1 cm, and hence, all cracks, no matter how minor, will show

up in the gamma density profile. With significant gas expansion in many cores, this effect shows up as a very "noisy" data set. These data are, in fact, quite accurately representing the state of the core but of course do not represent the *in situ* condition. The closest representation of the *in situ* condition is achieved by taking the upper values of the gamma density data envelope. However, even these values are often lower than the *in situ* densities because of gas in the matrix.

Electrical resistivity measurements increase as a result of small gas bubbles that have formed in the sediment matrix and increases dramatically around the major gas cracks. The largest excursions caused by the major cracks have been edited from the processed data sets but most remaining data is still affected by the core disturbance.

Gas expansion has the largest effect on the measurement of ultrasonic P-wave velocity (V_P). Even very small amounts of free gas in the sediment matrix (<1%) will cause a significant decrease in velocity. More importantly, the very high attenuation of P-waves at ultrasonic frequencies in sediments with even very low volumes of free gas makes the measurement of velocity all but impossible. During the GOM-JIP expedition, we generally encountered gas-rich sediments, in which P-wave velocity measurements were possible only in the upper few meters. In practice, we observed that P-wave velocity was generally only measurable above the sulfate/methane interface. Below the sulfate-methane interface, the gas exsolved generally prevented the acquisition of any reliable data.

Vertical Multi Sensor Core Logger (MSCL-V) Measurements

The MSCL-V accommodates cores vertically, and the sensor cluster moves up and down along the stationary core. For the GOM-JIP, the MSCL-V was configured to accommodate HYACINTH storage chambers in order to measure gamma density of pressure cores (Figure 5). The gamma density sensors and detectors are the same as used on the MSCL-S (see above, MSCL-S Sensor Descriptions and Operating Principles), and calibration was performed in a similar fashion (see Sensor Calibration). The stepped aluminum calibration sample was logged in the two different pressure core liners (FPC and HRC) within a pressure vessel to provide the appropriate calibration.

Pressurised Multi Sensor Core Logger (MSCL-P) Measurements

The MSCL-P (Figure 16) enables geophysical measurements to be made on HYACINTH pressure cores while maintaining them at *in situ* pressures. As used on the GOM-JIP, the MSCL-P system had 2 different Central Measurement Chambers (CMCs):

a) a Geotek CMC, which, for the GOM-JIP, had a set of P-wave transducers that enabled detailed P-wave profiles to be obtained rapidly and automatically along the core.

b) a Georgia Tech CMC that enabled a suite of measurements to be made manually as the core was moved through the chamber. These measurements generally relied on holes being drilled in the core liner (see separate Georgia Tech Report).

The core transport/manipulation system is based on existing HYACINTH technology and philosophy with modifications and adaptations to suit this particular application. In operation, the CMC was joined to a standard HYACINTH storage chamber (stainless steel or aluminum) which contained the original core to be logged. On the other side of the CMC was an extension chamber that provided enough space for the core to completely pass through the CMC. On both ends of the system, linear manipulators (pressurized, precision push rods) were fitted that allowed the

core to be pushed in both directions. The manipulators allowed the core to be securely held between the two ends of the push rods during the manipulation process. Mechanisms were designed to ensure that the core did not rotate during the linear translation and that small end confining pressures could be applied to the core material (if the core liner were full). All the components in the system were coupled together using the HYACINTH quick fit couplings, which fit around the flanged ends of the chambers. To ensure precise motion of the core, the manipulators were driven synchronously using servo motors under computer control. Before opening the storage chamber to begin logging the pressure core, the system was bled and filled with seawater using a compressed-air-driven high pressure water pump.

Figure 16. MSCL-P with Geotek P-wave Central Measurement Chamber in place (yellow arrow). The Georgia Tech measurement chamber (not in use) is sitting behind the Geotek CMC.

The system enables pressurized cores to be incrementally moved from a HYACINTH storage chamber through the CMC under computer control to any predetermined position with a precision of about 0.1 mm, enabling multiple probes to enter the same hole in the liner as required by the Georgia Tech measurement devices. The Geotek P-wave velocity profiles were generally collected at a spatial interval of 0.5 cm, using an automated core logging program.

Calibration of the Geotek CMC P-wave velocity measurement system is done as with the MSCL-S over the pressure range of interest using water with a known temperature and salinity. The process is repeated for both types of core liner (FPC and HRC).

Split-Core (multi-section) Multi Sensor Core Logger (MSCL-XYZ) Measurements

The MSCL-XYZ (Figure 17) contains multiple trays to hold up to nine split core sections. The sensor array, on a robotic arm, moves along each of these trays in turn. The MSCL-XYZ can make contact measurements or non-contact measurements. For the GOM-JIP, the MSCL-XYZ

was equipped for color linescan imaging, color spectrophotometry, high-resolution magnetic susceptibility, and measurement of natural gamma radiation.

Figure 17. MSCL-XYZ installed in the DSDP West Coast Repository at the Scripps Institution of Oceanography, where the split cores from the GOM-JIP were logged. The MSCL-WYZ is configured for natural gamma measurements in this photo.

MSCL-XYZ Sensor Descriptions and Operating Principles

Color Linescan Imaging: Color linescan images were collected with the Geoscan color linescan camera. The Geoscan color line scan camera uses 3 * 1024 pixel CCD arrays: one for each color, red, green and blue (RGB). The light unit uses 2 high frequency 'white' fluorescent tubes that illuminate the core evenly from both sides of the image line. This provides a flooded illumination that minimises some of the shadow effects caused by microtomographic effects. The camera is arranged directly above the light and "looks" through a slot in the top surface of the light unit.

High-Resolution Magnetic Susceptibility: High-resolution magnetic susceptibility was measured with a Bartington point sensor operating at 565 Hz. The frequency of the low-intensity, alternating magnetic field produced by the sensor is sensitive to changes in the magnetic susceptibility of material within and near the sensor. The instrument has two fixed integration periods of ~1 and 10 s. During the GOM-JIP, magnetic susceptibility was normally measured at a spacing of 2 cm, using the 10 s integration time as the susceptibilities were generally low. The instrument automatically zeroes every five measurements to compensate for drift. The magnetic susceptibility point sensor has a field of influence of approximately 5 mm. Magnetic susceptibility, a dimensionless number, is reported in SI units with an accuracy typically around +/- 4%. The user should be aware that because the point sensor has a very high spatial resolution the data can be significantly affected if the sensor happens to be positioned directly on a small crack.

Color Spectrophotometry: The Minolta color spectrophotometer collects light in 10 nm increments from 360 nm to 740 nm, thus providing complete spectral data in the visible wavebands

(400-700 nm) with small extensions into the ultraviolet (360-400 nm) and infrared (700-740 nm) regions. The diffraction grating creates a Gaussian distribution of wavelengths, centered on the reported value with a 10 nm width at half maximum. Therefore, in practice, the reported value at 360 nm contains photons from 355 to 365 nm with a contribution (about 30%) from wavelengths both larger and smaller.

Natural Gamma Radiation: Gamma radiation is measured on split core sections using a single 3 in. x 3 in. NaI(Tl) detector mounted in a heavily-lead-lined shield. The detector is positioned just above the split core surface during the measurements with additional lead shielding surrounding the core and detector. To further reduce background radiation from the concrete floor in the laboratory, and general background from the Earth, additional half-inch-thick lead tiles were used on the floor beneath the complete instrument. Natural gamma measurements have a down-core resolution of approximately 10 cm (detector diameter 7.5 cm). The precision of the measurement is dependent upon the total number of counts; on the GOM-JIP cores, this intrinsic error is approximately plus or minus 5% (95% confidence interval).

Laser Depth Profiler: The laser depth profiler measures the distance to the surface of the core, allowing the sensor array to contact the core without doing damage. This core thickness is also used in volume correction of natural gamma measurements. The laser depth profiler has a working range of 40 mm.

Sensor Calibration

All sensors were calibrated to ensure that measurements were accurate and comparable throughout the GOM-JIP Expedition as described below.

Color Linescan Imaging: The Geotek MSCL-XYZ software saves calibration files containing the black and white calibrations for each element in the CCD. This ensures that all CCD pixels are scaled to the same black (minimum) and white (maximum) values. White calibrations are performed on a special white ceramic tile. The camera travels a short distance to remove the effects of any dust on the tile. Black calibrations are performed with the lens cap on; data is collected for few seconds and then averaged.

High-Resolution Magnetic Susceptibility: The magnetic susceptibility sensor system is precalibrated by the manufacturer who provides a check piece to ensure the calibration is accurate.

Color Spectrophotometry: The spectrophotometer is calibrated internally by using a “white” calibration reference spectrum and a “zero” calibration reference spectrum. These calibration spectra must be acquired each time the Minolta color spectrophotometer is turned off, since they reside in the spectrophotometer memory and cannot be stored elsewhere. The white calibration spectrum is simply acquired by collecting the spectra with the sensor placed on a special white ceramic calibration tile. For convenience, the same white calibration tile can be used for both the Geoscan camera and the Minolta color spectrophotometer. The “zero” calibration spectrum is simply acquired by collecting a spectrum with the sensor in free air, away from any surfaces. In practice, if the sensor is about 20 cm above the empty core trays an accurate “zero” calibration is obtained.

Natural Gamma Radiation: Although the Natural Gamma measurements are only reported as total count rates (across the complete energy spectrum) the raw data does in fact consist of spectral data up to 3MeV. The NaI(Tl) detector is energy calibrated using Cobalt and Barium check

sources. In addition, the background radiation levels were measured along all the trays on the XYZ table so that the raw data could be appropriately corrected.

Laser Depth Profiler: The laser depth profiler is automatically calibrated by the Geotek MSCL-XYZ software by keeping the depth profiler stationary while the z-axis motor moves a target by incremental known distances.

Core Logging Protocols

Core sections were imaged with both a down-core and cross core resolution of 0.1 mm. The lens aperture was normally set at either f8 or f11 (this information is stored in the Geotek image files as well as the RGB datafiles). Labels with full section names were imaged at the bottom of each section.

Color spectra and magnetic susceptibility were collected every 2 cm, with 10 second integration times for the magnetic susceptibility.

Measurements of natural gamma radiation were taken every 5 cm for 5 minutes apiece, on selected cores only. Background radiation was subtracted from the data set and the core data was corrected for differences in core volume, as measured by the laser depth profiler.

Data Files & Formats

Data files are organized on the DVDs by site: Atwater Valley AT13 (& AT14 ROV cores), Atwater Valley Mound (ATM1&2), and Keathley Canyon (KC151). For each site, the DVDs include each of the data types below.

Pressure Core Data

MSCL-V data: Data from the MSCL-V is stored in folders, labeled by core number and an indication of conditions (pressure, depressurization). The files inside (,CAL, .DAT) are meant to be read by the Geotek MSCL software, with the exception of the .RAW file, which is fixed-width, tab-delimited plain text. Fields in the .RAW file are Core Depth (m), Section Number, Section Depth (cm), and Gamma Attenuation (cps). Pressure cores only have one section; pressure core files that appear to have multiple sections are actually repetitive logs of the same core.

MSCL-P data: Data from the MSCL-P is stored in folders, labeled by core number and an indication of conditions (pressure, depressurization). The files inside (,CAL, .DAT) are meant to be read by the Geotek MSCL software, with the exception of the .OUT file, which is fixed-width, tab-delimited plain text. Fields in the .OUT file are Core Depth (m), Section Number, Section Depth (cm), P-wave Amplitude (0-100), and P-wave Velocity (m/sec). Pressure cores only have one section; pressure core files that appear to have multiple sections are actually repetitive logs of the same core.

Processed Data: The .RAW & .OUT files from the MSCL-V & MSCL-P have been imported into Excel (.XLS) files with names that indicate when the data was taken (full pressure before depressurization, during depressurization, or post-depressurization). Plots of the data taken at full pressure are in Adobe Illustrator (.AI) format and .PDF files, and include the X-ray images. The Excel spreadsheet “Hydrate Calculations.xls” contains the calculation of hydrate content for the pressure cores.

Fields in the “Hydrate Calculations” spreadsheet are divided into four sections: Pore Volume Calculation, In Situ Methane Concentration from Xu, Calculation of Methane Oversaturation, and Calculated Hydrate Volume. Section “Pore Volume Calculation” contains Core Diameter, in mm (entered); Core Length, in mm (entered); Core Volume (calculated); Sediment Porosity, in percent, estimated from gamma density (entered); and Pore Volume, in liters (calculated). Section “In Situ Methane Concentration from Xu” contains Water Depth (m), Depth Below Mudline (m), Bottom Water Temp (Temperature, ˚C), Temp Gradient (Temperature Gradient, C˚/m), and Salinity (kg salt/kg water). All these values must be entered into the Xu spreadsheet (included) to get the final column, Methane Saturation from Xu (mM), Section “Calculated Methane Oversaturation” contains Total Volume of Methane Released During Degassing (liters, entered); Molar Gas Volume at Degassing Temp (liters, entered), calculated from experimental temperature, generally 10˚C, and PV=nRT; Total Moles Methane (mmol, calculated); Methane Saturation at Degassing T&P (mM), the concentration of methane remaining in the pore fluids when degassing is complete; Total Methane Concentration, if all dissolved (mM, calculated), calculated by dividing the total moles of methane by the pore volume; and Excess Methane Concentration (Oversaturation), in mM (calculated). Section “Calculated Hydrate Volume” contains Amount Excess Methane (mmol, calculated); Volume of Excess Methane as Gas (STP), liters (calculated); Volume of Excess Methane as Hydrate (ml, calculated), using the conversion 164 volumes of methane at STP can create one volume of methane hydrate; and Hydrate as a Percentage of Pore Volume (%, calculated), the volume of hydrate divided by the pore volume.

Temperature Data

Infrared Raw Data: Each folder contains the sequential images captured by the FLIR infrared camera on the Geotek IR track for a single core. File 01_0000.X is the top of the core. The four digits after the "_" indicate the distance downcore in millimeters of the center of the image. The image is 14 cm wide in the along-core direction. Each image is stored as a .IMG file (FLIR image file) and a .BMP file. The .IMG file can be read by ThermaCam Researcher (FLIR Systems) and quantitative data can be extracted. The .BMP file is just a picture used to create the core bitmap files. The .INI file allows the images to be read back into the Geotek Infrared Imaging Software, where montages can be created or images can be adjusted, in conjuction with ThermaCam Researcher (FLIR Systems). The temperature range for each set of images is in the folder name. There is a temperature scale included in each folder. Cores imaged in two sections (due to difficulty in removal from the core barrel) are labeled "a" & "b".

Infrared Core Images: The core bitmap (.BMP) files are montages created from the center 5 cm of 14 cm long (downcore) infrared images. Each folder of bitmaps has a temperature scale with it. The ruler is generated electronically in the Geotek imaging software.

Core Temperature Data: Data from the core-section-end thermistors and the infrared images were combined to create Excel (.XLS) files for each hole. Cores are contained on individual worksheets. A hole summary worksheet is also included. Columns are sub-bottom depth (m), core depth (m), IR temperature (˚C) from the infrared camera, and HOBO temperature (˚C) from the core-section-end thermistors.

Core Temperature Plots: Summary plots for each hole are included as .PDF files.

MSCL-S (whole-core log) Data

MSCL-S Logsheet: Logsheet in Excel (.XLS) format giving details, lengths, and any problems with core logging.

MSCL-S Calibrations: Processing parameters used by the Geotek MSCL software (.PRO), derived from on-board calibrations, including the gamma calibration piece logged in the folder Gamma Cal. Calibrations are calculated in "FHPC MSCL Cal.xls."

MSCL-S Raw Data: Data from the MSCL-S is stored in folders by core number. The files inside (,CAL, .DAT, .DEL, .SBD) are meant to be read by the Geotek MSCL software, with the exception of the .OUT file, which is fixed-width, tab-delimited plain text. Fields in the .OUT file are explained in MSCL-S Spreadsheets, below.

MSCL-S Spreadsheets: The .OUT files for each core have been imported as worksheets into Excel (.XLS) files for each hole. The columns are SBD (m), sub-bottom depth; Sediment Thickness (cm); P-wave Amplitude (0-100); P-wave Velocity (m/s); Gamma Density (g/cc); Magnetic Susc (SI), magnetic susceptibility in SI units; Acoustic Impedance (m•g/sec•cc, or 10^3 kg/m^2•sec), acoustic velocity multiplied by density, Fractional Porosity (0-1), calculated from gamma density; and Resistivity (ohm•m). A hole summary worksheet is also provided. Sub-bottom depths with numbers less that zero are beginning-of-core check pieces. Magnetic susceptibility data in core worksheets (but not Hole Summary worksheets) may contain extremely low (-200 to -600) erroneous values ("dropouts").

MSCL-S Plots: Summary plots for each core and each hole are included as Adobe Illustrator (.AI) and .PDF files.

MSCL-XYZ (split-core log) Data

RGB Linescan Images

Raw Images and RGB: Each section has a set of files, designated as Hole_Core_Section, contained in folders by hole. The .TIF file is the original raw image collected by the linescan camera. Each pixel is 0.1 mm on a side. The .RGB file is a tab-delimited text file, which starts with the core designation on multiple lines, followed by the lens aperature (f8 or f11 for most GOM-JIP cores), other numbers used by the Geotek imaging software that define the image resolution and cropping, and, just above the word START, the downcore resolution of the data in cm. After the word START, the RGB data, whose values range from 0-255, begins as tab-delimited columns of Section Depth (cm), Red, Green, and Blue. The .ICO and .XML files are for use with the Geotek Imaging Software.

JPEGS Large: These folders contain, by hole, jpeg files (.JPG) created from the .TIF files mentioned above. Jpegs are near full resolution of the original .TIF files. File sizes range from 2-8 Mb.

JPEGS Small: These folders contain, by hole, jpeg files identical to those above, only at a lower resolution. File sizes are less that half a Mb.

Concatenated Images: Small jpeg images of core sections have been concatenated to re-create the entire core (with missing core intervals in black). Files are named Hole-Core.

Magnetic Susceptibility Point Sensor & Minolta Color Spectrophotometry

Mag Susc-Spec Raw Data: Data from each core is stored in an .XML file, titled with the core name, meant to be read by the Geotek MSCL-XYZ software. These files are stored in folders named for the cores, and the cores are grouped into folders by hole.

Mag Susc-Spec CSV Files: Data from each core has been exported as comma-separated value files (.CSV) that can be read into most spreadsheet programs. Fields in the .CSV files are explained in Mag Susc-Spec Spreadsheets, below.

Mag Susc-Spec Spreadsheets: The .CSV files from each core have been imported as worksheets in Excel (.XLS) files for each hole. Columns are Sub-Bottom Depth (m), or Core Depth (m) for single-core worksheets; Core, GOM-JIP core number; Section; Laser Profiler (mm), the height of the core relative to a full half-core; Magnetic Susceptibility (SI); Munsell Color, the Munsell value of the color measured by the Minolta color spectrophotometer; and Reflectance (Xnm), where X varies from 360 to 740, and the values range from 0 to 100, calibrated across all GOM-JIP cores.

Natural Gamma Measurements

Natural gamma measurements were only made on Keathley Canyon cores.

Nat Gam Raw Data: Data from each core is stored in an .XML file, titled with the core name, meant to be read by the Geotek MSCL-XYZ software. These files are stored in folders named for the cores, and the cores are grouped into folders by hole.

Nat Gam CSV Files: Data from each core has been exported as comma-separated value files (.CSV) that can be read into most spreadsheet programs. Fields in the .CSV files are explained in Nat Gam Spreadsheets, below.

Nat Gam Spreadsheets: The .CSV files from each core have been imported as worksheets in Excel (.XLS) files for each hole. Columns are Sub-bottom Depth (m); Core; Section; Laser Profiler (mm), the height of the split core surface relative to a full half core; Corrected Natural Gamma (cps), the natural gamma data corrected for background and volume effects; Corrected Natural Gamma Smoothed (cps), the corrected natural gamma data averaged over four or five consecutive data points, where they exist; and Natural Gamma from LWD (API), the downhole natural gamma data from the Schulmberger Logging While Drilling tool. The worksheets representing single cores have Natural Gamma (Raw) (cps); these data have not been corrected for volume or background effects.

Atwater Valley, Hole AT13-2

HYACINTH Tool Operations

Fugro Pressure Corer (FPC)

The FPC recovered Core AT13-2-7P at full *in situ* pressure from Atwater Valley Hole AT13-2. AT13-2-7P was from 35.7 mbsf and contained 53.5 cm of core (Table 1). Unfortunately, the latching mechanism jammed in the shear transfer chamber and the core had to be depressurized, precluding any measurements at *in situ* pressure. Other FPC deployments were hampered by problems associated with over-penetration (Table 1): the tool was coring but extending too far, which meant that it could not retract the core into the autoclave. For instance, Core AT13-2-12P overshot, broke the central rod, and could only be recovered with the use of an improvised fishing tool. This over-penetration was occurring because a) the sediments were generally very soft and b) because there was no landing ring at the bit to prevent excessive movement of the core barrel. Bottom-hole assembly compromises to accommodate all the different tools meant that the smaller bit with the landing ring could not be used.

HYACE Rotary Corer (HRC)

Two HRC deployments were made at Atwater Valley Hole AT13-2 (Table 2). A good core (AT13-2-5R) was recovered from 27.1 mbsf, which demonstrated that the more recent modifications to the HRC enabled it to core in softer formations than its original design. However, this core did not retract into the autoclave and hence the *in situ* pressure was not retained. A shear pin failed on the next coring run (AT13-2-10R) and hence the motor and coring stroke did not take place. In addition, the inner rod broke and it was tentatively concluded that the shock load on the landing ring may have been too severe. It was noted that there was little fine control on the *Uncle John*'s sand line when trying to lower gently, and hence the shock load at the time of contact would vary for each deployment.

Pressure Cores

Pressure Core AT13-2-7P

Core AT13-2-7P was recovered under full pressure, but it became stuck in the shear transfer mechanism and had to be depressurized to remove it from the equipment. No measurements were made on core AT13-2-7P in its initial pressurized state. When it was depressurized, very little gas was observed.

FHPC & FC Cores

Temperature Measurement via Infrared Logging

The temperatures of each of the cores from Hole AT13-2 were monitored in order to detect any signs of hydrate dissociation, in the form of localized, centimeter-scale thermal anomalies or large cold zones that might span multiple cores. The infrared camera track provided a continuous record of the liner temperature, and temperature probes placed in the center of section ends recorded the actual core temperatures. However, no thermal anomalies were found in this hole that could be linked to gas hydrate.

Figures 18 &19 summarize the temperature data collected for Hole AT13-2. Cores AT13-2-6H & 8H were 3-6 C˚ colder than other cores from this hole (Figure 18). These two cores were very expansive, containing many gas voids. Gas expansion can cool cores (Shipboard Scientific Party, 2003) and could explain the cooling seen in these cores. If there had been very low levels of disseminated hydrate within these cores, it would be impossible to differentiate between the cooling effects from gas expansion and/or hydrate dissociation.

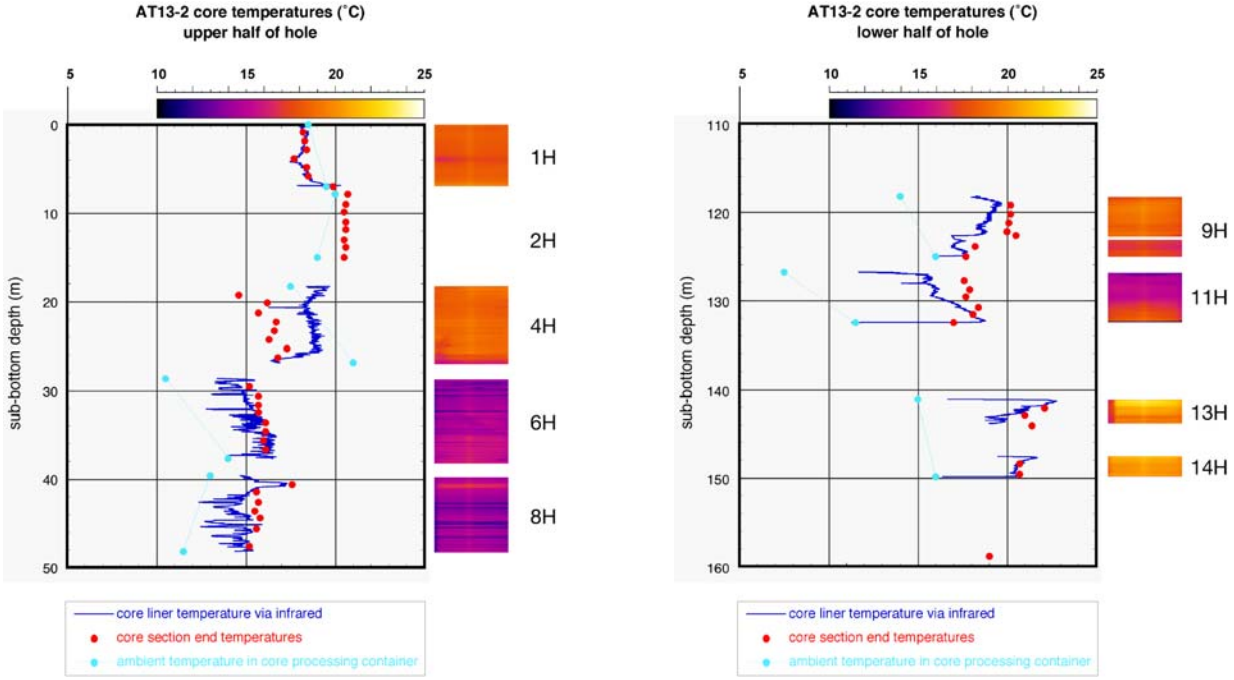

Figures 18 & 19. Plot of temperature data from infrared imaging, which takes the temperature of the core liner, and from direct measurement of the center of the core at core section ends for the top of Hole AT13-2. Two-dimensional infrared image is shown to the right of plot.

These two cores had many local thermal anomalies, most of which are definitely associated with gas voids. The gamma density logs (Figure 20) and the X-ray scans that were taken after the core was cut into sections were examined as void detectors . From Figure 20, it is evident that the very cold spots with sharp boundaries are gas voids. Unfortunately, in gas sampling, cutting, and general handling, voids and sediment move within the liner, causing the infrared record to be

decoupled from the gamma and X-ray scans, making this analysis qualitative rather than quantitative. In future, a visual image of the uncut core would be very helpful in later distinguishing voids from sediment. If there were small amounts of disseminated hydrate in these cores, on meter or centimeter scales, it would be extremely difficult to detect against the background of core variably cooled by gas expansion.

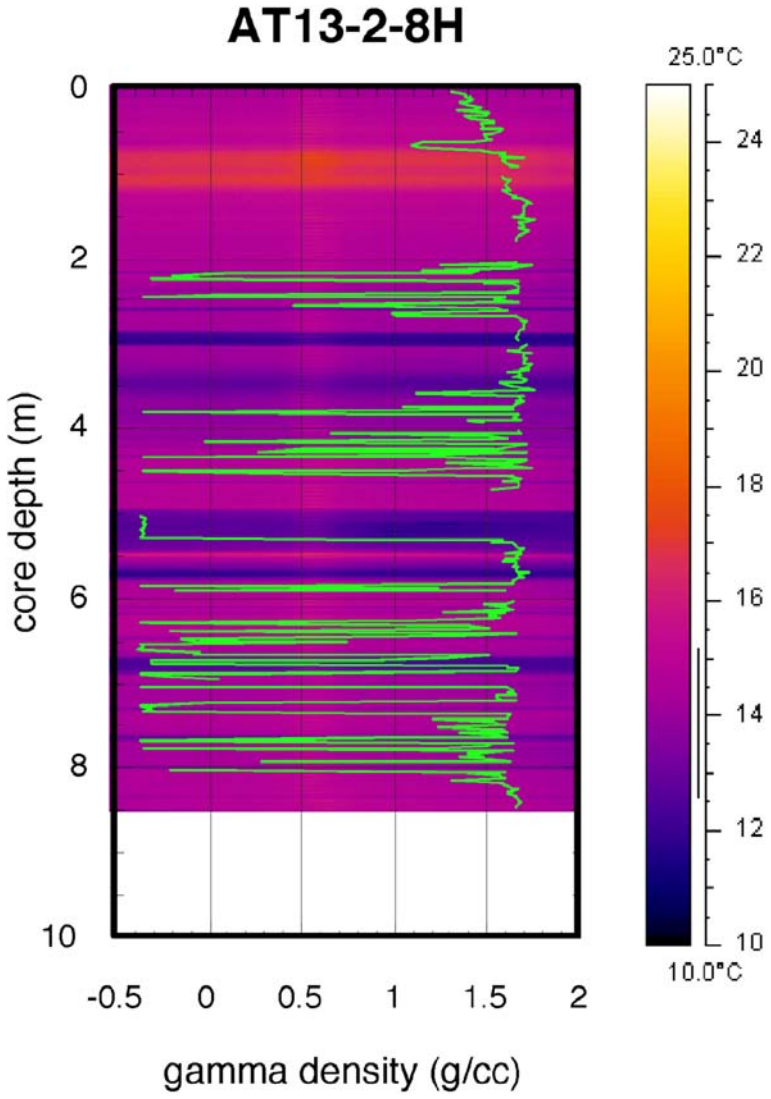

Figure 20. Gamma density (green line) and infrared image for Core AT13-2-8H. Sharply bounded cold regions are voids, but the voids had shifted by the time the gamma density is measured. Gamma density was not calibrated for air, so empty liner appears to have negative densities.

Nonuniform handling explains much of the remaining temperature variations within and between cores. For instance, Core AT13-2-11H had extended handling time and was then placed in ice; the internal core temperatures no longer reflect the *in situ* temperatures to any extent. The core processing container was cooler than the core but with a strong thermal gradient, causing a strong gradient in liner temperature that was not reflected in the internal temperature of the core (Figures 19 & 21). These variations make the thermal baseline for cores difficult to determine, and subtle anomalies hard to identify.

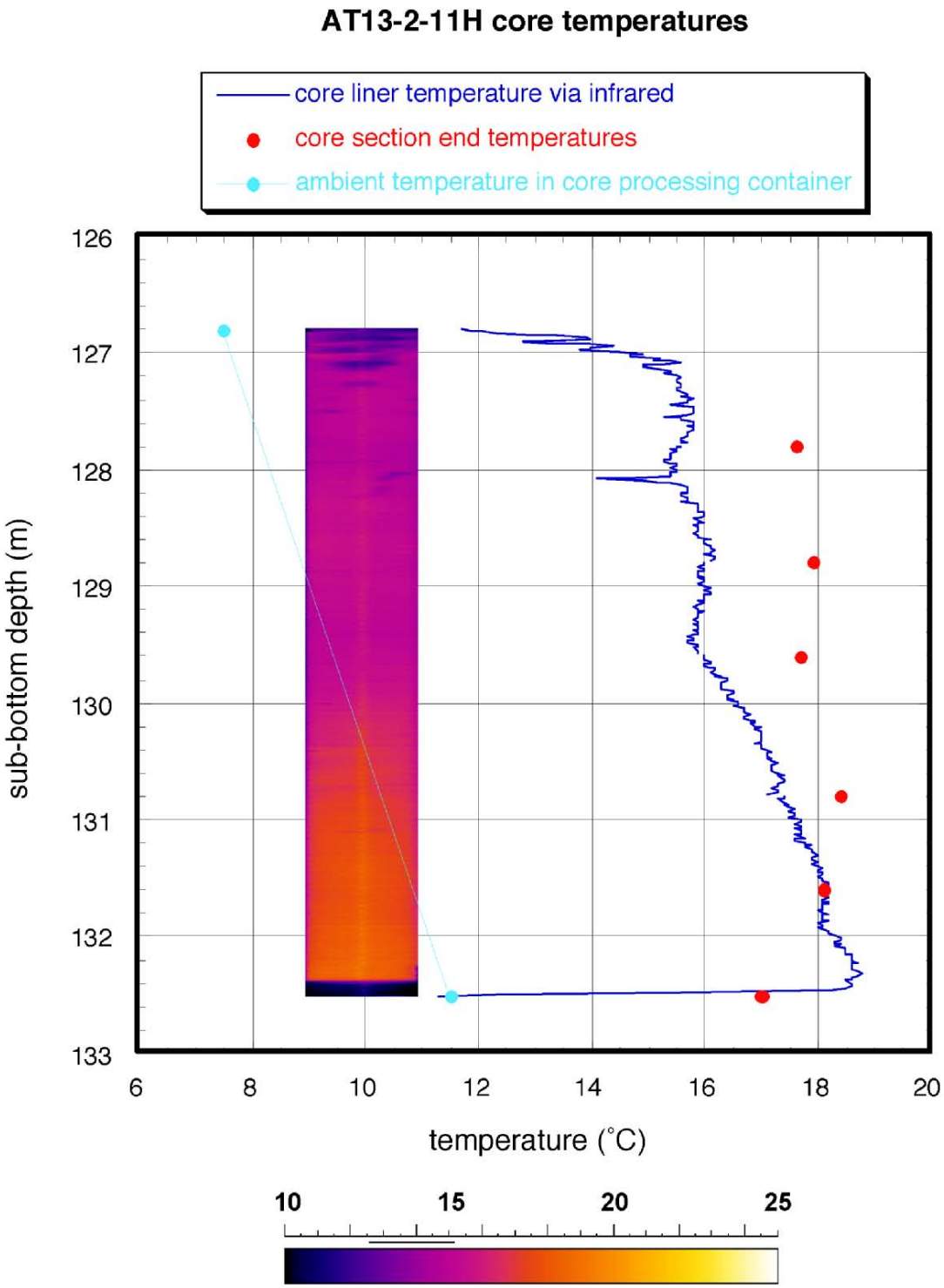

Figure 21. Temperature data for Core AT13-2-11H, including infrared image. Internal temperatures and core liner temperatures from infrared scanning did not match due to handling of the core.

The temperature data indicate that actual recovery of small amounts or concentrations of hydrate under these conditions was very difficult. Average cores reached the rig floor with temperatures of 18-22˚C, having warmed during the trip up the drill pipe. The data from the Seabird CTD (Figure AT-5) showed that the thermocline was extremely extended at this site and that over half of the water column was warmer than the cores were *in situ*. Data from the Fugro Pressure Corer temperature and pressure logger shows the temperature of the corer as it was recovered at AT13-2 (Figure AT-6); the corer warms quickly during its 17-minute trip up the drillpipe. This temperature profile is likely to be similar to what was experienced by the Fugro Hydraulic Piston Corer, accounting for the very warm FHPC cores.

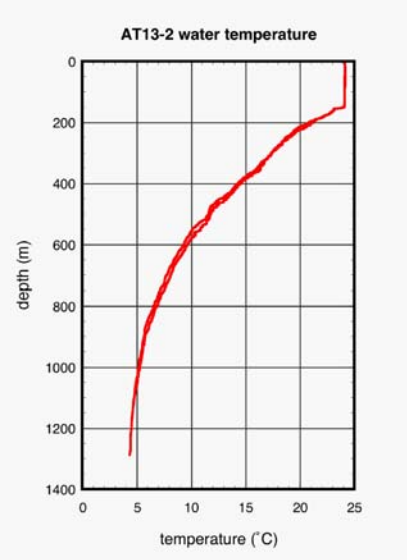

Figure 22. Temperature data from the Seabird CTD cast over Site AT13-2.

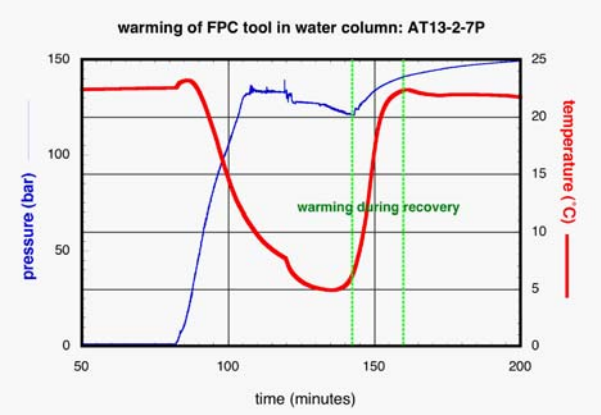

Figure 23. Temperature and pressure data versus time for core AT13-2-7P. The retrieval of the tool up the drillpipe is bounded by green dashed lines.

MSCL-S Measurements

Cores from Hole AT13-2 were logged with the MSCL-S, using the gamma density, P-wave velocity, electrical resistivity, and magnetic susceptibility sensors. All cores and hence data were adversely affected by gas expansion below the sulfate-methane interface (around 7 mbsf). Figure 24 shows a summary plot of all the data along with data envelopes bounding the data least affected by gas expansion. The P-wave data were almost non-existent below the sulfate-methane interface, and while resistivity values are shown, they are not representative of *in situ* conditions (see "Gas Expansion Effects & GOM-JIP Core" under Explanatory Notes). The gamma density data correlated well with the LWD data from the Hole AT13-1 (including the drop in density around 130 mbsf). The magnetic susceptibilty data does show some significant variations, especially in the zone 120-130 mbsf. Variations in magnetic susceptibility indicate changes in the source of the material, which may be useful when developing a sedimentological unit classification or sampling program.

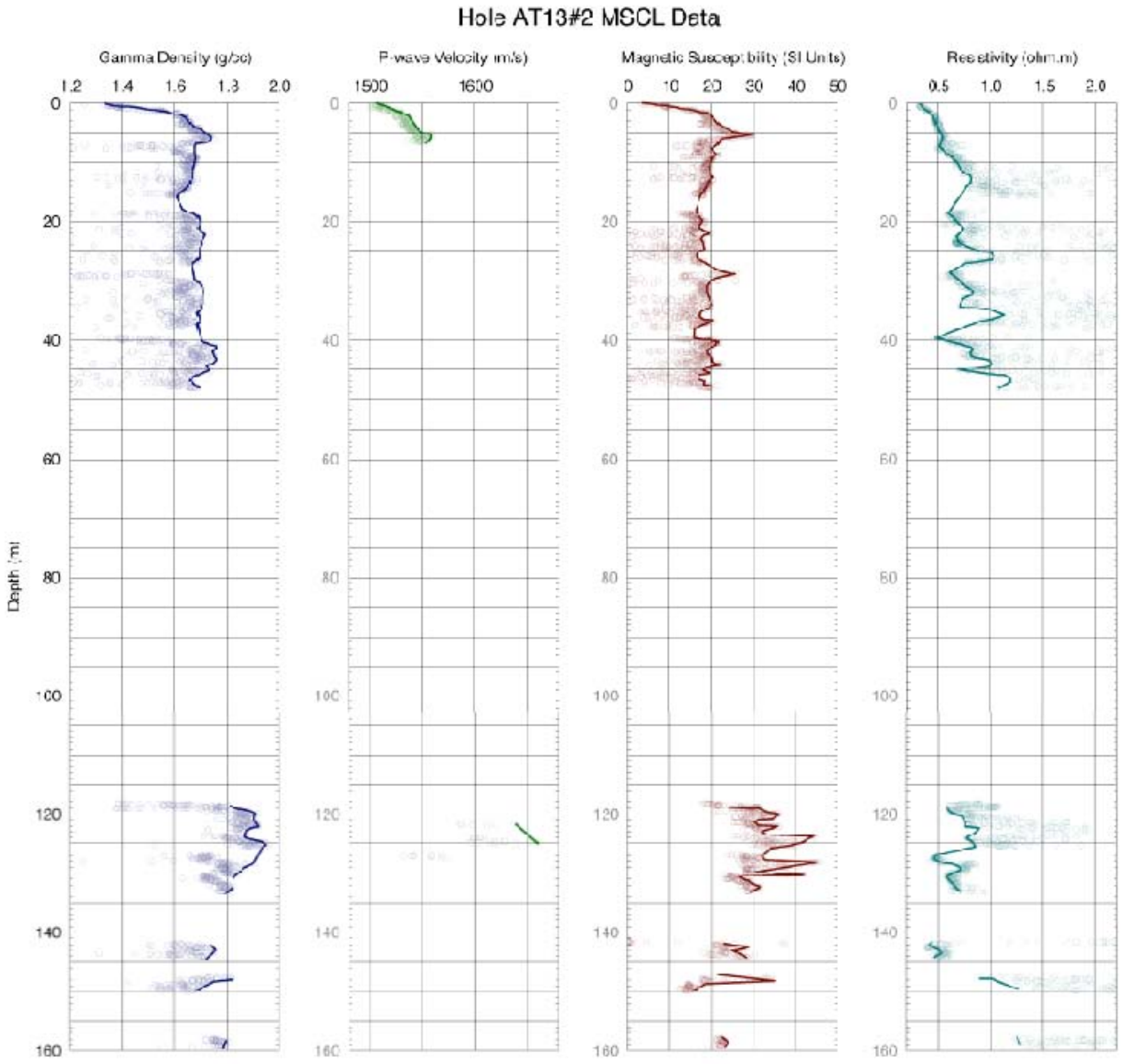

Figure 24. MSCL-S data, including gamma density , P-wave velocity, Magnetic susceptibility, and electrical resisitivity, for Hole AT13-2

MSCL-XYZ Measurements

Cores from Hole AT13-2 were imaged in the MSCL-XYZ. An example section is shown in Figure 25. A summary plot of the Minolta Spectra and Color spectra and magnetic susceptibility measurements are shown in Figure 26. The magnetic susceptibilty data shows the same overall trends as the loop sensor but contains another level of detail in the high resolution data that could prove useful when examining the sedimentology.

Figure 25. Linescan color image taken with the MSCL-XYZ using the Geoscan camera of typical GOM-JIP core section (AT13-2-4H-5)—clay with expansion voids. Pixels are 100 microns on a side. Color fringing on edges of image results from registration of camera CCDs.

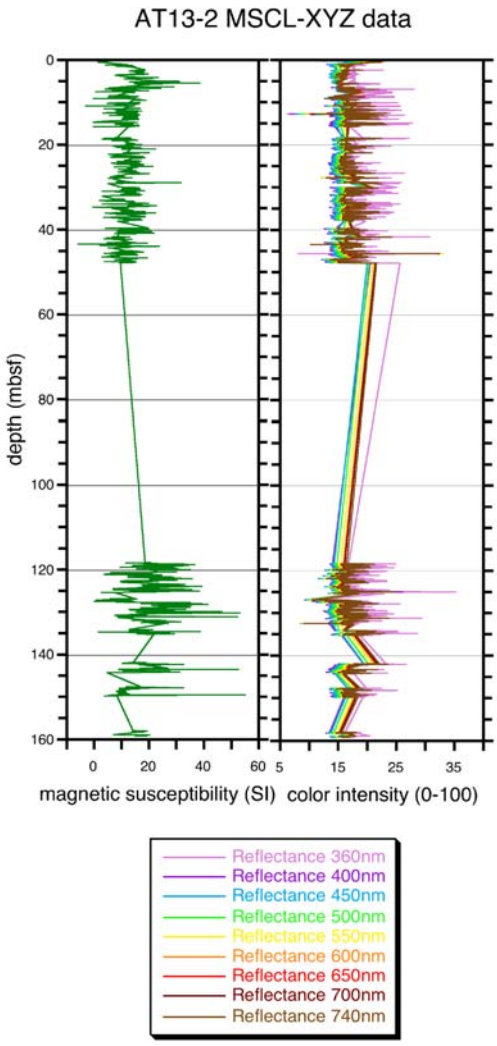

Figure 26. MSCL-XYZ data summary plot, in cluding matgnetic susceptibility and color spectrophotometry for Hole AT13-2.

ROV Push Cores (from AT13 & AT14)

MSCL-S Measurements

An ROV push core, Core AT14-7PC, collected from Atwater Valley in short fiberglass liners was logged with the MSCL-S (Figures 27 & 28). This core was taken specifically for measurements of physical properties (see separate Fugro Physical Properties Report), and the MSCL-S

data was meant to complement these measurements. The resistivity data is adversely affected by the core end effects and is not calibrated, however, all other data is calibrated and valid.

Figure 27. ROV push core AT14-7PC, collected in fiberglass liner, in the MSCL-S. Small fiberglass core sections had end-caps taped on for logging to prevent the core from oozing out of the liner.

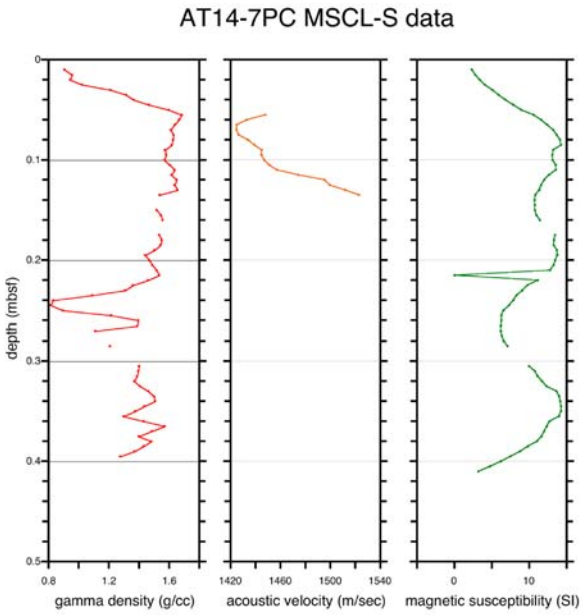

Figure 28. MSCL-S data summary plot, including gamma density, P-wave velocity, and magnetic susceptibility, for push core AT14-7PC.

MSCL-XYZ Measurements

The ROV push cores taken in plastic liners from Atwater Valley (AT13-2PC, AT14-5PC, AT14-6PC, AT14-8PC, AT14-10PC) were imaged in the MSCL-XYZ. Color spectra and magnetic susceptibility point sensor measurements were also made.

Atwater Valley, Holes ATM1 & 2

HYACINTH Tool Operations

Fugro Pressure Corer (FPC)

The FPC recovered one core at full *in situ* pressure from the Mound sites at Atwater Valley (Table 1). Core ATM2-5P was recovered at full pressure from 26.82 mbsf. This core was sheared with some difficulty in the shear transfer chamber and ended up in the storage chamber with the piston assembly and some broken bits of core liner. A portion of the core had been extruded during the transfer process but the rest of the core, containing gas hydrate, did have measurements made at *in situ* conditions. The other 2 pressure coring attempts were unsuccessful.

HYACE Rotary Corer (HRC)

All 3 HRC pressure coring attempts at the mounds sites failed because of jamming issues inside the tool during activation (Table 2). It was concluded that these deployments functioned correctly on the bottom but failed to fully retract because the top of the core cutter was not engaging correctly as it retracted into a sleeve in the autoclave.

Pressure Cores

Pressure Core ATM2-5P

Pressure core ATM2-5P (Figure 29), recovered with the FPC from 26.82 mbsf at 130 bar, was imaged with the X-ray CT scanner, logged for gamma density in the MSCL-V, logged in the MSCL-P using the Geotek P-wave system in a manual mode, and finally depressurized.

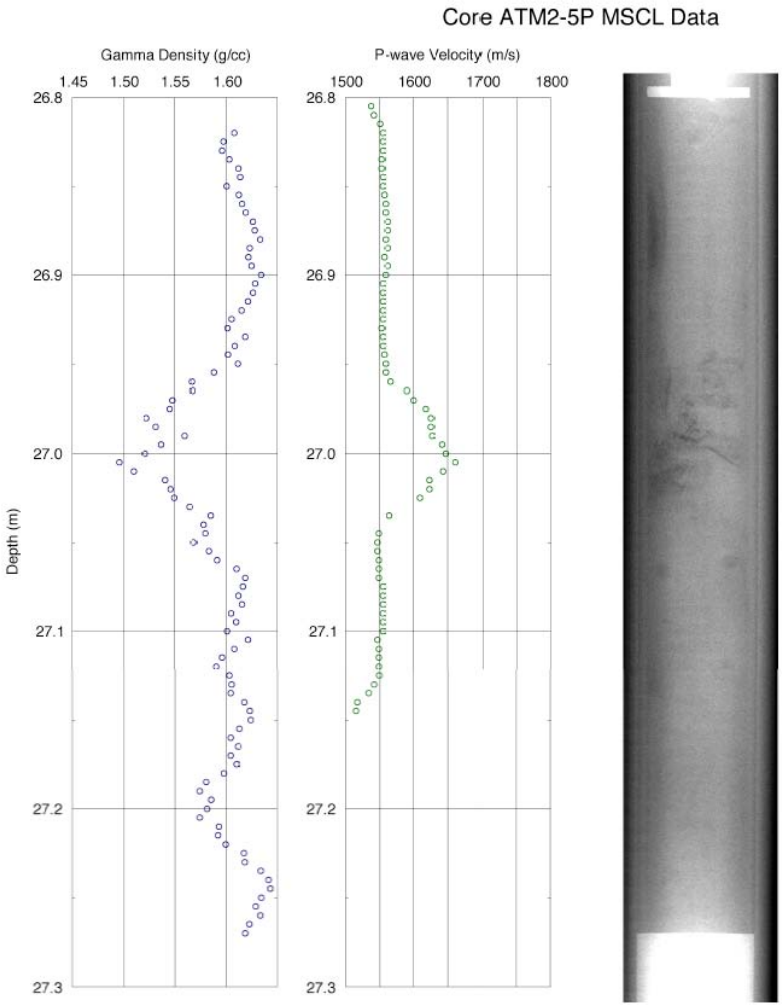

Figure 29. Data from pressure core ATM@-5P, collected from 26.82 mbsf at a pressure of 130 bar. Figure shows gamma density data, collected in the MSCL-V; P-wave velocity, collected in the MSCL-P; and linear X-ray scan, collected in the X-ray CT scanner. Low density/high velocity zone at 27 cm core depth, corresponding to odd X-ray texture, may be a hydrate-bearing layer.

After a difficult transfer process (see FPC operations) it was known that the FPC corer/piston mechanism (technical portion of core) was inside the aluminum storage chamber together with the recovered core material. The complete storage chamber was X-ray CT scanned, which revealed that there was a coherent core 52 cm long surrounded by an intact liner. Within the core there was a zone of lower density material that contained some very interesting and unusual structural features (see separate Lawrence Berkeley X-ray Report). However, the liner was broken around the piston assembly, which was to impede further core manipulations.

The storage chamber was loaded into the MSCL-V, where a detailed density profile was obtained (Figure 29) indicating a low density zone that correlated with the zone revealed by the X-ray scan. After connecting the storage chamber to the MSCL-P and balancing the pressures, the core was moved carefully through the system using the manipulators. However, the resistance (caused by the broken liner) was such that we decided against automated logging and collected the P-wave information manually as the core passed the transducers. This data is also shown in Figure 29 and reveals a high velocity interval that correlates with the low density interval as shown by both the gamma density profiles and the X-ray profiles.

Further movement of the core in the system became more difficult and it was concluded that we had extruded some more core inside the apparatus. This was confirmed when the MSCL-P system was opened (sediment around the transducers) and the chamber (still under full pressure) was X-rayed again. Because of the jamming issues we could not use the core with the Georgia Tech central measurement chamber.

The final core was only 30 cm long. This remaining length of core (which, fortuitously, contained the low density/high velocity anomaly) was depressurized. The MSCL-V could not be used during the depressurization due to the presence of the technical portion of the core. The total volume of methane released was 1015.7 ml (lower estimate; some gas remaining in the corer at 1 bar could not be measured). Over a liter of air was also released; this gas presumably came from the technical portion of the FPC core, which is not normally transferred into the logging chambers.

The final core was sub-sampled and squeezed for pore water analysis that showed significant porewater freshening around the low density zone (see separate Scripps Porewater Chemistry Report). The retrieval of this core and the experiments conducted were far from ideal, but the combination of information retrieved indicated that the core did contain some gas hydrate. Our calculations show that this was about 0.3% of the total pore volume in the core.

It is likely that the gas hydrate was concentrated in the 10-cm-long high velocity interval, which would indicate that this layer had a hydrate concentration of about 3% of total pore volume. While the velocity anomaly shown in Figure ATM-1 could have been due to hydrate within this zone, the density anomaly cannot be explained simply by the presence of 3% hydrate. This layer has a low density independent of hydrate presence and the low density of the layer may have provided space for preferential hydrate growth.

FHPC & FC Cores

Temperature Measurement via Infrared Logging

The temperatures of each of the cores from Holes ATM1&2 were monitored in order to detect any signs of hydrate dissociation, in the form of localized, centimeter-scale thermal anomalies or

large cold zones that might span multiple cores. The infrared camera track provided a continuous record of the liner temperature, and temperature probes placed in the center of section ends recorded the actual core temperatures (Figures 30 & 31).

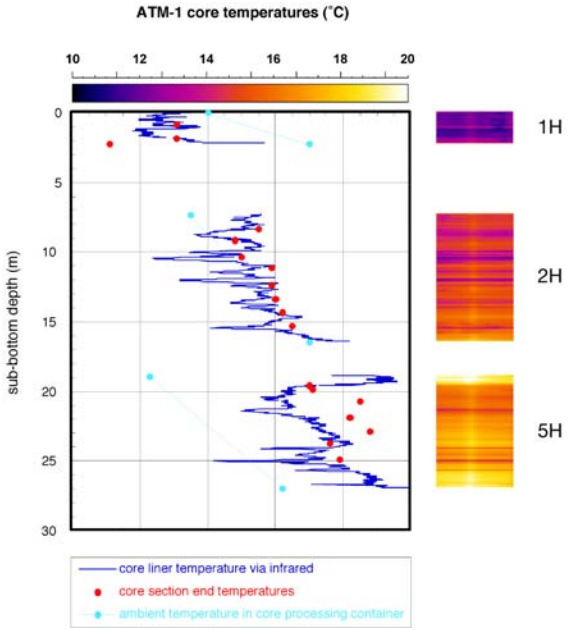

Figure 30. Plot of temperature data from infrared imaging, which takes the temperature of the core liner, and from direct and from direct measurement of the center of the core at core section ends for the top o f Hole ATM1. Two-dimensional infrared image is shown to the right of the plot.

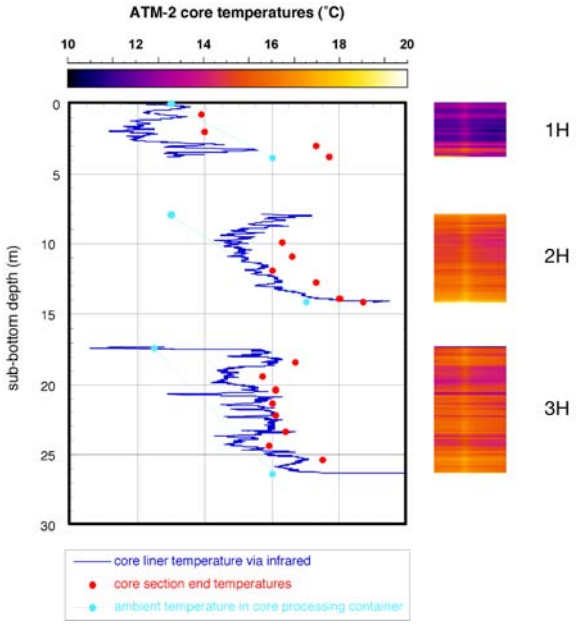

Figure 30. Plot of temperature data from infrared imaging, which takes the temperature of the core liner, and from direct and from direct measurement of the center of the core at core section ends for the top o f Hole ATM2. Two-dimensional infrared image is shown to the right of the plot.

The moussy texture of all six of the cores from the Atwater Mound site (Figure 1), which was first observed while cutting the core into sections and inserting temperature probes, indicates that there may have been gas hydrate in these cores. The mudline core from each hole was colder than the deeper cores, though the rest of the cores were similar in temperature to the cores from AT13-2. However, some of the cores may have been cooled in the ice trough or processing van, as their centers, as measured by the temperature probes, were warmer than the outside, as measured by the infrared camera.

Plenty of small thermal anomalies existed in these cores, many of which are likely due to gas expansion effects. The moussy, frothy expansion of the cores would have chilled the cores in a qualitatively different fashion than the dry gas expansion cracks seen in Hole AT13-2. This small-scale gassy nature can be seen in the split-core images (see ATM MSCL-XYZ) and in the gamma density logs (see ATM MSCL-S). Gas expansion cracks were also present. Attempts to remove these two gas expansion effects using the density data from either the gamma attenuation (Figure 32) or the X-ray images proved complex and beyond the scope of this report.

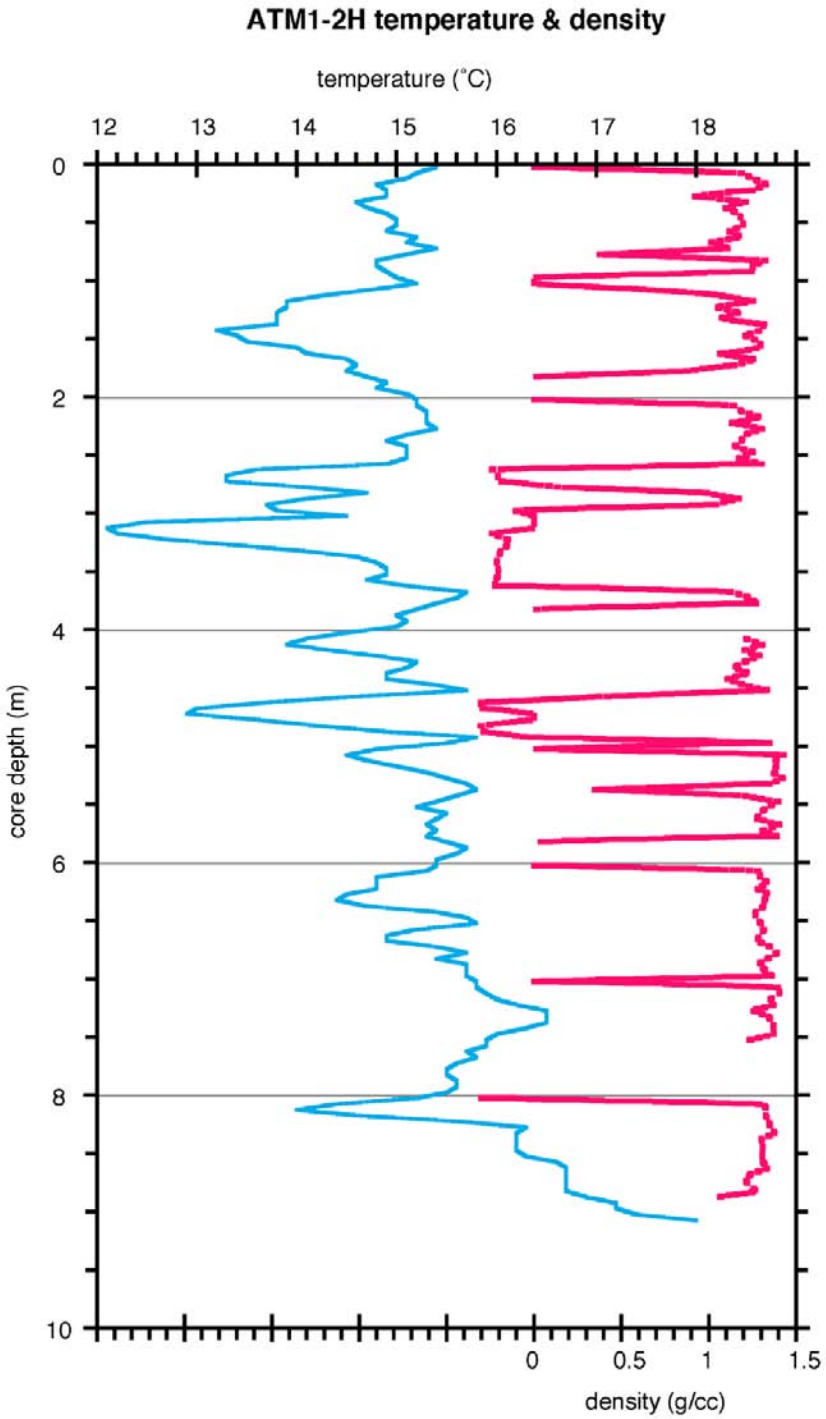

Figure 32. Plot of gamma density and infrared-derived temperature for ATM1-2H, which shows the difficulty in distinguishing cold regions due to voids from cold regions corresponding to gas hydrate. Voids had shifted an unknown distance between the two measurements.

Comparison of the thermal anomalies with the salinity data provided by the geochemists showed that most thermal anomalies directly associated with gas hydrates at this site were probably lost

in recovery and handling. There is a large, low-salinity zone that encompasses the center of Core ATM1-2H that might be due to hydrate dissociation, but there is no corresponding thermal anomaly at the center of this core (Figure 33). Core ATM2-3H may have retained some thermal anomalies due to hydrate dissociation, based on the salinity anomalies (Figure 34).

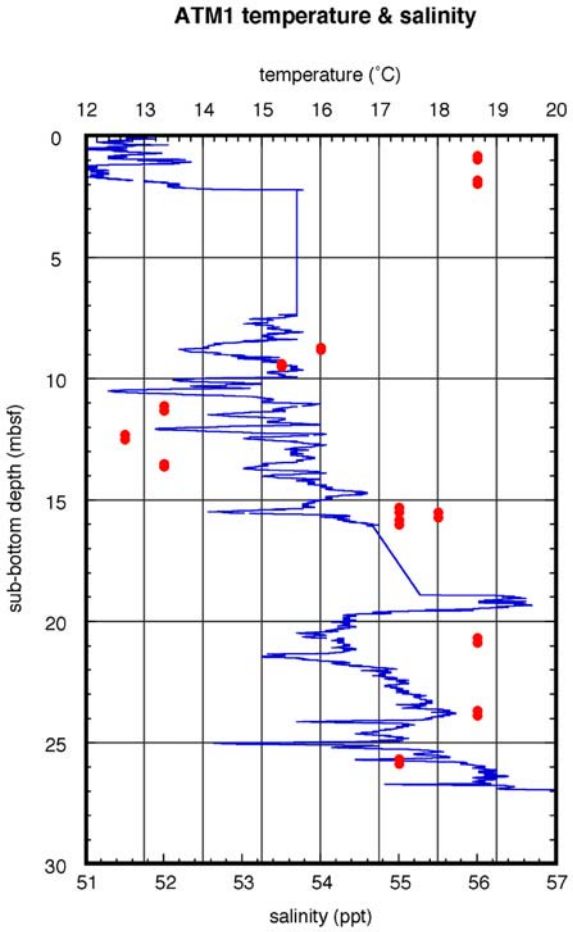

Figure 33. Temperature from infrared track (blue) and porewater salinity (red) for Hole ATM1. Freshening trend from 8-15 mbsf is not reflected in the recorded thermal anomalies.

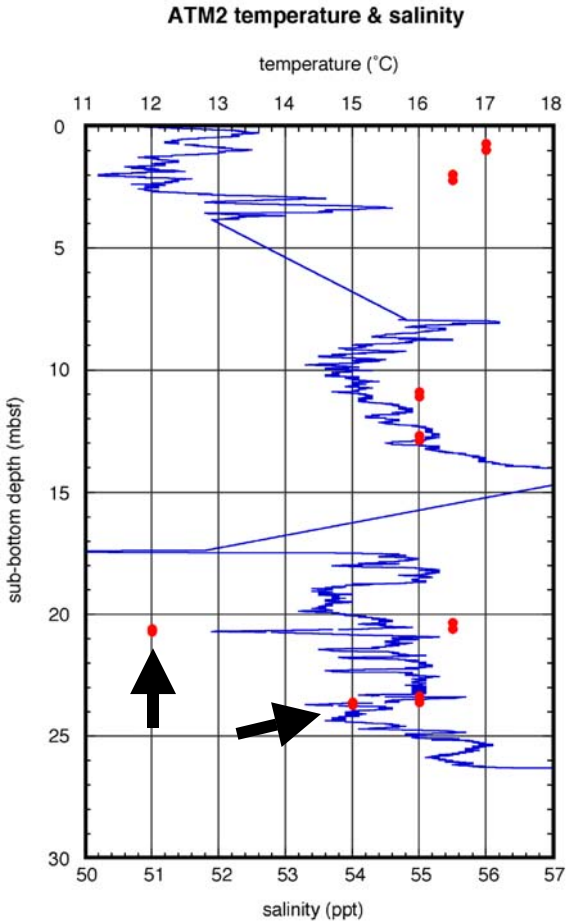

Figure 34. Temperature from infrared track (blue) and porewater salinity (red) for Hole ATM2. The two pore water freshening anomalies in bottom core (arrows—ATM2-3H) may correspond with negative thermal anomalies.

The Atwater Mound site was very close to AT13-2, so the water column temperature profile is likely very similar (Figure 22), where the thermocline was quite extended. The Adara temperature shoe attached to the FHPC on Cores ATM1-5H and ATM2-3H (Figure 35) as well as the temperature logger on Core ATM2-5P (Figure 36) show that the core would warm substantially during the trip up the pipe and any remaining thermal anomalies from hydrate dissociation were likely to be subtle.

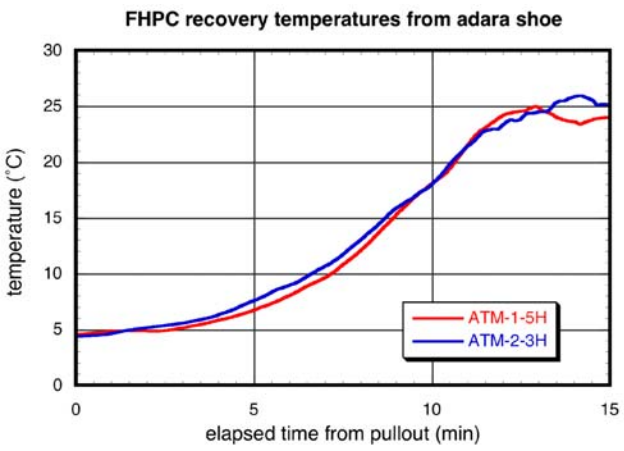

Figure 35. Temperature data from the temperature shoe fitted on the FHPC for cores ATM1-5H and ATM2-3H.

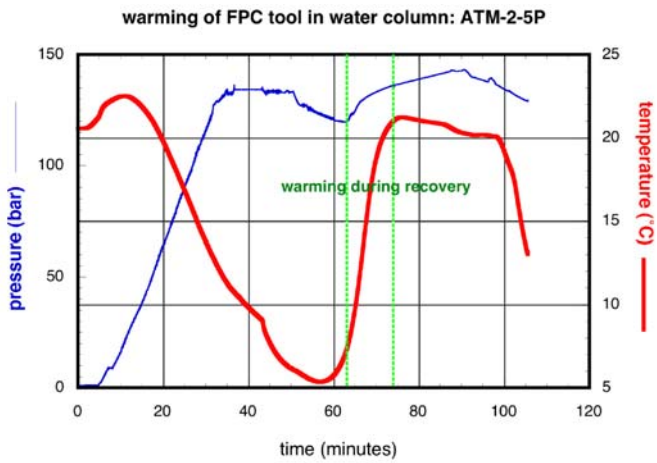

Figure 36. Temperature and pressure data versus time for Core ATM2-5P. The retrieval of the tool up the drillpipe is bounded by green dashed lines.

MSCL-S Measurements

Cores from Holes ATM1&2 were logged using the MSCL-S, using the gamma density, P-wave velocity, electrical resistivity, and magnetic susceptibility sensors (Figures 37 & 38). The cores exhibited moussy textures and contained much gas, potentially from dissociated hydrate. No P-wave velocity measurements were possible at any depth and all the other parameters are significantly affected by the core disturbance. Even the gamma density is likely to be significantly low; the density measured in the MSCL-S in ATM1 at full depth (27 mbsf) is around 1.5 g/cc, whereas the density measured from the pressure core just beneath it is 1.6 g/cc. Note the significant differences in the magnetic susceptibility data, taking into account the density, for both holes below 15-20 mbsf, indicating rapid horizontal variation at the Mound site.

MSCL-XYZ Measurements

Cores from Holes ATM1&2 were imaged in the MSCL-XYZ. Even after transport, storage for over a month, and splitting, the moussy texture of the cores was still evident (Figure 1). Color spectra and magnetic susceptibility measurements, made with a point sensor, were also taken (Figure 39). The quality of the data in these cores is compromised because of the very moussy texture. Care should be used when interpreting the data.

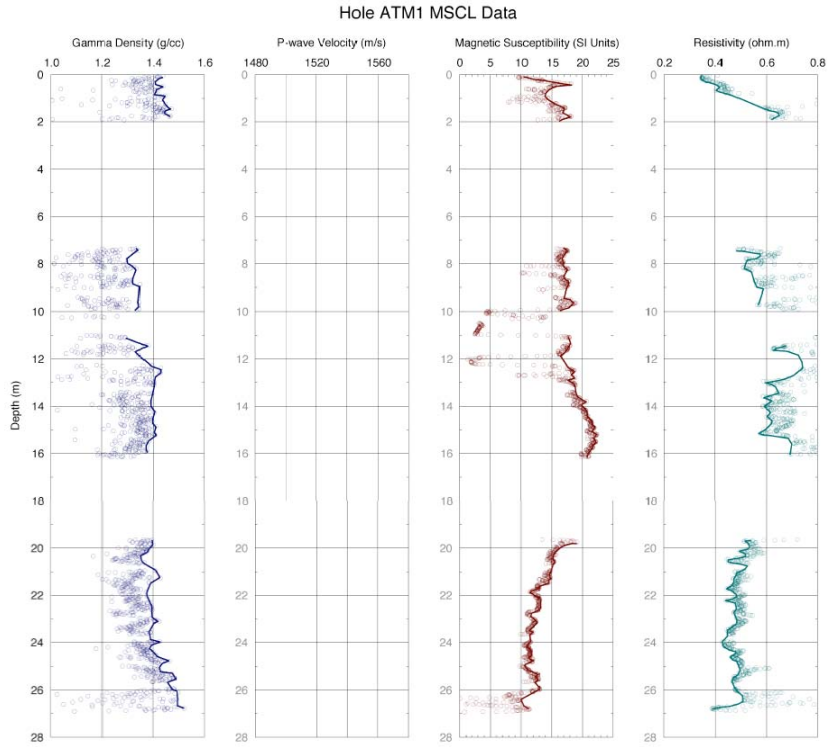

Figure 38. MSCL-S data, including gamma density, P-wave velocity, magnetic susceptibility, and electrical resistivity for Hole ATM2.

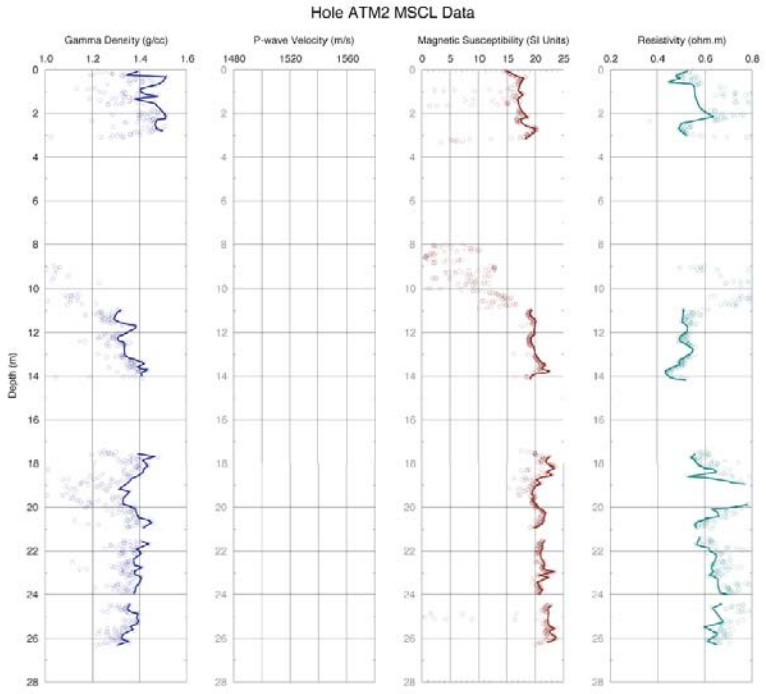

Figure 38. MSCL-S data, including gamma density, P-wave velocity, magnetic susceptibility, and electrical resistivity for Hole ATM2.

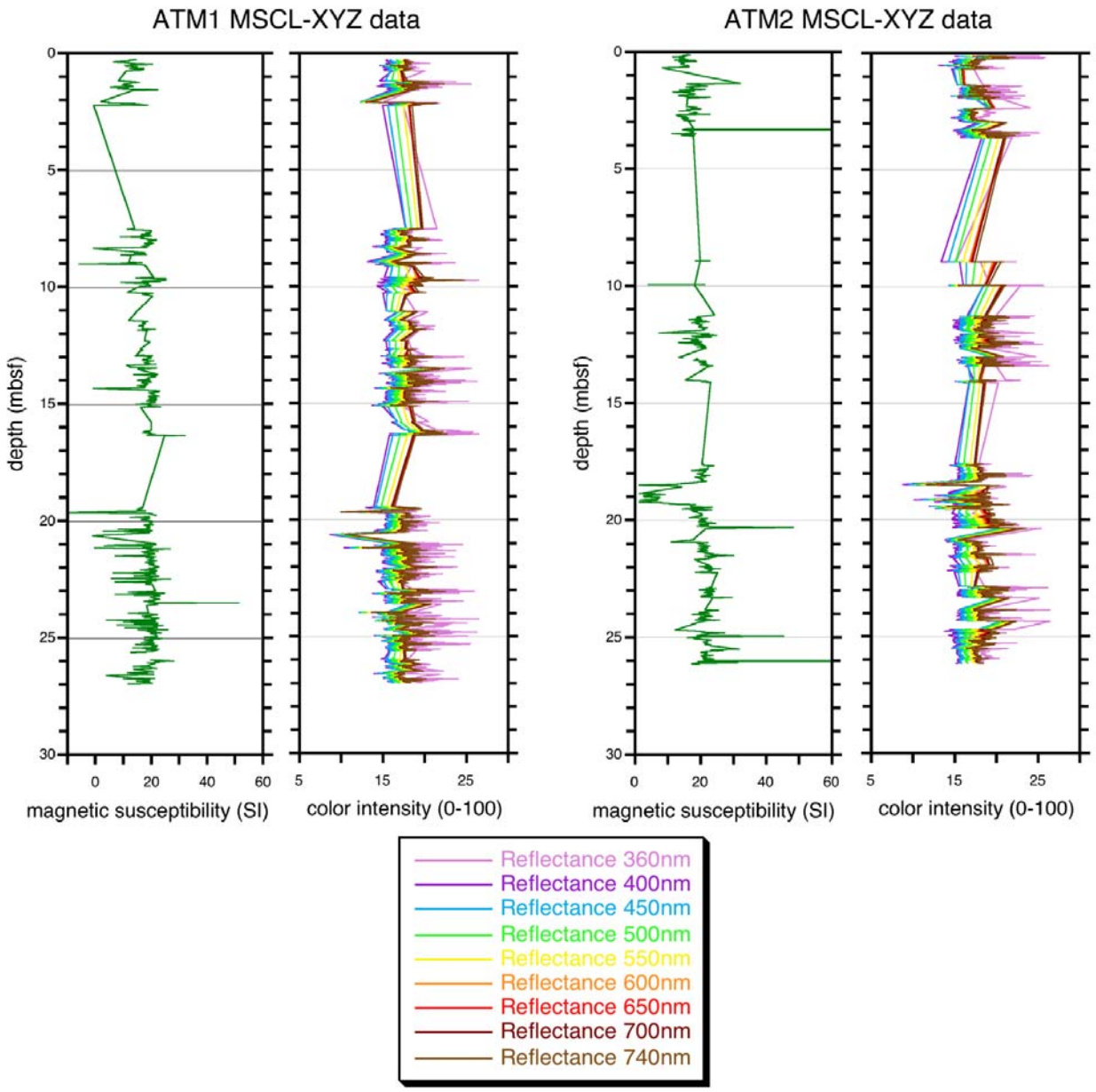

Figure 39. MSCL-XYZ data summary plot, including magnetic susceptibility and color spectrophotometry, for Holes ATM1 and ATM2.

Keathley Canyon, Hole KC151-3

HYACINTH Tool Operations

Fugro Pressure Corer (FPC)

The first attempted pressure core at Keathley Canyon (KC151-3-6P; Table 1) was thwarted by a backwash of sand in the BHA (bottom hole assembly). The deployment went smoothly but there was no pressure drop indicating the tool had fired. The tool had become stuck in the BHA and the sand line could not free the tool. After many hours of attempting to free the tool from the

BHA, the sand line was finally cut and the pipe tripped. It was discovered that the tool had never landed on the landing shoulder because of fine sand that had filled the BHA.

After this deployment it was thought that a number of the pressure corer failures may have been caused by some sediment "sticking up" in the BHA, which might have prevented the tools landing properly. Consequently, it was decided to run the center bit prior to all remaining pressure cores to ensure the BHA was clear of any obstructions. The subsequent 3 resulting successes (FPC and HRC; Tables 1 & 2) may have been partially due to this new procedure. The second FPC deployment (KC151-3-11P) at 227.08 mbsf was a total success and recovered 88.5 cm of core at full *in situ* pressure. This core was logged in the X-ray CT scanner, the MSCL-V, and the MSCL-P (see Keathley Pressure Cores).

The last 2 deployments with the FPC at Keathley Canyon were deep in the hole and did not recover cores under pressure essentially because the sediments were stiffer than the tool was designed for (Table 1). In the case of KC151-3-18P at 265.18 mbsf, the pull-out forces broke the liner and the top half of the liner (which was empty) was recovered under full pressure. The 59 cm core was recovered in the unpressurized outer barrel. During the final FPC deployment at 384.96 mbsf (probably below the depth of gas hydrate stability), the sediment completely jammed the liner in the outer barrel and prevented it being retracted into the autoclave. Excessive pull-out forces on this deployment showed that we had gone beneath the level at which the corer could operate.

HYACE Rotary Corer (HRC)

The HRC operations at Keathley Canyon provided 2 good pressure cores recovered from the 4 deployments in what were difficult coring conditions (Table 2). KC151-3-13R was recovered from a depth of 235.92 mbsf, which was just into the region predicted (from the LWD data) to contain significant amounts of gas hydrate. The second core retrieved under pressure came from a depth of 383.13 mbsf and was thought to lie just above the base of the gas hydrate stability zone. Both cores were logged in the X-ray CT scanner, the MSCL-V, and MSCL-P before being subjected to depressurization experiments (see Keathley Pressure Cores). The other 2 HRC deployments suffered technical difficulties, as at Atwater Valley, caused by the retraction of the sleeve when the inner core barrel enters the autoclave.

Pressure Cores

Pressure Core KC151-3-11P

Pressure core KC151-3-11P (Figure 40), recovered with the FPC from 227.08 mbsf at 160 bar, was imaged with the X-ray CT scanner, logged for gamma density in the MSCL-V, and logged in the MSCL-P using both the Geotek P-wave system and the Georgia Tech sensors (see separate Georgia Tech Report). The gamma density log showed a relatively uniform core, with slightly higher densities in the lower third of the core (Figure 40). The P-wave velocity log showed somewhat higher velocities (1625 vs 1600 m/sec) in the same interval (Figure 40). P-wave amplitudes were high throughout the core.

The core was stored under pressure in the cold for sub-sampling on shore. Prior to sub-sampling, the water surrounding the core was replaced by nitrogen. The core was sub-sampled under pressure. The top 5 cm of the core was trimmed off and archived. The interval 8.5-34.5 cm was transferred under pressure into a modified Parr vessel for transport to USGS Woods Hole for

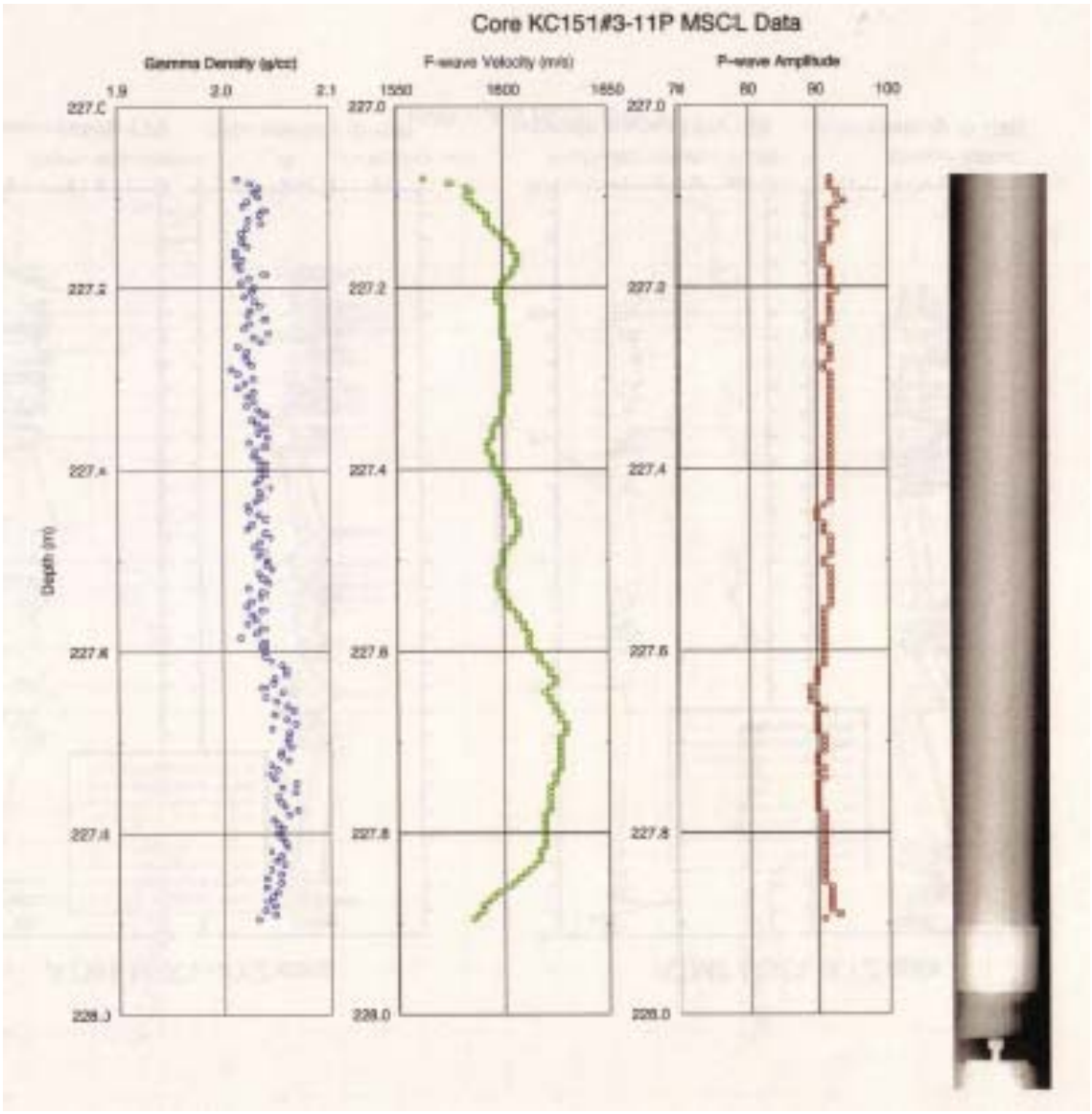

Figure 40. Data from pressure core KC151-3-11P, collected from 227.08 mbsf at a pressure of 160 bar. Figure shows gamma density data, collected in the MSCL-V; P-wave velocity and amplitude, collected in the MSCL-P; and linear X-ray scan, collected in the X-ray CT scanner. Top two-thirds and bottom third of core are distinct in density and velocity.

physical properties studies using the GHASTLI system. The Parr vessel was flushed with methane and reduced to 100 bar pressure before transport. The intervals 5-8.5 cm and 34.5-42.5 cm were depressurized and sent to Woods Hole so the investigators could examine the surrounding core material before opening the pressure vessel.

The interval 42.5-51 cm of the core was cut, depressurized, and archived. The interval 51-54 cm was transferred into a microbiological sub-sampling apparatus for microbiological studies at Cardiff University. The nitrogen surrounding the remaining core (54-90 cm, 46 cm total length)

was replaced with water and the core was depressurized. Gas sub-samples were sent to USGS Menlo Park for analysis (see separate USGS Gas Report).

None of the rapidly depressurized core portions showed any evidence of hydrate or increased gas content. The hydrate content of this core is not yet known, but the log and visual evidence points to little or no hydrate.

Pressure Core KC151-3-13R

Pressure core KC151-3-13R, recovered with the HRC from 235.92 mbsf at 160 bar, was imaged with the X-ray CT scanner, logged for gamma density in the MSCL-V, and logged in the MSCL-P using both the Geotek P-wave system and the Georgia Tech sensors (see separate Georgia Tech Report). The gamma density log showed that the upper part of the core is more uniform than the lower part of the core which has some lower density intervals (Figure 41). The P-

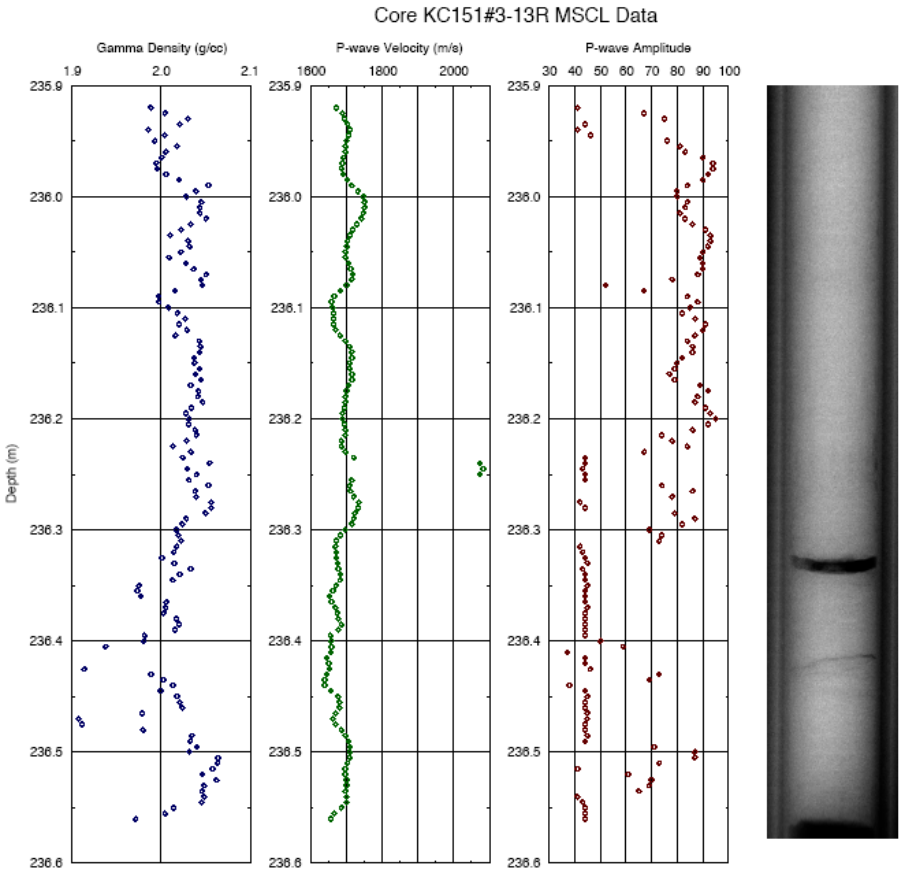

Figure 41. Data from pressure core KC151-3-13R, collected from 235.92 mbsf at a pressure of 160 bar. Figure shows gamma density data, collected in the MSCL-V; P-wave velocity and amplitude, collected in the MSCL-P; and linear X-ray scan, collected in the X-ray CT scanner. Lower half of core is distinguished by low P-wave amplitudes, slightly lower P-wave velocity and more variable density. High-velocity spike at center of core may have been a thin hydrate vein.

wave velocity log showed a prominent high velocity spike (2074 m/s) at the midpoint in the core (Figure 41), which may correspond to a thin vein of hydrate. There is no density evidence for a

hydrate layer, either from the gamma density or an initial examination of the X-ray scans; if this velocity spike was caused by a hydrate vein, it must have been extremely thin.

The P-wave amplitude was distinctly lower below the velocity spike (Figure 41) and may indicate the presence of microbubbles from partially dissociated dispersed hydrate. Bubble size and density would have been small, as good P-wave signals were still recorded in this interval. P-wave velocity was slightly lower in the bottom half of the core and is also consistent with small amounts of gas in the core. Destabilization of disseminated hydrate due to warming during core recovery could account for these results.

Following the logging, the core was depressurized and gas collected while being repetitively logged in the MSCL-V (Figure 42). Gas was evolved from a point in the core corresponding to the high velocity spike and throughout the core below that point; very little gas was generated from the upper half of the core. Once the core was completely depressurized, it was repressurized to *in situ* pressure (140 bar) and re-logged in the MSCL-P (Figure 43). The high velocity spike had disappeared and the lower portion of the core was completely disturbed, showing velocities near that of water. In contrast, the upper half of the core was relatively unchanged in velocity, with preservation of the basic characteristics.

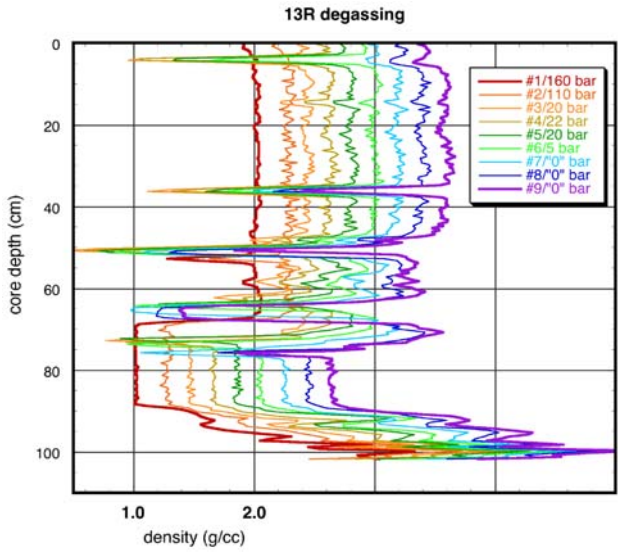

Figure 42. Gamma density data from pressure core KC151-3-13R, collected on repetitive scans during depressurization. Legend shows density scan number and pressure. Each scan is offset from the next by 0.2 g/cc. The high-velocity spike in Figure 41 may correspond to the crack in the core that formed at about 35 cm core depth.

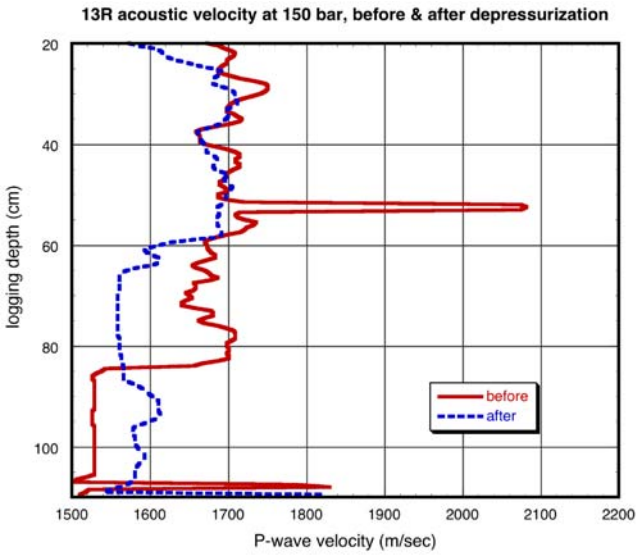

Figure 43. P-wave velocity data from pressure core KC151-3-13R, collected on pristine core and represurized core, after depressurization. Core starts at about 20 cm logging depth. Note that the high-velocity spike in the center of the core disappeared following following depressurization.

The core was then cut into subsections for subsequent pore water analysis, which is ongoing (see separate Scripps Porewater Chemistry Report). A total volume of 7,894 ml of gas and 557 ml of liquid was given off during the depressurization process, corresponding to about 6.2 liters (gas

only) to 6.7 (gas and liquid) of methane. The 6.2 liters of methane is equivalent to about 30 cc of methane hydrate, or a hydrate content of approximately 4-5% by pore volume throughout the core.

The interpretation of Core KC151-3-13R was that the core had two distinct halves. There was little if any hydrate in the top half of the core: the top of the core had high P-wave amplitudes and generated very little gas during depressurization. In the bottom half of the core, hydrate was disseminated in the pore space: the lower half had low P-wave amplitudes, possibly from gas produced by hydrate dissociation during core recovery; generated gas during depressurization; and appeared significantly disturbed in the P-wave log taken after depressurization. Hydrate presence within this layer may have been influenced by the lower densities within the sediment. If the hydrate was confined to the low-P-wave-amplitude region of the core, the hydrate content would have been over 10% hydrate by pore volume.

It is possible that a thin, horizontal hydrate vein, no more than a millimeter thick, divided this core in two: this location in the core exhibited a spike in the P-wave velocity, could be seen generating gas during the depressurization, and had disappeared from the P-wave profile after depressurization. Because there is no conclusive evidence from the density data, however, this interpretation is tentative.

Pressure Core KC151-3-26R

Pressure core KC151-3-26R, recovered with the HRC from 383.13 mbsf at 180 bar, was imagedwith the X-Ray CT scanner, logged for gamma density in the MSCL-V, and logged in the MSCL-P using the Geotek P-wave system. Variability in the gamma density and P-wave velocity mirrored one another (Figure 44), and low velocity and density zones were also visible on the

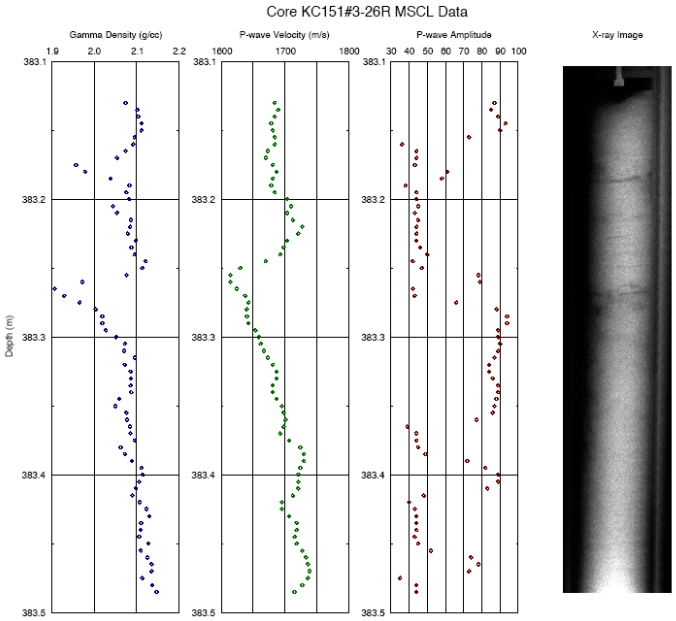

Figure 44. Data from pressure core KC151-3-26R., collected from 383.13 mbsf at a pressure of 180 bar. Figure shows gamma density data, collected in the MSCL-V; P-wave velocity and amplitude, collected in the MSCL-P; and linear X-ray scan, collected in the X-ray CT scanner. Low velocity near center of the core and low amplitudes may indicate core disturbance by hydrate dissociation during core recovery.

X-ray image. The variability in the core logs is a reflection of variations in the sediment, which may have been caused by coring disturbance of the rotary corer in the clay substrate. The low P-wave amplitudes seen in the upper and lower portions of the core may be due to microbubbles of gas formed by partial dissociation of disseminated hydrate (see Core KC151-3-13R).

Following the core logging, the core was depressurized while being repetitively logged in the X-Ray scanner (see separate Lawrence Berkeley X-ray Report). A total volume of 2491 cc of gas and 566 cc of liquid was given off during the depressurization process, corresponding to about 1.4 liters (gas only) to 1.7 liters (gas and liquid) of methane. This is equivalent to 1-2 cc of methane hydrate, or a hydrate content of about 0.5% by pore volume.

FHPC & FC Cores

Temperature Measurement via Infrared Logging

The temperatures of each of the cores from Hole KC151-3 were monitored in order to detect any signs of hydrate dissociation, in the form of localized, centimeter-scale thermal anomalies or large cold zones that might span multiple cores. The infrared camera track provided a continuous record of the liner temperature, and temperature probes placed in the center of section ends recorded the actual core temperatures (Figures 45, 46, 47, 48).

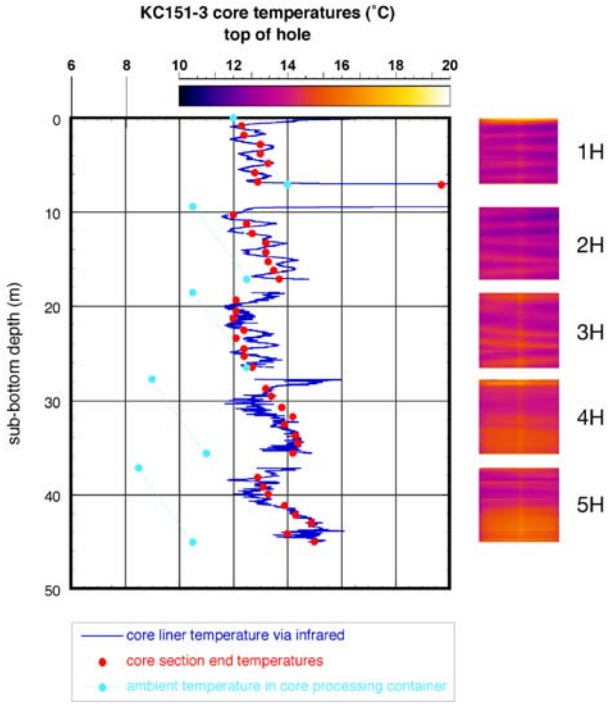

Figure 45. Plot of temperature data from infrared imaging, which takes the temperature of the core liner, and from direct measurement of the center of the core at core section ends for top of Hole KC151-3. Two-dimensional infrared image is shown ot the right of the plot.

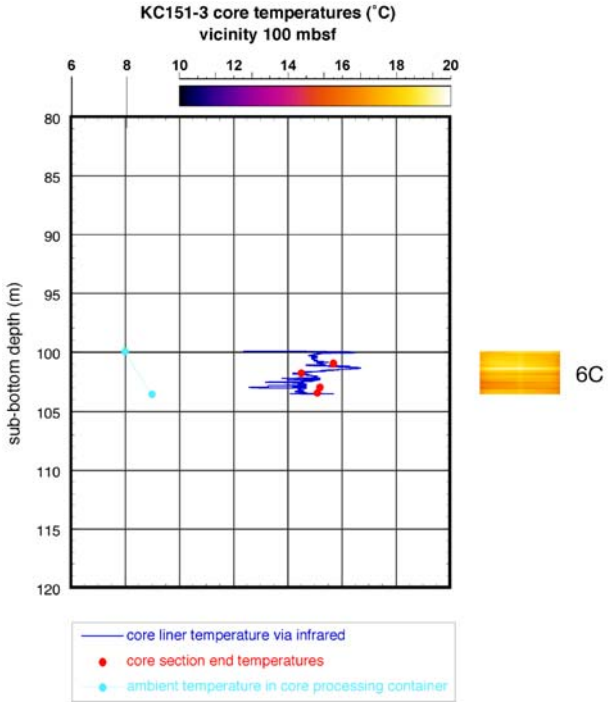

Figure 46. Plot of temperature data from infrared imaging, which takes the temperature of the core liner, and from direct measurement of the center of the core at core section ends for top of Hole KC151-3. Two-dimensional infrared image is shown ot the right of the plot.

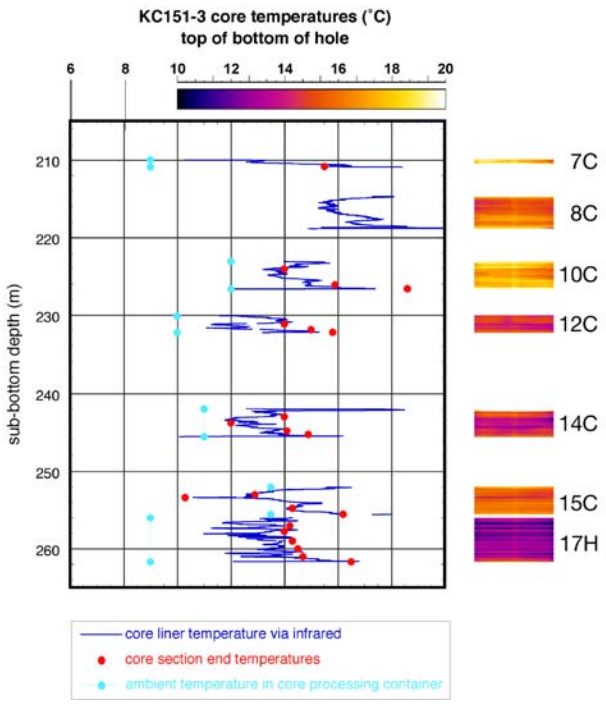

Figure 47. Plot of temperature data from infrared imaging, which takes the temperature of the core liner, and from direct measurement of the center of the core at core section ends for top of Hole KC151-3. Two-dimensional infrared image is shown ot the right of the plot.

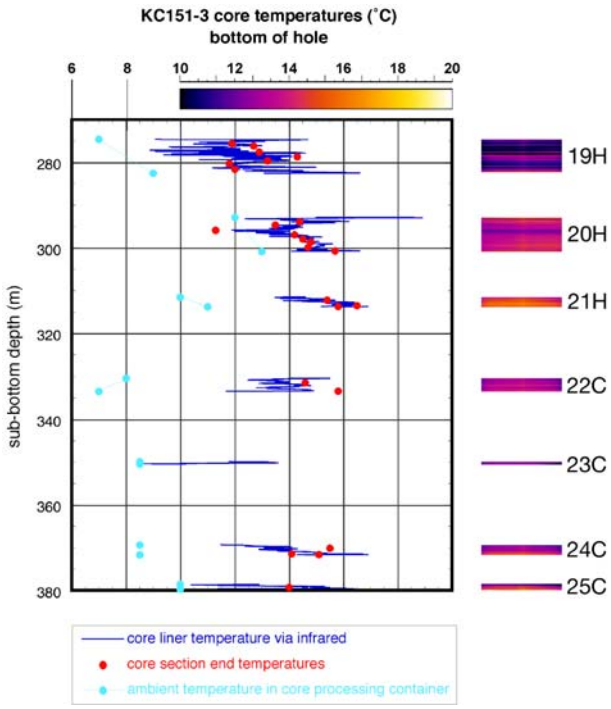

Figure 48. Plot of temperature data from infrared imaging, which takes the temperature of the core liner, and from direct measurement of the center of the core at core section ends for top of Hole KC151-3. Two-dimensional infrared image is shown ot the right of the plot.

Hole KC151-3 contained the only obvious thermal anomaly likely to be associated with gas hydrate on the entire expedition. Core KC151-3-15C (Figure 49), taken with the Fugro Corer, contained a 2.2 C˚ thermal anomaly centered 136.5 cm below the top of the core. This anomaly was similar in morphology and magnitude to nodular or vein hydrate seen on ODP Leg 204 (Shipboard Scientific Party, 2003).

No other cores showed thermal anomalies likely to be hydrate, either centimeter-scale or whole-core scale. Periodic thermal variation in the top three cores was of unknown origin but was potentially an artifact of data collection. Core KC151-3-19H (Figure 48) was relatively cool, but also was extremely expansive. FHPC and FC cores were distinctly different in this respect. FHPC cores tended to have a dry contact between the core and the liner, while the FC core-liner contact tended to be quite wet. Because the FHPC cores were dry, they created a seal against the liner, which allowed cores to be pushed aside by gas expansion, forming voids within the core. FC cores may have experienced the same amount of gas expansion (and cooling) but the gas could escape along the sides of the core. FC cores therefore had a much more uniform infrared thermal profile. This uniform background was one reason that the thermal anomaly in Core KC151-3-KC could be identified and differentiated from thermal anomalies associated purely with gas expansion.

The Keathley Canyon site had a steeper thermocline than that at Atwater Valley (Figure 50).

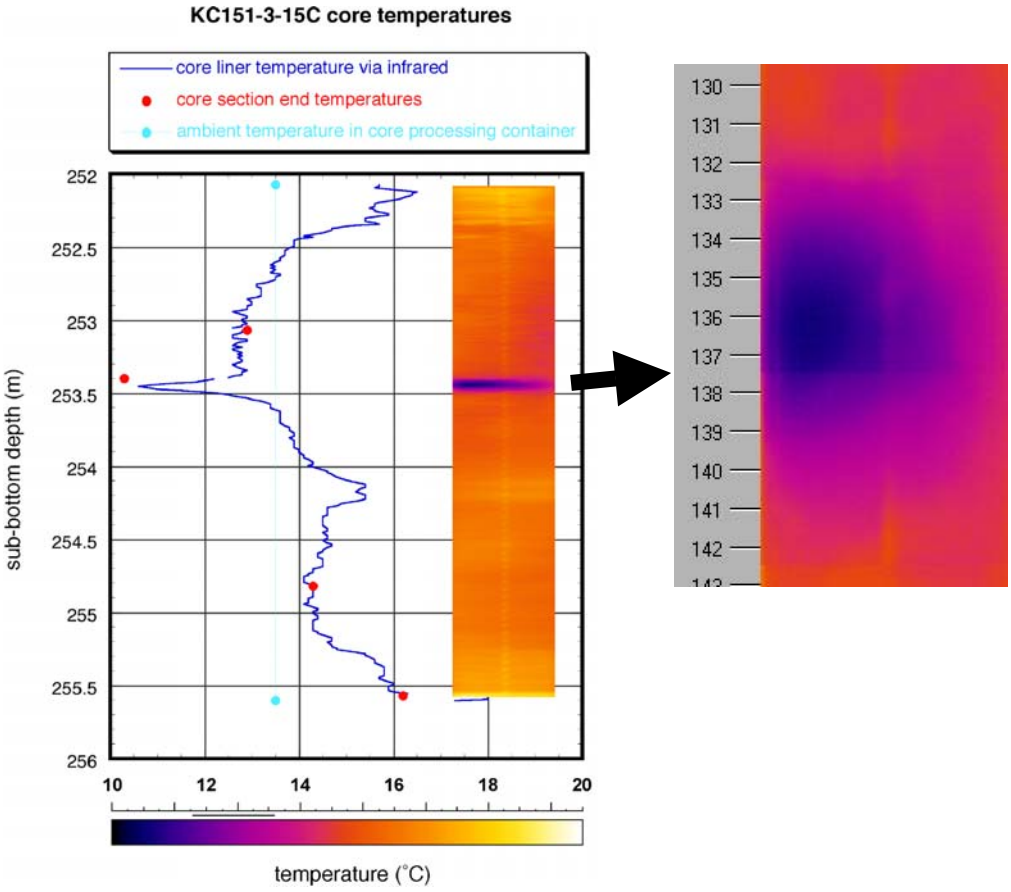

Figure 49. Temperature data for Core 151-3-15C, including infrared image. The negative thermal anomaly at 253.45 mbsf displayed classic magnitude and morphology for a hydrate generated thermal anomaly. Slight discontinuity at 137.5 cm is a result of joining the adjacent infrared images.

The Adara temperature shoe attached to the FHPC on Core KC151-3-3H (Figure 51) and the temperature logger on Core KC151-3-11P (Figure 52) showed that the warming for Keathley Canyon cores, while possibly less drastic than that at Atwater Valley, was still substantial and probably enough to mask all but the most intense thermal anomalies. Thermal anomalies, like hydrate itself, are ephemeral beasts: the absence of thermal anomalies does not indicate absence of gas hydrate! The pressure cores taken at Keathley Canyon indicated that there was gas hydrate in the sediment column, but at levels of hydrate at 1-5% of pore volume, the thermal anomaly created by the dissociation of this amount of hydrate could easily be erased during the pipe trip.

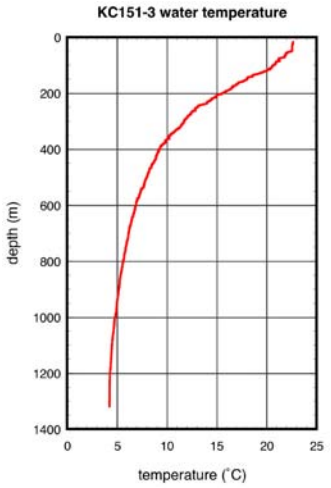

Figure 50. Temperature data from the Seabird CTD cast over Site KC151-3.

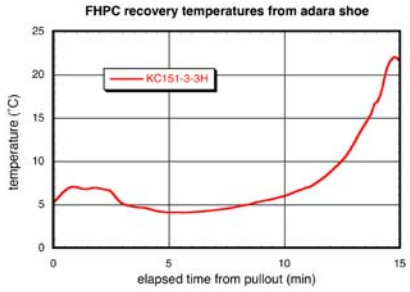

Figure 51. Temperature data from the temperature shoe fitted on the FHPC for core KC151-3-3H.

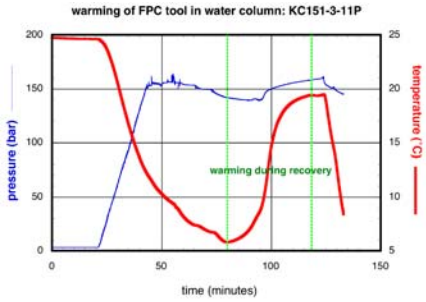

Figure 52. Temperature and pressure data versus time for core KC151-3-11P. The retrieval of the tool up the drillpipe is bounded by green dashed lines.

MSCL-S Measurements

Cores from Hole KC151-3 were logged with the MSCL-S, using the gamma density, P-wave velocity, electrical resistivity, and magnetic susceptibility sensors (Figure 53). As at the previous

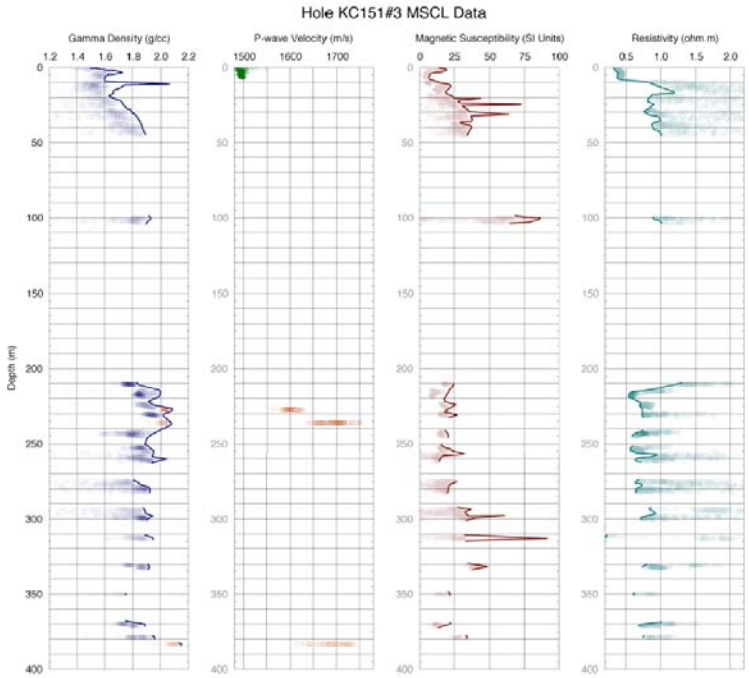

Figure 53. MSCL-S data, including gamma density, P-wave velocity, magnetic susceptibility, and electrical resistivity, for Hole KC151-3. Gamma density and P-wave velocity from pressure cores KC151-3-11P, -13R, and -26R, measured under in situ pressure, are included in the composite in orange. High-velocity spike in Core KC151-3-13R of 2074 m/sec is off scale.

sites, all data are affected by gas expansion below the sulfate-methane interface at about 7 mbsf, the P-wave and resistivity data especially so. The density and magnetic susceptibility data show a number of distinct features that might be used, in conjunction with sedimentological observations, to describe sedimentary units. The density maximum near 230 mbsf was also seen on the LWD logs for Hole KC151-2.

The composite plot for this hole also incorporates the measurements made on the pressure cores at full *in situ* pressure in the MSCL-V and MSCL-P. The densities are slightly higher in the pressure cores, as expected, as there is no gas expansion and therefore these are truer indications of *in situ* densities. The only P-wave velocities below the sulfate-methane interface are from the pressure cores, and a very high velocity peak that is tentatively interpreted as hydrate is not shown on Figure KC151-14.

MSCL-XYZ Measurements

Cores from Hole KC151-3 were imaged in the MSCL-XYZ. Most notable in the images were generally subhorizontal millimeter-thick white horizons (e.g., Figure 54), which are presumably carbonate layers. Color spectra and magnetic susceptibility measurements, made with a point sensor, were also taken (Figure 55). High frequency variations in the magnetic susceptibility may aid in the sedimentological description of the cores.

Figure 54. Color linescan image of Core KC151-3-20H, 55-65 cm, showing millimeter-thick, sub-horizontal white veins that may be carbonate.

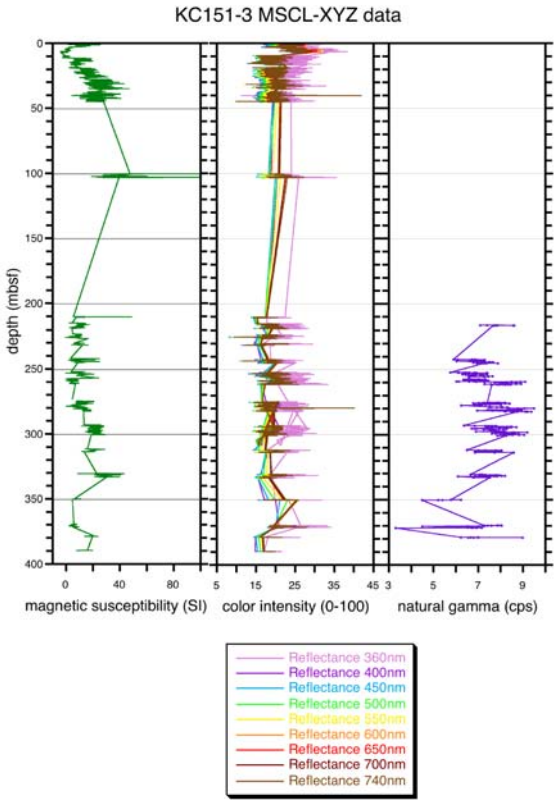

Figure 55. MSCL-XYZ data summary plot, including magnetic susceptibility, color spectrophotometry, and natural gamma radioactivity, for hole KC151-3. Data for natural gamma was only collected on cores below 200 mbsf.

Measurement of naturally-occurring gamma radiation was made to aid in correlation with the LWD logs from nearby Hole KC151-2. Because the natural gamma measurements collected on the split core were collected at a much higher spatial resolution than the downhole measurements, the core data were smoothed for comparison (Figure 56). The vertical offset in the strata between the two holes appears to be between 0-7 meters and varies downhole; some of the variation may be due to curatorial issues with short cores. However, this does not mean that all features in the two holes should be assumed to be similar. One of the most notable features of the LWD logs from KC151-2 was the high resistivity layers, which were dipping at extremely high angles and are likely to cross strata.

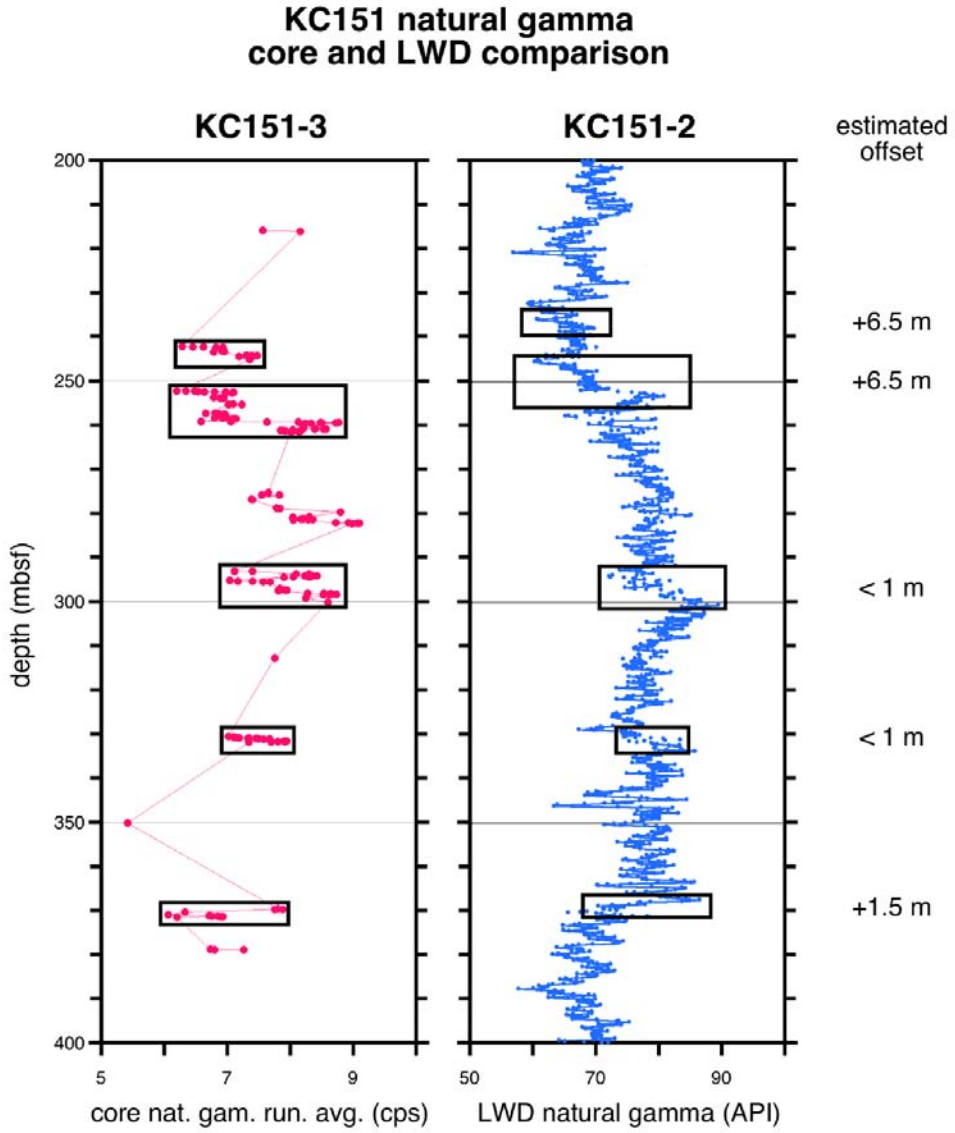

Figure 56. Natural gamma data collected on split cores from KC151-3 compared to logging-while-drilling natural gamma data from Hole KC 151-2. Core data has been smoothed for comparison with the downhole data. Boxed zones are provisional matched strata, and offsets of KC151-3 from KC151-2 are at right.

ROV Push Cores

MSCL-S Measurements

An ROV push core, Core KC151-2PC, collected from Atwater Valley in short fiberglass liners was logged with the MSCL-S (Figure 57). This core was taken specifically for measurements of physical properties (see separate Fugro Physical Properties Report), and the MSCL-S data was meant to complement these measurements. The resistivity data is adversely affected by the core end effects and is not calibrated, however, all other data is calibrated and valid.

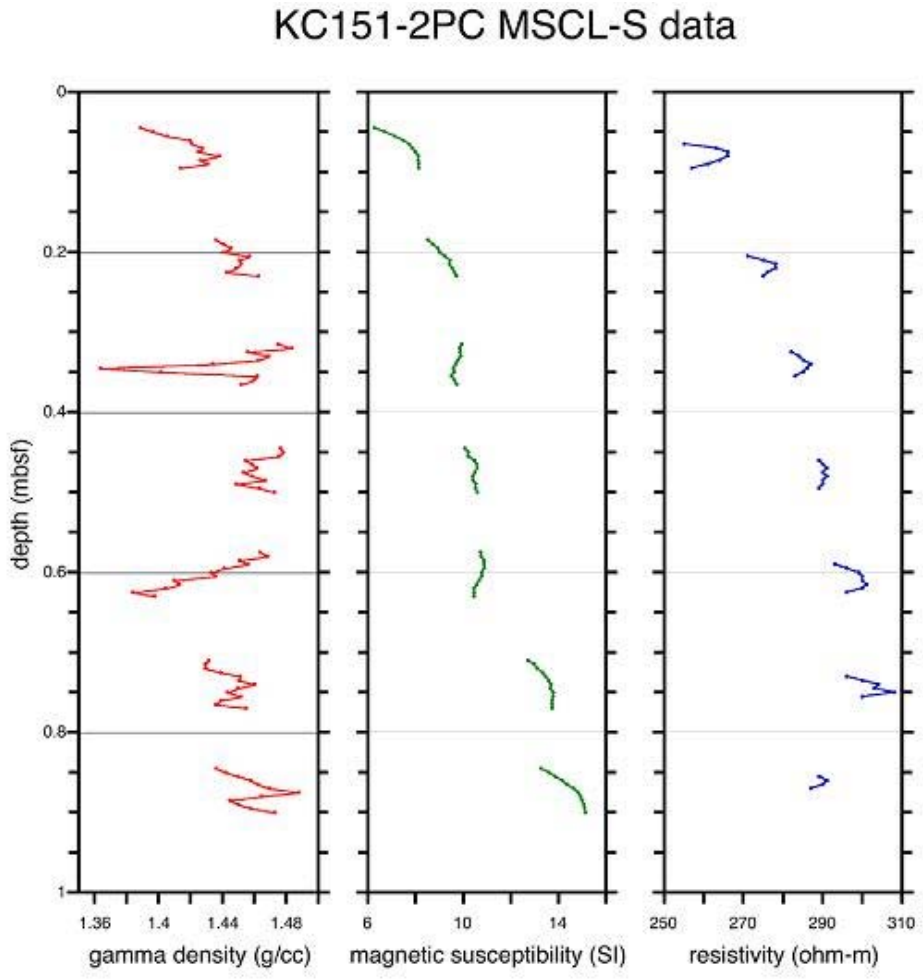

Figure 57. MSCL-S data summary plot, including gamma density, P-wave velocity, and magnetic susceptibility, for push core KC151-2PC.

References

Ford, K.H., Naehr, T.H., Skilbeck, C.G., and the Leg 201 Scientific Party, 2003. The use of infrared thermal imaging to identify gas hydrate in sediment cores. In D'Hondt, S.L., Jørgensen, B.B., Miller, D.J., et al., Proc. ODP, Init. Repts., 201, 1-20 [CD-ROM]. Available from: Ocean Drilling Program, Texas A&M University, College Station TX 77845-9547, USA.

Schultheiss, P.J., Francis, T.J.G., Holland, M., Roberts, J.A., Amann, H., Thjunjoto, Parkes, R. J., Martin, D., Rothfuss, M., Tyunder, F., & P.D. Jackson, 2005. Pressure Coring, Logging and Sub-Sampling with the HYACINTH System, in "New ways of looking at sediment cores and core data", Geological Society Special Publication, in press.

Shipboard Scientific Party, 2003. Explanatory notes. In Tréhu, A.M, Bohrmann, G., Rack, F.R., Torres, M.E., et al., Proc. ODP, Init. Repts., 204, 1-102 [CD-ROM]. Available from: Ocean Drilling Program, Texas A&M University, College Station TX 77845-9547, USA.

Tool Run ID	Core ID	Date	SBD (m)	Core Length (cm)	Comments
FPC1	AT13-2-3P	26-Apr-05	15.54	0	Core overshot and core washed out.
FPC2	**AT13-2-7P**	**27-Apr-05**	**35.70**	**53.5**	**Core recovered under full pressure**
FPC3	AT13-2-12P	29-Apr-05	134.11	119	No pressure. Core overshot–tool left in hole and fished out.
FPC4	ATM1-3P	4-May-05	15.85	0	Core overshot and core washed out.
FPC5	ATM1-6P	4-May-05	26.82	0	Corer did not fire.
FPC6	**ATM2-5P**	**5-May-05**	**26.82**	**52 (initial), 30 (final)**	**Core recovered under full pressure. Partially extruded in STC and MSCL-P.**
FPC7	none	5-May-05	~100	0	No core recovered. Sand filled BHA, tool stuck, pipe tripped.
FPC8	**KC151-3-11P**	**14-May-05**	**227.08**	**88.5**	**Center bit run prior. Core recovered at full pressure.**
FPC9	KC151-3-18P	15-May-05	265.18	59	Center bit run prior. Sediment too stiff for pull out. Liner broke–top recovered at full pressure, bottom depressurized. Core in bottom half.
FPC10	KC151-3-27P	17-May-05	384.96	0	Center bit run prior. Sediment too stiff. Core jammed in tool barrel and could not be retracted into autoclave.

Table 1. FPC deployments on the GOM-JIP Expedition.

Tool Run ID	Core ID	Date	SBD (m)	Core Length (cm)	Comments
HRC1	AT13-2-5R	26-Apr-05	27.10	93	No pressure. Valve did not close
HRC2	AT13-2-10R	28-Apr-05	126.19	0	Motor start mechanism destroyed due to overloading.
HRC3	ATM1-4R	4-May-05	17.37	0	Liner shoe jammed; core liner broken.
HRC4	ATM2-4R	4-May-05	25.30	0	Liner shoe jammed; core liner broken.
HRC5	ATM2-6R	5-May-05	28.96	0	Liner shoe jammed.
HRC6	KC151-3-9R	14-May-05	220.98	0	No penetration into formation (sediment in BHA?)
HRC7	**KC151-3-13R**	**15-May-05**	**235.92**	**64**	**Center bit run prior. Core recovered at full pressure.**
HRC8	**KC151-3-26R**	**17-May-05**	**383.13**	**51**	**Center bit run prior. Core recovered at full pressure.**
HRC9	KC151-3-29R	17-May-05	389.53	25	Center bit run prior. No pressure. Core liner broken.

Table 2. HRC Deployments on the GOM-JIP Expedition.

Georgia Tech – JIP Methane Hydrates Program

Preliminary Results

Georgia Tech Instrumented Pressure Testing Chamber Deployed on JIP Gas Hydrate Drilling Program in Gulf of Mexico, April to May 2005

Submitted June 5, 2005

PIs: Carolyn Ruppel and J. Carlos Santamarina
Georgia Institute of Technology

Data in this report were collected and analyzed by shipboard scientists Dr. T-S Yun and Ph.D. Candidate G. Narsilio with support from the Georgia Tech JIP contract

Summary

We provide an overview of data collected with the Georgia Tech instrumented pressure testing chamber constructed under contract with the ChevronTexaco JIP. The Georgia Tech instrumented pressure testing chamber for the first time ever in the drilling community measures mechanical properties, strength, and electrical conductivity on pressure cores maintained at pressure. The chamber was used to test cores obtained during drilling in the Gulf of Mexico in April and May 2005. Due to difficulties retrieving pressure cores, the Georgia Tech sampling plan was modified shipboard and measurements were completed on 68 whole rounds from conventional cores, 2 re-pressurized cores, and 2 pressure cores. For conventional cores, Georgia Tech independently measured some parameters being measured by other groups for the purpose of comparison methods and results. The results yield a set of correlative plots that may yield important insights into the behavior of the sediments at the microstructural level. For the re-pressurized and pressure cores, Georgia Tech conducted through liner measurements of Vp and invasive measurements of Vp, Vs, electrical conductivity, and strength. Despite some difficulty with the third-party manipulator, the Georgia Tech data provide proof-of-concept that the vessel operated as planned. A preliminary comparison between Vs data obtained on a pressure core and on conventional core whole rounds at comparable depths demonstrates the potential importance of pressure coring. The Vs data from the conventional cores show wide scatter and have significantly lower velocity than the Vs result measured on a pressure core, probably due to the disturbance of the conventional core's soil structure by gas expansion during retrieval.

Non-Pressure Cores (FHPC and FC)

Due to early difficulties with acquisition of pressure cores, the Georgia Tech sampling plan was altered aboard ship to include tests on conventional cores. A total of 68 5- to 10-cm long whole rounds were obtained near the pore water sampling locations. Specimens are sealed to prevent moisture loss. Most properties were measured shipboard in the Georgia Tech instrumented pressure testing chamber. In some cases, Georgia Tech and others measured the same properties using different techniques, as a means to compare methodologies and results later.

Conventional cores: Measured properties

Properties		Method	Party responsible
Elastic wave velocity (vertical)	P-wave	Pinducer	GeoTek (horizontal) Georgia Tech
	S-wave	Bender element	Georgia Tech
Electrical conductivity		Needle probe	Georgia Tech
Undrained shear strength		Penetrometer / torvane	Fugro
pH		pH strip (resolution: ±0.25)	Scripps
Specific surface (S_a)[1]		Methylene blue method	Georgia Tech
Gravimetric water content[1]		ASTM standard (GT)	Fugro Georgia Tech

1: on-shore measurement (at Georgia Tech)

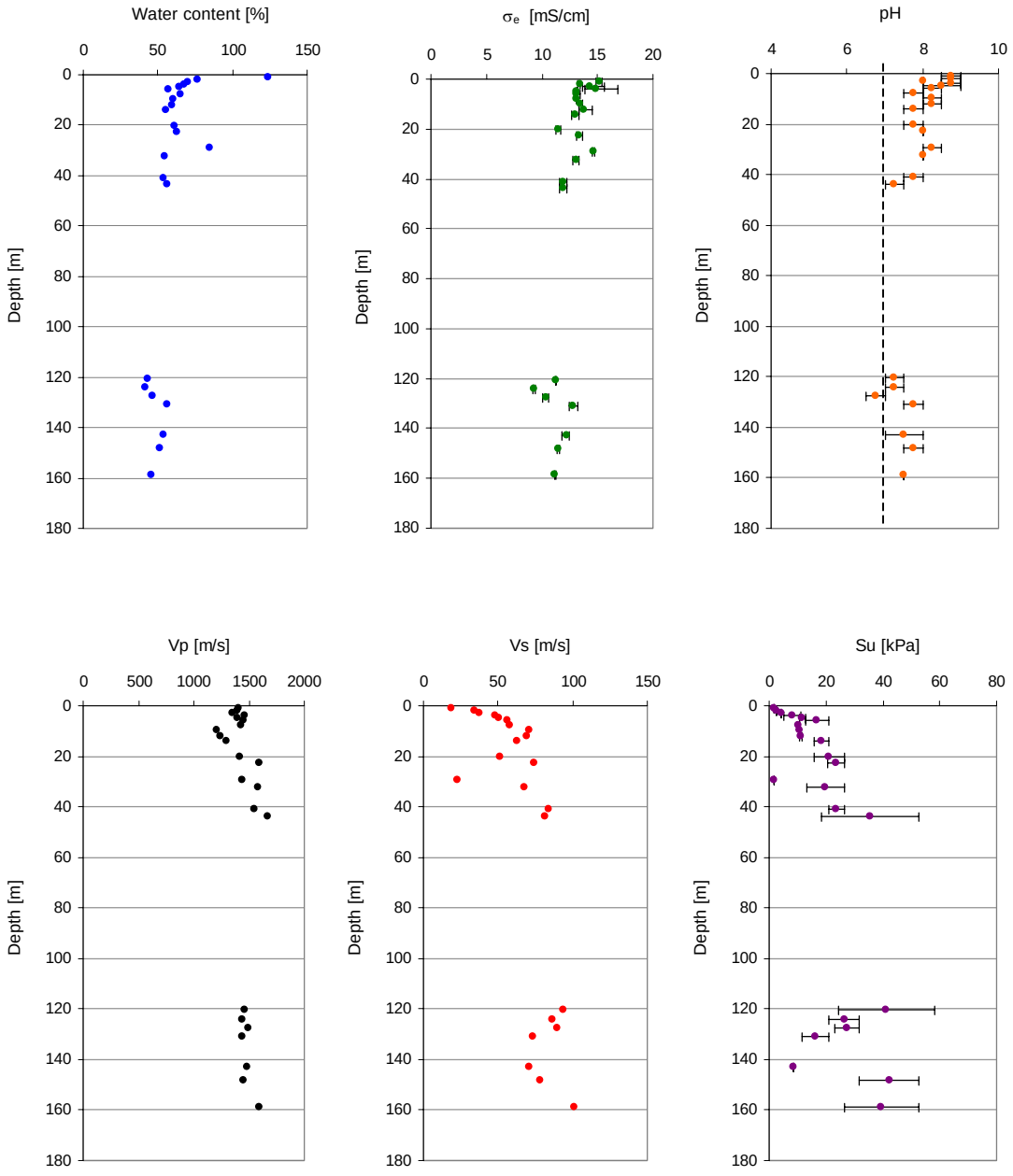

Figure 1. Stacked data from conventional core whole rounds analyzed at AT 13-2 site.

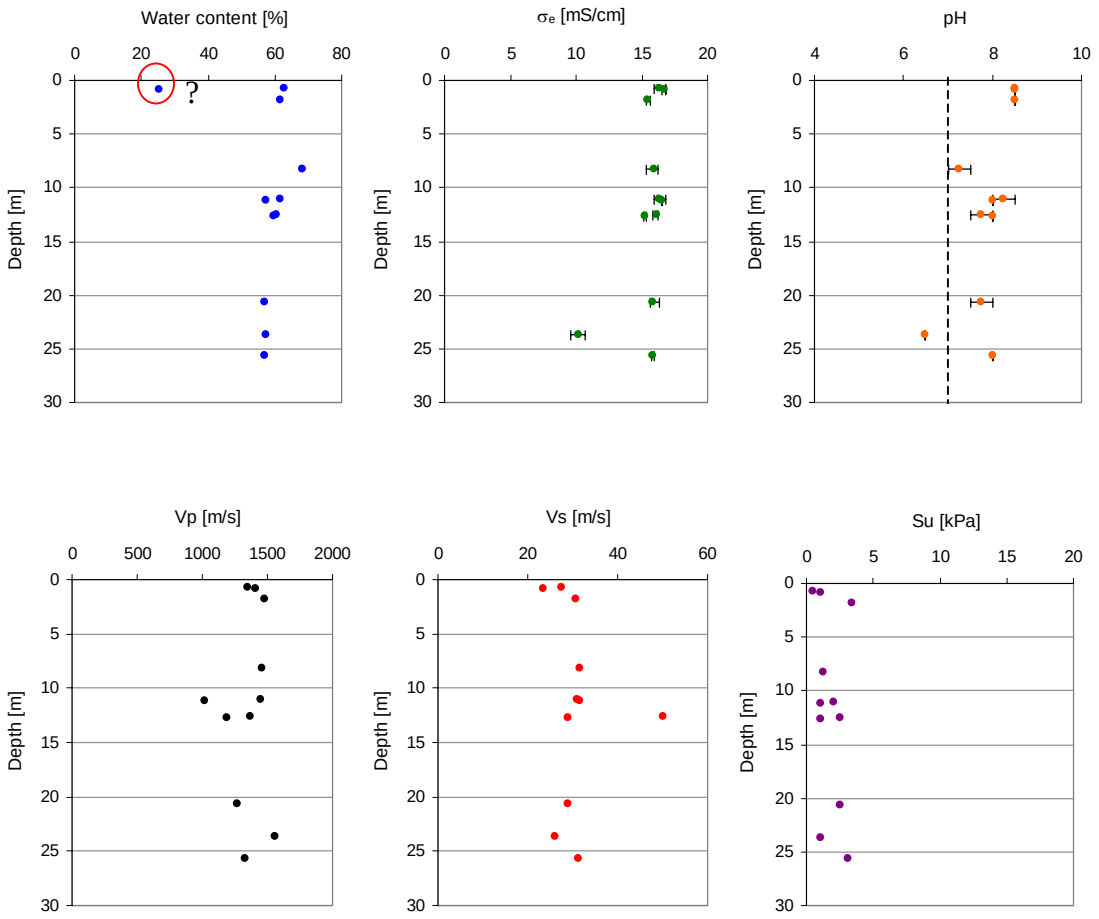

Figure 2. Stacked data measured on whole rounds from conventional cores at the AT Mound sites (ATM 1 and ATM 2).

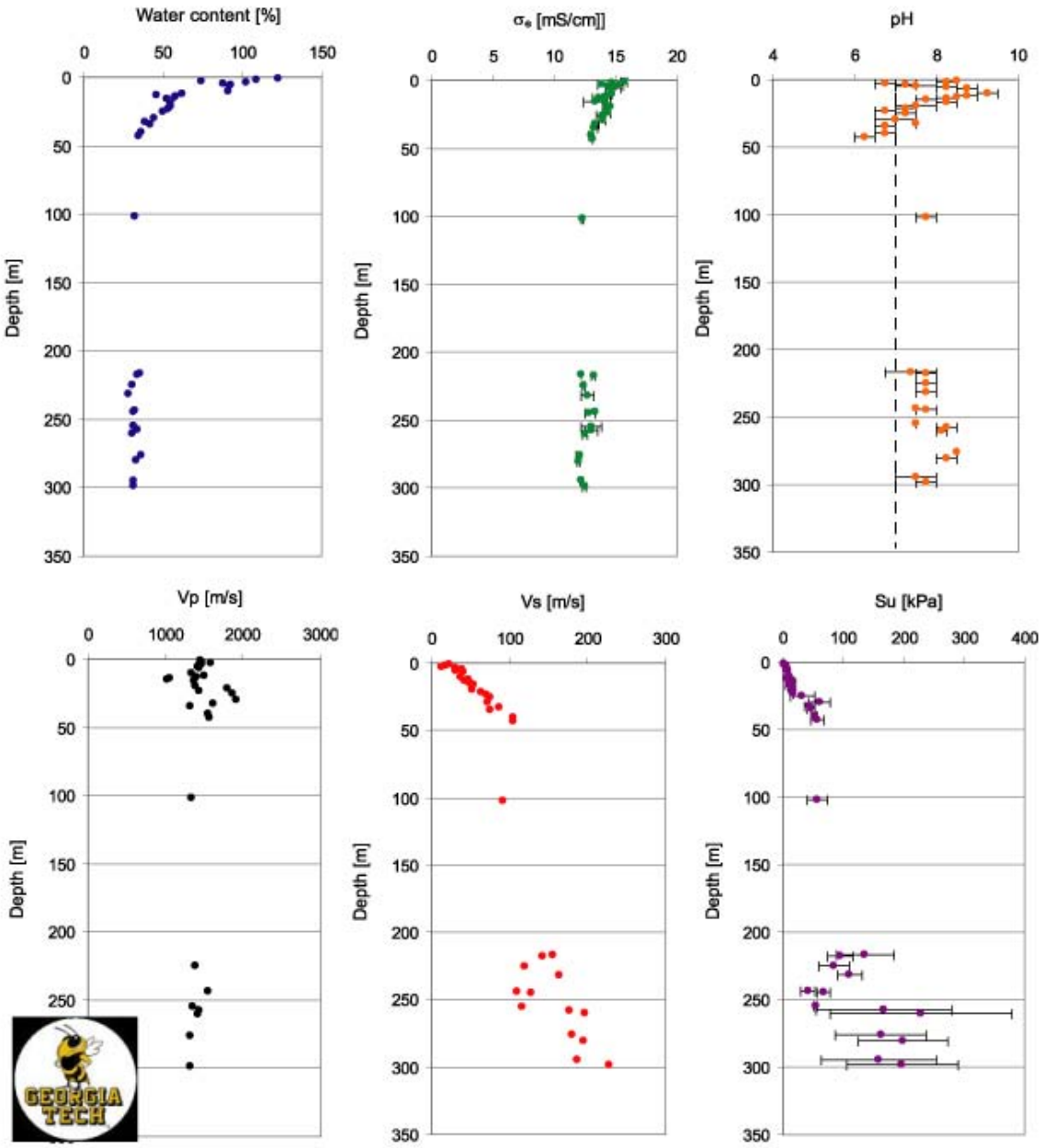

Figure 3. Stacked data from conventional core whole rounds obtained at site KC 151-3.

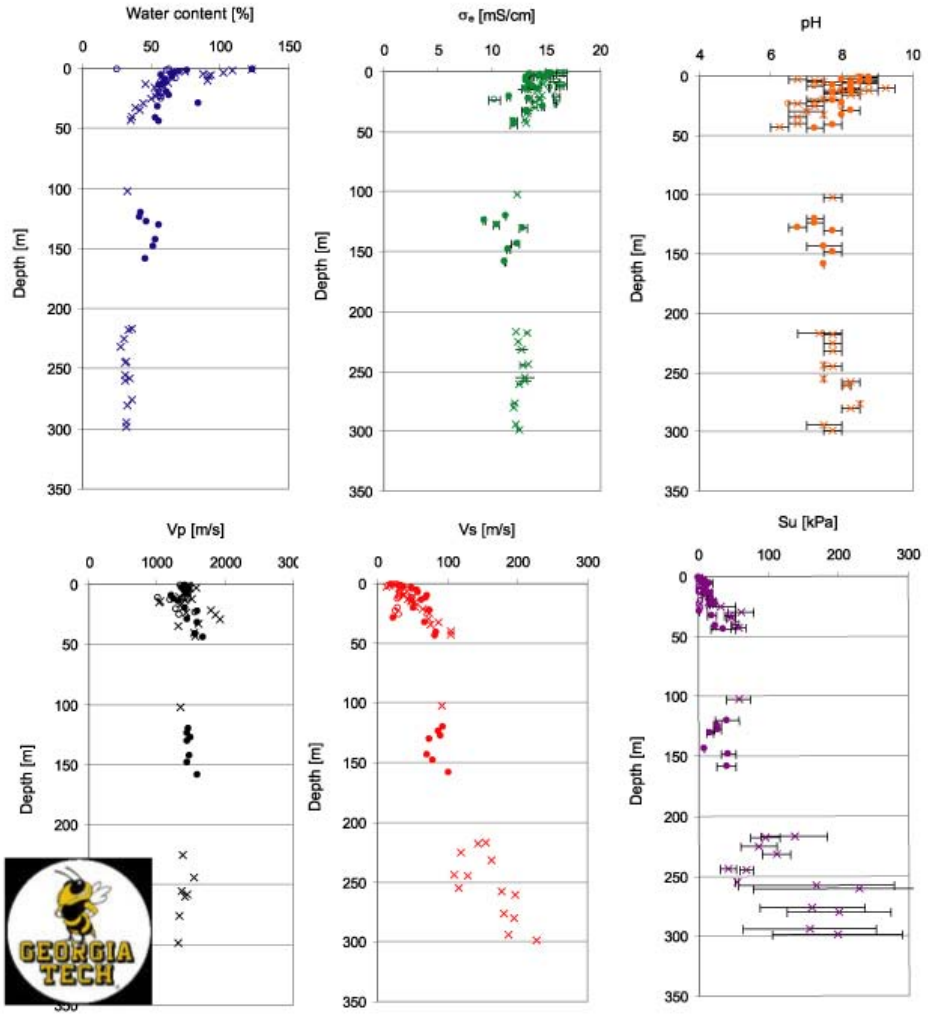

Figure 4. Compilation of data from measurements on conventional core whole rounds at all sites. Closed circles denote AT 13-2; open circles represent ATM 1 and 2, and crosses show data for KC 151-3.

Correlations / Observations

Here we present only raw data correlations, without any interpretation. Some of the interpretations in Francisca et al. (revised for EPSL, June 1, 2005) for shallow cores obtained elsewhere in the Gulf of Mexico may provide insight into these results.

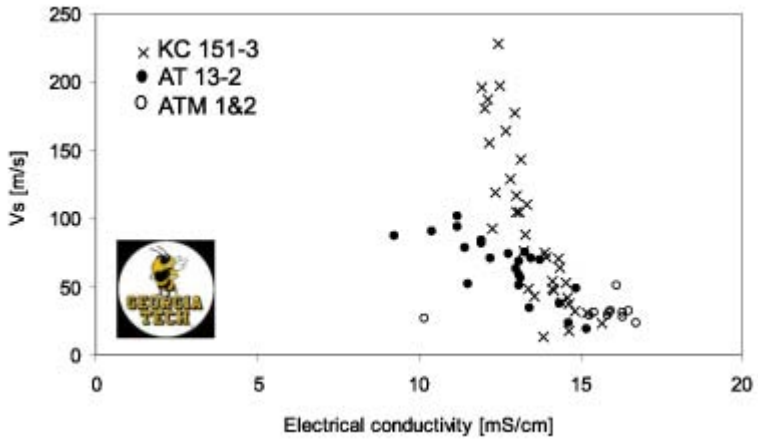

Figure 5. S-wave velocity vs. electrical conductivity for conventional cores. V_s decreases with increasing electrical conductivity. V_s/σ_e at the different locations have different slopes.

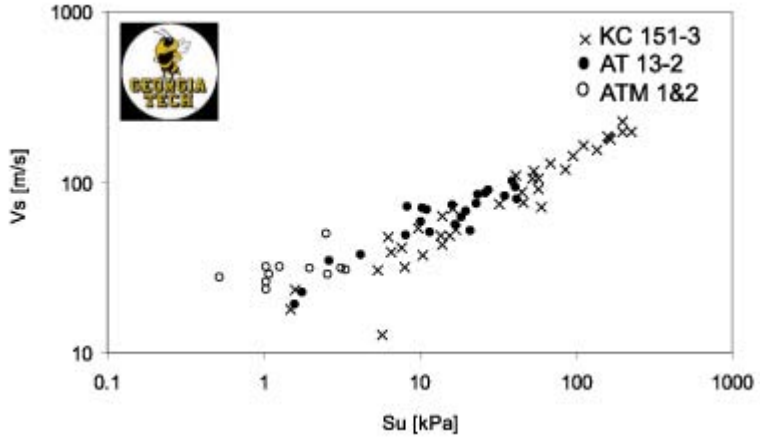

Figure 6. S-wave velocity vs. undrained shear strength for conventional cores. Best fit line is: $V_s = 20[m/s] \cdot \left[\frac{S_u}{kPa}\right]^{0.4}$

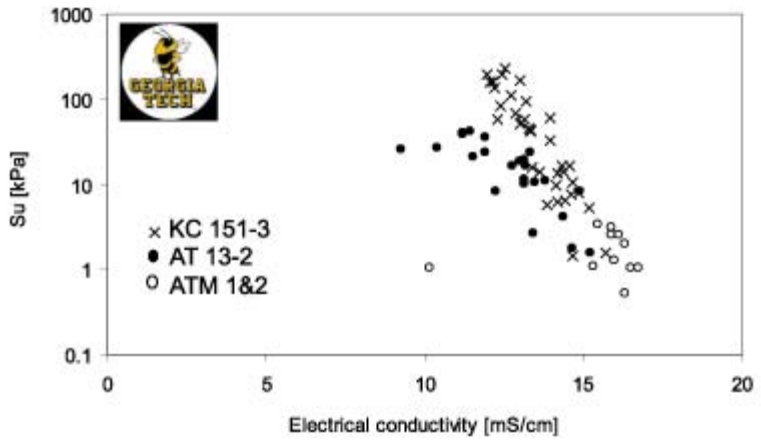

Figure 7. Undrained shear strength vs. electrical conductivity for conventional cores.

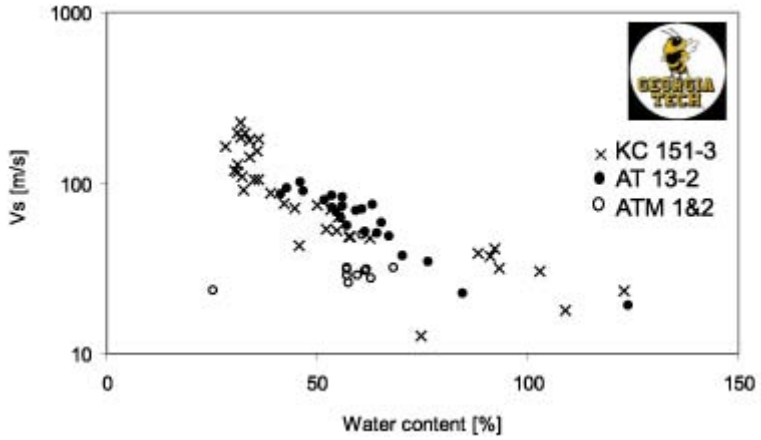

Figure 8. S-wave velocity vs. water content for conventional cores.

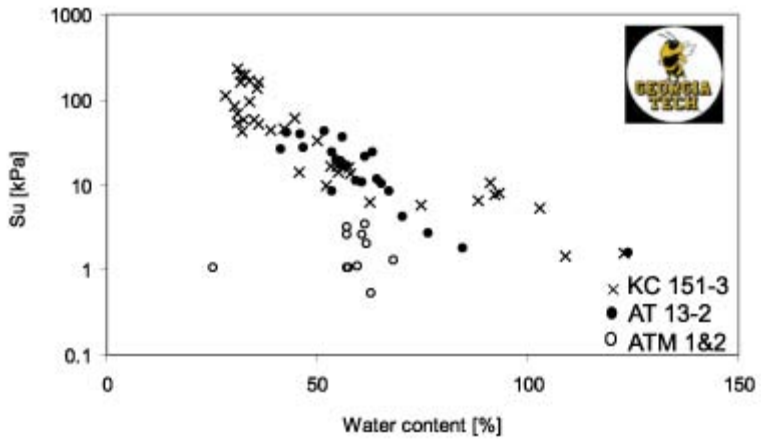

Figure 9. Undrained shear strength vs. water content for conventional cores.

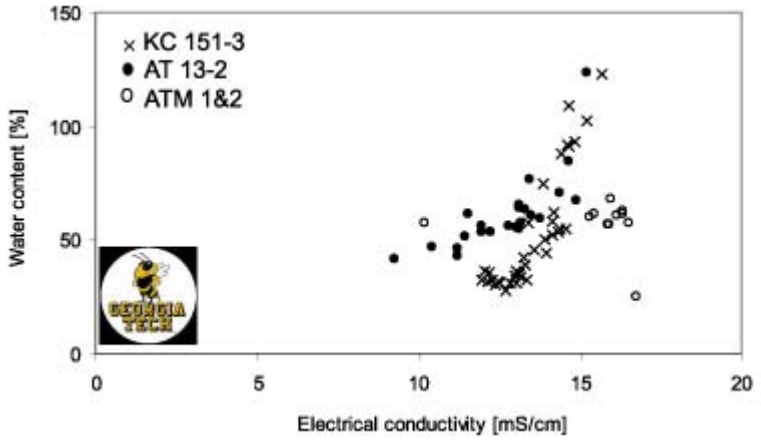

Figure 10. Water content vs. electrical conductivity for conventional cores.

Pressure cores (FPC and HRC)

Georgia Tech originally planned no work on re-pressurized cores since these cores have experienced significant disruption of their mechanical properties. However, the sampling plan was modified aboard ship, and Georgia Tech analyzed two re-pressurized cores and two pressure cores. Measurements are performed after X-ray and CT-scanning in all cases, another modification to the original sampling plan.

Measured properties

Sites		V_p			V_s	S_u	R	Depth	Applied pressure
		Scan	Non-invasive	Invasive					
Re-pressurized cores	AT13-2-3P	O	O	O	O	O	O	1291.1m water 15.54mbsf	14MPa
	AT13-2-12P	O[1]	O	O		O[2]		1291.1m water 134.1mbsf	14MPa
Pressure cores	KC151-3-11P	O	O	O	O	O	O	1322.5m water 227.1mbsf	14MPa
	KC151-3-13R	O	O	O			O	1322.5m water 235.9mbsf	14MPa

[1]: without and with fluid pressure.
[2]: Penetrometer and vane shear test

Electrical resistance has not been converted to conductivity due to problems with corrosion of the sensor.

Strength measurements are currently being calibrated.

Sample: AT13-2-3P

P-wave scan

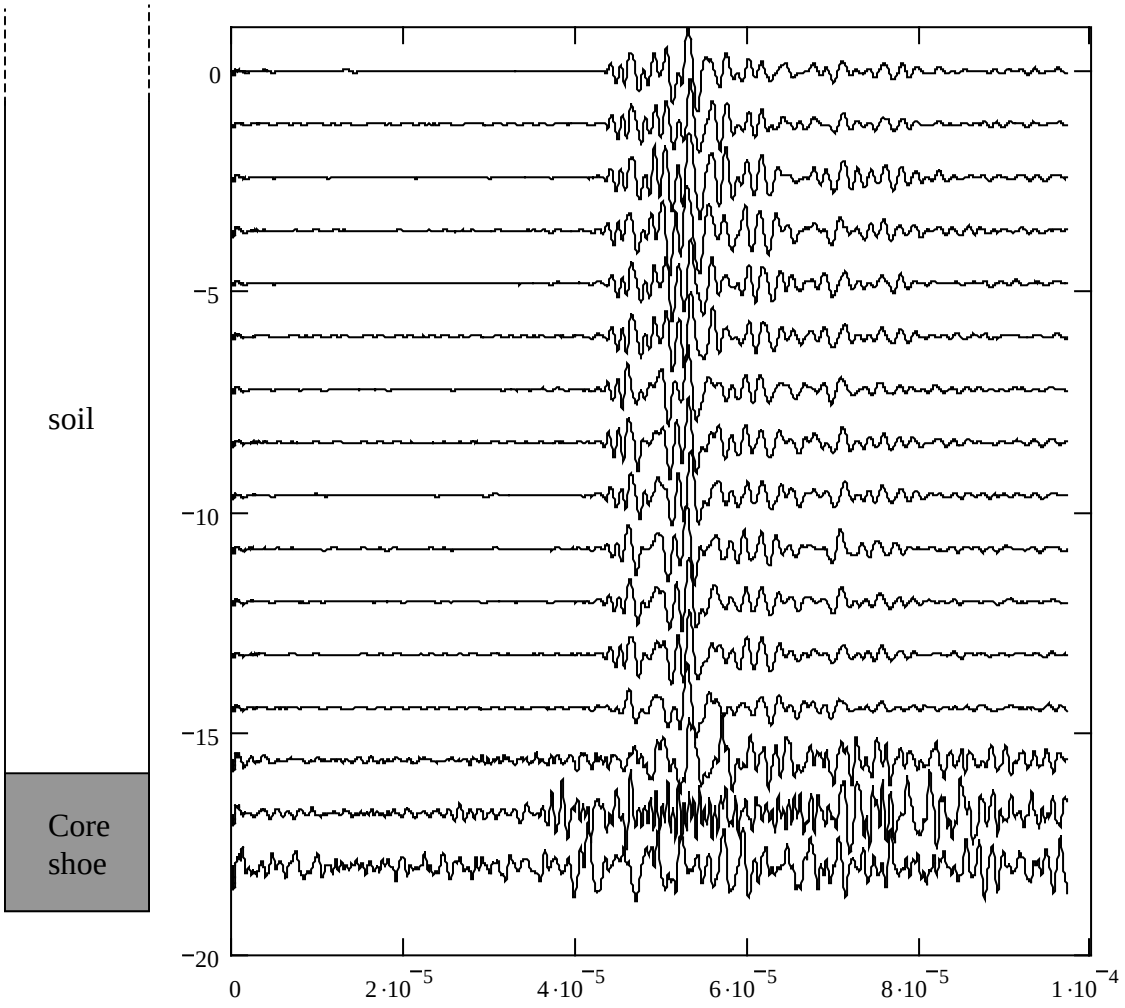

Figure 11. P-wave scan measurements every 3cm with 14MPa (re-pressurized).

Elastic wave velocities

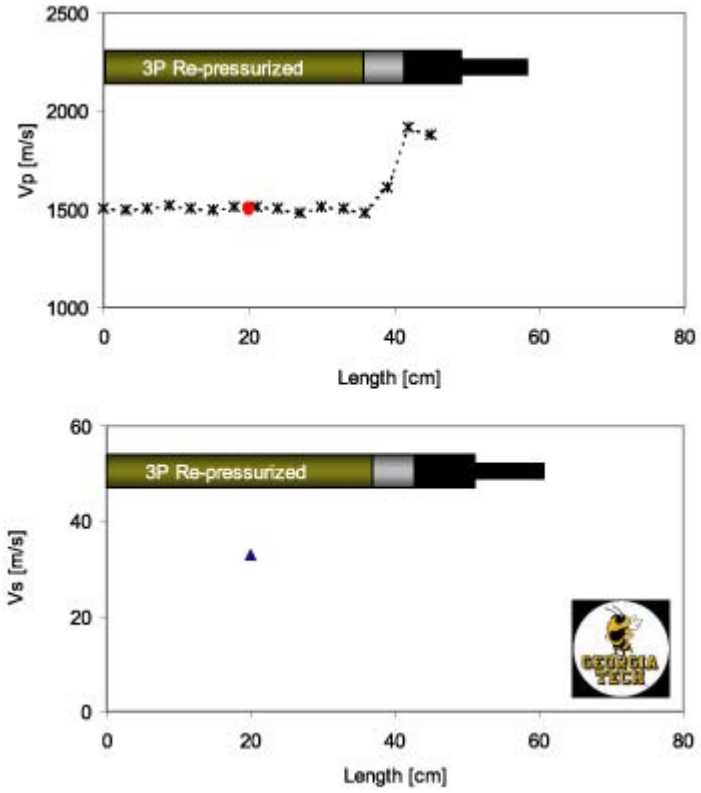

Figure 12. Measured elastic wave velocities. The dotted line with asterisks indicates the P-wave scan while red symbol shows V_p through a liner hole. The triangle (Δ) shows the measured V_s. Symbols are the same in other seismic velocity figures that follow.

Strength

Specimen stregth is too low to measure with penetration proble.
Pocket vane shear test confirmed very soft sediment.

Electrical Resistance

Values oscillate between 1135 and 1131 ohms (single wedge needle). This high value results from using iced water to saturate the system.

OBSERVATIONS

- The estimated P-wave velocity by non-invasive P-wave measurement ranges from 1480 to 1510m/s.
- The invasive P-wave measurement shows similar values.
- S-wave velocity ranges from 33 to 45 m/s.

- Strength is appropriate for very soft sediment.
- Electrical conductivity: The resistance is higher than seawater because the system was saturated with an ice water/seawater mixture rather than pure seawater.

Sample: AT13-2-12P

P-wave scan – 0MPa

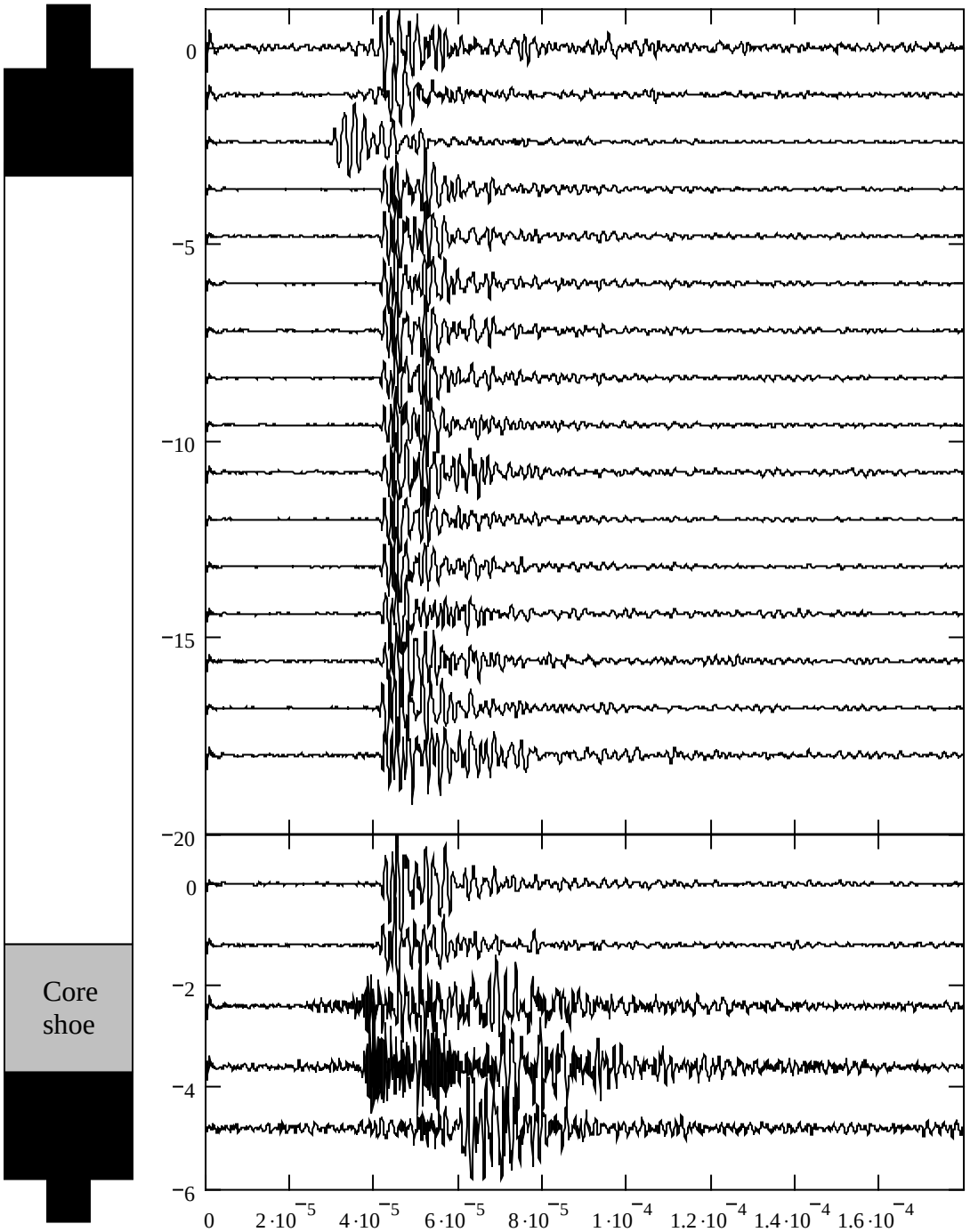

Figure 13. P-wave scan measurements every 3cm without pressure.

P-wave scan – 14MPa

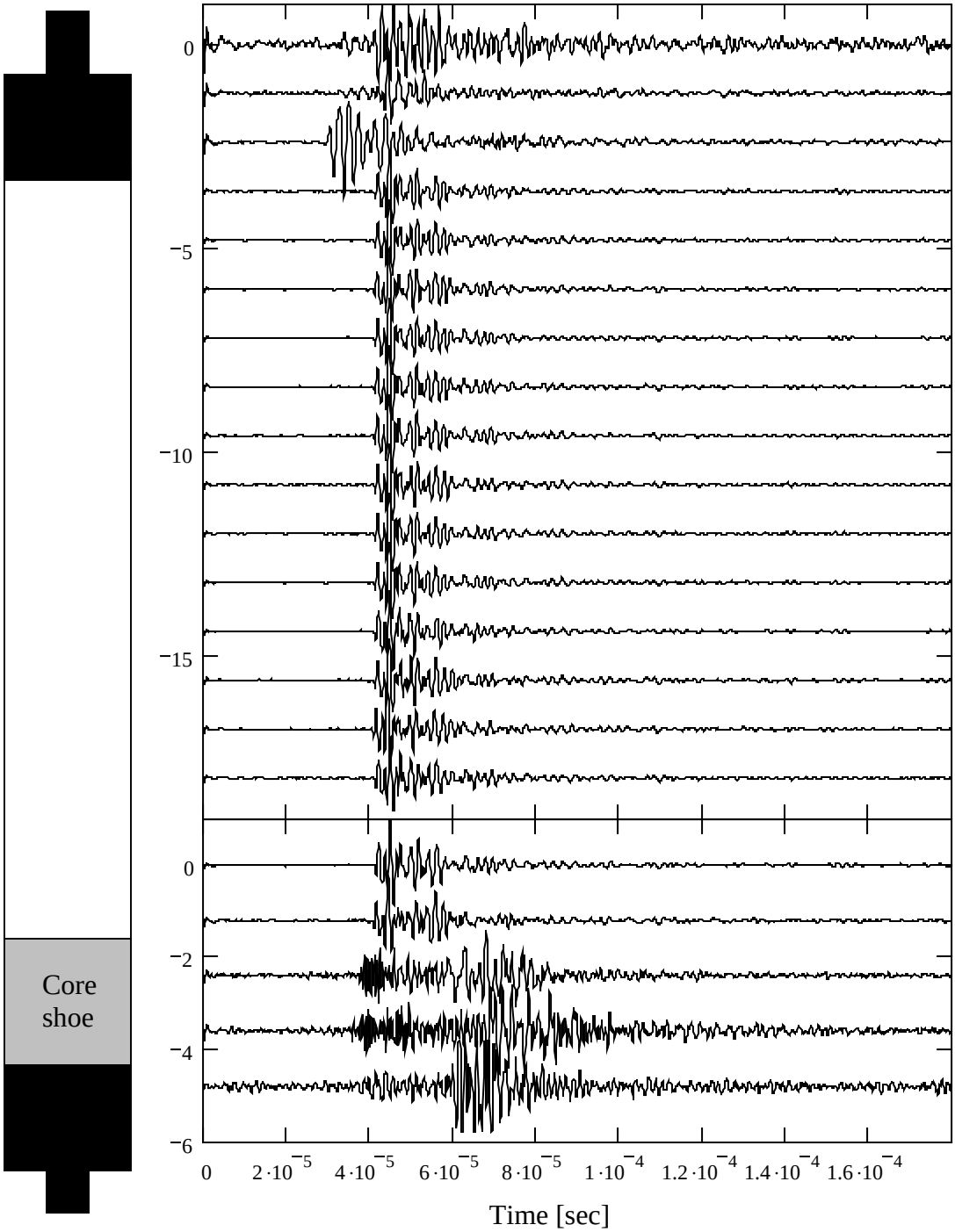

Figure 14. P-wave scan measurements every 3cm (re-pressurized to 14MPa).

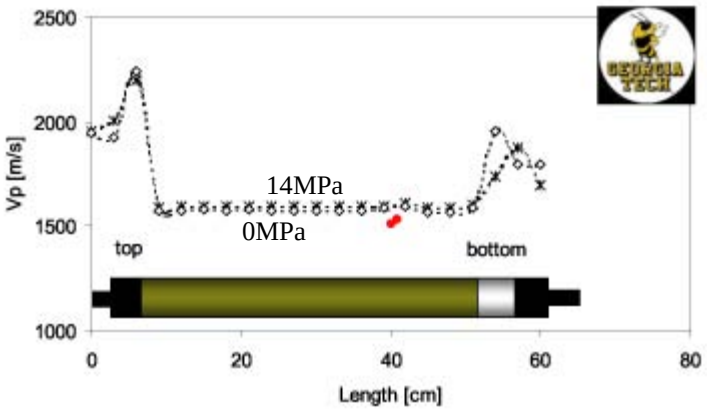

Figure 15. Invasive and non-invasive P-wave measurements under atmospheric pressure (diamonds) and under 14 MPa (asterisks). Red dots indicate invasive P-wave velocities. Higher velocity is measured under pressure, which may reflect gas dissolution into the fluid.

P-wave velocity (without and with pressure / invasive and non-invasive)

	Without pressure (0 MPa)	With pressure (14 MPa)
Invasive	1512 m/sec	1531 m/sec
Non-invasive	1515 m/sec	1529 m/sec

Strength – pocket penetrometer and vane shear test

Penetrometer: 28.7 kPa (at 0 MPa fluid pressure)
Vane shear test: 95.8 to 144 kPa (at 0 MPa fluid pressure)

Sample: KC151-3-11P

P-wave scan

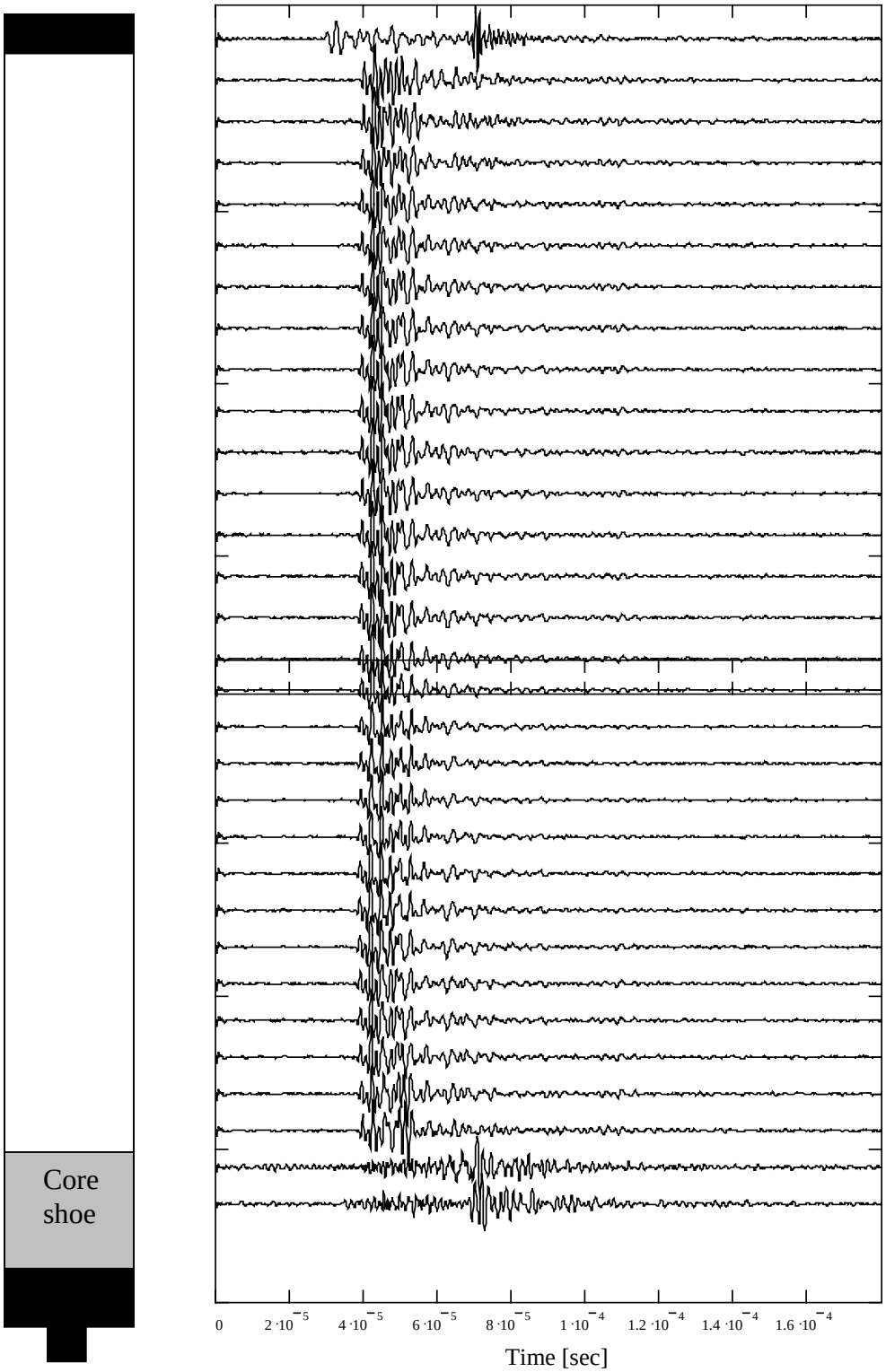

Figure 16. P-wave scan measurements every 3cm (pressure core).

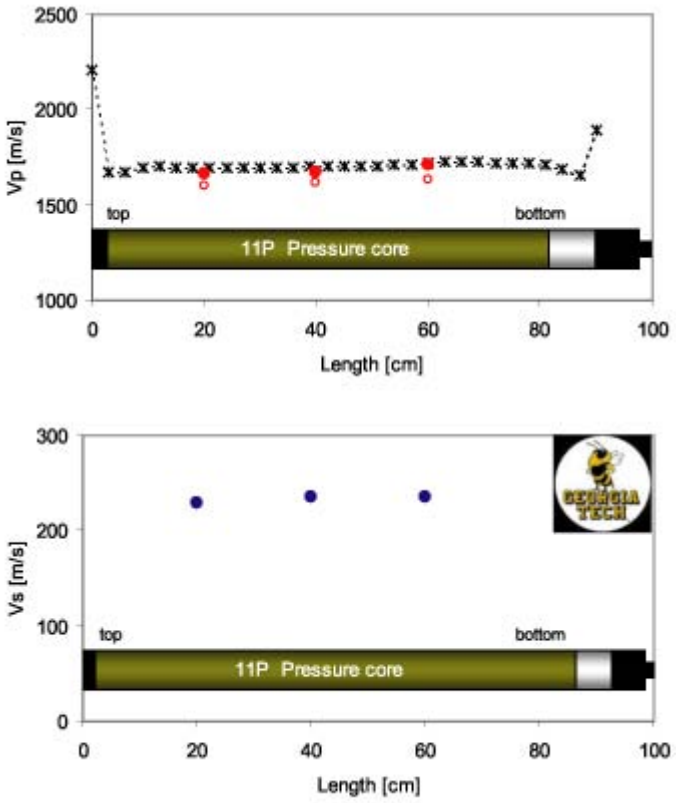

Figure 17. Elastic wave velocity measurements. Measured P-wave velocity is ~ 1700m/s and S-wave velocity is ~ 230m/s. In this and subsequent diagrams, asterisks marks the results of the 3-cm interval seismic wave scan, filled circles mark the invasive velocity measurement, and open circles are the non-invasive velocity measurement.

Electrical Resistance

The measured values are: 609 ohm, 555 ohm and 514 ohm.

Strength

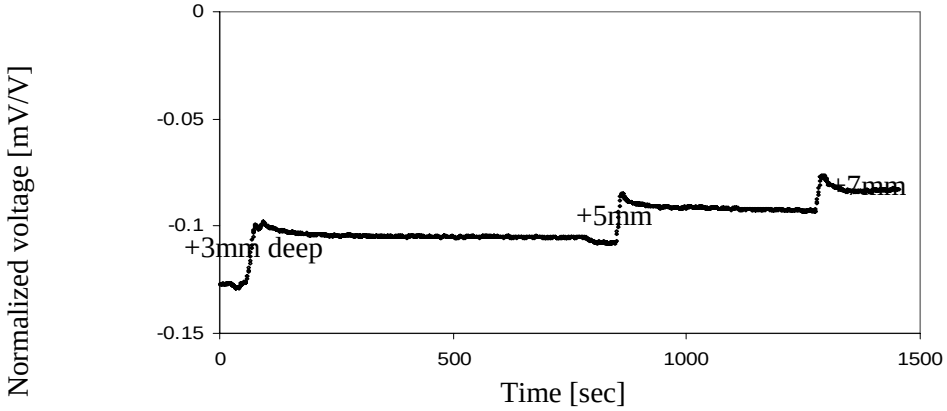

Figure 18. Voltage evolution with time for the strength determination test. Analysis is in progress.

Sample: <u>KC151-3-13R</u> (HRC specimen-chamber with chamber reducer)

<u>P-wave scan</u>

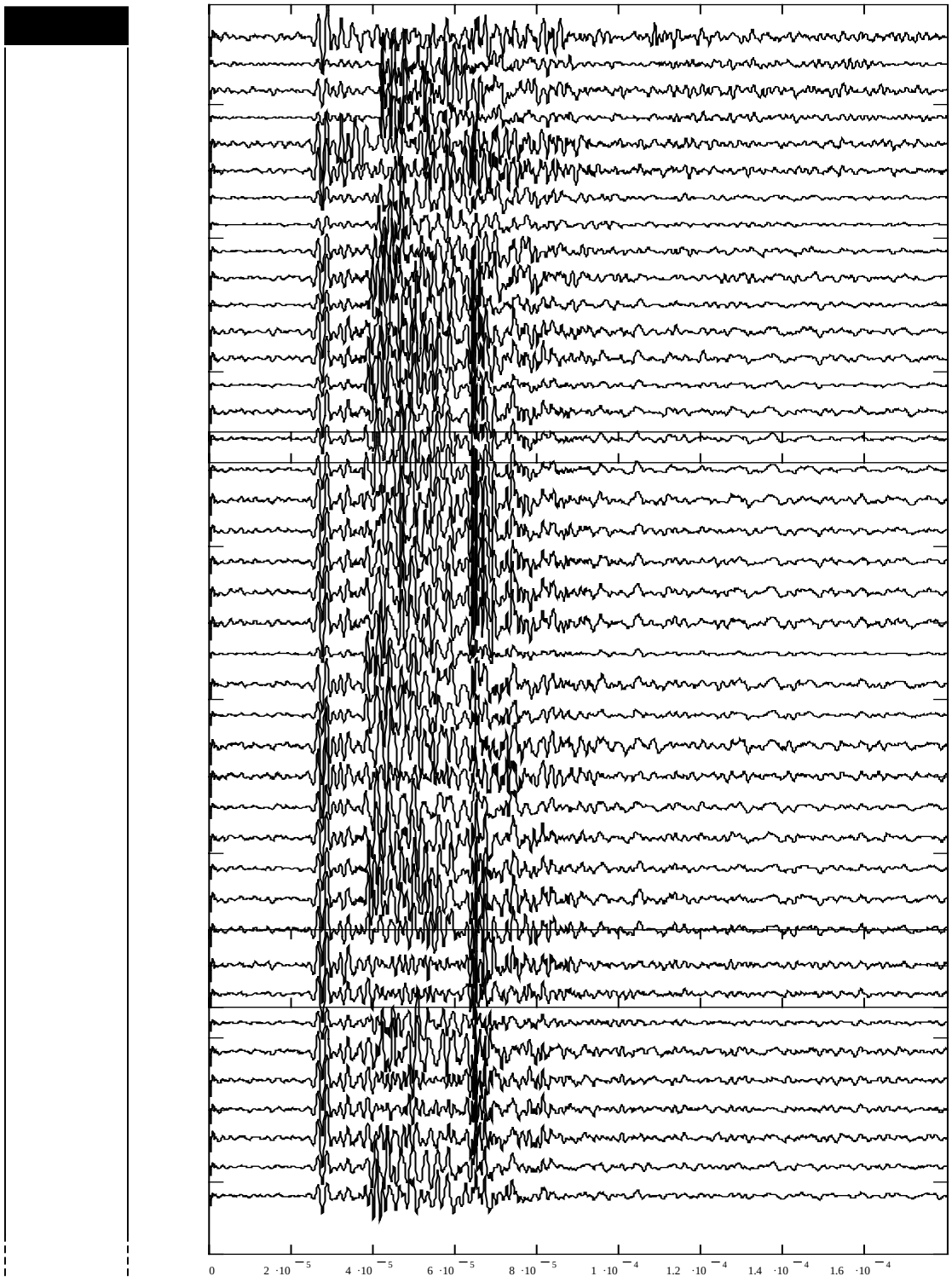

(Previous page)
Figure 19. P-wave scan measurements every 2cm (pressure core).

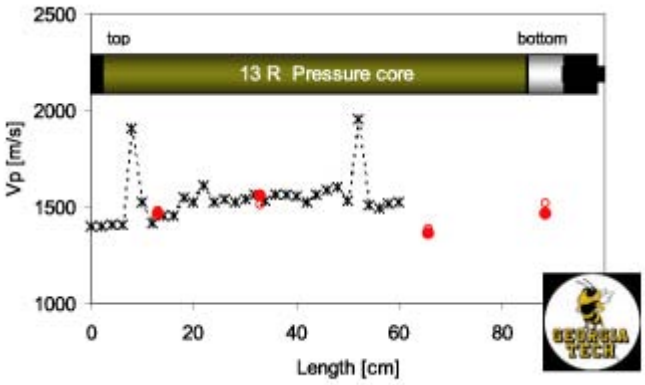

Figure 20. Noninvasive and through liner hole V_p measurements. See caption of Figure 17 for more information.

NOTES: 1. The explanation for the two high velocity peaks in the noninvasive measurements is not yet certain. The first arrival for the peak at ~55cm is not clear, and the received signal at this location is different from the surrounding recorded signals.

2. The third party manipulator had a motor control failure and positioning in the core was lost after the 2nd hole.

Electrical Resistance

The measured values are: 572 ohm, 542 ohm and 593 ohm.

Comparison of conventional cores and pressure cores

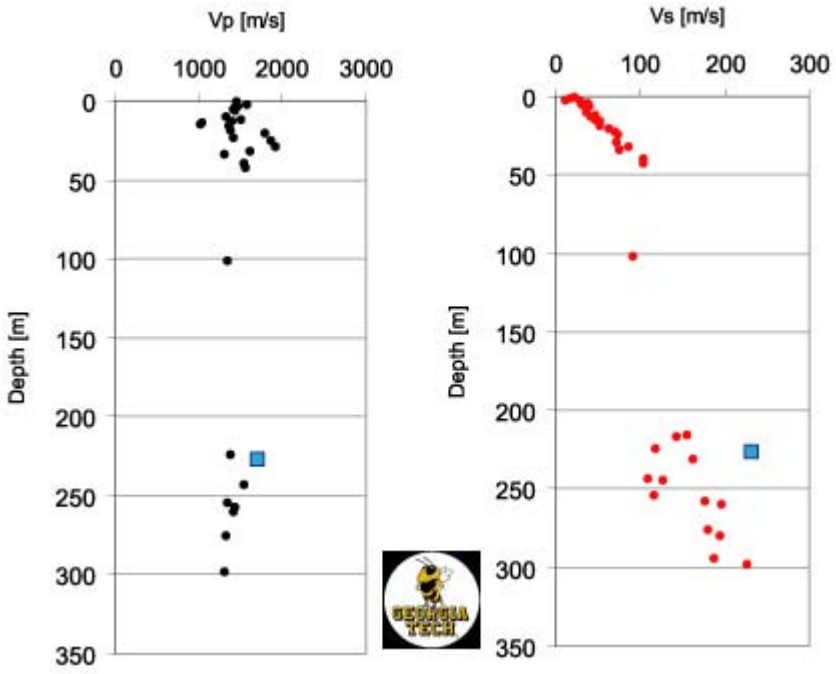

Figure 21. Conventional core P-wave and S-wave velocity data for KC151 with data measured in the pressure core denoted by the blue square. In particular, the S-wave result for the pressure core may have significance for demonstrating the effect of sampling (coring) on the sediments. Although the pressure core apparatus maintains only hydrostatic, not effective, stress, the pressure core prevents gas expansion that disturbs the soil microstructure. Such gas expansion probably contributes to the dramatically lower and much more scattered S-wave velocities measured in conventional cores from the same depth as the pressure core.